EFFECTS

OF

WASTE GLASS ADDITION

ON THE PROPERTIES

OF

FIRED CLAY BRICK

EFFECTS

OF

WASTE GLASS ADDITION

ON THE PROPERTIES

OF

FIRED CLAY BRICK

By

LISA MARIE FEDERICO, B.ENG.

A Thesis

Submitted to the School of Graduate Studies

in Partial Fulfilment of the Requirements

for the Degree

Master of Applied Science

McMaster University

MASTER OF APPLIED SCIENCE (2006) McMASTER UNIVERSITY

(Civil Engineering) Hamilton, Ontario

TITLE: Effects of Waste Glass Addition on the Properties of Fired Clay Brick

AUTHOR: Lisa Marie Federico, B.Eng. (McMaster University, 2004)

SUPERVISOR: Dr. Samir Chidiac

NUMBER OF PAGES: xii, 201

ABSTRACT

The optimization of the production of fired clay brick is essential in order to maintain a sustainable industry in Ontario. While there exists areas for improvement of the properties of bricks used in severe climates, concerns including non-renewable resource depletion, increasing energy costs, and waste management have become increasingly important in Canadian and global industries. One method to address these concerns is the use of waste additives as fluxing agents in bricks. While a fluxing agent reduces the firing temperature required for sintering of the brick and improves properties, the use of a waste additive can decrease the dependency of the industry on non-renewable resources such as mined clay or crushed shale. Waste additives can improve strength, durability, and absorptive properties, while decreasing firing temperature, and diverting waste from landfills.

A testing program was developed to determine the effects of several variables in brick production, including extrusion and firing, and to investigate the effect of the addition of non-recycled waste glass in the properties of fired clay brick. The addition was varied in the particle size of the waste glass and the percentage by mass of additive. The effects of waste glass addition were determined in terms of absorption, strength, and freeze-thaw durability of the individual specimens. Microstructure was also investigated using SEM images and mercury intrusion porosimetry to determine the effect on pore structure and vitrified matrix of the bricks. The results of the testing program determined an optimal addition of waste glass, and the expected effects of the implementation of this addition to the production of fired clay brick in an industrial setting.

ACKNOWLEDGEMENTS

I would like to thank the many people and organizations to which I am indebted for contributions made throughout the years of work leading up to the completion of this thesis. I wish to acknowledge the kind support and encouragement of my supervisor, Dr. Samir Chidiac, without whom this thesis would never have been. Thank you to the Civil Engineering faculty, staff, and students for all their assistance. The technicians of the Applied Dynamic and Geotechnical Laboratories at McMaster University, Maurice Forget, Dave Perrett, Bernard Nieuwenhuis, and Peter Koudys for their knowledge and assistance, to Dr. Charles Wu and Tim Stephens of University of Western Ontario for the XRF and Mercury Intrusion Porosimetry expertise, as well as Steve Koprich of McMaster University's BIMR facility for training and assistance in SEM analysis. Thank you to Brampton Brick for the donation of materials, laboratory time and equipment, as well as the technical knowledge required to complete this project, especially to Brad Duke and Brad Cobbeldick for their encouragement and support, Paul-Francis D'Arcey and Claudio Sacilotto for many hours of assistance. Thank you to the Ontario Graduate Scholarship Program and the Natural Sciences and Engineering Research Council of Canada for much appreciated financial support. Materials Manufacturing Ontario for financial support and project inspiration. The Centre for the Effective Design of Structures and the Department of Civil Engineering for providing financial support and the opportunity to share ideas. Very special thanks are due to my family and friends for their understanding, encouragement and support every step of the way. *Lisa Federico*

TABLE OF CONTENTS

LIST OF TABLES

LIST OF FIGURES

CHAPTER 1 INTRODUCTION

1.1 Fired Clay Brick

Clay brick, a crystalline ceramic, is one of the oldest known building materials, with the use of simple bricks dating back to the first civilizations and structures at least ten thousand years ago (Drysdale, Hamid, and Baker, 1994). Although there have been great efforts made to improve our understanding of the mechanisms which influence the strength and durability of brick, as well as technological advancements that have led to more efficient production, there still exists opportunity to further optimize brick production based on the challenges facing current and future generations. The art of fired clay brick making is an ancient one; however there are still gains to be made by increasing the efficiency and reducing the material requirements of large scale productions.

The process by which fired clay brick is produced has remained essentially unchanged since its development. Clay is extracted from naturally occurring deposits, or is mined as shale and crushed into small particles. A small amount of water is added to this base material in order to improve its plasticity. The material is either pressed into moulds or extruded under vacuum pressure through a die. The finished form of the brick is dried before being heated in a firing process at temperatures in excess of 1000°C for up to 36 hours. The firing process sinters the particles of clay together to form a bond which gives the brick its characteristic strength and durability. The sintering process is achieved by heating SiO_2 (quartz), which occurs naturally in clay and shale, to high temperatures,

causing it to soften. Upon cooling, the quartz forms a bond between adjacent clay or shale particles at the points of contact. Due to the high energy demands of the sintering process, additives called fluxes are often used to lower the temperature required to form the glassy bond. Common additives include Na_2O (soda) and CaO (lime) (Grimshaw, 1971).

1.2 Objective of the Thesis

In Ontario alone, 700 million bricks are produced per year (Ontario Ministry of Northern Development and Mines, 2003). This production is supported by extensive mining of natural resources. Although there is no immediate local shortage in the supply of clay and shale for brick production, several issues still exist within the industry. Despite being in great supply, natural clay and shale deposits on a scale large enough to make mining feasible are non-renewable resources and are finite in amount and location. Once used, these deposits cannot be replaced. As a result, mines will become more remote, smaller, and of a lower quality. The increasing cost of transporting material from a remote location to a factory, or else from an on site facility to a more populated area for sales and construction will become a growing threat to the profitability of the industry.

By replacing a portion of the raw shale mined for brick production with an alternative, renewable or waste material, the environmental and material demands of the industry could be greatly reduced. Specifically, the use of waste material as a clay body additive is attractive both environmentally and economically. By adding waste components to building materials, the volume of material sent to land fills is reduced, and the waste is instead stably contained within an affordable structural building material.

The use of waste materials as an additive not only reduces the consumption of raw materials and diverts waste from landfills, but also provides potential profit in tipping fees for manufacturers. In addition to mining, transportation, and storage costs, the firing process is an aspect of brick production which is energy intensive. By reducing the firing temperature by even a few degrees while still maintaining strength and durability, the energy requirements of the firing process could be reduced.

A waste material which has potential as an additive to bricks is glass. Much of the common bottle glass produced is difficult to recycle due to colouring additives, and may therefore end up in landfills. As a brick additive, glass acts as a flux due to its Na_2O content and its noncrystalline composition, lowering the temperature required to sinter bricks. The increased glassy phase in the finished brick has the potential to improve both structural and durability properties, while reducing manufacturing costs.

1.3 Thesis Outline

This thesis contains seven chapters. The first chapter is an introduction to fired clay brick and the objectives and scope of the research performed in developing this theses.

In chapter two, a literature review on waste additives in ceramic bodies provides several mixture compositions and the resulting brick properties based on experimental specimen preparation dating back as far as 1972. Variables of prior work include, but are not limited to, waste chemical composition and size, clay composition and particle size,

extrusion aids, percent waste addition, extrusion procedure, firing procedure and firing temperature.

Based on the literature review, an experimental procedure was created and is presented in chapter three. The procedure involves the preparation of numerous specimens for strength, absorption, durability testing, and microstructural analysis. The materials used in the production of specimens are discussed, and the procedure for their production is presented in detail.

In chapter four, the testes performed for the determination of the properties of the prepared specimens are discussed. The methods for testing follow those required by CAN/CSA standard A82.1-M87 for Burned Clay Bricks, and CSA CAN3-A82.2-M78 for Testing of Clay Fired Samples. In the case where the standards are not followed, a detailed description of the modified method, as well as justification for the modification are provided.

The results of the testing are presented in chapter five, along with a statistical analysis of the data which uses the difference in mean values of repeated testing. This method is used in order to identify significant trends in the properties tested as the percentage of waste glass is increased and the particle size of the waste glass decreased. The results of the microstructural analysis are presented in this chapter without a statistical analysis due to the limited number of tested specimens.

In chapter six, more complex statistical analysis is employed in order to formulate the relationships between the resulting physical properties of the bricks and the variables tested. Using linear regression, the significance of each tested variable is determined by

hypothesis testing. This analysis also helps to support the reliability of the testing methods used, especially the modified methods.

The conclusions of this thesis, based on the results of the testing program, are presented in chapter seven. A number of recommendations are also provided which are intended to further promote research in this area as well as to build on the information obtained through this testing program.

CHAPTER 2 LITERATURE REVIEW

The first step in determining the feasibility of adding waste material, particularly waste glass, to fired clay bricks within the North American production industry is to conduct a literature review to accumulate knowledge and data produced by similar past experimental initiatives. The review covers extensively, but not exclusively, additives such as waste container glass, fly ash, biological waste, and slag. The feasibility of adding such materials to fired clay bricks is based on the reported experimental results of testing for strength, durability to extreme weather exposure, shrinkage and distortion, appearance, compatibility in production facilities, and environmental and cost benefits. Variables common to several of the testing programs include the chemical composition of the base material, combinations of added waste material, percentages of waste material added, particle size and distribution of waste additive, and kiln firing temperature. These variables and resulting properties are compared and discussed in the following sections.

The studies reviewed involving waste glass addition to fired clay brick were carried out as early as 1970. As such, it is necessary to note that although the variables of interest are generally comparable, there are often significant differences in the laboratory testing programs as well as differences in the production procedures. Some of the tested specimens were produced in laboratory facilities and others in industrial production facilities. This implies that the specimens have experienced different firing environments. Moreover, some specimens were extruded while others were pressed. The implications of changing production procedures on the properties of the brick are important and are

therefore explained inclusively in this study. The review will examine the material and waste additives used in the production of fired clay brick and the corresponding resulting properties.

2.1 Materials

The material used in the production of fired clay brick is clay or shale. The source of the raw clay material is usually local to the area of the study, while the glass is commonly crushed, post consumer or non-recycled manufacturing waste glass. The waste additives are varied depending on the study; however they generally containing silicon dioxide (SiO_2).

2.1.1 Shale and Clay

The type and source of clay used in the production of bricks varies greatly depending on location and selection. Locally, clay used for brick production is surface mined from shale deposits along the Niagara Escarpment, which are identified by their depth below the surface and approximate age of formation. Brick produced in Brampton uses Queenston Shale, while British production uses Carboniferous Shale and Glacial Lacustrine Clay (Smith, 2004). The properties of each clay or shale material, including green and fired colour, particle size and distribution, ease of extrusion, fired shrinkage and deformation, porosity, strength, and durability, vary depending on the unique microscopic composition of the material.

The ability of clay to form a ceramic bond upon firing is due to the large amount of silicon dioxide, or more commonly, quartz (SiO_2) present in its particles. Upon heating, this compound softens into a glassy form, which bonds the remaining particles to one another where they are in contact in a process known as sintering. At these particle interfaces, pores are formed as a result of incomplete contact of the particles as well as the formation of gasses as the organic components of the clay or shale are burnt off. The strength, durability, and absorption of the resulting product depend on the state and nature

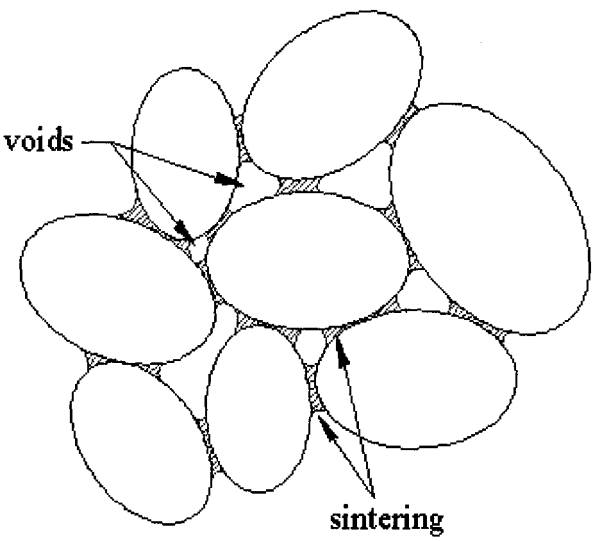

Figure 2.1 Sintered Clay Particles

of sintering within the brick. The formation of the glassy bond through sintering can be seen in Figure 2.1. A comparison of the types of clay and shale used to produce test specimens in the reviewed work shows similar chemical composition, with the average silicon dioxide content close to 60%, aluminium oxide average close to 20%, and iron

oxide averaging close to 5% by mass. As previously discussed, the content of silicon dioxide influences the ability of the clay or shale body to form a strong sintered bond in the firing process; however, a very high silicon dioxide content can cause increased warping and deformation in the fired product, and can increase the temperature required to cause softening of the silicon dioxide present. An increased level of aluminium oxide can also contribute to a high firing temperature, but improves the strength of the final sintered bond. The presence of iron oxide contributes to the traditional deep red colour associated with fired clay brick. A summary of the chemical composition of the clay and shale material examined in this review is presented in Table 2.1.

Table 2.1 Chemical Composition of Several Common Types of Brick Clay and Shale

Compound (%)	Etruria Marl[1]	Carboniferous Shale[1]	Quatrenary Glacial Lacustrine Clay[1]	Westerwald Ball Clay[2]	Egyptian Body Mass[3]
SiO_2	61.1	58.48	68.71	61.06	62
TiO_2	1.27	0.95	0.48	1.57	Traces
Al_2O_3	18.74	19.32	11.73	25.24	21
Fe_2O_3	9.58	7.73	3.61	1.2	4
CaO	0.3	0.61	2.7	0.18	2
MgO	0.51	1.61	1.84	0.46	<1
K_2O	1.96	2.5	3.02	2.21	2
Na_2O	0.1	0.68	0.33	0.18	0.5
P_2O_5	0.09	0.21	0.11	0	0
Mn_3O_4	0.06	0.15	0.06	0	0
Cr_2O_3	0.01	0.02	0.01	0	0
LOI	6.16	7.82	6.57	7.9	6.5
Total	99.88	100.08	99.17	100	98

[1] (Smith, 2004) [2] (Matteucci, Dondi, and Guarini, 2002) [3] (Youssef, Abadir, and Shater, 1998)

2.1.2 Additives

The review included specimens containing waste materials such as container glass (Leshina and Pivnev, 2002; Liu, Li, and Zhang, 1991; Matteucci, Dondi, and Guarini, 2002; Shutt, Campbell, and Abrahams, 1972; Sanders, 2003; Youssef, Abadir, and Shater, 1998; Smith, 2004), float glass waste (Matteucci, Dondi, and Guarini, 2002), blast furnace slag (Arkhipov, Nemchenok, and Rempel, 1979; Malhotra and Tehri, 1996; Shih, Wu, and Chiang, 2004; Nishigaki, 1999), sewage sludge ash (Anderson, Elliot, and Hickson, 2002), waterworks sludge (Liew, Idris, Samad, Wong, Jaafar, and Baki, 2004), and carpet yarn (Anderson, Elliot, and Hickson, 2002).

Waste container glass, or bottle glass, consists of soda-lime glass. Container glass is manufactured in a number of colours depending on the addition of oxides. Common container glass colours include green, amber, and clear. Although all three types of glass have the ability to be recycled, commonly only clear glass, which has the highest value, is retained for recycling purposes. Amber container glass gains its colour from the addition of Fe_2O_3 (Ferric Oxide) and FeO (Ferrous Oxide), while green glass is coloured with the addition of Cr_2O_3 (Chrome Oxide) (Hlavac 1983). During the recycling process, these additives cause difficulty in obtaining a consistent required end product, and are therefore undesirable. Coloured waste glass has other possible uses outside of bottle production, including fibreglass insulation, and is often processed into sand sized particles for use in such applications. Glass is desirable because it has a high SiO_2 content, and a chemical composition comparable to that of natural shale and clay. The highly vitreous state of glass is a desirable attribute for a potential sintering agent in clay brick.

Blast furnace slag is a by-product of the steel making industry, and is abundant locally in Southern Ontario. Slag produced from a variety of metal working furnaces is used extensively in civil engineering applications as aggregates for roadways and cement. According to Motz and Geiseler (2001), slag mainly consists of dicalcium silicate (C_2S) and dicalcium ferrate (C_2F), with a SiO_2 content ranging from 10% to 18% and a lime content ranging from 45% to 55%. The high content of lime can lead to volumetric instability as a result of hydration; however treatments are available to minimize this effect (Motz and Geiseler, 2001). On the other hand, lime can act as a very effective flux in the sintering process and it is therefore necessary to optimize its content when using slag as a waste additive in brick. The temperature required to melt slag is 1600°C (National Brick Research Centre, 2003). This high temperature demand limits its use within the brick making process.

The remaining prospective waste materials represent the use of biological waste as additives to bricks, which include sludge in the form of water treatment residue (WTR), industrial wastewater residue (IWR), wastewater treatment residue (WWTR), and incinerated sewage sludge ash (ISSA), to name a few possible sources. Following water purification, the remaining WTR is high in water content and must be dried prior to use as an additive. On the contrary, ISSA results from the incineration of sewage treatment sludge, and is highly absorbent (Anderson, Elliot, and Hickson, 2002). As a result of the use of different flocculation agents and chemicals during the treatment process, the chemical compound of biological waste can vary greatly between sources, which will directly influence its suitability as a waste additive in brick.

Table 2.2 compares some of the chemical compositions of waste additives used in previous research programs. As can be seen, the waste compositions vary greatly in chemical content, especially SiO_2, Fe_2O_3, CaO, and Na_2O.

Table 2.2 Chemical Composition of Several Possible Waste Additives

Compound (%)	Waste Container Glass	Waste Float[1]	Waste Container Glass[2]	Steel Slag[3]	Granulated Slag[4]	BOF Slag[5]	Water Treatment Residue[6]
SiO_2	63.79	71.92	63.64	19.15	36.75	12-18	9.06
TiO_2	0.2	0.06	0.43	-	-	-	1.1
Al_2O_3	3.02	1.22	2.16	1.18	17	<3	2.85
Fe_2O_3	1.57	0.36	0.14	7.64	0.6	14-20	83.9
CaO	9.9	7.45	0.66	41.98	39	45-55	0.92
MgO	0.89	3.95	0.22	1.16	5.2	<3	0.4
Na_2O	11.72	14.15	6.9	2.32	-	-	<0.05
K_2O	0.54	0.36	7.36	2.89	-	-	0.18
LOI	4.55	0	0	15.73	-	-	51.5

[1](Matteucci, Dondi, and Guarini, 2002), [2](Sanders, 2003), [3](Shih, Wu, and Chiang, 2004), [4](Malhotra and Tehri, 1996), [5](Motz and Geiseler, 2001), [6](Anderson, Elliot, and Hickson, 2002)

2.2 Past Experimental Work

Several experimental procedures and scopes have been explored, where a sample of both clay and waste material from various sources are combined in different concentrations by mass and waste particle sizes. In these procedures, the resulting strength, absorption, and durability properties of the bricks are then compared with a control brick to gauge the resulting effect. Temperature effects are also studied, where the temperature for a constant composition is varied in order to find the optimal firing temperature for the mixture. Although the experimental procedures are not exactly

comparable, the results of the addition of the different types of waste material can be interpreted for comparison in order to establish the feasibility of production. The following discussion summarizes the results of these studies for three waste additives; glass, slag and sludge.

2.2.1 Waste Glass

The addition of waste glass to brick specimens ranged from 0.5% to 94% by mass; however, most studies tended toward a range of between 5% and 20% glass by mass. The glass particle size ranged from 600μm to 45μm. In all reported test results, shrinkage was found to increase as glass addition increased, as well as with increased temperature of firing. Figure 2.2 and Figure 2.3 depict the results obtained by Sanders (2003) as well as Matteucci et al. (2002) and Smith (2004) for shrinkage effects. For lower percentages of added glass, shrinkage effects were dependant on particle size. Sanders (2003) indicated that while a glass particle size of less than 75 μm added at 4% mass produced similar shrinkage values to a control brick, the addition of coarse glass, with particle sizes ranging between 132 μm and 150 μm at 4% caused shrinkage to decrease. According to the National Brick Research Council (NBRC) (2003), larger particle sizes lead to incomplete sintering, where glass particles act more as an aggregate with sintered edges than a completely sintered medium.

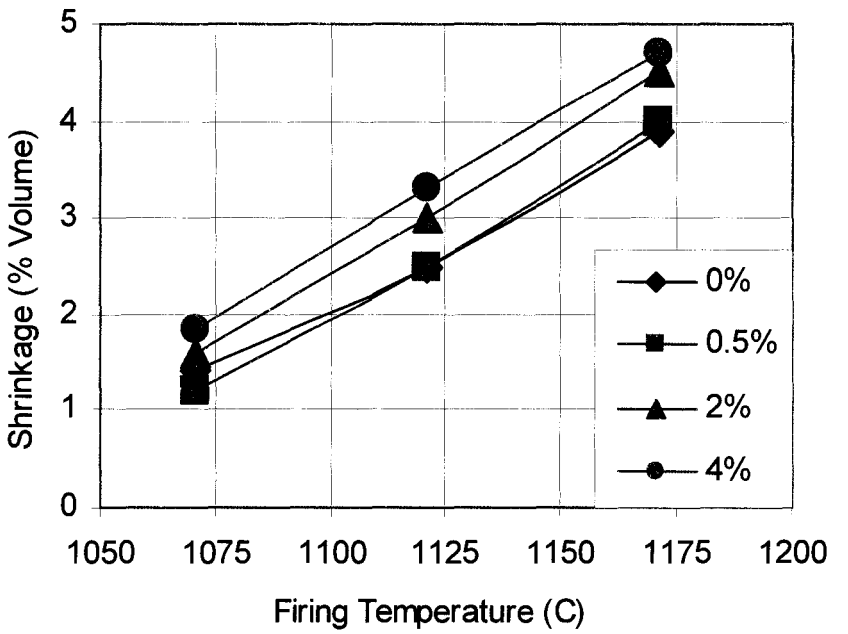

Figure 2.2 Effects of Glass Addition on Shrinkage (Sanders, 2003)

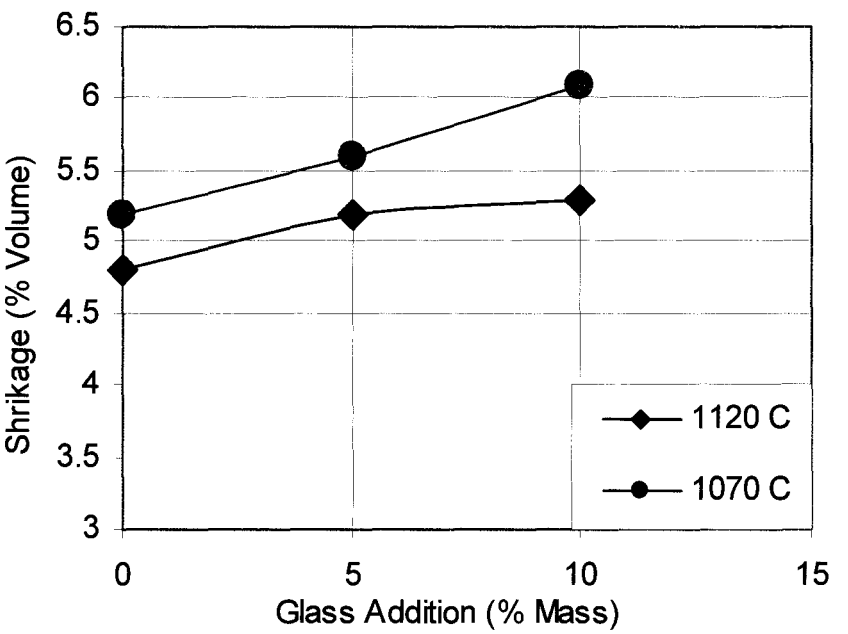

Figure 2.3 Effects of Glass Addition and Temperature on Shrinkage (Matteucci, Dondi, and Guarini, 2002) (Smith, 2004)

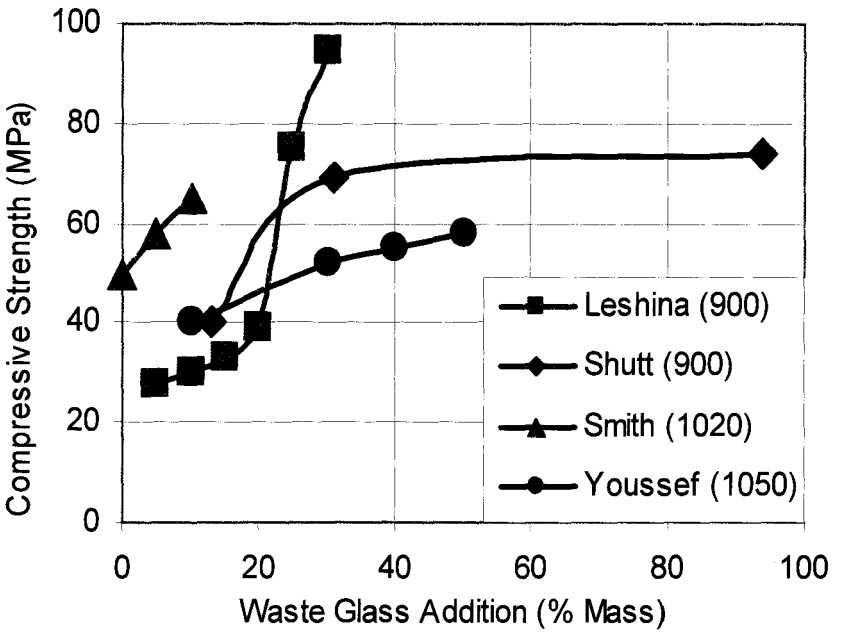

Figure 2.4 Compressive Strength Achieved for Various Waste Glass Additions (Shutt, Campbell, and Abrahams, 1972) (Leshina and Pivnev, 2002) (Smith, 2004) (Youssef, Abadir, and Shater, 1998)

The strength properties of specimens containing waste glass were determined by both compressive strength and modulus of rupture testing. Figure 2.4 illustrates some of the results reported for various additions of waste glass. The range of compressive strength values varies between specimens, which may be attributed to slight variations in particle size, specimen size and firing temperature for each testing method. The trend for all results, however, clearly indicates an increase in compressive strength with increased addition of waste glass, especially between 10% and 30% by mass. Values obtained for modulus of rupture (MOR) demonstrates a similar trend. As can be seen in Figure 2.5, the actual MOR values obtained by two methods are not necessarily similar due to

differences in methodology; however the trend displays an increase in strength with increased waste glass addition.

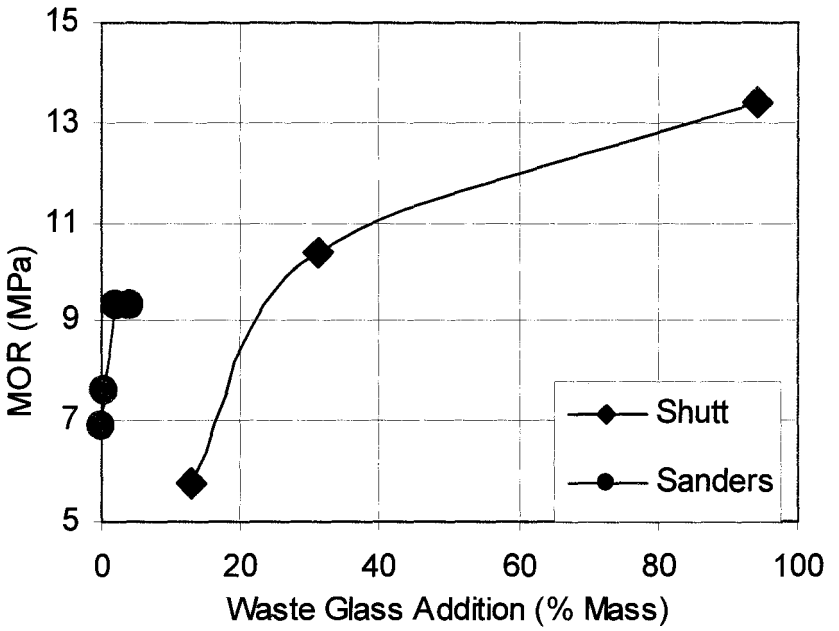

Figure 2.5 Modulus of Rupture Achieved for Various Waste Glass Additions (Shutt, Campbell, and Abrahams, 1972) (Sanders, 2003)

There is a lack of comparable data available with respect to durability testing of bricks with waste glass additives. The only presented results came from Leshina and Pivnev (2002), who used sodium sulphate to simulate freeze-thaw testing. Specimens containing 5% waste glass were found to be resistant to at least 70 cycles of freezing and thawing. Current code requirements, according to CAN/CSA-A82.1-M87, define resistance as 50 cycles of freeze-thaw with less than 0.5% dry mass loss. Since freeze-thaw tests are time consuming to perform, often absorption properties are used to establish the expected durability of a brick, as well as its performance in construction

applications. The absorption coefficient (C/B), a ratio of cold water absorption to boiling water absorption, is often provided as a means of estimating durability, where a lower C/B value indicates greater durability and better performance in extreme conditions. Several C/B ratios were reported for comparison and are shown in Figure 2.6. This trend indicated an apparent decrease in C/B ratio with increasing waste glass addition. This trend further suggests increased durability.

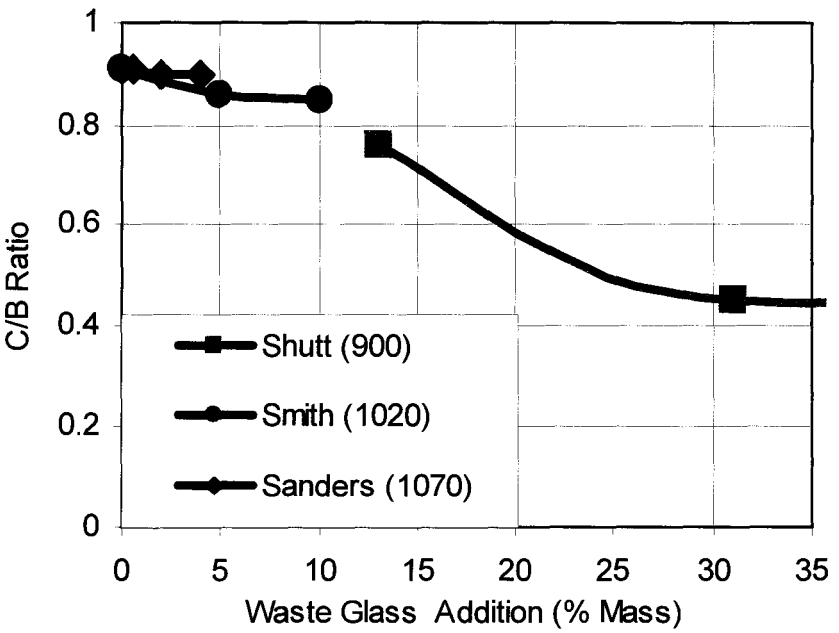

Figure 2.6 Absorption Coefficient for Various Waste Glass Additions at Indicated Firing Temperature (Sanders, 2003) (Shutt, Campbell, and Abrahams, 1972) (Smith, 2004)

2.2.2 Blast Furnace Slag

The high lime content in slag (Table 2.2), which can often cause volumetric instability in hydrating environments, tends to act as a sintering agent within fired clay

bricks. Therefore, the application of slag in clay bricks may be appealing. Research on the use of slag as an additive has not been as extensive as for waste glass. Nonetheless there were attempts to incorporate slag at 5% to 30% by mass into fired clay brick. Unfortunately, these studies often incorporated the slag with other waste materials to optimize the benefits.

Work by Arkhipov et al. (1979) and Nishigaki (2000) suggests that reasonable values of shrinkage, acceptable in a production environment, are achievable with the addition of up to 20% slag, and it was shown by Shih et al. (2004) that values of shrinkage varied only moderately with increased slag addition, as seen in Figure 2.7. Results presented for compressive strength indicate that the values remain relatively consistent for additions ranging from 5% to 30%; however, the values were low with respect to those achieved through the addition of waste glass. Other reported data comparing strength, absorption, and durability properties with varying slag addition to bricks include combinations of additional materials such as glass, grog, and coal. Values presented, do however, indicate that the addition of slag up to 20% by mass does not hinder the properties of interest, while displacing non-renewable body material, and potentially lowering firing temperature (Shih, Wu, and Chiang, 2004). Given that these results were obtained using a combination of slag and other waste material, it is difficult to ascertain the contribution of blast furnace slag in fired clay brick. Therefore, a more comprehensive study is needed in order to better interpret the feasibility of the addition of blast furnace slag in fired clay brick.

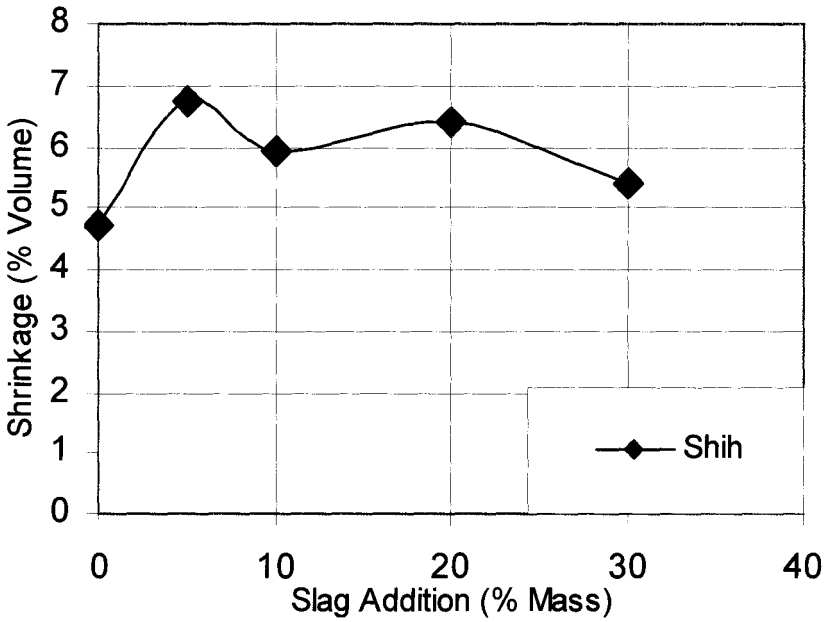

Figure 2.7 Shrinkage for Various Slag Additions (Shih, Wu, and Chiang, 2004)

2.2.3 Sludge

Sludge in the form of water treatment residue (WTR), industrial wastewater residue (IWR) and wastewater treatment residue (WWTR) has been added to fired clay brick in various percentages by mass. It should be noted that other additives were required to overcome processing complications, including incinerated sewage sludge ash (ISSA) (Anderson, Elliot, and Hickson, 2002). Work by Anderson et al. considered the addition of sludge ranging from 0% to 6% by mass, with the addition of ISSA and carpet yarn in order to control excess moisture and improve plasticity, while work by Liew et al. (2003) considered only sludge. The procedure followed by Weng, Lin, and Chiang (2003) was not comparable to that of Liew, which used manual pressing methods for brick formation.

Values reported for shrinkage by Liew and Weng et al. were not comparable. The difference in values can be attributed to the preparation of specimens and the composition of the added waste material. Liew reported an apparent decrease in firing shrinkage, which is contradictory to the results recorded by Weng et al. Weng attributed the increase in the amount of shrinkage to the higher tendency to swell of the organic matter in the sludge. According to Liew (2004), a similar contradiction was reported by Alleman and Ang. While Alleman reported an increase in shrinkage comparable to the results of Weng, Ang reported a decrease in firing shrinkage similar to Liew. The range in shrinkage results could be due to any number of factors, including sludge and clay chemical composition, particle size, or additives used. The shrinkage results reported by Weng (2003) and Liew et al. (2004) are reproduced in Figure 2.8. Testing of specimens prepared in a full factory setting tend to exhibit overall higher strength properties due to the highly pressurized extrusion process required to overcome the lack of plasticity in the green material, as can be seen in Figure 2.9. The resulting compressive strength of specimens tested by Anderson et al. are not comparable to those presented for the laboratory specimens. The trend in compressive strength of the specimens is, however, comparable, where an increase in sludge addition tends to decrease compressive strength, albeit at varying rates.

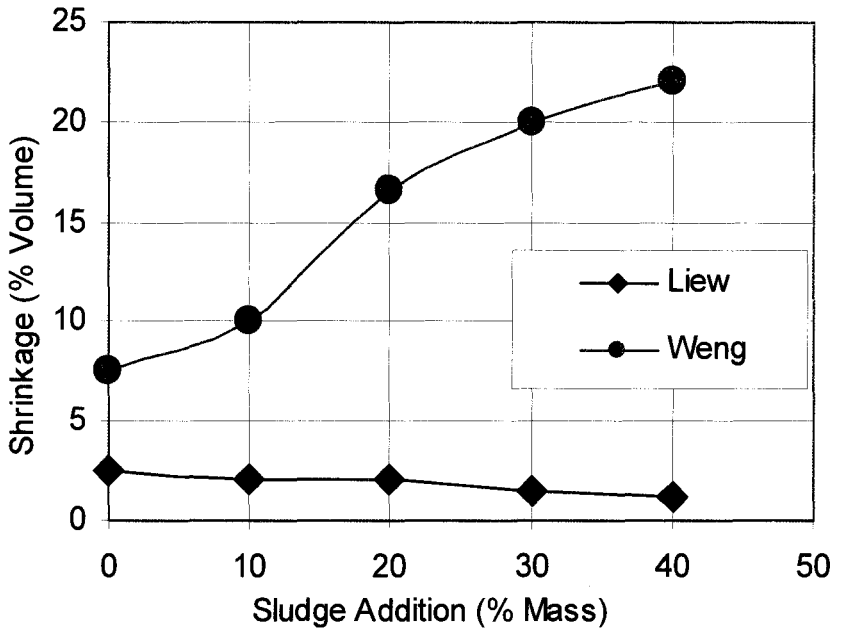

Figure 2.8 Effects of Sludge Addition on Shrinkage (Liew et al., 2004) (Weng, Lin, and Chiang, 2003)

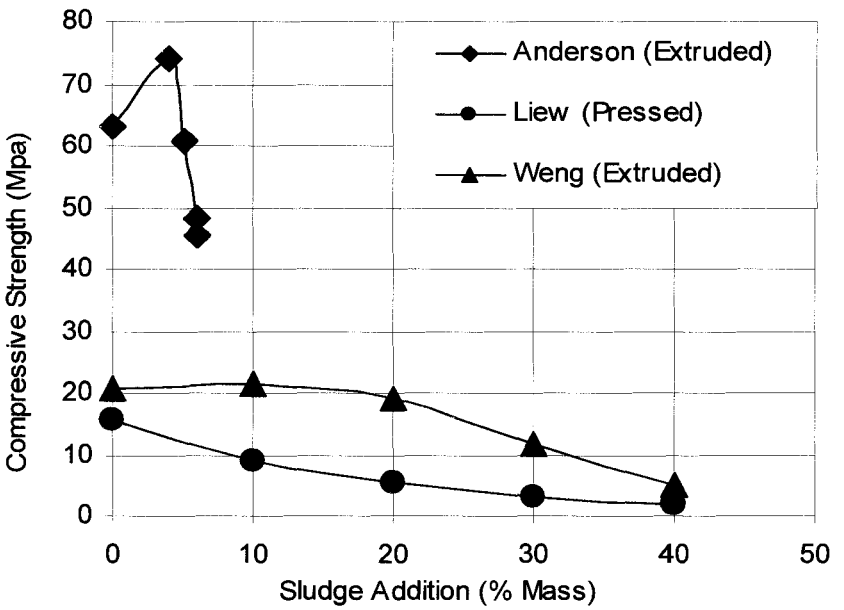

Figure 2.9 Effects of Sludge Addition on Compressive Strength (Anderson, Elliot, and Hickson, 2002) (Liew et al., 2004) (Weng, Lin, and Chiang, 2003)

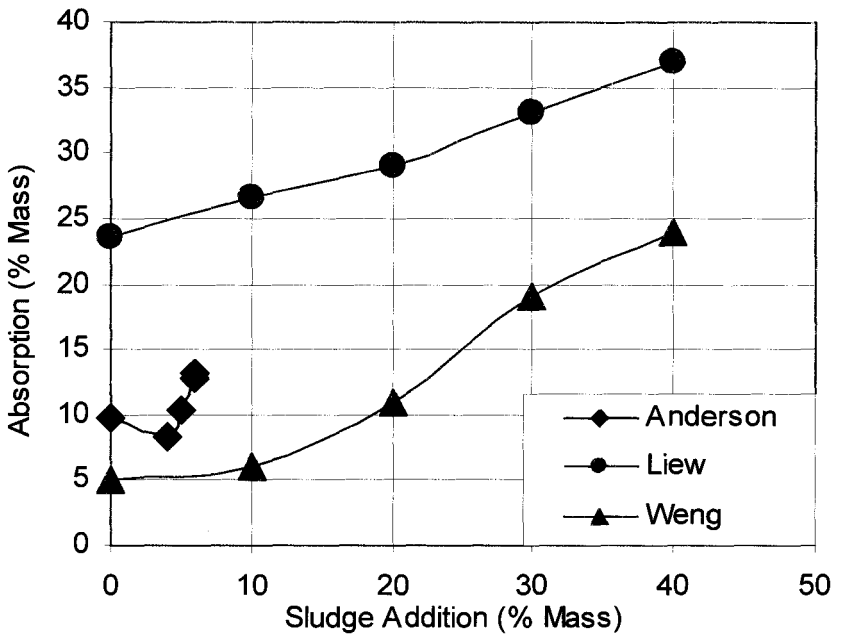

Figure 2.10 Effects of Sludge Addition on Absorption (Anderson, Elliot, and Hickson, 2002) (Liew et al., 2004) (Weng, Lin, and Chiang, 2003)

Figure 2.10 shows similar trends in absorption values in fired clay bricks with waste sludge addition. Although the manually pressed bricks are observed to have absorption values 30% to 80% higher than mechanically produced bricks, the general trend of increased absorption is similar for the addition of sludge between 10% and 40% by mass. Results presented by Anderson, Elliot, and Hickson (2002) with additional additives had a similar trend. Durability results were also discussed by Anderson et al., where some difficulties were observed in meeting durability requirements without the addition of alternative additives, including incinerated sewage sludge ash and carpet yarn.

There is not sufficient absorption data presented for specimens containing solely sludge to comment with respect to expected durability performance.

2.3 Summary of Literature Review

From the literature review of work completed on the addition of waste material to clay bricks, the preceding comparisons and discussions demonstrate the feasibility of such additions in an industrial setting, especially in the case of waste glass. The addition of waste glass showed an increase in strength, decrease in absorption, and improved durability properties. Addition of waste glass in an industrial setting in the order of 10% to 15% by mass should be feasible as a waste material additive while producing acceptable quality bricks. Additional benefits observed include the possibility of a decreased firing temperature. As the addition of glass tends to improve the quality of the bricks, a lower firing temperature could maintain quality while significantly decreasing energy requirements. Other benefits of waste glass addition include emission reduction. It was reported by Smith (2004) that the emissions monitored in a factory scale waste glass addition trial lead to the lowering of Hydrogen Fluoride by 33%.

The addition of slag waste in bricks is considered especially attractive for the southern Ontario area, where blast furnace slag is readily available. The current use of slag in concrete and paving materials may increase the appeal of a product combining slag into bricks, however the results studied lacked comparison specific to slag addition without the combination of other waste materials and additives. It is therefore necessary to carry out a testing program focusing on the addition of slag, and following a testing protocol comparable to the work already completed for waste glass.

The addition of wastewater and water treatment sludge to bricks demonstrated possible feasibility based on the results of prior work. Inconsistency in the test results and

processes, as well as a lack of information with respect to actual chemical composition, consistency in materials, and product durability creates a need for additional laboratory tests. The tests should be representative of production facilities in order to determine whether or not this process is possible and would be desirable in North American industry. It was noted by Weng et al. (2003) that despite processing and product success, this concept may be beyond current legal and public acceptance.

2.4 Problem Statement

The waste materials discussed and their feasibility as additives in fired clay brick to improve quality while decreasing resource depletion and production cost, are only a narrow sample of the possible alternatives and combinations thereof. The use of waste glass is a promising additive to displace clay body material while improving strength and durability properties and diverting waste from landfills. The use of this additive could further optimize the North American brick industry and therefore merit a comprehensive investigation. Furthermore, the effects of changing production procedures (ie plant versus laboratory) on the properties of clay brick should be studied in order to correlate the two procedures.

CHAPTER 3 EXPERIMENTAL PROGRAM

In order to examine the feasibility of adding waste glass to fired clay brick, a comprehensive testing program was developed. The variables studied included waste glass particle size and combinations of particle sizes, percentage of waste glass addition, production method, and firing method. The specimens were tested in correspondence with the requirements of the Canadian Standards Association (CSA) and the American Society for Testing and Materials (ASTM). Pore structure, strength, absorption, and freeze-thaw durability properties were analyzed for comparison.

3.1 Specimen Materials

Test specimens were prepared in the laboratory and production facilities at Brampton Brick in Brampton, Ontario. The base body material consisted of pure crushed Cheltenham (Queenston) Shale removed from the grinding room conveyor belt of the production line, which directly feeds the mixer prior to extrusion. Approximately 300 kg of material was removed from the conveyor belt on June 29, 2004 and stored in a covered container in the laboratory in order to preserve the moisture level for future use. The waste glass was obtained from a recycling supplier, Glass Recycling Technologies of Florida, Inc. and consisted of a sample of 30:70 mix of back dust and super fines, respectively, and a sample of 100% back dust. On June 29, 2004, approximately 40 kg of the mixed back dust and super fines sample was obtained, and 30 kg of the 100% back dust sample was obtained.

3.1.1 Sieve Analysis of Crushed Shale

A sieve analysis was preformed on the shale sample obtained on June 29, 2004 according to the procedure specified by Bowles (1992) and in accordance with the ASTM D421 and D422. The grain size distribution for the crushed shale is presented in Figure 3.1. From this analysis, it can be seen that the crushed shale has a coefficient of uniformity C_U of 5.7 and a coefficient of concavity, C_C of 1.1 according to Equations 3.1 and 3.2 respectively.

$$C_U = D_{60}/D_{10} \qquad \text{Equation 3.1}$$

$$C_C = (D_{30})^2/(D_{60}*D_{10}) \qquad \text{Equation 3.2}$$

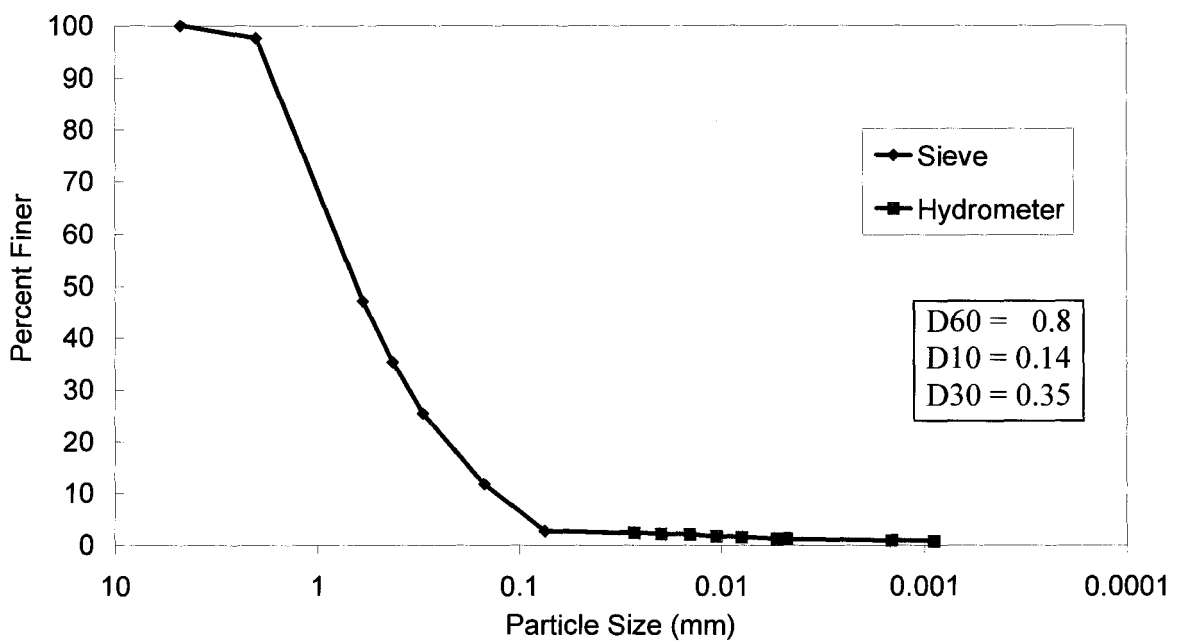

Figure 3.1 Sieve Analysis of Crushed Shale

Due to the mechanical preparation of the soil, the limits of the Unified Soil Classification System cannot be accurately applied to the classification of the crushed shale; however, the use of C_U and C_C can indicate that the crushed shale is relatively well graded, and cannot be considered a strictly fine grained material.

3.1.2 Sieve Analysis of Waste Glass

A sieve analysis performed on the 30:70 back dust and superfine waste glass obtainted on June 29, 2004 followed the same procedure as 3.1.1, and the results are presented in Figure 3.2. The waste glass has a coefficient of uniformity C_U of 4.3 and a coefficient of concavity C_C of 0.83. The evidence of gap grading is not unexpected due to the nature of the sample of glass tested, namely a combination of two distinct sizes of waste glass.

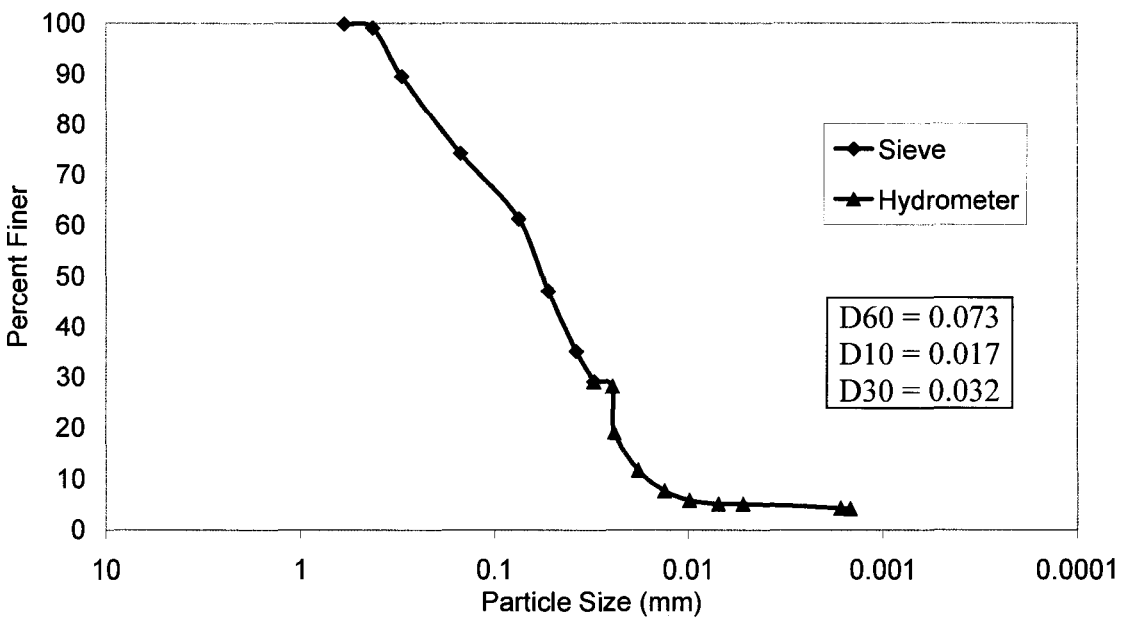

Figure 3.2 Sieve Analysis of Waste Glass

3.1.3 XRF Chemical Composition

Samples of both the clay and waste glass were prepared from the material collected on June 29th 2004 for conducting X-Ray Fluorescence (XRF) analysis. XRF is a technique used for determining the chemical composition of the material, particularly the elemental oxide composition. The test was carried out at the University of Western Ontario, London, Ontario. Results, reported in Table 3.1, show that, the clay used in the preparation of the specimens had slightly lower silicon dioxide content in comparison to previous chemical investigations where SiO_2 content ranges between 58% and 69%, Table 2.1.

Table 3.1 X-Ray Fluorescence Oxide and Trace Element Analysis

Compound	Shale (wt%)	Glass (wt%)	Compound	Shale (ppm)	Glass (ppm)
SiO_2	46.83	63.79	Nb	18.5	3.7
TiO_2	0.77	0.2	Zr	135	101.9
Al_2O_3	16.33	3.02	Y	32.9	8.8
Fe_2O_3	5.83	1.57	Sr	151.9	157
CaO	9.9	13.01	Rb	124.8	14.8
MgO	2.96	0.89	Ba	552.4	362.2
K_2O	4	0.54	Ga	21.9	65.5
Na_2O	0.25	11.72	Pb	14	165.5
P_2O_5	0.07	0.04	As	11.5	10.2
MnO	0.11	0.16	Zn	85.4	616.3
SO_3	0.2	0.165	Cu	20.2	34
LOI	12.5	4.55	Ni	49.2	16.1
Total	99.75	99.655	Co	8.9	6.6
			Cr	69.9	352.3
			V	112.7	18.3
			Total	0.14092	0.19332

The content of both alumina and iron oxide were found to be slightly higher than expected. This chemical composition would indicate a higher required firing temperature due to the alumina content and iron oxide can influence colour darkening in the specimens, especially in the case of over firing (Grimshaw, 1971). With this clay composition, high values can be expected for modulus of rupture and compression strength.

The waste glass composition, given in Table 3.1, had average silicon dioxide content, and a slightly higher than average iron oxide and calcium content. This glass composition is expected to influence the fired colour of the specimens and to increase their strength.

3.2 Specimen and Material Preparation

To obtain the exact amount of material required for the preparation of specimens, a sampling protocol was devised to ensure the correct proportions and particle sizes of waste glass. Details of the protocol are described in the following sub-sections.

3.2.1 Material Preparation

A tube sampler was used to obtain the glass, which was dried for one hour at 110°C to remove latent moisture, Figure 3.3. Using the sieve stack, the glass was sieved 200g at a time for five minutes, Figure 3.4. The glass remaining on the number 100 sieve, 200 sieve, and 325 sieve was separated into individual clean, dry, marked buckets.

The sieve sizes on which glass was retained for use were –50 to +100, -100 to +200, and –200 to +325. Table 3.2 lists the corresponding particle sizes.

Table 3.2 Sieve Stack

Sieve No.	Particle Diameter
50	0.3 mm
100	0.15 mm
200	0.075 mm
325	0.045 mm
Pan	<0.045 mm

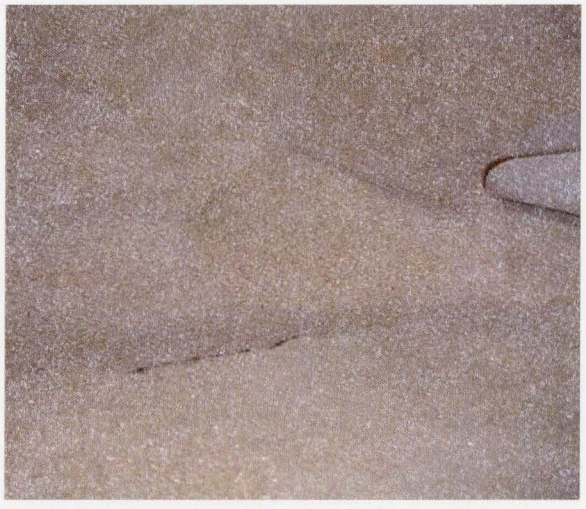

Figure 3.3 Crushed Glass

Figure 3.4 Sieve Stack in Shaker Apparatus

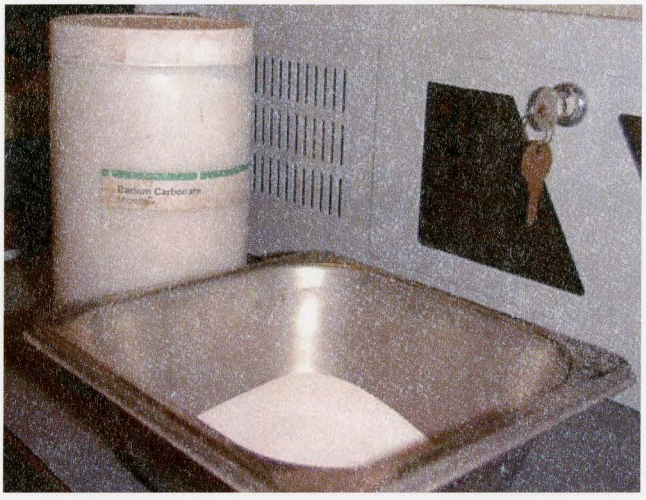

Figure 3.5 Barium Carbonate

In addition to the main crushed shale body material, 2.25% Barium Carbonate was added to control the post firing efflorescence of natural salts, Figure 3.5. Although the presence of efflorescence was not influential in the testing program, the addition of barium carbonate was included to more accurately reproduce the conditions of factory brick production.

During the mixing process, 20mL of lignosulfonate, a chemical additive, was added to the water used in preparing the wet mixture. Lignosulfonate, which is a deflocculating agent referred to as a plasticizer, is a byproduct of paper production. When added to clay, it acts as an extrusion aid by increasing the plasticity of the material. When the clay is fired, the lignosulfonate burns off at a low temperature and does not impact the properties of the brick.

3.2.2 Laboratory Specimens and Variables

Specimens were produced in two phases based on the variables of interest. The first set of specimens was designed to investigate the influence of percentage of waste glass addition by mass, as well as the influence of waste glass particle size on the properties and durability of the brick. The second set of specimens was designed to investigate the influence of production and firing methods, specifically, the effect of laboratory extrusion and firing versus plant extrusion and firing. Table 3.3 lists the specimen labels, variables, and sizes of the specimens produced for both testing phases. Specimens containing 50% -50 and 50% -100 glass particles will be referred to as containing coarse waste glass, while those containing 50% -100 and 50% -200 glass will be referred to as containing fine waste glass.

Table 3.3 Specimen Production Schedule

Sample Label	Shale %	Glass %	Glass Mesh Size	14x1¼x¼ (Gradient)	24.7x7.6x9 (Plant)	6x2x1 (Lab)	1¾ x ¼ x ¼ (Dilatometer)
A1 to A30	100	0	0	1	0	30	1
B1 to B30	95	5	50% 150-300µm 50% 75-150µm	1	0	30	1
C1 to C30	95	5	50% 75-150µm 50% 45-75µm	1	0	30	1
D1 to D30	90	10	50% 150-300µm 50% 75-150µm	1	0	30	1
E1 to E30	90	10	50% 75-150µm 50% 45-75µm	1	0	30	1
F1 to F30	85	15	50% 150-300µm 50% 75-150µm	1	0	30	1
G1 to G30	85	15	50% 75-150µm 50% 45-75µm	1	0	30	1
L1 to L30	100	0	0	0	0	30	0
X1 to X30	100	0	0	0	0	30	0
FL1 to FL30	100	0	0	0	30	0	0
FX1 to FX30	100	0	0	0	30	0	0

3.3 Procedure for Laboratory Specimen Preparation

The 270 laboratory sized specimens (6x2x1cm) were produced in the weeks of July 5th 2004 to July 30th 2004 and the week of May 9th 2005 in accordance with the following procedure.

3.3.1 Material Requirement

For each batch, material requirements included 17 to 19 kg of crushed shale and 1kg to 3 kg of pre-sieved glass, depending on the composition of the batch mixture. In addition to the body material, 45g of Barium Carbonate, 20ml lignosulfonate, and 2000 ± 300ml water were required for each batch.

3.3.2 Equipment

Equipment used for the preparation and extrusion of the laboratory specimens include:

- 2 medium plastic buckets with lids
- Large scale (0.1 kg) (Figure 3.6)
- Small scale (0.01g)
- Large electric mixer (Figure 3.8)
- 2 1L graduated cylinders
- Damp cloth
- Extruder with vacuum (Figure 3.9)
- Small metal dish
- Measuring Tape
- Utility knife
- Stamp set

3.3.3 Mixing and Extrusion Procedure

The following procedure was adopted to produce at least 30 testing specimens, 3 gradient bars, and 6 dilatometer samples.

1. Combine required amounts of clay and specified mesh size glass in a bucket for a total mass of 20 kg.
2. Add 45g of barium carbonate to the dry mixture to avoid scumming and efflorescence due to the natural presence of excess salt in the shale.
3. Blend the dry mixture in the Eirich RV02E mixer for 10 minutes at a frequency of 20Hz.
4. Remove 10kg of the dry mixture and place in a clean, dry bucket.
5. Prepare a solution consisting of 1000ml of water and 20ml of lignosulfonate.
6. Reduce the mixing frequency to 10Hz and add 500ml of the water and lignosulfonate solution to the 10kg dry mixture at the approximate rate of 100ml/min.
7. Add the remaining 500ml of water to the mixture at the approximate rate of 100ml/min.
8. Remove the mixture and place in a small, dry bucket marked with the mesh size of the glass additive, as well as the percentage of glass added. Cover with a wet cloth and lid.
9. Repeat steps 6, 7, and 8 for the remaining 10kg of dry mixture.
10. Remove approximately 100g of wet material. Place in weighed metal dish and record the total mass. Place the dish in the drying oven for 24 hours, record mass.

11. With the extruder set to medium speed (speed 4), extrude required specimens, ensuring a constant vacuum of at least 19in Hg. Measure extrusion to required length with measuring tape, and cut specimens in one perpendicular motion with utility knife.

12. Mark extruded specimens with stamps for identification, ensuring less than 5% of the surface area is marked.

13. Allow specimens to air dry for at least 24 hours.

14. Place specimens in drying oven for 12 hours at a temperature of at least 110°C.

15. Fire specimens in electric kiln at required temperature, ensuring TempChek keys are positioned in various locations in the kiln.

3.3.4 Production Method Details

The dry mixture, Figure 3.6, was combined in an Eirich model RV02E electric mixer at a speed of 20Hz for approximately 10 minutes. Half of the material was removed from the mixer, and the remaining 10kg of material was mixed with water and lignosulfonate solution. Once the desired water content and plasticity was reached, the wet material was removed to a bucket and covered with a damp cloth and lid while the remaining 10kg of the material was prepared. This process was followed due to size limitations of the mixer used, Figure 3.8. Extrusion was performed using a Plymouth Locomotive International vacuum extruder, along with various sizes and shapes of extrusion plates, Figure 3.7 and Figure 3.9, in order to create the necessary specimens. The vacuum within the extruder was maintained between 18 and 22 inches Hg and the auger speed of the extruder was set between 2.5 and 4 depending on the workability of

the wet material and the plate shape. Use of the equipment was provided by Brampton Brick Limited.

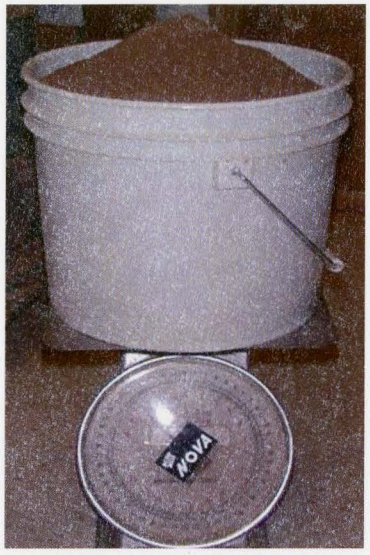

Figure 3.6 Dry 20kg mixture

Figure 3.7 Extrusion Plates

Figure 3.8 Electric Mixer

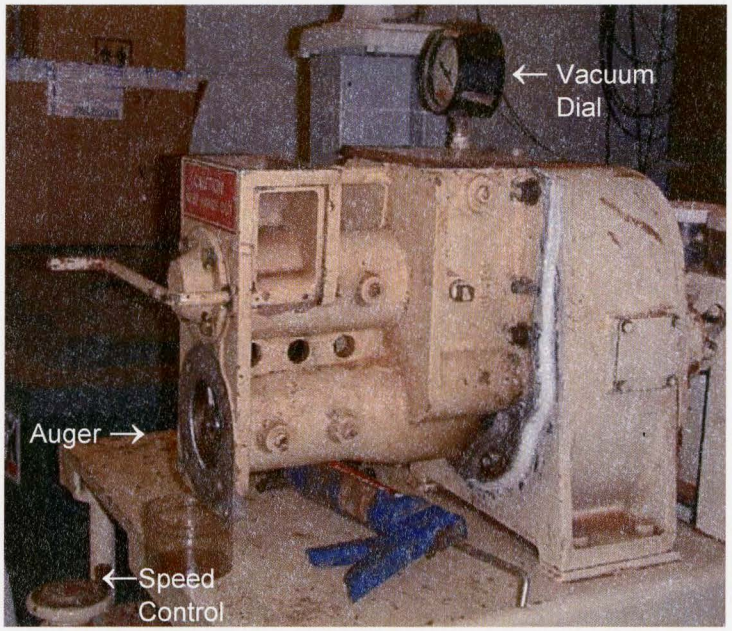

Figure 3.9 Laboratory Extruder

The extruded specimens were marked with a metal stamp set for identification before air drying for 24 hours. The specimens were then placed in an oven to dry for an additional 24 hours at 100°C. For specimens FX and FL, 60 bricks were removed from the Brampton Brick production line immediately after being loaded on a kiln car, prior to being loaded into the drying oven. The specimens were removed from the west side of the car on line 1. The removed full sized bricks were marked for identification. Bricks marked FX1 to FX30 were replaced on the west end of the kiln car, see Figure 3.10. Specimens X1 to X30, extruded in the laboratory, were also placed on the west side of the kiln car for firing in the production line. Bricks marked FL1 to FL30 were removed from the plant and brought to the laboratory for drying and firing.

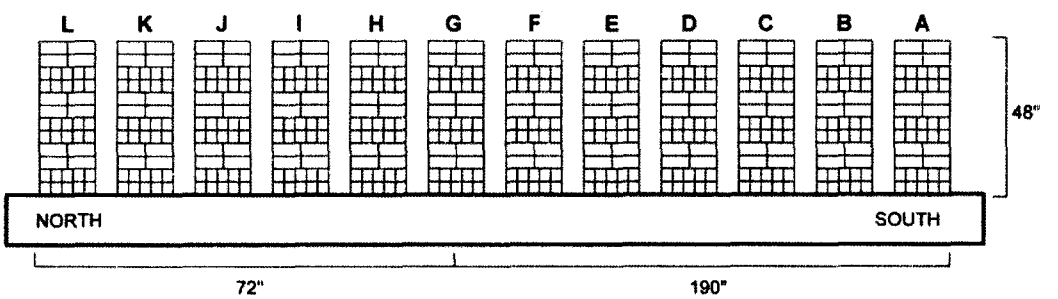

Figure 3.10 Production Line Kiln Car

Table 3.4 Ramping Rate

Ramp Rate (°C/Hr)	Dwell Temp. (°C)	Dwell Time (Hr)
120	475	0.5
90	850	1
60	1035	3.5
-600	25	END

After drying was complete, specimens A-G, as well as specimens X and XF were fired in the electric laboratory kiln, Figure 3.11. The specimens were fired 21 at a time in order to reduce the risk of loss in case of a kiln element failure. The firing schedule for the kiln was programmed to a maximum temperature of 1035°C with a one hour soak time, Table 3.4, and the heat work within the kiln was measured using a pyrometric shrinkage product, known as a key, with the commercial name TempCheck. By measuring the product after placement within the kiln during firing, a map of temperatures achieved within the kiln could be determined in order to establish the exposure range, and an average temperature within the kiln calculated. Specimens 1 to 30 of mixtures A to G were fired over the course of 3 weeks, with specimens 1 to 30 of X and FX fired at a later date.

Figure 3.11 Electric Laboratory Kiln

The TempChek keys were measured in order to compare the firing temperature experienced by the specimens. As can be seen in Figure 3.12, a much higher firing temperature was achieved for the kiln batch containing specimens 7, 8, and 9. As a result, these specimens were excluded from testing due to the expected change in properties resulting from such a large difference in firing temperature.

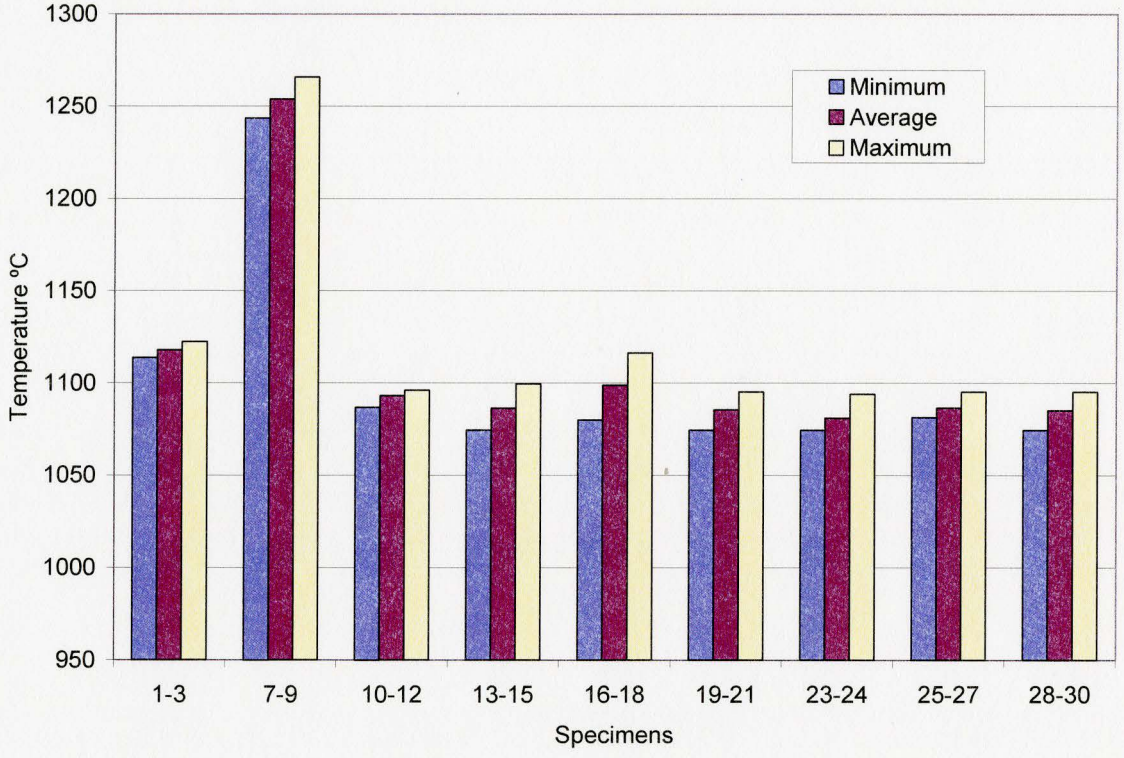

Figure 3.12 Specimen Firing Heat Work

3.3.5 Finished Specimen Dimensions and Appearance

The small scale laboratory specimens used for the testing of mechanical, absorption and durability testing had a smooth extruded finish and a core hole in the

centre of the specimen in order to improve the firing of the specimens. The finished dimensions were 2.4cm high by 4.8cm wide. The length of the specimens varied from 14 to 15.5cm. An unfired specimen is shown in Figure 3.13, while Figure 3.14 shows a fired specimen.

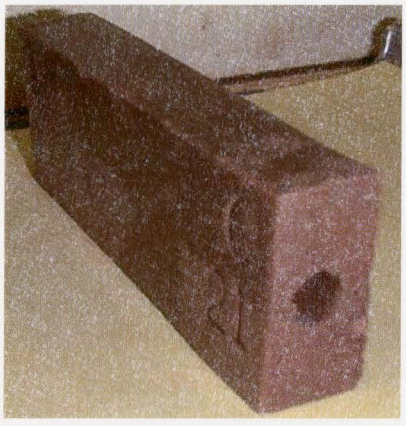

Figure 3.13 Green Extruded Specimen

Figure 3.14 Fired Specimen

The full scale plant specimens were extruded to the standard dimensions of the Brampton Brick "Premier" line of bricks, for which dimensions were provided as 24.7cm long by 7.57cm high by 9.0cm wide. The bricks were finished with coloured sand and a texture before they were removed from the production line, as seen in Figure 3.15.

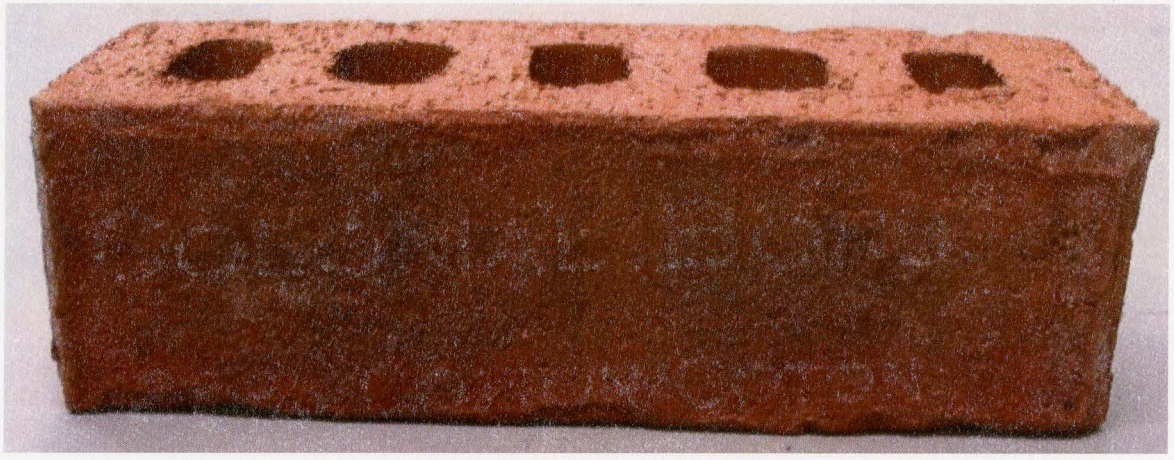

Figure 3.15 Full Scale Brick Finish

3.3.6 Shrinkage

Shrinkage, which occurs between the extrusion and firing stage of brick production, was measured using two methods. The shrinkage occurring from the green to fired phases was measured using callipers in the freshly extruded specimens. Callipered shrinkage measurements were not performed on specimens A and B. The green bricks were marked at 50 mm. They were allowed to dry for at least 24 hours, and once again the calliper imprints were measured. After firing, the calliper marks were measured for a final time, and from the difference in measurements, the shrinkage was determined. This shrinkage measurement depended heavily on both the water content of the extruded mixture, and the placement of the callipers within the original marks. The use of calliper measurement was therefore deemed unreliable and unrepeatable as a method of measuring shrinkage. The results of this method of measurement will not be presented.

The second method for the measurement of shrinkage was the dilatometer, Figure 3.16, which measures shrinkage as a change in length of a small sample over the course of the firing process. The dilatometer can also be used to track the reactions taking place within the brick during firing, and at what temperature they occur.

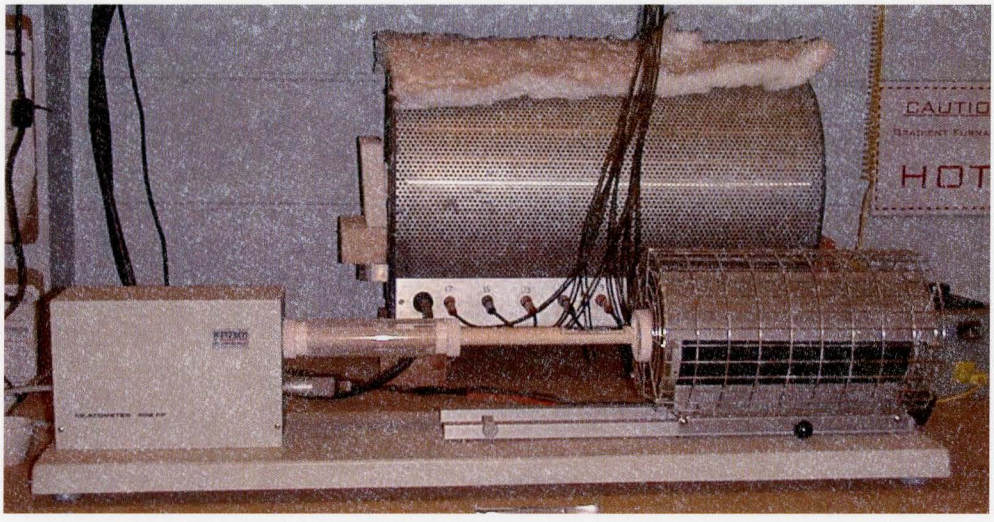

Figure 3.16 Dilatometer Apparatus

From Figure 3.17, the dilatometer testing indicates a similar rate of expansion for each of the mixtures in the early stages of the firing process, where at 800°C, the difference in expansion is within 0.1% for all specimens from A to G. After the quartz conversion process begins within the clay particles of the specimen at 800°C, the samples begin to shrink as sintering takes place. As can be seen from Figure 3.17, specimen B, containing 5% coarse glass, expanded 0.2% more than specimen A, containing 0% glass, with a final shrinkage 0.4% lower than that of specimen A. Similarly, specimen D with

Figure 3.17 Dilatometer Shrinkage, Specimens A to G

10% coarse glass experienced shrinkage of 0.1% lower than specimens A and C. Specimens containing coarse glass, including B, D, and F, experienced a greater expansion during the quartz conversion phase of firing than those specimens containing fine glass. The final shrinkage of the coarse glass specimens was lower than for those specimens containing the same percentage of fine glass, namely specimens C, E, and G.

Both specimens B and D had an even lower shrinkage than the control specimen, A, containing 0% glass, while the difference in final shrinkage between specimens F and G is greater than the difference in shrinkage between all other specimens. Therefore, not only is the shrinkage of specimens containing fine particles potentially more than twice that of the specimens containing coarse particles in high concentrations, the addition of low percentages of coarse particles of glass may actually reduce the shrinkage currently experienced in production of a brick with 0% waste glass.

Table 3.5 Specimen Shrinkage

Specimen	Shrinkage (%)
A	0.5
B	0.1
C	0.5
D	0.4
E	0.65
F	0.85
G	1.9

When compared to prior findings, the shrinkage results, Table 3.5, support the findings of the NBRC (2000), where the addition of coarse glass below 5% lowered

shrinkage when compared to the control specimen, while the addition of below 5% fine glass gave results similar to the control specimen.

3.3.7 Firing Temperature

The firing temperature for bricks produced with Queenston shale in a continuous kiln generally ranges between 1040°C and 1060°C. Any brick fired between these temperatures is generally expected to meet the standards of acceptable strength, absorption, durability, and appearance. The larger the firing range, the greater the percentage of bricks likely to be accepted from each car, and the fewer bricks which will be either over or under fired, and deemed unacceptable.

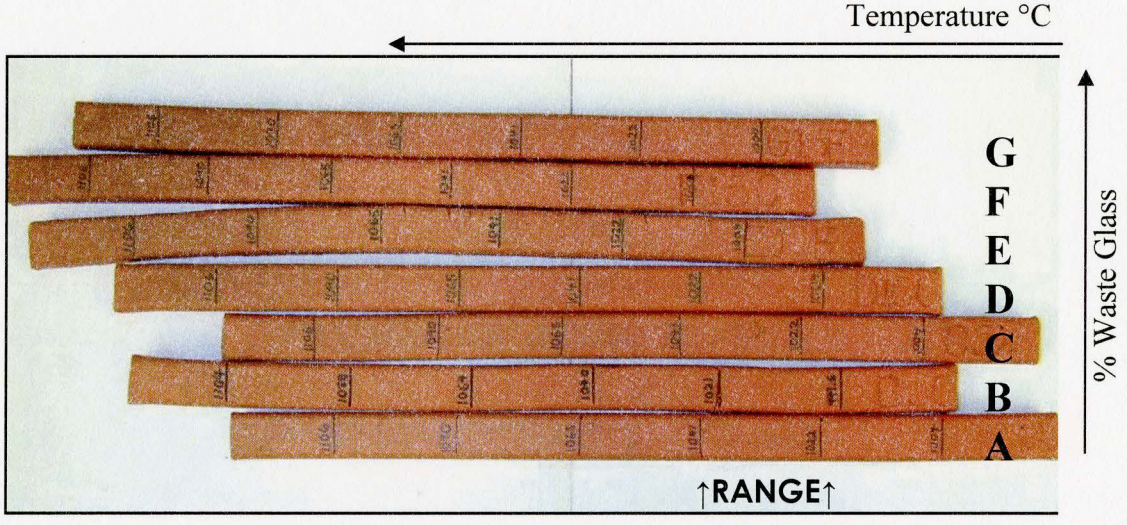

Figure 3.18 Gradient Bars

The gradient bars seen in Figure 3.18 correspond to specimens A to G, and were extruded at the same time as the testing specimens. Each bar was fired in the gradient kiln

at the same firing schedule, with a minimum temperature of 999.6°C and a maximum temperature of 1106°C. The bars are arranged to demonstrate the location and length of the acceptable firing range by visibly comparing areas of similar colour and texture to that of the control bar, bar A.

Table 3.6 Firing Temperature, Shift, and Range for Various Waste Glass

Bar	Low °C	High °C	Shift °C	Range °C
A	1018	1038	0	20
B	1005	1025	13	20
C	1015	1030	3	15
D	1008	1022	10	14
E	1000	1010	18	10
F	985	998	33	13
G	998	1012	20	14

The visibly noticeable effect of increased glass content is the shortening of the firing range from 20°C to less than 10°C, as well as lowering the temperature at which the range occurs. For gradient bar F, corresponding to 15% fine waste glass addition, a shift in firing range of almost 40°C is apparent.

A staggered pattern of firing range was also observed due to the particle size of the glass. In all cases, the coarse glass resulted in an even larger downward shift in the firing range temperature. Despite the greater shift in average firing temperature, the coarse glass bars, namely B, D, and F, were more tolerant of a range in temperature. The fine glass bars, C, E, and G had a much shorter range, but a less prominent shift in

temperature. Table 3.6 lists the observed shift in firing temperature and firing range as a result of the addition of waste glass based on the visual inspection of the gradient bars.

CHAPTER 4 TEST PROGRAM

Evaluation of the specimen properties was carried out in accordance with the procedures prescribed in "Testing of Clay Fired Samples", CSA CAN3-A82.2-M78 (Canadian Standards Association, 1978). The testing program included the evaluation of mechanical properties, absorption properties, durability, and pore structure. With the exception of the microstructure evaluation, all of the tests were repeated for five specimens.

Mechanical properties tested included the compressive strength and the modulus of rupture. The testing was performed in the Geotechnical Laboratory and Applied Dynamics Laboratory at McMaster University, as well as the research laboratory at Brampton Brick. The results were compared to the requirements of CAN/CSA standard A82.1-M87 for Burned Clay Bricks (Canadian Standards Association (CSA), 1987), and analyzed for trends related to the addition of waste glass.

The permeation tests performed on the specimens included the Initial Rate of Absorption (IRA), the 24-Hour Cold Water Absorption test (CWA), and the 5-Hour Boiling Water Absorption test (BWA). These tests aimed to indicate changes in the pore structure of the brick due to the addition of waste glass. The results were analyzed for trends related to the addition of waste glass and changes in the production method. The tests were performed in the Applied Dynamics Laboratory at McMaster University.

Durability of the fired clay brick was evaluated by subjecting the specimens to freeze-thaw cycles as well as by evaluating the coefficient of absorption. The tests were

carried out to determine the impact of adding waste glass and changes in the production method on the durability of the specimens. Scanning electron microscopy and mercury intrusion porosimetry tests were carried out to assess the changes in the microstructure of the specimens due to the addition of waste glass and the effect of the changes on the properties, in particular the effect of the changes on durability.

4.1 Compressive Strength

Compressive strength was tested parallel to the direction of extrusion. The height of the small scale laboratory specimens (A to G, L, X) was halved for testing in order to overcome the effects of slight firing and extrusion warping. The length of the full scale plant specimens (FX, FL) was also cut in half in accordance with the testing specifications of CSA CAN3-A82.2-M78. Each specimen was measure in three locations along each side of the testing surface, and the dimensions were used to calculate an individual average area for each specimen. Specimens were capped using hydrostone to ensure a level testing surface in accordance with section 4.2a of CSA CAN3-A82.2-M78. The hydraulic actuator used for compressive testing was equipped with a spherically seated hardened metal block as the testing surface in all cases, Figure 4.1. The rate of loading was set so that failure occurred within one to two minutes. The results of the compression tests were recorded as the maximum achieved load.

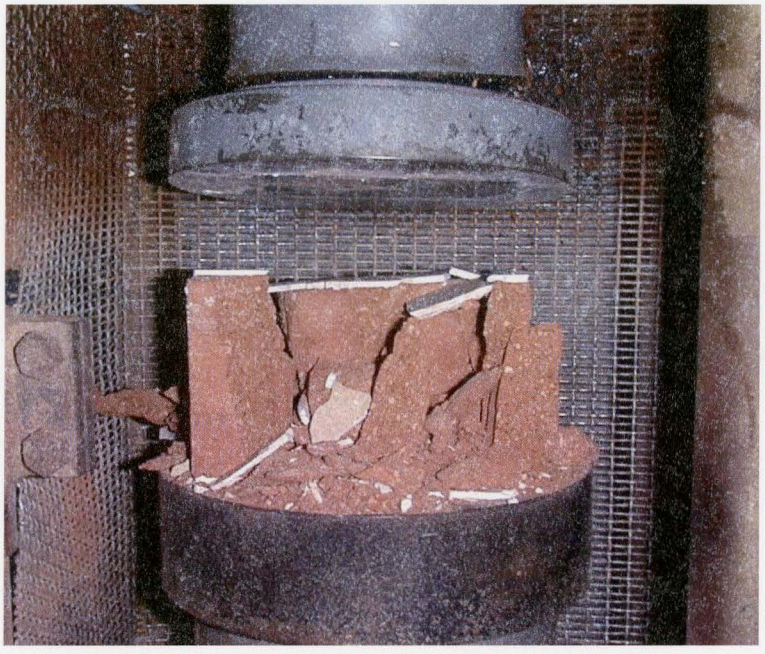

Figure 4.1 Compression Testing at Brampton Brick

4.2 Modulus of Rupture

Modulus of rupture is a measure of the tensile strength of the material, in which the specimen is loaded in flexure at points along a third of its length until it fails due to cracking on the tension face.

$$f_r = 6M/bh^2 \qquad \text{Equation 4.1}$$

The flexural tensile strength or modulus of rupture, f_r, is calculated using Equation 4.1, where M is the moment, b is the width of the specimen and h is the depth of the specimen.

In this regard, the test was carried out in accordance with CSA CAN3-A82.2-M78 on specimens A to G. However, the use of the three point bending test has led to unacceptably high variation in the results due to specimen seating issues, which led to premature failure caused by warping, which occurred in the extrusion and firing process. As a result, an alternative four point constant moment method was adopted. The test setup is shown in Figures 4.2 and 4.3. It should be noted that constant moment is calculated using Equation 4.2, with L_1 and L_2 defined in Figure 4.2.

$$M = P*[(L_1-L_2)/2]/2 \qquad \text{Equation 4.2}$$

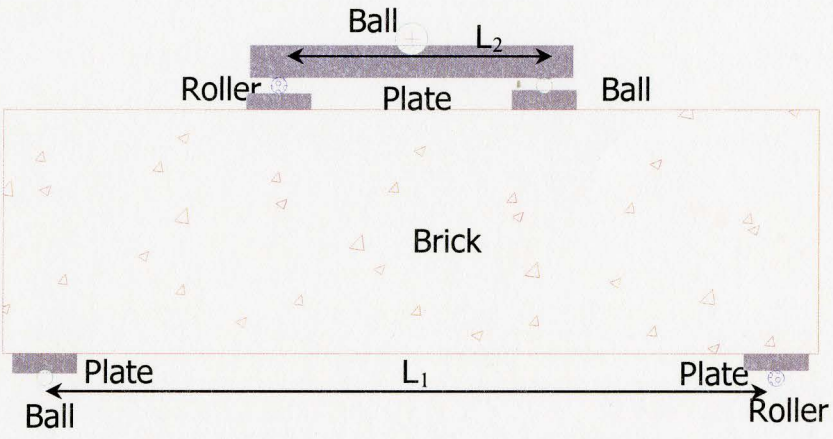

Figure 4.2 Four Point Loading Modulus of Rupture Apparatus

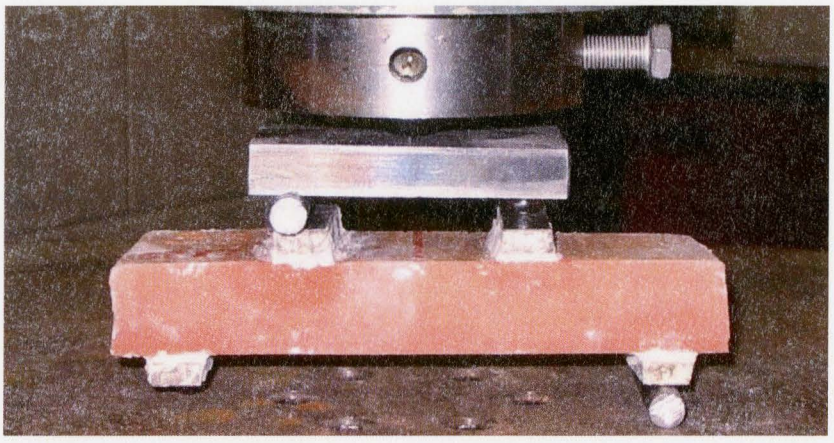

Figure 4.3 Four Point Loading Setup for MOR

Laboratory specimens were tested with bending stresses perpendicular to the direction of extrusion for modulus of rupture, while full scale plant specimens were tested with bending stresses parallel to the direction of extrusion. This discrepancy was necessary due to the nature of the extruded shape, the reduced size of which made testing parallel to extrusion impossible. Five test specimens were selected at random. Specimens previously used for absorption testing were considered appropriate for use in modulus of rupture testing once properly dried according to the specifications of CAN3-A82.2-M78. The specimens were marked for identification purposes.

The marked bricks were prepared by attaching the four top and bottom plates to the brick at the appropriate location using hydrostone, and ensuring that once placed, the plates were level and parallel. For the full scale bricks, L1 is 214mm and L2 is 80mm, while for the small scale specimens, L1 is 125mm and L2 is 60mm. Before applying the load, the specimen was seated on the bottom ball and roller, and the topmost plate was placed on the top ball and roller. The topmost plate was aligned with the topmost ball,

and a small seating load was applied. The load was then applied in such a way that failure occurred between one and two minutes of testing. The maximum load was recorded and the failure documented for crack location.

4.3 Initial Rate of Absorption

The initial rate of absorption (IRA) test was performed in accordance with CAN3-A82.2-M78, section 7. The purpose of the IRA is to evaluate the expected bond strength of the specimen when used in the field. Too high an IRA value may lead to a weak mortar bond at the joint depending on the curing condition of the mortar. An IRA value that is too low, on the other hand, will result in a weak bond between the mortar and the brick due to a lack of mortar penetrating into the pores of the brick. According to CSA specifications, an acceptable IRA should be below $30g/min \cdot 194cm^2$. The initial rate of absorption can be used as an indicator of the specimen pore structure. This stems from the fact that IRA is mainly due to capillary forces, which are a function of pore size and distribution.

A large, level tank, with a surface area in excess of $1m^2$ was filled with deionized water, Figure 4.4. The tank was equipped with a drainage spout in order to ensure the water level remained consistent. Triangular stainless steel angles were used to achieve minimum surface area contact during testing. The height of the angles ensured the required water height for the full scale plant specimens, FX and FL. For the small scale laboratory specimens, stainless steel lifters were used to decrease the height of the water

relative to the size of the brick. The water heights were 3mm for the full scale and small scale specimens.

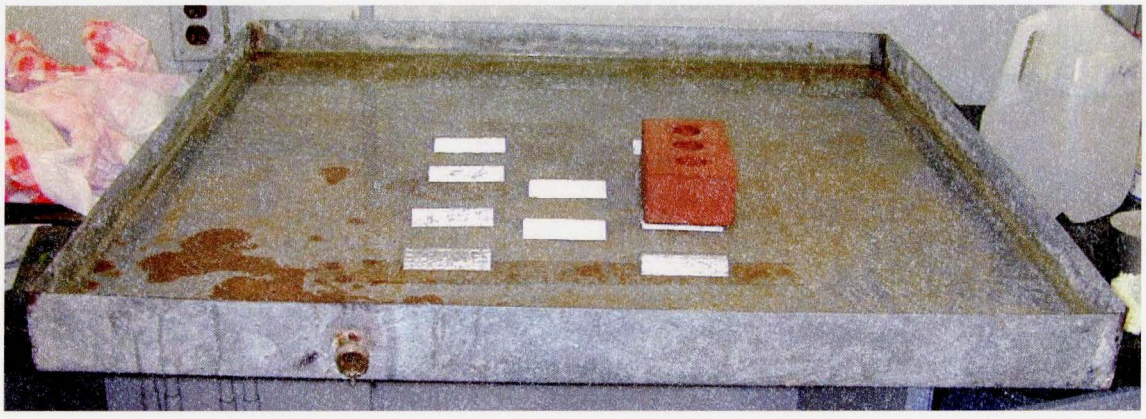

Figure 4.4 Initial Rate of Absorption Testing Tank

The IRA was calculated by first oven drying the specimens for 24 hours to remove latent moisture. When cool, the specimens were weighed, and the initial weight was recorded. They were then placed individually in the IRA tank for one minute, after which they were removed, and the surface was blotted with a damp towel. They were immediately weighed, and the final weight was recorded. The IRA values were calculated in g/min·194cm^2, which is the standard unit size. Note that neither the full scale plant specimens nor the laboratory specimens are a standard unit size, and therefore the results were scaled based on measurements taken of the surface area of each actual tested specimen.

4.4 Cold Water Absorption

The 24 hour cold water absorption (CWA) is a measure of the amount of water easily absorbed by the specimen due to capillary forces and pressure head. This procedure provides a measure of capillary pores as well as the capillary channels present in the brick. The method used for the determination of the cold water absorption follows the method prescribed in CAN3-A82.2-M78, section 5. After proper drying to remove latent moisture, the specimens were weighed, and the initial mass recorded. They were then placed in a deep plastic container, stacked in two layers. The bottom of the container was lined with plastic screen to decrease the surface area in contact with the container, and plastic screen was placed between the two layers of specimens. The container was filled with room temperature, deionized water and covered for 24 hours. After 24 hours had elapsed, the specimens were individually removed and their surface was blotted with a damp towel to remove surface moisture. They were weighed immediately, the mass being recorded as the final mass. The specimens were then placed directly into a boiling tank for boiling water absorption testing.

4.5 Boiling Water Absorption

The 5 hour boiling water absorption (BWA) provides a measure of the liquid and water vapour diffusion due to thermal and mass fluxes. After being submerged in the CWA test, the specimens are then exposed to five hours in boiling water. The increased pressure forces the liquid and vapour present in the pores to diffuse further into the

smaller pores of the brick, resulting in additional absorption. The relative amount of absorbed water due to high temperature provides an indirect measure of the ability of the material to diffuse the large internal pore forces generated by hydraulic pressure without generating micro cracking. This process simulates to some degree the mechanical process of freeze-thaw action.

Figure 4.5 Boiling Tank

The method used for the determination of the boiling water absorption follows the method prescribed in CAN3-A82.2-M78, section 5. After the specimens were removed from the CWA container, their mass was recorded prior to beginning the BWA test. The specimens were placed in a boiling tank, Figure 4.5, in which the temperature of the water had been preheated to 30°C. The tanks were lined with wire mesh to decrease the

surface area of brick in contact with the tank during testing. The temperature of the water was electrically heated to 100°C within an hour, or as close to an hour as possible, depending on the size of the specimens and the volume of water required in the boiling tank. Subsequently, the water level and temperature of 100°C was maintained for five hours. The tank was then allowed to return to room temperature for no less than 16 and no more than 18 hours. The specimens were removed individually and their surface was blotted with a damp towel to remove excess moisture. They were weighed immediately and the value was recorded as the final mass.

4.6 Calculation of the Coefficient of Absorption

The coefficient of absorption, also known as the C/B ratio, is the ratio of the CWA divided by the BWA. The coefficient of absorption is used as an indicator for the expected durability of the specimen. Durability of fired clay brick is most often dictated by the ability of the brick to withstand the cyclic freezing and thawing associated with a severe climate. This freeze-thaw cycle causes the liquid absorbed within the pores of the brick, to freeze and expand. As it expands, the hydraulic pressure created pushes unfrozen liquid into the adjacent and unfilled pores, which are typically smaller in size and are not connected to the capillary pore structure. If the volume of pores is adequate to accommodate the volume of expanding water, damage will not occur. If, however, these pores are not adequate, the excess hydraulic pressure will break the sintered bonds of the brick, resulting in freeze-thaw damage to the brick. This damage will result in partial or complete disintegration of the unit depending on the degree of saturation and number of

freeze-thaw cycles. Accordingly, a low absorption ratio indicates that the pore structure can endure freeze-thaw cycles.

4.7 Durability Testing

The freeze-thaw durability of the clay brick specimens is generally evaluated in accordance with CAN3-A82.2-M78 (CSA, 1978). Specimens A to G were tested according to the method prescribed by CAN3-A82.2-M78, however difficulties were encountered mainly due to specimen shape. According to the recommended method, specimens were oven dried to remove latent moisture, and their mass was recorded. The specimens were submerged in a tank filled with deionized water for 4 hours. The water temperature was kept at 22 ±2°C. The specimens were then placed in metal trays and set into a 10mm depth of water. The trays were subsequently placed in a freezer at -20°C for 20 hours. After 20 hours, the trays were removed and submerged in the thawing tank filled with deionized water for 4 hours. This process of freezing and thawing was repeated five times, after which the thawed specimens were allowed to dry for 40 hours. Once dry, the state of the specimens was visually determined. Testing was carried out for 50 cycles, after which the specimens were oven dried and a final mass was recorded for each specimen.

Although the test procedure is straightforward, extracting meaningful and reliable measurements of the mass loss was found to be very difficult. Measurement of the mass loss after each cycle was problematic. Moreover, the extruded shape of the specimens did

not accommodate the testing method. Core holes created at the centre of the specimens during extrusion allowed columns of water to freeze, creating an internal pressure at the center of the specimen. This pressure caused the majority of the specimens to split apart rendering those split specimens as failures. Figure 4.6 shows a schematic illustration of the failure mode, where actual failure is shown in Figure 4.7

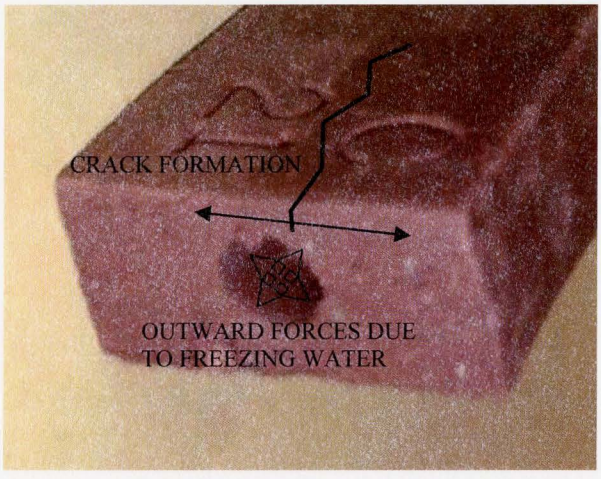

Figure 4.6 Failure Mode of Specimens

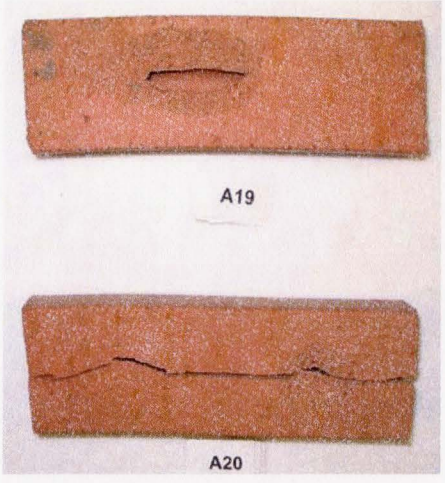

Figure 4.7 Failed F/T Specimens

As a result of the unexpected specimen failures, and the lack of quantifiable data from the testing method, an alternative method was developed to allow for a quantification of mass loss as the test progressed through the cycles of freezing and thawing, as opposed to the reliance on a visual estimation to determine a termination point for the test. The test method adopted followed largely the specifications of ASTM C 1262-98, Standard Test Method for Evaluating the Freeze-Thaw Durability of Manufactured Concrete Masonry Units and Related Concrete Units, (ASTM

International, 2006). This approach provided a reliable test method to accurately quantify the mass loss due to freeze-thaw action; however, the results of this method are relative in nature and cannot be directly compared to the CSA standard. For this reason, the results are not expected to be directly indicative of field performance.

A precedent was set by Koroth, Surej, Dorel, and Fazio, (1998) regarding the reliability of the durability testing methods endorsed by ASTM and CSA who stated that "evaluation procedures using these requirements and test methods are time consuming and were criticized as being inadequate and unreliable in certain cases." (Koroth et al., 1998) They attempted to remedy the inadequacy through the development of a durability index which would allow the prediction of durability based solely on absorption properties including Boiling Water Absorption and 4 hour capillary suction. The calculated results obtained by Koroth et al. were then compared to accelerated laboratory freeze-thaw test results. In this thesis, Koroth et al.'s methods for laboratory testing have been improved upon through the development of a modified freeze-thaw test, which incorporates methods of both CSA and ASTM, while allowing a more quantitative analysis of specimen performance than the traditional pass/fail system. The setup and method followed for testing the freeze-thaw resistance of both small scale and full sized brick specimens is outlined below.

Five specimens were selected at random for testing. The specimens were not oven dried. The length of the specimens, being the longest dimension, was cut in half, and each half specimen clearly marked on the non-testing surface for identification with markings covering no more than 5% of the marked surface. The marking "A" was used to identify

specimens tested in deionized water, while "B" indicated testing of the specimen in 3% NaCl solution. The specimens were not previously used in any other testing, including absorption testing. They were visually examined, and any loose or extraneous material associated with the manufacturing process was removed. Any cracks or chips were noted and marked. A small scale laboratory specimen, X29 can be seen in Figure 4.8 a), while a full scale plant specimen, FL5, is seen in Figure 4.8 b).

(a) (b) (c)

Figure 4.8 (a) Marked Small Scale Specimen (b) Marked Full Scale Specimen (c) Freezer and Racking System

The testing face of each full sized specimen was measured at three locations along height and length, and an average of the three values was used to calculate the surface area. For the small scale specimens, the testing face was measured in three locations along width and length, and an average of the measurements was used to determine the surface area. According to ASTM C1262, the minimum surface area of the test specimen

must exceed 161cm². Due to the small scale nature of the testing specimens, this minimum value was not possible to achieve. Although ASTM C1262 advises the use of two small specimens in place of one undersized specimen, the minimum surface area would still not be achieved, and as a result, the variation between the ASTM standard recommendations was noted for observation and for any possible effects on the final freeze-thaw results. Specimen dimension locations are shown in Figure 4.9.

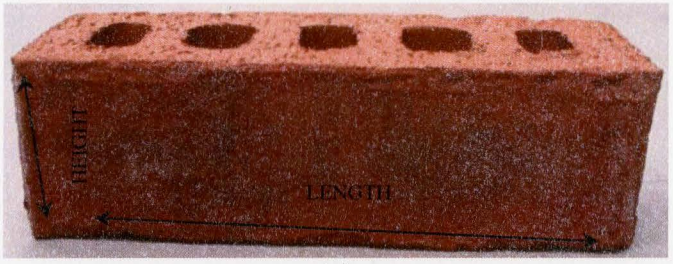

(a)

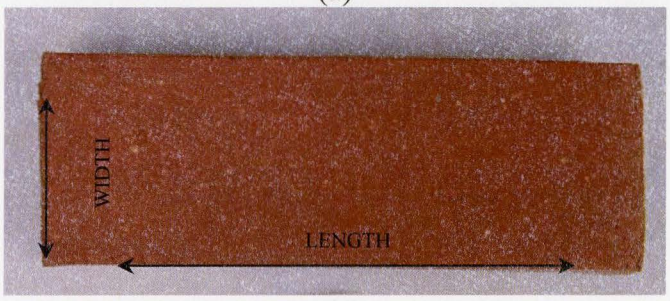

(b)

Figure 4.9 (a) Full Size Brick Testing Face (half brick) (b) Small Scale Brick Testing Face (full brick)

The freezing apparatus was a General Refrigeration model RSW-40SF. The capacity of the unit was such that the air within the freezing chamber would reach -9°C ±1°C within 1 hour ±5 minutes once the specimens were placed within the unit, and an interior temperature of -20°C ±2C was maintained for at least six hours within the next

twenty hours of testing. The temperature within the unit was monitored by an electronic sensor during the first week of testing to ensure proper operation.

A steel rack was constructed with several shelves in order to stack the containers in such a way as to allow adequate air flow around each container, and to facilitate moving specimens in and out of the freezing apparatus. The racking system is shown in Figure 4.8c). The racking system was lifted in and out of the freezer using a battery operated fork lift.

Figure 4.10 Scale and Airtight Container

The scale used to measure the mass loss was a Denver Instrument electronic scale with a capacity of 500g and a sensitivity of 0.0001g. Due to the incredibly sensitive nature of this particular scale, it was necessary to enclose the dried filter papers in a re-sealable, airtight container in order to prevent absorption of moisture from the air while

weighing the specimen. This procedure allowed for a stable mass reading to be obtained. The sealable containers used for this application were small glass mason jars with screwed on metal lids and a rubber coated gasket. Figure 4.10 shows the setup of the scale using the airtight container to preserve the filter paper while weighing.

The specimens were each placed in a plastic container which contained a lining of plastic grate material in order to minimize the contact area between the specimen and the supporting surface. The containers were fitted with air tight lids. The size of the containers were such that one half specimen could be placed in the container with a distance of at least 10 mm separating the specimens from the container walls. Figure 4.11 shows the setup of a small scale specimen in a container. Each container lid was clearly marked with the name of the specimen and solution being tested.

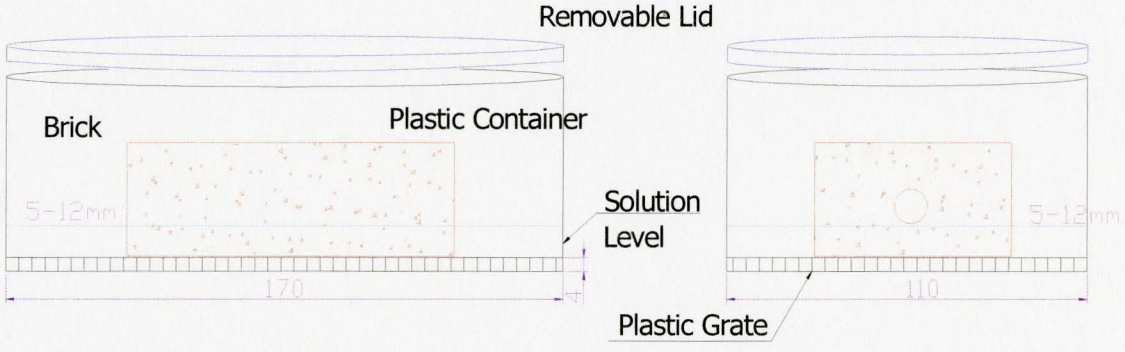

Figure 4.11 Container Setup

Two liquids were used to test the freeze-thaw durability of the specimens. The first liquid was deionized water, and the second one consisted of 3% NaCl in deionized

water. The solution was prepared using the Mass/Volume method (Chang, 1998), where the required percent, in mass, per 100ml of solvent, gave the correct concentration.

$$M = (\%\ m/V) * 10 / 58.4427 \qquad \text{Equation 4.3}$$

The molarity of the solution, M, was 0.513 moles as determined by Equation 4.3, where m is mass, V is volume of solution, and 58.4427g/mol is the molecular mass of NaCl.

Prior to beginning the 100 cycles of freeze thaw testing, the specimens were placed in the soaking tank for 4 hours ±15 minutes. The soaking tank was filled with deionized water at room temperature (22±2°C). The specimens were then removed from the soaking tank and placed with the largest face down in the containers atop the plastic grate, ensuring adequate spacing. For full scale plant specimens, the tested surface was the finished surface, which is the surface on which decorative texture had been applied, and it is parallel to the direction of extrusion. For the small scale laboratory specimens, the tested surface was also parallel to extrusion. The appropriate solution, either deionized water or 3% NaCl, was then added to the containers. For full sized specimens, solution was added to a depth of 12mm of submersion. For small scale specimens, solution was added to a depth of approximately 5mm of submersion, ensuring no solution reached the core holes. The specimens were lifted from the container to remove any air bubbles trapped beneath the specimen in the plastic grating, as well as to drain any

solution which may have pooled on the untested face of the specimen, which is the top of the specimen. The lids of the containers were secured.

The containers were placed on the racking system and moved into the freezing apparatus. The specimens remained in the unit for 14 to 16 hours, at least 6 of which consecutively maintained at a temperature of -20°C ±2°C. The racking system was removed from the freezing apparatus using the forklift and the containers and their contents thawed for 8 to 10 hours at room temperature before repeating the freezing cycle.

The filter papers used were Whatman No.2 qualitative circles, 185mm diameter. The filter papers were labelled with ink for each specimen to be filtered and then placed in a drying oven at 110°C for 48 hours. After 48 hours of drying, each filter paper was weighed by sealing it in an airtight container and recording the mass to an accuracy of 1/10000 of a gram.

After inspection, the specimens were replaced in the containers, which were refilled with the appropriate solution to the specified depth. The lids were replaced, containers placed on the racking system where after each cycle, the position of the specimens on the racking system was rotated along the height of the rack, and the rack was placed back in the freezing apparatus to begin another freeze cycle. The test was carried out in this manner, five full freeze-thaw cycles at a time, for a total of fifty cycles. After the completion of fifty cycles, the cycle length between filtrations was increased to ten until the completion of a total of 100 cycles.

Occasionally, due to unavoidable or unforeseen circumstances, it was necessary to extend a cycle. In this case, the specimens were left in the frozen state, and the thawing cycle recommenced the following day.

After the completion of 5 freezing and thawing cycles, the lids of the containers were removed. The specimens were removed, and a small, labelled syringe, one corresponding to each solution, was used to rinse any lose particles from the surface. The specimens were inspected and documented for cracks, damage, or breakage. The solution from each container was poured through a pre-weighed and labelled sieve paper. Any material remaining in the container was rinsed into the sieve paper using the syringe and the solution being filtered. The sieve papers and any material within were placed in individual glass containers and into a drying oven for 48 hours at 110°C to remove all moisture. After at least 48 hours of drying, the mass of the dried sieve paper and material was determined using the method described in Section 4.7.5, and recorded as the final mass. The weighed filter papers and their contents were retained and sealed individually in plastic bags.

The loss of mass for each specimen was calculated as the cumulative loss of mass of the initial surface area of the specimen of interest, in kg/m². Mass loss was calculated according to Equation 4.4 in order to determine the percentage of mass lost based on the total available mass, where M_C is the cumulative mass loss and M_D is the final dried mass of the specimen.

$$\text{Mass Loss} = \sum M_C / (\sum M_C + M_D) \qquad \text{Equation 4.4}$$

4.8 Scanning Electron Microscopy

The use of a scanning electron microscope (SEM) for image analysis can increase spatial resolution of the observer from greater than 100μm, the resolution of the human eye, to less than 100 Å (Botton, 2005). A beam of electrons of known energy and size is aimed at a specimen within a vacuum sealed chamber. These electrons interact with the specimen and the environment to create several measurable results, including backscattered electrons, secondary electrons, characteristic x-rays, and Auger electrons. The basic mechanism by which SEM works is to measure variations in the secondary electrons produced by surface variation. In addition to the measurable emissions, it is possible to predict the path and depth of electron interaction within the specimen using Monte Carlo statistical simulations. Generally speaking, the higher the energy of the incident electron beam, the greater the interaction volume of the electrons within the specimen.

The SEM allows not only for a more detailed view of the microscopic properties of the specimen, but also a measure of the intensity of the components of the chemical composition of the material based on the characteristic x-rays. This measurement is called Energy-Dispersive Analysis of X-rays (EDAX) and provides a relative value of chemical composition based on the number of electrons emitted onto the sample, which is usually a time dependant value.

The purpose of investigation using SEM technology is to further understand the relationship between pore size and structure and the resulting strength and durability properties of the specimens. Moreover, the use of SEM technology permits the

visualization of the addition of waste glass on the sintering and pore structure of fired clay brick.

4.8.1 Sintering and Pore Formation

In order to investigate the effect of waste glass addition on pore structure, a more comprehensive understanding of the sintering process is required. This process forms the pore structure and solid phases in the finished product, which influence the strength, durability, and absorptive properties of the brick. The three major steps in the sintering process are water smoking, oxidation and vitrification. Although the firing process is influenced by the specific properties of the raw material, the type of kiln used and the product being manufactured, the three main steps in the sintering process remain the same. Materials used in the production of bricks generally contain various chemical phases including quartz (SiO_2), phyllosilicates (including all clay phases), feldspars (AlSiO), calcite ($CaCO_3$), dolomite ($CaMg(CO_3)_2$), and hematite (Fe_2O_3) (Bauluz et al., 2004) (Cultrone et al., 2004). After firing, the transformation of phases leads to the development of wollastonite ($CaSiO_3$), anorthite ($CaAl_2Si_2O_8$), and gehlenite ($Ca_2Al_2SiO_7$) (Riccardi, Messiga, and Duminuco, 1999).

During the first stage of firing, the chemically bound water within the clay or shale particles is removed. This is not to be confused with the surface water, or hygroscopic water, added to the crushed shale or clay during extrusion to improve plasticity, which is lost during the first stage of oven drying (Grimshaw, 1971). Once this process of chemically bound, or hydrate, water removal has begun, around approximately

200°C, the sintering process has also begun, as the chemical state of the shale or clay has been altered (Brick Industry Association, 2004). After approximately 400°C, the OH^- is removed in the form of water vapour (Bauluz et al., 2004) in a process known as dehydroxilation (Monteiro and Vieira, 2004). The conversion of quartz from its alpha to beta phase occurs at 575°C, marked by a sudden increase in expansion of the samples (Toledo et al., 2004). At 700°C, the oxidation process has begun, also known as carbonate decomposition. In this process, calcite and dolomite begin to disappear, resulting in calcium oxide (CaO), magnesium oxide (MgO) and the release of CO_2. The calcium decomposition is an exothermic process and causes an increase in volume (Cultrone et al., 2004), while release of CO_2 leads to the sudden shrinkage of the brick (Cultrone et al., 2001), as seen in Figure 3.17, beginning at approximately 825°C. At 900°C, the carbonate decomposition process is completed and the vitrification process begins (Bauluz et al., 2004). Up to approximate temperatures of 800°C, the bond created at particle contact points is a solid state sintering, where particles have bound due to slight softening and phase regeneration. As temperatures approach 1000°C, vitrification begins, where the crystalline phases become amorphous, characterised by the elongation of pores and clumping of remaining phyllosilicates in to globular forms (Cultrone et al., 2004).

There are two common methods for the measurement of firing reactions, which are thermogravimetric analysis and dilatometry. Thermogravimetric analysis measures the change in weight of the specimen during firing, corresponding to reactions taking place within the specimen, while dilatometry measures the change in specimen length during firing, the expansion and contraction of which corresponds to reactions within the

specimen. The results of a dilatometer analysis performed on the specimens containing waste glass, along with the control specimen A can be found in Section 3, Figure 3.17. The analysis shows, for each specimen, a consistent rate of bloating between the temperatures of 0°C and 575°C until the quartz conversion causes a sudden increase in the rate of expansion. At the temperatures between 500°C and 800°C dehydration occurs followed by an expansion due to calcium conversion to approximately 850°C and the sudden shrinkage between approximately 850°C and 900°C as carbon dioxide is released, and the rate of vitrification increases.

Grain growth of non-metals during heat treatment can hinder the sintering process by preventing the diffusion of atoms toward the pore (Shackelford, 2005) as opposed to the glassy vitrified phase, which allows a more complete densification. A pure glass is completely non-crystalline in structure, while ceramics are crystalline. The use of scanning electron microscopy allows the investigation of the sintered specimens on the micro level, in order to determine which phase is dominant, as well as the degree of vitrification and the influence of waste glass on the firing results.

4.9 Mercury Intrusion Porosimetry, Pore Size and Distribution

There is a known correlation between the porosity and pore distribution of a specimen and its durability performance which is discussed by several authors in the review by Mallidi (1996) of methods for the measurement of this correlation. In order to develop a quantifiable connection between the two factors, detailed measurement of pore size and distribution using liquid porosimetry or gas sorption (Jena and Gupta, 2005) is

required. The use of these methods of pore measurement is beneficial in determining quantitatively the change in pore size distribution and volume with increased waste glass addition. According to Wardeh and Perrin (January, 2006), specimens with smaller and more widely distributed pores (0.001μm to 1μm) performed poorly in freeze-thaw tests when compared to specimens containing larger and more narrowly distributed pores (0.1μm to 10μm). The stresses developed in the specimens with smaller pores during freezing were nearly 4.5 times larger than those in the specimens with pores up to 5.5 times larger (Wardeh and Perrin, April, 2006). Another theory proposed by Ravaglioli (1976) states that at a certain pore diameter (less than 5μm), water cannot freeze. For this reason, there is a definite range of pore sizes which are directly correlated to durability. Specifically, at pore sizes less than 0.25μm, the water cannot freeze in the pores and damage is minimal. When the range of the pore size is between 0.25μm and 1.4μm, freezing occurs at relatively low temperatures and damage is likely. Finally, at a pore size greater than 1.4μm, the lack of capillary prevents complete saturation, and crystallization can take place without increased pressure and consequently damage (Ravagioli, 1976). In general, according to Maage (1984), an increase in the pore size percentage below 0.74μm can decrease the ultimate durability of the specimen.

Mercury intrusion porosimetry is performed using a porosimeter capable of achieving pressures close to 7000MPa which forces mercury into the pores of the specimen while measuring both applied pressure and volume of intruded mercury. Pore diameter, D, is calculated according to the Washburn equation, Equation 4.6 (Koroth,

Feldman, and Fazio, 1998), where γ is surface tension, θ is the contact angle, and p the applied pressure.

$$D = -4\gamma\cos\theta/p \qquad \text{Equation 4.5}$$

The pore sizes which can be measured are limited only by the pressure achievable by the porosimeter. From the data, several porosity properties of the specimen can be determined, including the total pore volume (ml/g or cc/g), the median, mean, and average pore diameter, as well as the density and porosity of the specimen (León y León, 1998). Of the three types of pores present, namely through, blind, and closed pores, mercury intrusion porosimetry can directly measure both through and blind, and closed pores can be calculated using the measured bulk and true densities (Jena and Gupta, 2005).

The porosity of all eleven specimens was measured using mercury intrusion porosimetry performed at the University of Western Ontario. The resulting measurement of the pore size and distribution will provide information necessary to develop a correlation between durability and pore structure, as well as to numerically quantify any influence of changes in pore structure as a result of the addition of waste glass or modification of the production process.

According to work by Maage (1984), the porosity is directly related to the freeze-thaw durability, F_c, given in Equation 4.7, where PV is the intruded pore volume, and P_3 is the percent of pores in the intruded pore volume with diameter greater than 3 μm.

$$F_c = 3.2/PV + 2.4*P_3 \qquad \text{Equation 4.6}$$

Using this quantitative scale, a durability value greater than 70 can be considered durable, while a value below 55 is non-durable.

CHAPTER 5 EXPERIMENTAL RESULTS

In this chapter, the results of the experimental program discussed in Chapter 4 are presented. A synthesis of the results achieved due to the addition of waste glass of various particle sizes and due to the method of production is presented. A statistical analysis of the results is performed to determine the significance of the measured properties.

5.1 Statistical Analysis

The statistical analysis is carried out in order to evaluate the similarities and differences in the experimentally measured properties of control specimens and those of specimens both containing waste glass and produced through differing methods. Statistical process control methods, which consider more than one variable, enable the use of simple calculations for the comparison of large sets of data. When employing this method, the goal is to determine whether a significant difference exists between two sets of data (Quinn, 2004). For this thesis, the aim of the statistical analysis is to investigate the difference in the mean experimental value, μ, assuming that there is no pairing of data. This implies that there is no relationship between the data sets. Due to the relatively small population size (5 specimens), the population variances, σ, are assumed to be unknown, and a pooled estimate is calculated based on the standard deviation of the sample. It is also necessary to assume that the variances are equal when using this method.

In order to determine whether or not the assumption of equal variance between compared sample populations holds true, the properties of normally distributed data are assumed, Equation 5.1. By rearranging this property, a set of upper and lower bound values can be determined, Equation 5.2. If the value 1, representing the ratio of equal variances, falls within the bounds, it can be assumed with confidence 100(1-α) % that the variances are in fact the same (Quinn, 2004). The degree of freedom, ν, of the sample is taken as n-1, where n is the number of tested specimens. The probability distribution used in this analysis is Snedecor's F-distribution, which is most commonly used in the testing of hypothesis, as well as regression and variance analysis.

$$(s^2_x \sigma^2_y) / (s^2_y \sigma^2_x) \sim F\nu_{x,}\, \nu_y \qquad \text{Equation 5.1}$$

$$[(s^2_x / s^2_y * F\nu_{x,}\, \nu_{y,\, \alpha/2)}, (s^2_x / s^2_y * F\nu_{x,}\, \nu_{y,\, 1-\alpha/2)}] \qquad \text{Equation 5.2}$$

In the case where the value 1 is not contained within the upper and lower bounds, an approximate method must be employed where the confidence interval for each variable is constructed using the standard deviation. If the confidence intervals for the compared values overlap, then there is no statistical evidence that a difference in the mean values μ_x-μ_y exists. In this case, the statistical significance of the results will not be certain, although it may be evident from the figures that there is a significant difference in the means of the control specimen and the particular specimen of interest based on the standard deviation confidence intervals presented.

If the value of 1 falls within the calculated upper and lower bounds, the variance of the two data sets is assumed to be equal, and based on this assumption, a pooled estimate of the variance is determined using Equation 5.3 (Quinn, 2004).

$$s^2_p = (\nu_x s^2_x + \nu_y s^2_y) / (\nu_x + \nu_y) \qquad \text{Equation 5.3}$$

The pooled variance is then used to calculate a confidence interval for the difference in mean values, with student's t-distribution representing the probability distribution. The confidence interval is determined using Equation 5.4. If the value 0 is contained within the bounds of Equation 5.4, it can be concluded that there is no statistically significant difference between the mean values, μ_x and μ_y with a confidence of 100(1-α) %. For this analysis, the confidence level will be 95%, with α set at 0.05.

$$[(\mu_x-\mu_y) - t_{\nu,\alpha/2}\sqrt{(s^2_p/n_x + s^2_p/n_y)},\ (\mu_x-\mu_y) + t_{\nu,\alpha/2}\sqrt{(s^2_p/n_x + s^2_p/n_y)}\ ] \qquad \text{Equation 5.4}$$

5.2 Compressive Strength

The failure mechanism of both the specimens produces in the plant and the laboratory scale specimens followed one of two patterns. The first mode of failure can be described as a shattering of the specimen about the central core hole or holes into at least four distinct sections, where the height of each section was approximately that of the specimen. The second mode is a conical shape where crushing is traced from the loaded surface towards the centre of the specimen. Figure 5.1 shows the first failure mode as

seen in a small scale specimen, while the second mode is depicted in Figure 5.2. According to CSA standards (CSA, 1987), for an average of five tested bricks, the minimum compressive stress required for a grade designation of SW (suitable for outdoor applications) is 20.68 MPa.

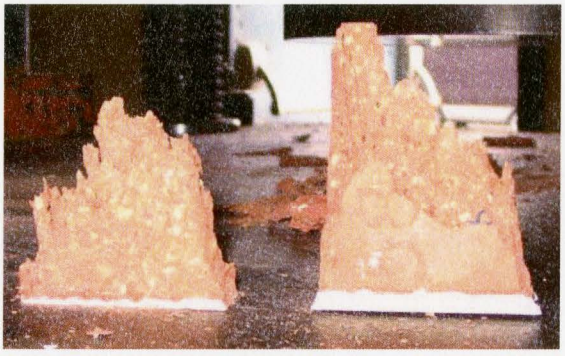

Figure 5.1 Compressive Failure, Conical

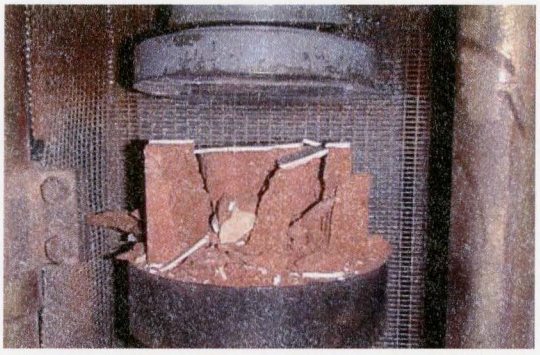

Figure 5.2 Compressive Failure, Bedding

The results of the compressive tests, in terms of average value and one standard deviation, are shown in Figure 5.3. The control specimen A, containing no waste glass, achieved an average compressive strength of 65 MPa, well above the minimum value for SW grade bricks. As waste glass addition is increased from 0% to 5%, 10% and 15%, compressive strength increases for both coarse and fine waste glass addition. In the case of coarse waste glass (particle sizes ranging from 300μm to 150μm), specimens B, D, and F corresponding to 5%, 10% and 15% coarse glass content show an increase of 41%, with compressive strength of 92.4 MPa at 15% waste glass content. In comparison, specimens C, E and G, corresponding to 5%, 10%, and 15% fine glass content, show an increase of 104%, with a compressive strength of 133.4 MPa at 15% waste glass addition.

Analysis of the results using variance and sample means indicates that the compressive strength of specimens D, F, G, and FX can be considered conclusively higher than that of the control specimen, A. Therefore, the addition of 10% fine waste glass, the addition of 15% coarse, and the addition of 15% fine waste glass, and production exclusively in the plant, led to a statistically significant increase in average compressive strength of 104% for specimen G, and 20% for specimen FX.

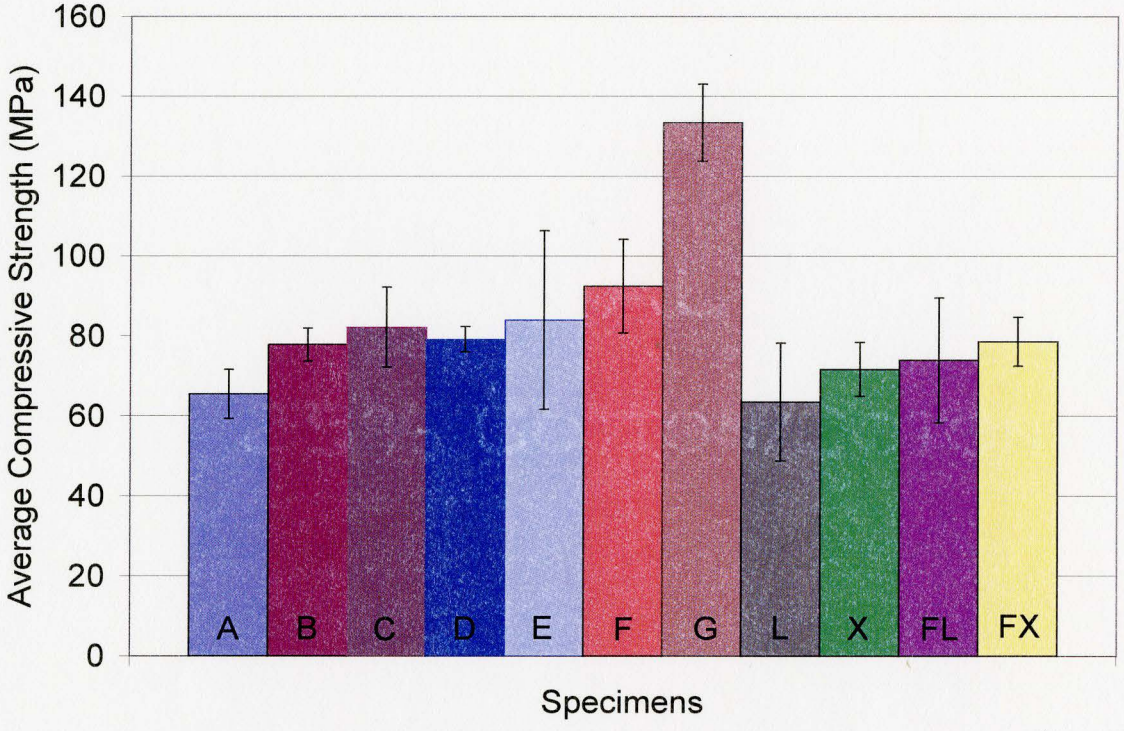

Figure 5.3 Average Compressive Strength

A comparison between the two control specimens, A and L, showed no significant difference in the mean strength values. Although there was no significant difference in the compressive strength for the various production methods based on the

comparison to specimen L, there was a slight increase in the compressive strength of specimen FX, produced in the plant, when compared to the control specimen A. Therefore the compressive strength results for specimens A to G may be considered slightly conservative in estimating the expected compressive strength of bricks produced in the plant and containing waste glass. The effect of the size difference between the specimens extruded in the lab and the plant is best determined by comparing specimens L and FL, as well as specimens X and FX, in order to keep firing location constant. Although the full size specimens had slightly higher average strength values, statistically, there was no apparent impact on the results due to the size of the specimens.

5.3 Tensile Strength – Modulus of Rupture

Specimens A to G were tested for modulus of rupture according to the method prescribed by CAN3-A82.2-M78; however, this method produced exceptionally low strength results. These results led to use of the four point loading method for testing of the remaining specimens. Figure 5.4 shows the original apparatus for testing. The specimens tended to roll out of alignment before the seating load could be applied, and warping along the extruded length caused uneven load distribution. As a result, failure tended to occur near the supports of the specimen and resembled shear failure.

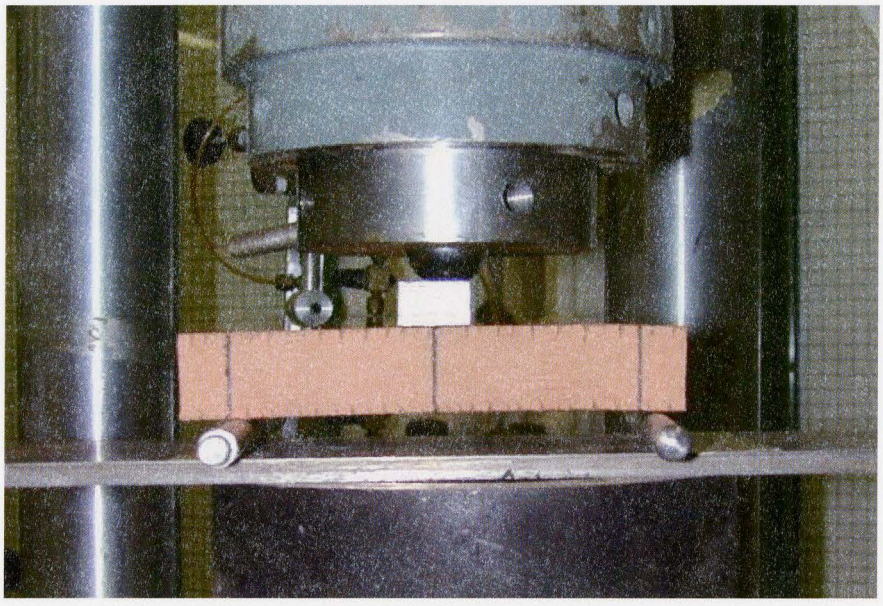

Figure 5.4 CSA MOR Apparatus

Specimens L, X, FL, and FX were tested according to the four point loading test method. Generally, the specimens failed as expected, in the zone of constant moment where the stress was the highest, see Figure 5.5. The results of the CSA and modified testing methods for the specimens are presented together in Figure 5.7. It was observed during testing of full scale specimens fired in the laboratory (FL) that premature failure tended to occur on the extreme edge of the zone of constant moment. The hairline crack is visible along the left plant indentation in specimen FL15 seen in Figure 5.6, while premature failure occurred in a similar crack in the right plant indentation. This premature failure occurred as a result of hairline cracks which had developed along the plant impression points during firing in the laboratory kiln, and were generally unnoticeable prior to testing.

(a) (b)

Figure 5.5 (a) Small Scale MOR Failure Mode (b) Full Scale MOR Failure Mode

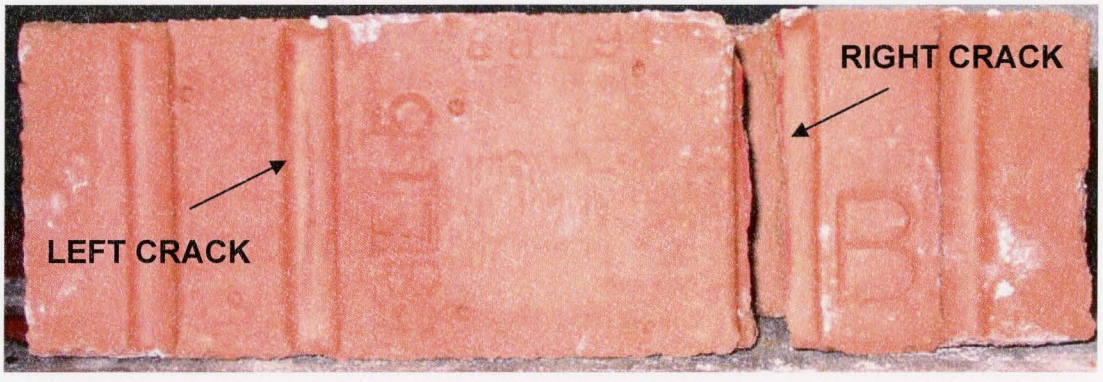

Figure 5.6 Hairline Crack Causing Premature MOR Failure

Based on the statistical analysis, the modulus of rupture values for the specimens tested according to the four point load test method were conclusively higher than the specimens tested using the prescribed three point load test method. Although, from the graph, there appears to be a trend of increasing MOR with increasing waste glass addition, statistically, this evidence is not conclusive for specimens A to G. Given the nature of the failure mechanism observed, no statistically supported conclusions can be made with respect to the effects on the modulus of rupture of adding waste glass. A comparison of control specimens A and L indicated that due to an extreme difference in

variance, the statistical evidence could not be considered conclusive. The results of the MOR testing for specimens A and L did not lead to comparable mean values, and the MOR value achieved for the laboratory specimen L tested using the four point loading method produced higher values.

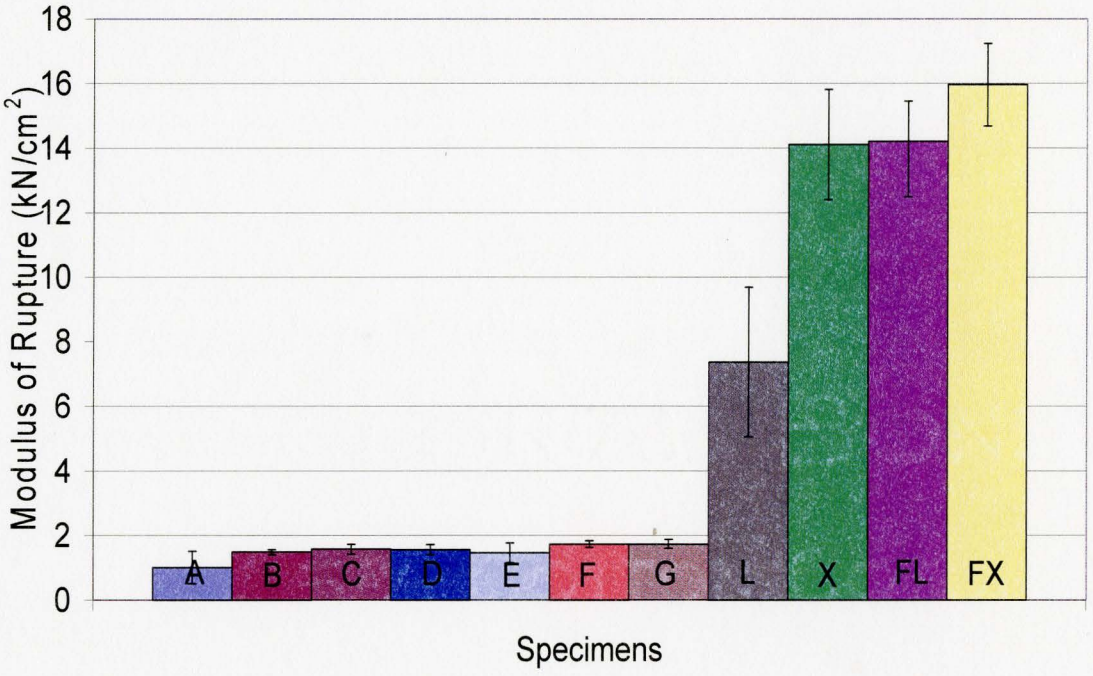

Figure 5.7 Modulus of Rupture Results

The size effects are evaluated by comparing specimens L and FL, as well as specimens X and FX. From Figure 5.7, there appears to be a size effect for the laboratory fired specimens since the results of L and FL are not comparable; however, when looking at the plant specimens there is no statistical difference due to size. The large difference in the values for L and X indicates either an effect of firing location, or another factor which

influences the performance of the small scale laboratory specimens. The latter can be linked to the increase in warping observed for the small scale specimens.

5.4 Initial Rate of Absorption

The initial rate of absorption results are presented in Figure 5.8 for specimens A to G, L, X, FL, and FX. Statistical comparison of the results indicates that there is a significant difference between the results achieved for the control specimen A, and the results of specimens E, F and G. The use of 10% fine waste glass, as well as the use of 15% coarse glass and 15% fine glass led to a decrease in IRA of at least 27%, and at most 71% as waste glass content increased from 10% to 15%. A comparison of the control specimen L, and the specimens prepared in the plant and laboratory show a statistically significant increase in the IRA of specimens extruded in the laboratory but fired in the plant (specimen X). The IRA results of the control specimen L are comparable to those of the specimens extruded in the plant, as well as the control specimen A.

The size effects of the specimens based on the IRA results indicates that the use of small scale specimens yields slightly higher values. The full scale specimens performed statistically better in IRA testing, with a decrease in IRA of up to 14% depending on variance. Based on the analysis of the statistics, the IRA results for specimens containing waste glass produced in a plant trail would be comparable to, if not slightly lower than, the results of the small scale testing.

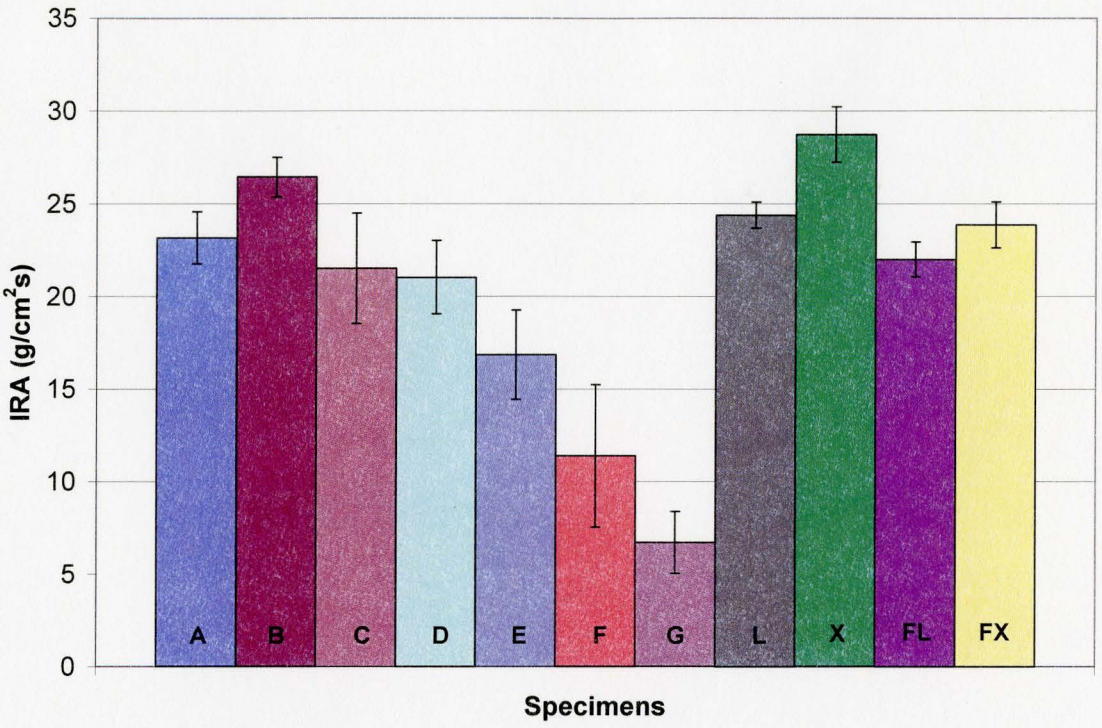

Figure 5.8 IRA Results

5.5 Absorption Ratio

The absorption ratio of the specimens was determined by obtaining the 24 hour cold water absorption and 5 hour boiling water absorption, and using the ratio of the two values to compute the average absorption ratio for the specimens. The 24 hour cold water absorption and 5 hour boiling water absorption values are presented and discussed individually, and consequently, the absorption ratio is developed and discussed.

5.5.1 Twenty Four Hour Cold Water Absorption

The cold water absorption (CWA) results are presented in Figure 5.9 for all specimens. The statistical analysis of the results indicates that when compared to the

control specimen A, there is a statistically significant difference in the mean values of CWA obtained for specimens E, F, and G, with 95% confidence. Therefore, when the fine waste glass content reaches 10%, there is an average 23% decrease in the initial rate of absorption of the brick. At 15% waste glass addition, the CWA decrease is even more substantial, where the specimens containing coarse waste glass achieved an average decrease in CWA of 32%, and the specimens containing fine waste glass had an average decrease in CWA of 43%.

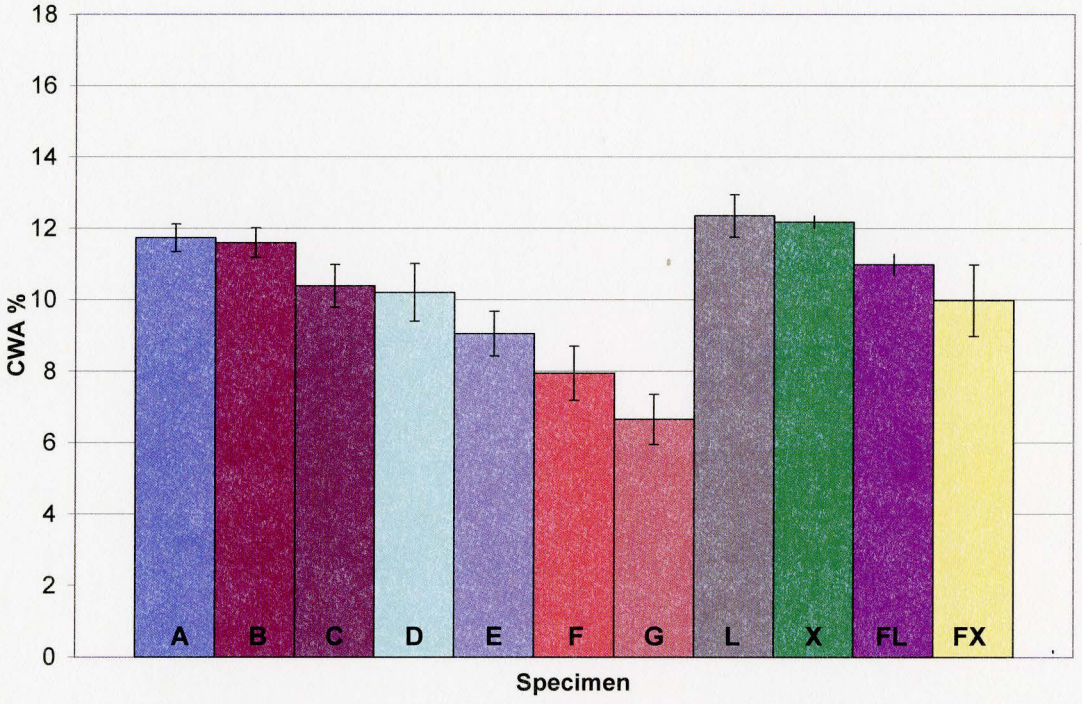

Figure 5.9 Cold Water Absorption Results

A comparison of the results with the control specimen L indicates that there is no statistically significant difference between the control specimens A and L, which were

produced and fired with the same composition and under the same conditions. There was a significant decrease in the CWA of specimens E, F, and G; there was also a statistically significant decrease in CWA for specimen FX when compared to both L and A. A 19% decrease in CWA was measured for the specimen produced in the plant, FX, when compared to the laboratory control specimens, which may indicate a better performance can be expected (lower CWA value) for specimens containing waste glass and produced in the plant.

5.5.2 Five Hour Boiling Water Absorption

The results of the five hour boiling water absorption (BWA) are presented in Figure 5.10. A statistical analysis indicates a similar trend to the one observed for the 24 hour cold water absorption test. The results for the two control specimens, A and L, are comparable, with no significant difference in their mean BWA value.

A significant decrease in BWA is observed for specimens E, F, and G. For specimen E, an average decrease in BWA of 14% was measured compared to the control specimen A. At 15% waste glass addition, specimens F and G had a decrease in BWA of 18% and 28%, respectively, compared to control specimen A. Specimen FX, produced in the plant, has a BWA value 15% lower than that of the control specimen, and specimen FL, which was produced in the plant but fired in the laboratory, has a BWA value13% lower than control specimen L.

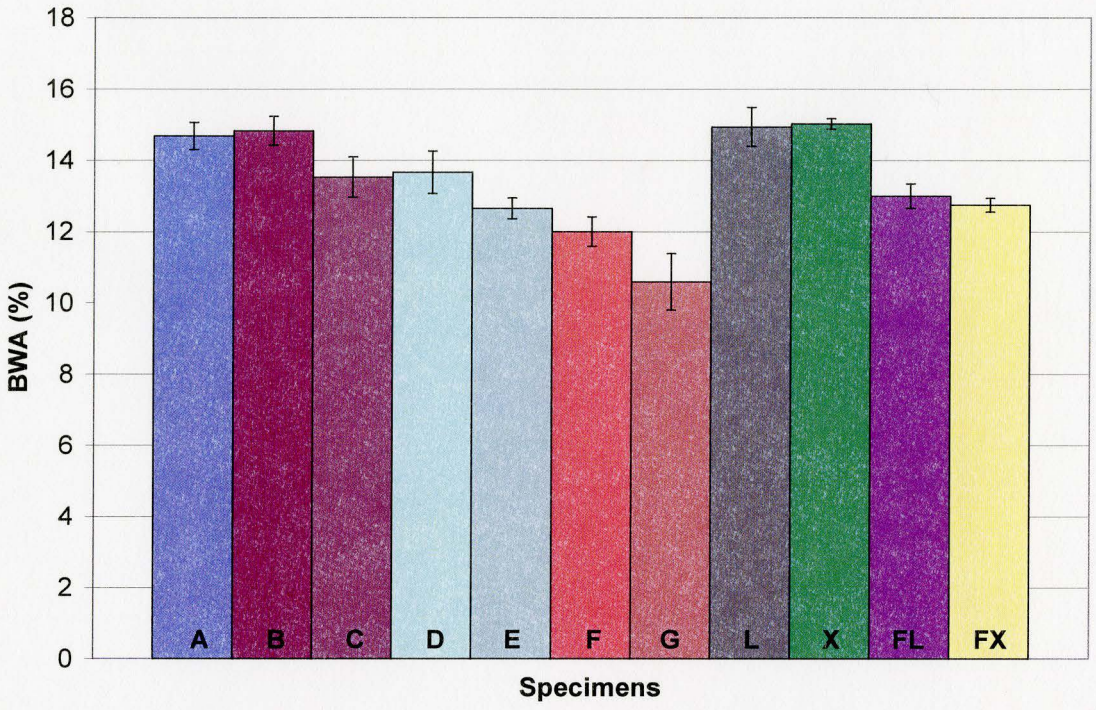

Figure 5.10 Boiling Water Absorption Results

5.5.3 Absorption Ratio

The absorption ratio is calculated by taking the ratio of the CWA and the BWA in order to estimate the durability potential of the specimens. A low absorption ratio indicates ideal durability. The absorption ratios for the specimens are presented in Figure 5.11.

Based on the statistical analysis, there was no conclusive evidence that a difference in the mean values existed, despite the apparent trend of decreasing C/B ratio observed in Figure 5.11. As discussed in Section 5.1, the variance of specimens D to G were not equal to the variance of the control specimen A, and therefore any comment on

the trend of decreasing absorption ratio can only be made relative to the standard deviation intervals presented in Figure 5.11. From these confidence intervals, it can be stated that specimens D to G display a decreased C/B ratio.

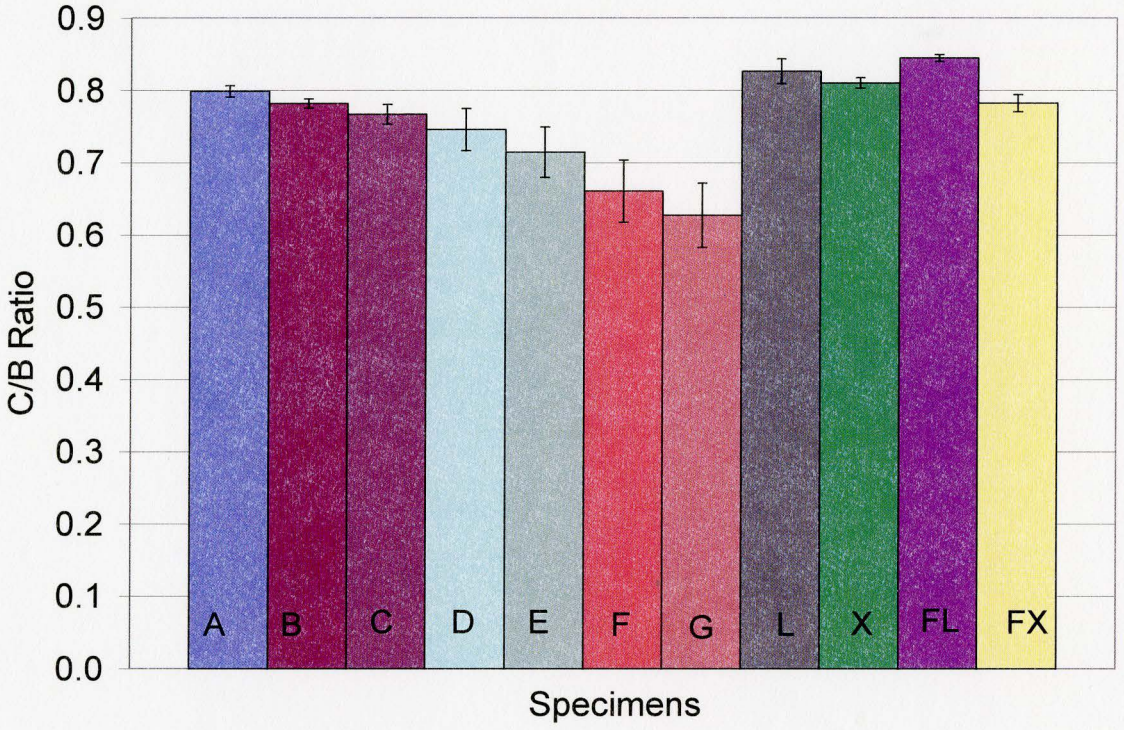

Figure 5.11 Absorption Ratio Results

The mean C/B value for the control specimen L is not statistically different from that of the control specimen A, and therefore the results of a comparison of mean values between specimen L and specimens D to G provides more useful results. Specimens C, E, F and G demonstrate a statistically significant decrease in C/B ratio when compared to specimen L. Specifically, specimen C, containing 5% fine waste glass, has a C/B ratio

7% lower than the control specimen L. Specimens E, F, and G have reductions in their C/B ratio of 14%, 20%, and 24% respectively, when compared to specimen L.

For the different manufacturing processes, the statistical analysis indicates no significant difference in the absorption ratios achieved for specimens X, FL, and FX. There is however a slight increase in the C/B ratio of specimen FL when compared to control specimen A. The results of the absorption ratio analysis indicate that the results achieved for specimens A to G are representative of what would be expected for full scale specimens containing waste glass produced in a plant setting since the values of FX and A are comparable.

5.6 Freeze-Thaw Durability

Freeze-thaw endurance of the fired clay specimens was tested over the course of five months, to a total of 100 cycles in both deionized water and 3% sodium chloride solution. For the first 55 cycles, a measurement of the mass loss was taken every five cycles. For the next 20 cycles, mass loss was measured every 10 cycles, and the final mass loss measurement encompassed 25 cycles. Deionized water was used in accordance with CAN/CSA-A82.1-M87. The use of 3% NaCl as a test solution was introduced to evaluate the effects of deicing salt on the scaling resistance of fired clay brick.

5.6.1 Specimens A to G in Deionized Water

Cumulative mass loss for specimens A to G after 50 cycles is presented in Figure 5.12. At the conclusion of the first 50 cycles, the mass loss of the control specimen A is

approximately average, while specimens B and C, containing 5% waste glass, performed slightly better, and specimens D, E, F, and G performed slightly worse based on cumulative mass loss. Specimens E, F and G were performing better than the control specimen until the 40th cycle, where they experienced a sudden increase in their rate of mass loss. At cycle number 40, chipping along the edges of specimens E, F, and G was observed, as well as a roughening of the extruded surface for some of the specimens, which resembled very mild scaling.

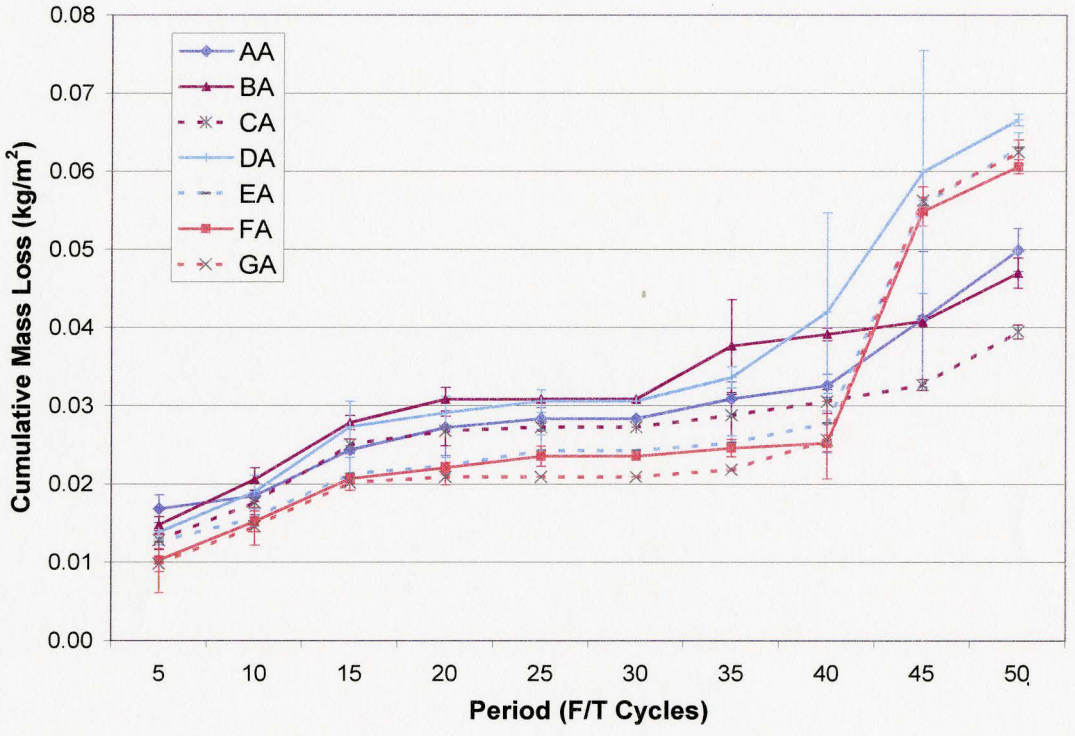

Figure 5.12 Cumulative Freeze-Thaw Mass Loss in Deionized Water After 50 Cycles

Specimens D, containing 10% coarse waste glass, showed early signs of deterioration. At the 10^{th} cycle, small and previously unnoticeable cracks began to open on two of the three tested specimens, Figure 5.13. As a result of these cracks, the rate of mass loss for these specimens increased dramatically in the first fifty cycles compared to the other tested specimens, despite the apparent stability of the cracks. The cracks were not observed to open or propagate, Figure 5.14. After 50 cycles, the maximum recorded cumulative mass loss, corresponding to specimen D, was 0.0667 kg/m².

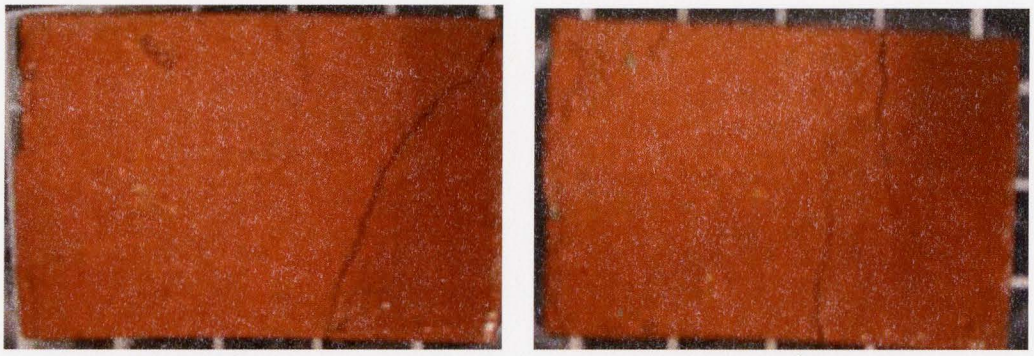

(a) (b)

Figure 5.13 After 10 F/T Cycles, (a) Specimen D4, (b) Specimen D5

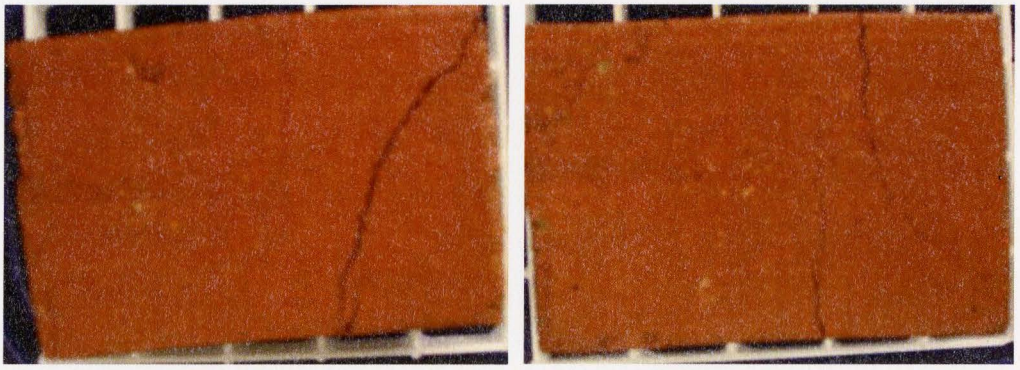

(a) (b)

Figure 5.14 After 50 Cycles, (a) Specimen D4, (b) Specimen D5

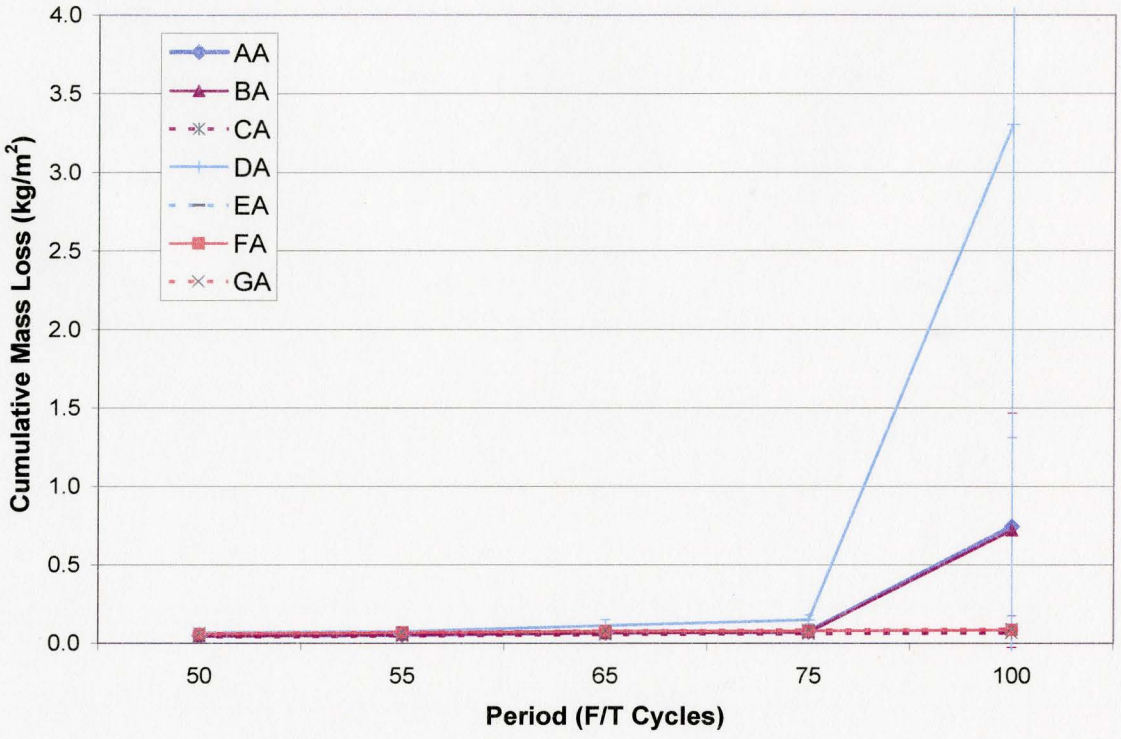

Figure 5.15 Cumulative Freeze-Thaw Mass Loss in Deionized Water for 100 Cycles

In the final 50 cycles, Figure 5.15, the average mass loss for specimen D increased dramatically due to the separation of the cracked sections, Figure 5.16. The variation of the mass loss was very high due to the increased loss for only two of the three tested specimens. The final average cumulative mass loss for specimen D was 3.3kg/m², more than triple the next highest total cumulative mass loss value for specimens A to G. Specimens A and B, which in the first 50 cycles performed at the mid range of the tested specimens, suffered major degradation in the final 25 cycles.

The specimens that experienced significant mass loss were observed to spontaneously decompose in a localized area and in areas where no previous cracks were

visible, as seen for specimens A4 and B5 in Figure 5.17. The mechanisms of failure did not resemble those observed during the first attempt at freeze-thaw testing according to the CSA method, where internal pressure developed along the core hole. The final cumulative mass loss for specimens A and B was 0.72 kg/m² and 0.74 kg/m², respectively. The cumulative mass losses for specimens A to G over the period of 100 cycles of freeze-thaw testing are presented in Figure 5.18.

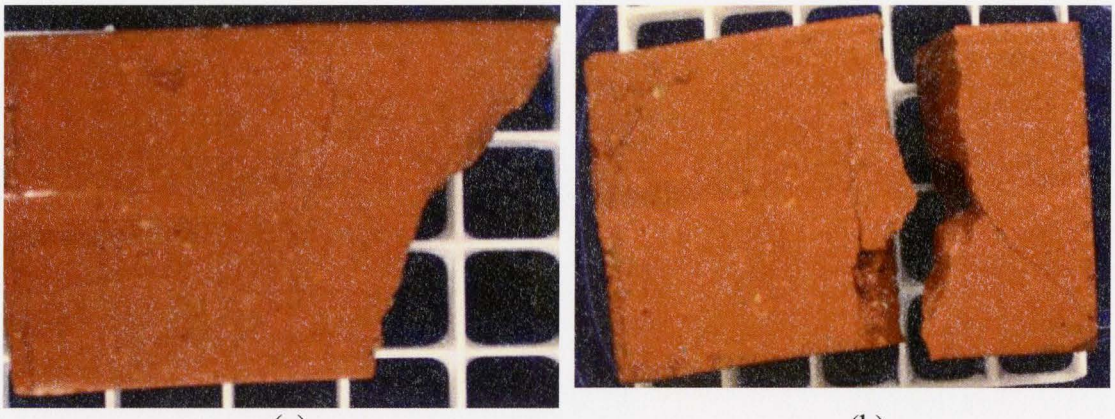

(a) (b)

Figure 5.16 After 100 F/T Cycles (a) Specimen D4, (b) Specimen D5

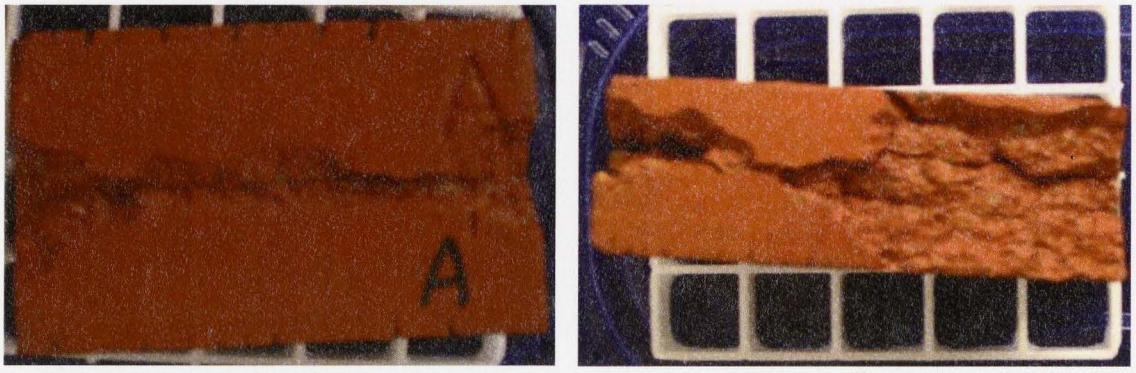

(a) (b)

Figure 5.17 After 100 F/T Cycles, (a) Specimen A4, (b) Specimen B5

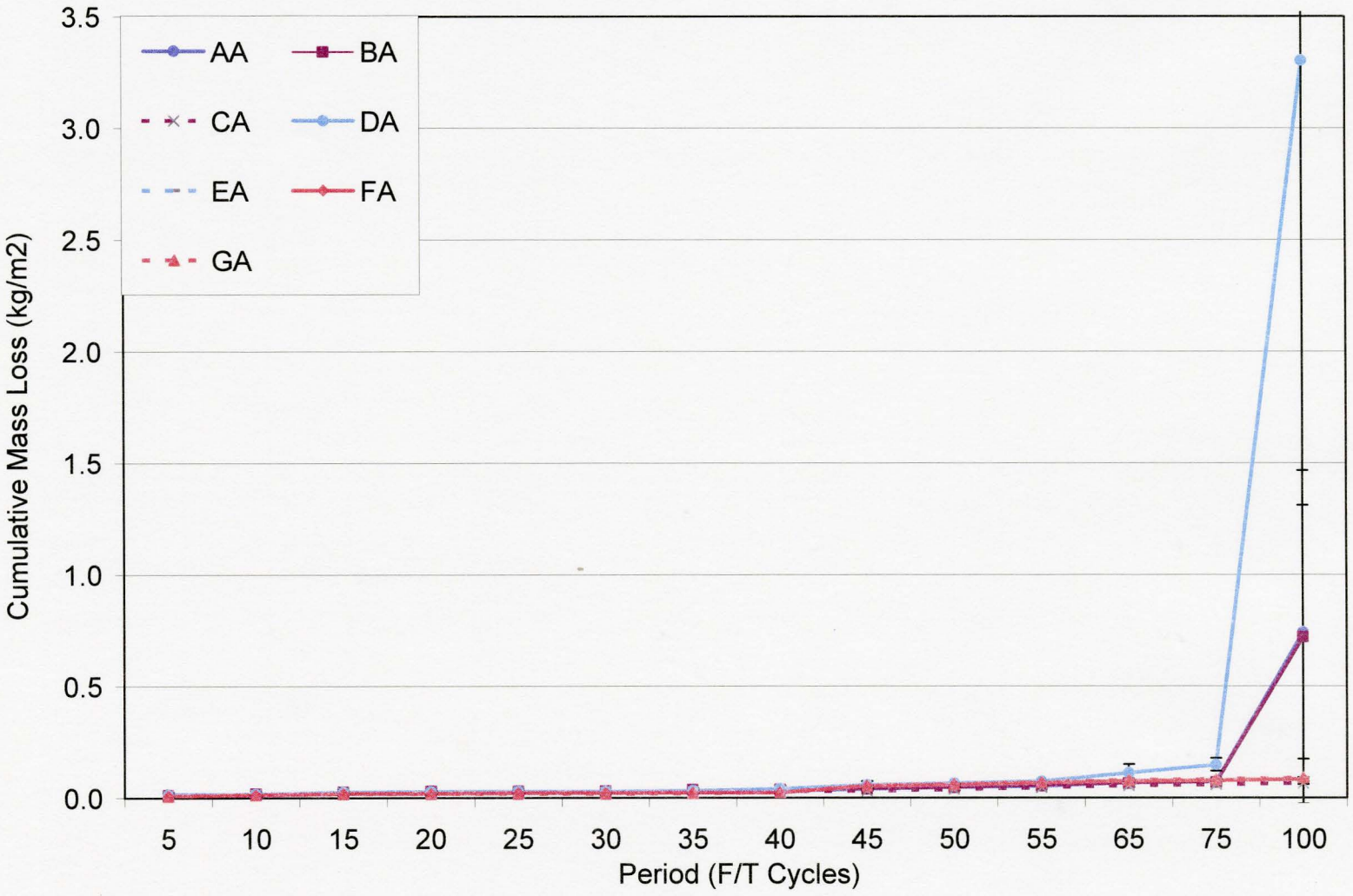

Figure 5.18 Cumulative Mass Loss in Deionized Water due to F/T Cycles

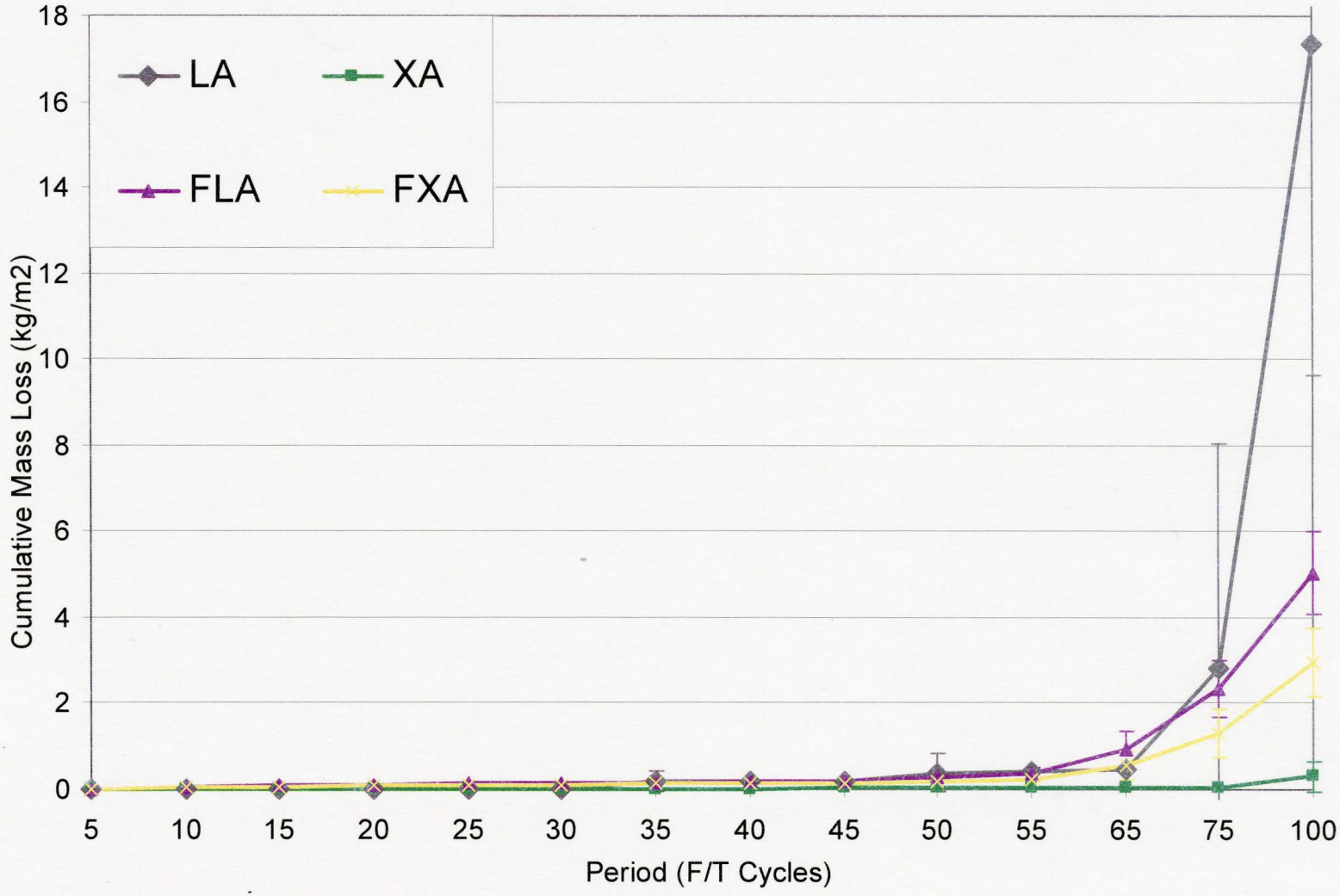

Figure 5.19 Cumulative Mass Loss in Deionized Water for Various Production Methods due to F/T Cycles

5.6.2 Specimens L, X, FL, and FX in Deionized Water

Cumulative mass loss for the specimens with varying production methods are presented in Figure 5.19 for the full 100 freeze-thaw cycles. During the first 50 cycles of testing, Figure 5.20, the specimens performed in an unexpected manner. In the initial weeks of testing, the majority of the mass loss occurred with the full scale specimens FL and FX, as a surface finish, consisting of coloured sand applied in the production plant, loosened and separated from the brick.

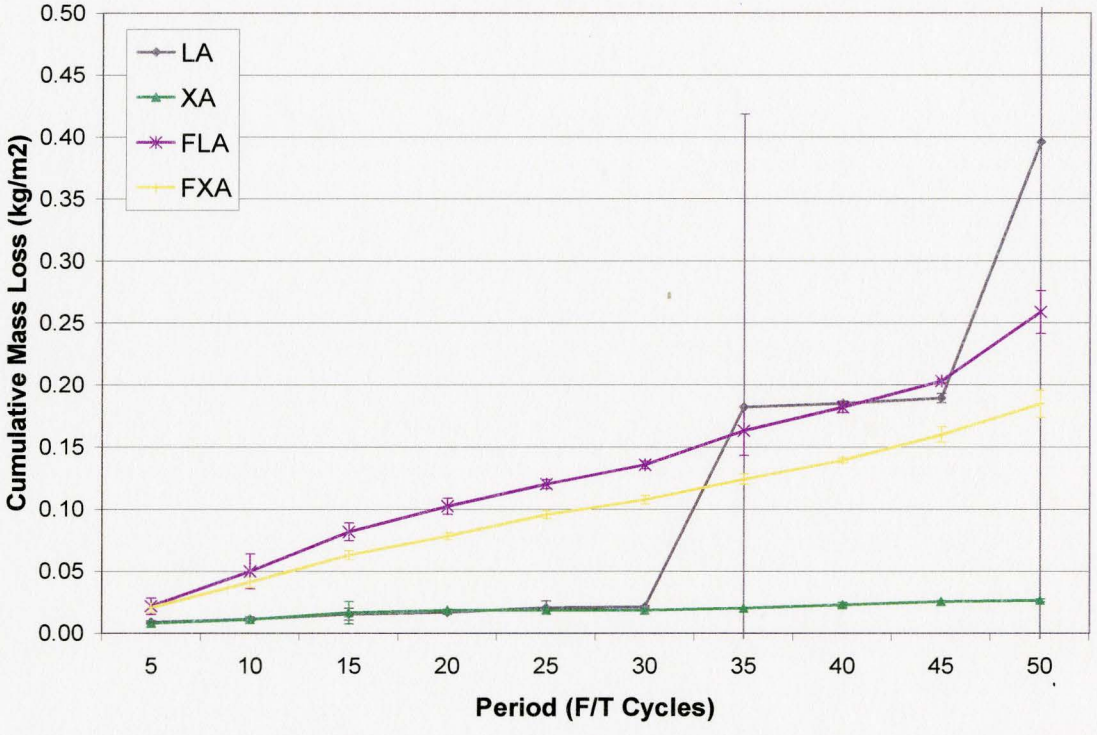

Figure 5.20 Cumulative Mass Loss in Deionized Water After 50 F/T Cycles

At the completion of 15 cycles, the edges of the full scale specimens began to feel soft to the touch as the specimens were handled during filtration. Material was easily removed using the syringe, especially from the specimen edges. No flaws or points of mass loss were evident; however this softening of the edges did increase the rate of material being lost by the specimens at each filtration. By the end of the first 50 cycles of freezes-thaw testing, the full scale specimens had lost at least 60% more mass than specimens A to G. Specimens FL and FX lost 0.26 kg/m^2 and 0.18 Kg/m^2 respectively by the conclusion of cycle number 50. Specimens L and X performed at a rate comparable to specimens A to G in the first 30 freeze-thaw cycles, and had the lowest rate of mass loss of all specimens tested in deionized water. After 35 cycles, the rate of mass loss for specimen L jumped dramatically.

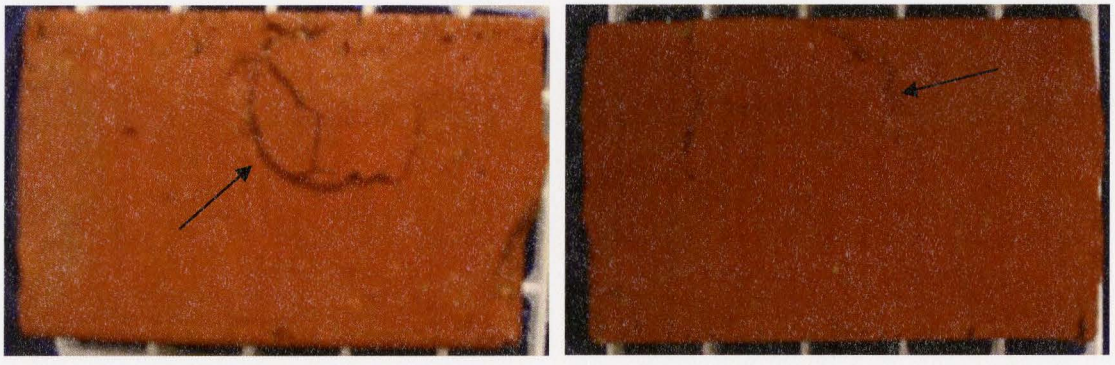

(a) (b)

Figure 5.21 After 30 F/T Cycles (a) Specimen L18 (b) Specimen L29

This jump in mass loss was due in part to minor chipping on the edges of the specimens, but mostly to the formation of small craters and pop outs on several of the L

specimens. Two pop outs are shown in Figure 5.21 on specimens L18 and L29. At cycle 50, the mass loss again spiked as specimen L18 split and lost a small piece of material. The crater formation noted at cycle 30 continued in specimen L2, causing increasing loss of mass, Figure 5.22. This high rate of mass loss resulted in a cumulative mass loss of 0.396 kg/m² by the end of cycle number 50. While the average mass loss for specimen L increased dramatically, specimen X performed very well, with only 0.026 kg/m² average cumulative mass loss after 50 cycles of freeze-thaw testing.

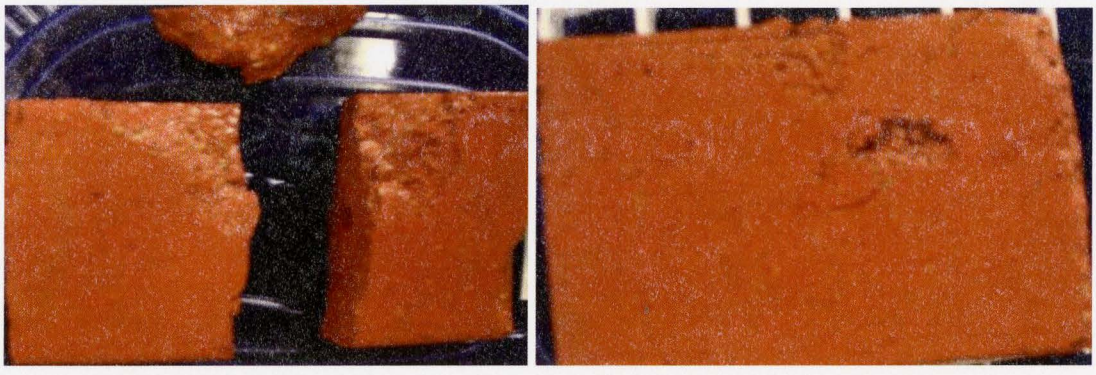

(a) (b)

Figure 5.22 After 50 F/T Cycles (a) Specimen L18 (b) Specimen L2

In the final 50 cycles of testing, the average rate of mass loss of specimen L continued to increase at an unexpected rate, Figure 5.23. In the final 35 cycles, specimens began to spontaneously decompose almost completely, where all surfaces, not exclusively the testing surface, were observed to deteriorate in a random cracking pattern, Figure 5.24. At the completion of 100 freeze-thaw cycles, cumulative mass loss was 17.33 kg/m²; however, this value is not an accurate representation of the mass loss per

area, since mass loss occurred on all surfaces of the specimen. A more accurate measure of the mass loss for specimen L is the total percentage mass loss. The rate of mass loss increased slightly for specimens X in the final 50 cycles; however, there was no observable failure until the completion of the final 25 cycles. Some surface failure was observed as shown in Figure 5.25 however, the deterioration was not on the tested surface. The final cumulative mass loss was relatively low at 0.316 kg/m².

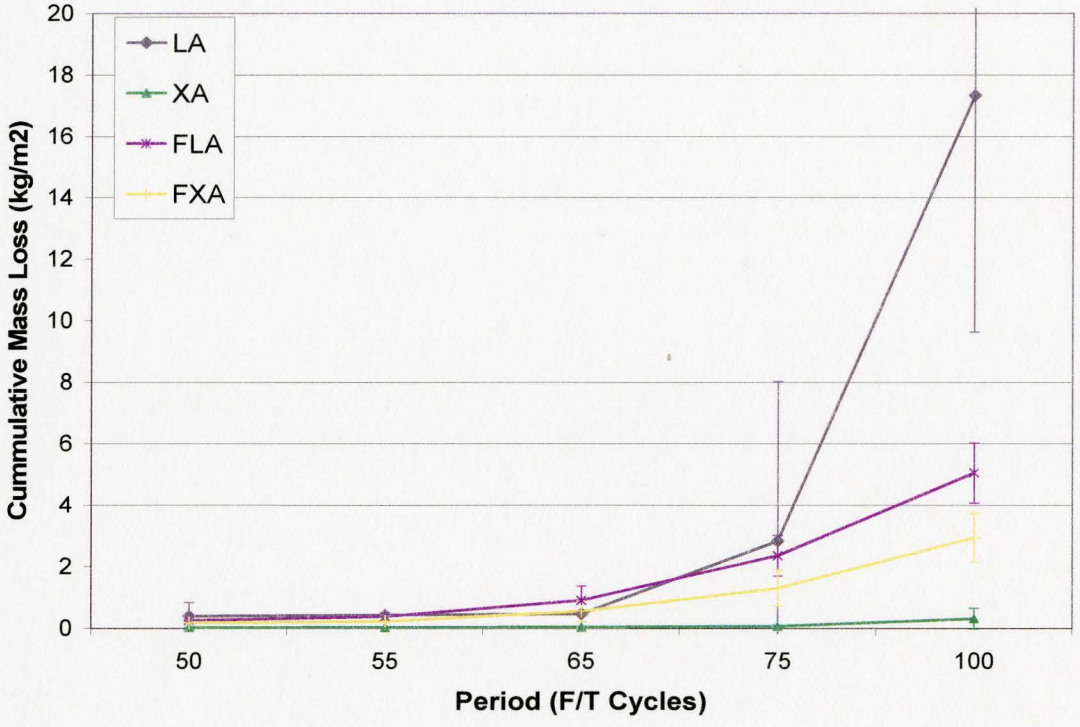

Figure 5.23 Cumulative Freeze-Thaw Mass Loss in Deionized Water After 100 Cycles

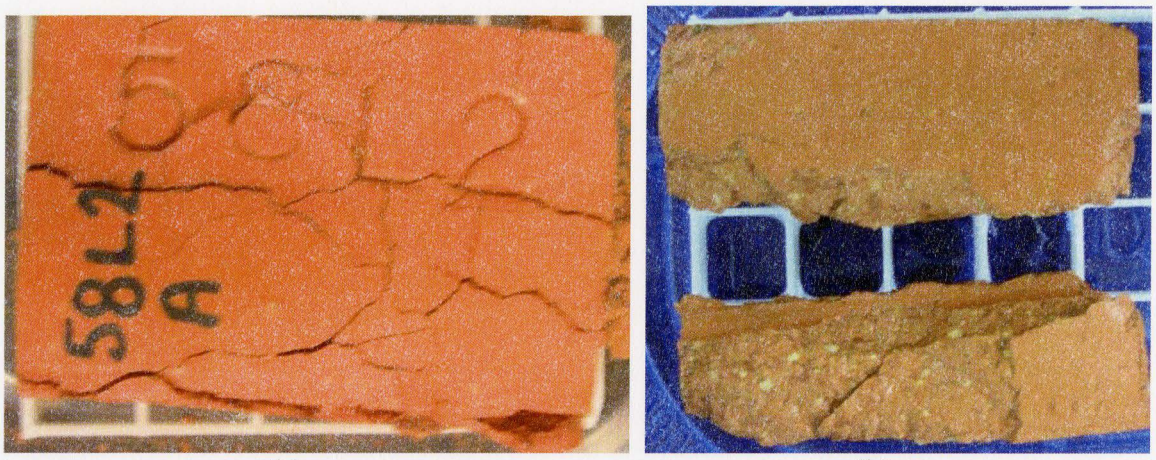

(a) (b)

Figure 5.24 Spontaneous Deterioration of L2 (a) Top, (b) Bottom Surface at Cycle 75

(a) (b)

Figure 5.25 Mass Loss for Specimens (a) X26 and (b) X29 at Cycle Number 100

The rate of mass loss for specimens FL and FX increased in the final 50 freeze-thaw cycles, especially for FL. The mass loss along the edges of the specimens expanded to the tested surface, for which the deterioration mode tended to be scaling of the first 1-2 mm of finished surface. This deterioration mode also occurred on some of the finished side surfaces. A small area was observed to scale at the top surface, which is the unexposed surface of the specimens. Figure 5.26 a) shows the typical deterioration mode

for specimen FL, while b) shows the mass loss occurring from surfaces other than the tested surface. This deterioration mode developed later for the specimens fired in the plant, with first signs of major surface deterioration occurring at cycle number 75. The specimens fired in the laboratory experienced surface failure at cycle number 65. The difference in the rate of cumulative mass loss between specimens FL and FX is apparent in Figure 5.19, which shows the results for the cumulative mass loss of the 100 tested freeze-thaw cycles for specimens L, X, FL, and FX. The final cumulative mass loss for FL was 5.05 kg/m², while the cumulative mass loss for FX was 2.95 kg/m².

(a) (b)

Figure 5.26 Surface Spalling of Specimens (a) FL2 and (b) FX20 after Cycle Number 65

The total average percentage of mass loss for all specimens tested in deionized water is presented in Figure 5.27. The statistical analysis indicates that for the specimens that have equal variance with the control specimen A, namely specimens B, X, FL, and FX, there is no statistically significant difference in the mean values of total average percentage mass loss. For the remaining specimens, it is necessary to look at the confidence intervals for the individual variances in order to make a statement about the difference mean values. From this comparison, the most significant is the difference in mass loss between the two control specimens A and L. The variances between the two specimens are not comparable, however the variance ranges of A and L do not intersect, which indicates that there is a difference between the mass losses experienced by the two specimens.

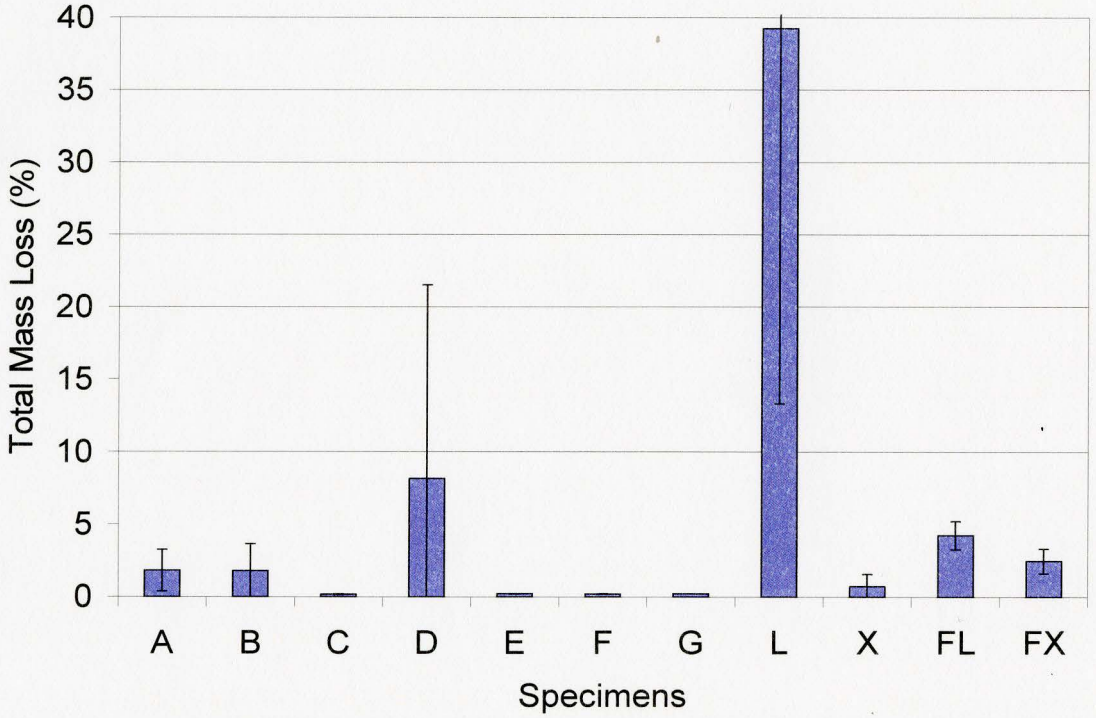

Figure 5.27 Total Mass Loss for Specimens Tested in Deionized Water

Due to the extreme mass loss experienced by specimen L, a comparison of the various process specimens would be more informative if conducted with control specimen A. When compared to the control specimen A, there was no statistically significant difference between the mean total mass loss percentage for specimens X, FL, and FX.

5.6.3 Specimens A to G in 3% Sodium Chloride Solution

The cumulative mass loss for the first 50 freeze-thaw cycles in NaCl solution is presented in Figure 5.28. The control specimen A had an average mass loss in the first 50 cycles of testing when compared to the other specimens. Specimens B and D, containing 5% and 10% coarse waste glass respectively, performed similarly to the control specimen. Specimen C, containing 5% fine waste glass, experienced the greatest cumulative mass loss over the first 50 cycles of testing, with a maximum cumulative mass loss of 0.177 kg/m^2. Specimens E, F and G performed slightly better than the control specimen A, where specimen F had the lowest cumulative mass loss after 50 cycles, 0.064 kg/m^2. In the first 50 cycles of testing, very little damage was observed on the surface of the tested specimens, which appeared nearly pristine.

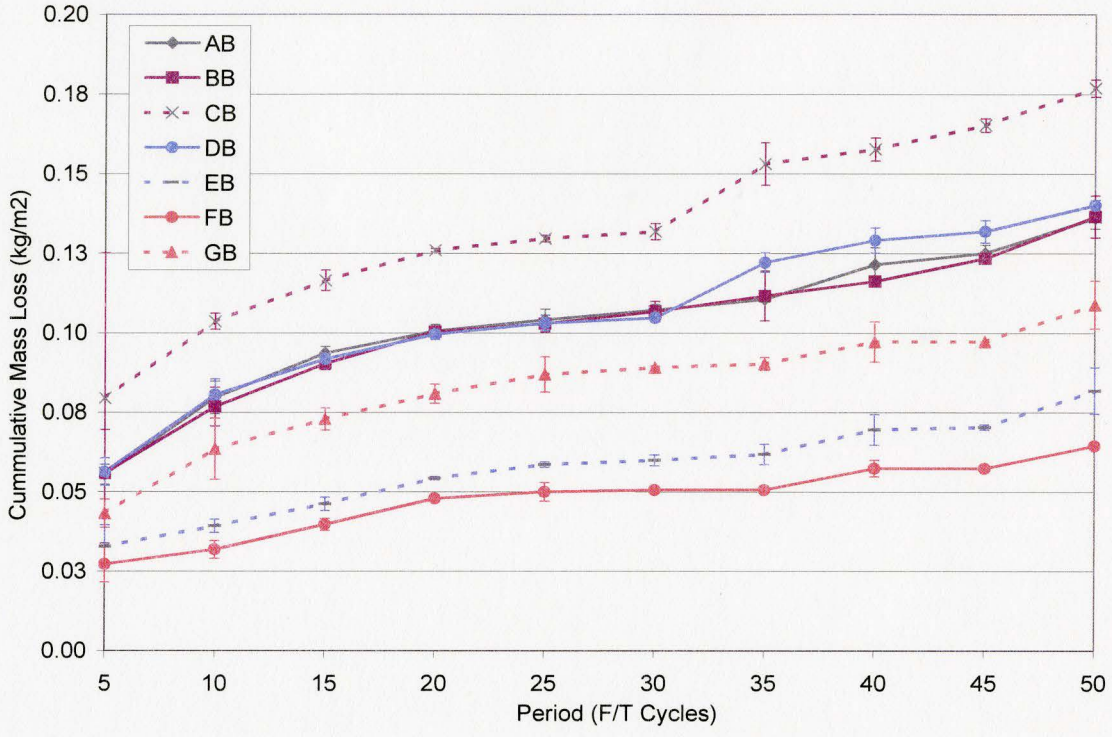

Figure 5.28 Cumulative Mass Loss, 3% NaCl Solution, Specimens A-G After 50 Cycles

In the final 50 cycles of freeze-thaw testing, Figure 5.29, the specimens continued to lose mass with the same linear pattern; however, the rate of mass loss decreased and seemed to level off. The cumulative mass loss for specimens A to G over the full 100 cycles of freeze-thaw testing in 3% NaCl solution is presented in Figure 5.30. As mentioned, there is a noticeable linear trend throughout the test. The variation is significantly lower for all specimens when compared to the results of testing in deionized water.

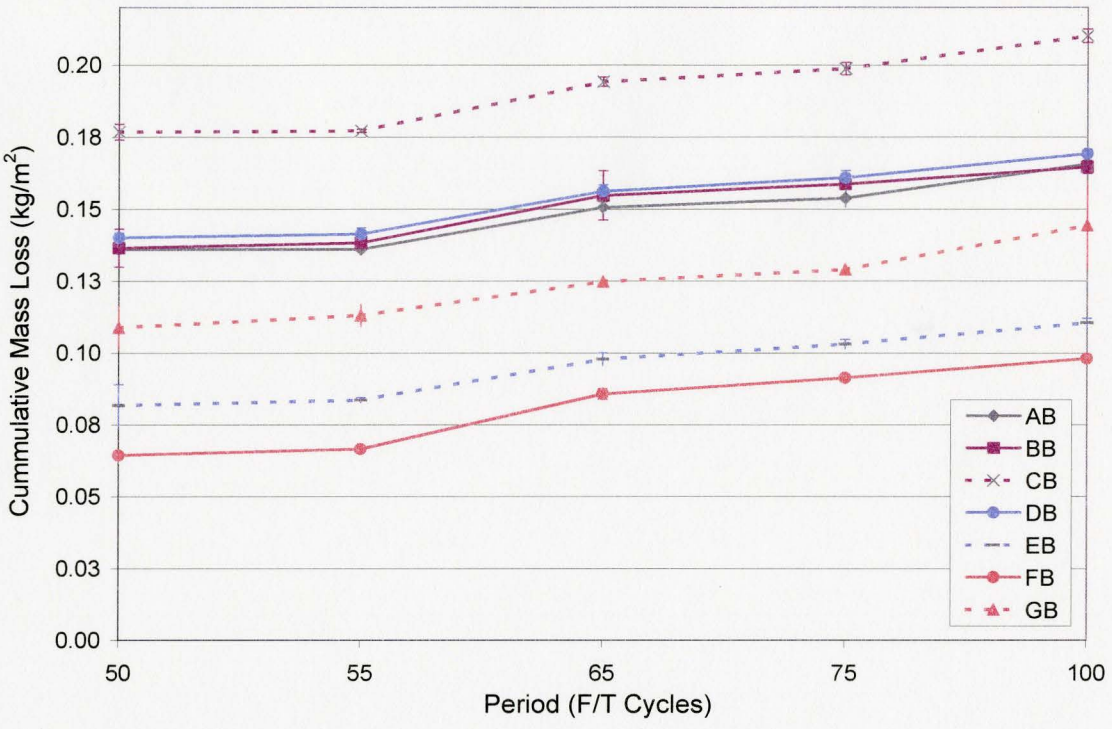

Figure 5.29 Cumulative Mass Loss, 3% NaCl Solution, Specimens A-G After 100 Cycles

A statistical analysis of the final percentage mass loss values for the specimens, Figure 5.31, confirms that the variance for the specimens could be considered equal in nearly all cases. A comparison of the mass loss of the control specimens A and L resulted in no statistically significant difference between the two in terms of total percentage mass loss. Despite what seems to be a pattern of increased mass loss for specimens C and D, and a decrease in mass loss for specimens E, F and G, there was no statistically significant difference at 95% confidence between the control specimen and the specimens containing waste glass.

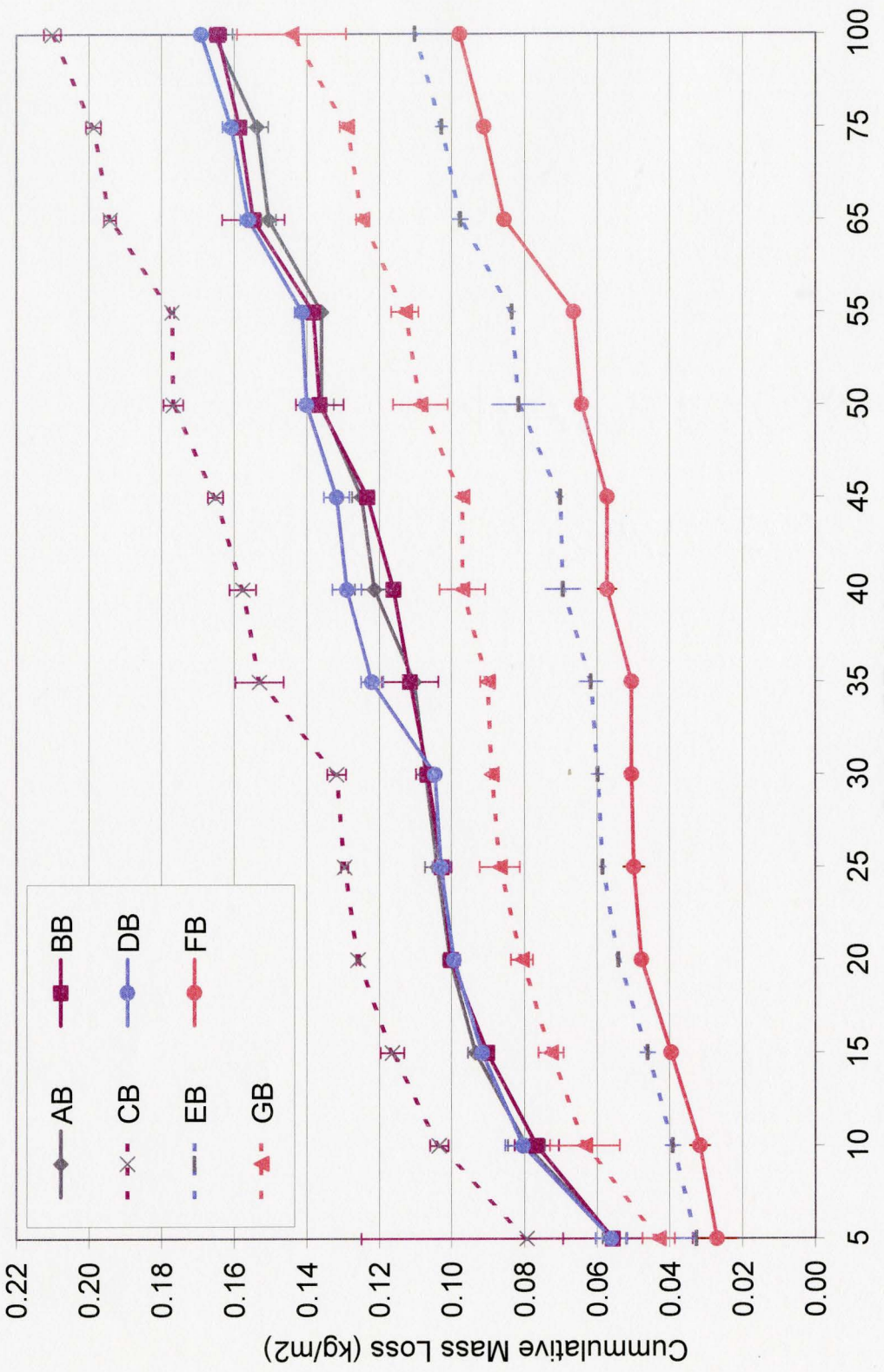

Figure 5.30 Cumulative Mass Loss in 3% NaCl Solution due to F/T Cycles

Due to the similarity in mass loss of the control specimens A and L, it is possible to look at specimen L in order to gain more incite into the performance of the specimens containing waste glass. When compared to control specimen L, there was a slight statistically significant decrease in the total mass loss for specimens E and F, containing 10% fine and 15% coarse waste glass, respectively. Specimen E has an average mass loss 47% lower than the control specimen L, while specimen F has an average mass loss 52% lower than the control specimen L.

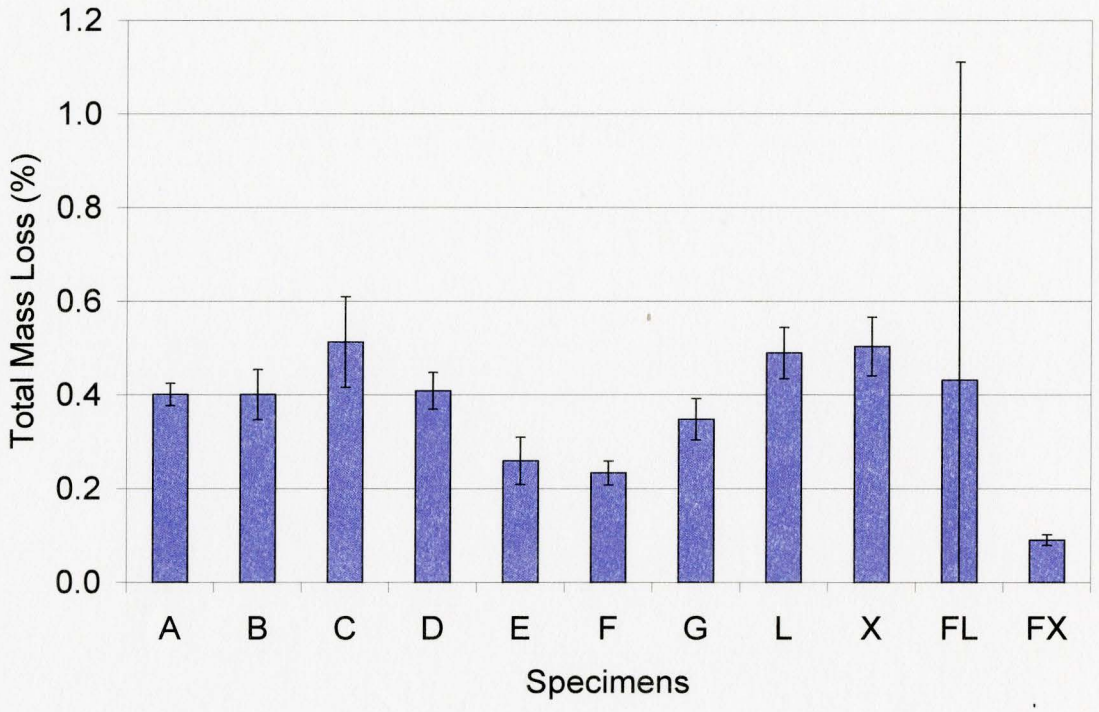

Figure 5.31 Total Mass Loss for All Specimens Tested in 3% NaCl Solution

5.6.4 Specimens L, X, FL, and FX in 3% Sodium Chloride Solution

The cumulative mass loss for specimens L, X, FL, and FX in the first 50 cycles of freeze-thaw testing is presented in Figure 5.32. Similar to the results of specimens A to

G, there is a linear trend in the cumulative mass loss. Initially, the mass loss is below that of the small scale specimens A to G, with the mass loss of the full scale specimens FL and FX being lower than average. The rate of mass loss for the small specimens, L, and X, was consistent and comparable. Although the rate of mass loss in specimens FL and FX is comparable; there was an increased mass loss in the laboratory fired specimens in the first 15 cycles of testing.

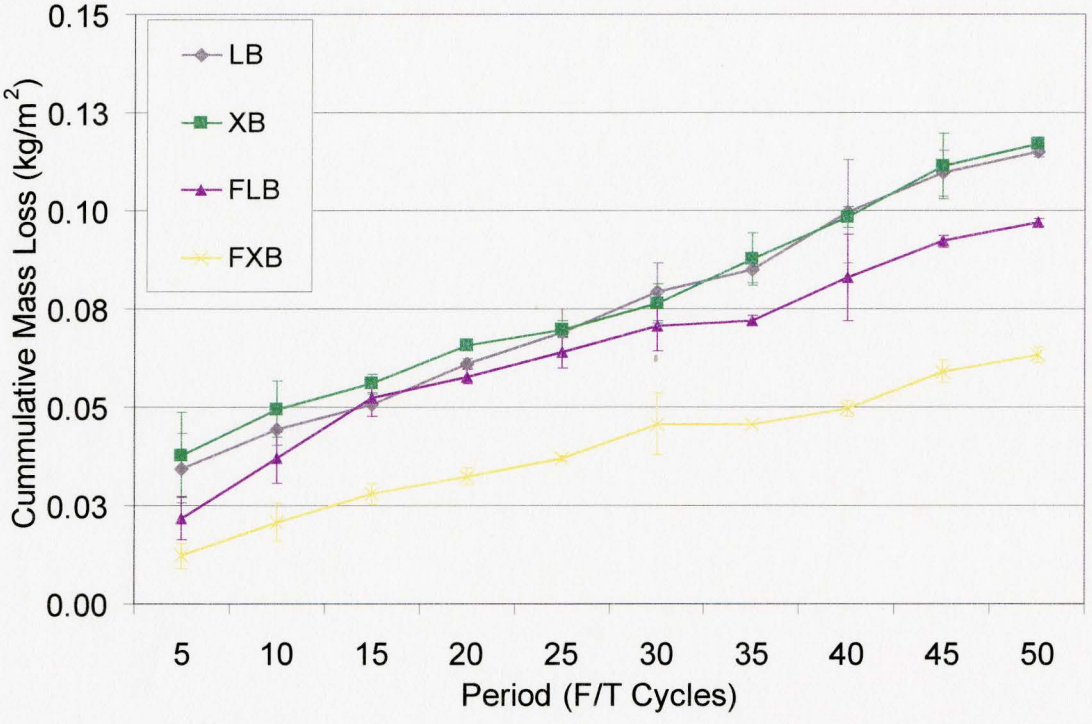

Figure 5.32 Cumulative Mass Loss in 3% NaCl Solution After 50 F/T Cycles

Figure 5.33 Specimen FL20 Flawed Edge After 10 F/T Cycles

The observed increase in mass loss for specimens FL was most likely due to the production flaw on the surface of specimen L20. The flaw on the edge of the specimen seen in Figure 5.33 was caused when the specimen contacted the grated metal floor of the production facility while still green, before being dried and fired. Initially this flaw seemed inconsequential due to its location on the untested surface of the specimen; however, it became evident within the first 10 testing cycles that mass was being lost from this location at an increased rate relative to the other specimens. This mass loss only slightly altered the results in the first 50 cycles, and when the values of the mass loss for specimen FL20 were removed, the difference in cumulative mass loss was not significant. As described for the specimens tested in deionized water, during the initial testing cycles, the decorative surface sand applied in the plant production process was loosened from the

testing surface, causing an initial increase in the mass loss. In the final 50 cycles of testing, the rate of mass loss for specimens L, X, and FX decreased rapidly, Figure 5.34. The cumulative mass loss for specimens L and X was very similar, while the mass loss for specimen FX was lower than most tested specimens at 0.08kg/m^2.

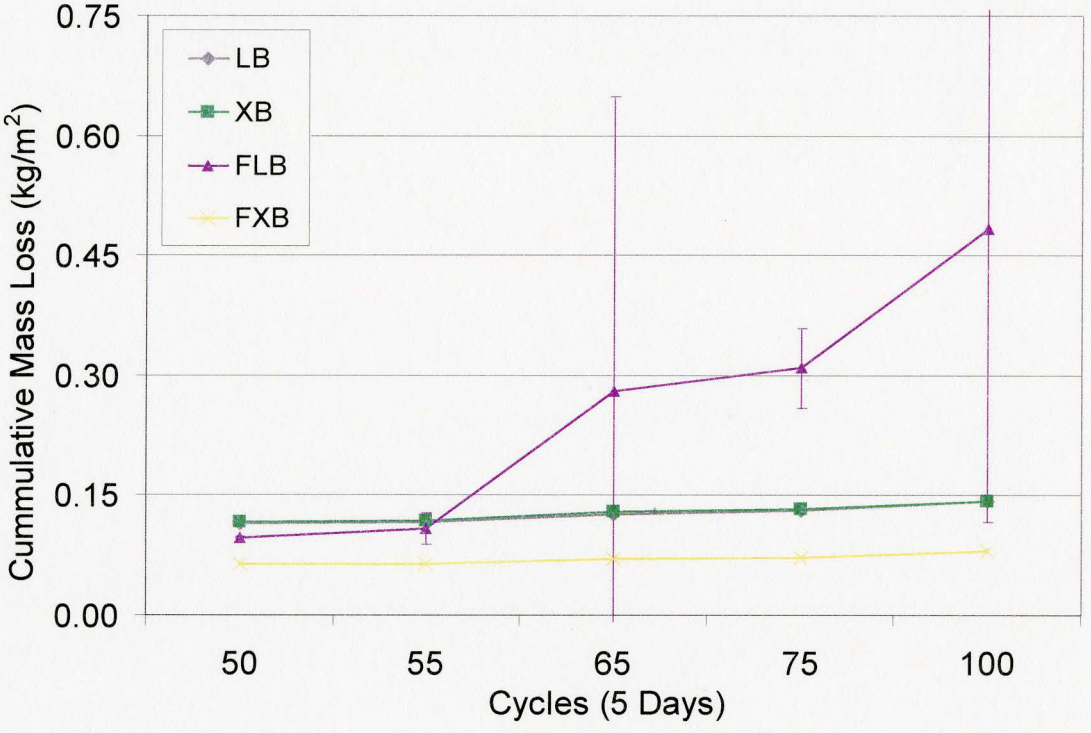

Figure 5.34 Cumulative Mass Loss in 3% NaCl Solution After 100 F/T Cycles

The cumulative mass loss for specimens FL increased dramatically in the final 50 cycles of freeze-thaw testing. At the completion of 65 cycles of testing, the mass loss associated with specimen FL20 alone was more than one hundred times greater than any of the other four FL specimens being tested. As discussed above, the majority of the mass

loss was attributed to the edge flaw of the specimen, Figure 5.35. This result is also evident in the increased variation in Figure 5.34. Measurements at the completion of cycle 100 showed another jump in cumulative mass loss for specimen FL, where the lost mass was again observed to occur at the point of the surface flaw. By including the results of the flawed specimen, the cumulative mass loss for specimens FL was unrepresentative of the performance of the majority of the specimens in that grouping. As a result, the mass loss of specimen FL20 was removed from the calculations for the statistical analysis.

Figure 5.35 Specimen FL20 Flawed Edge After 65 F/T Cycles

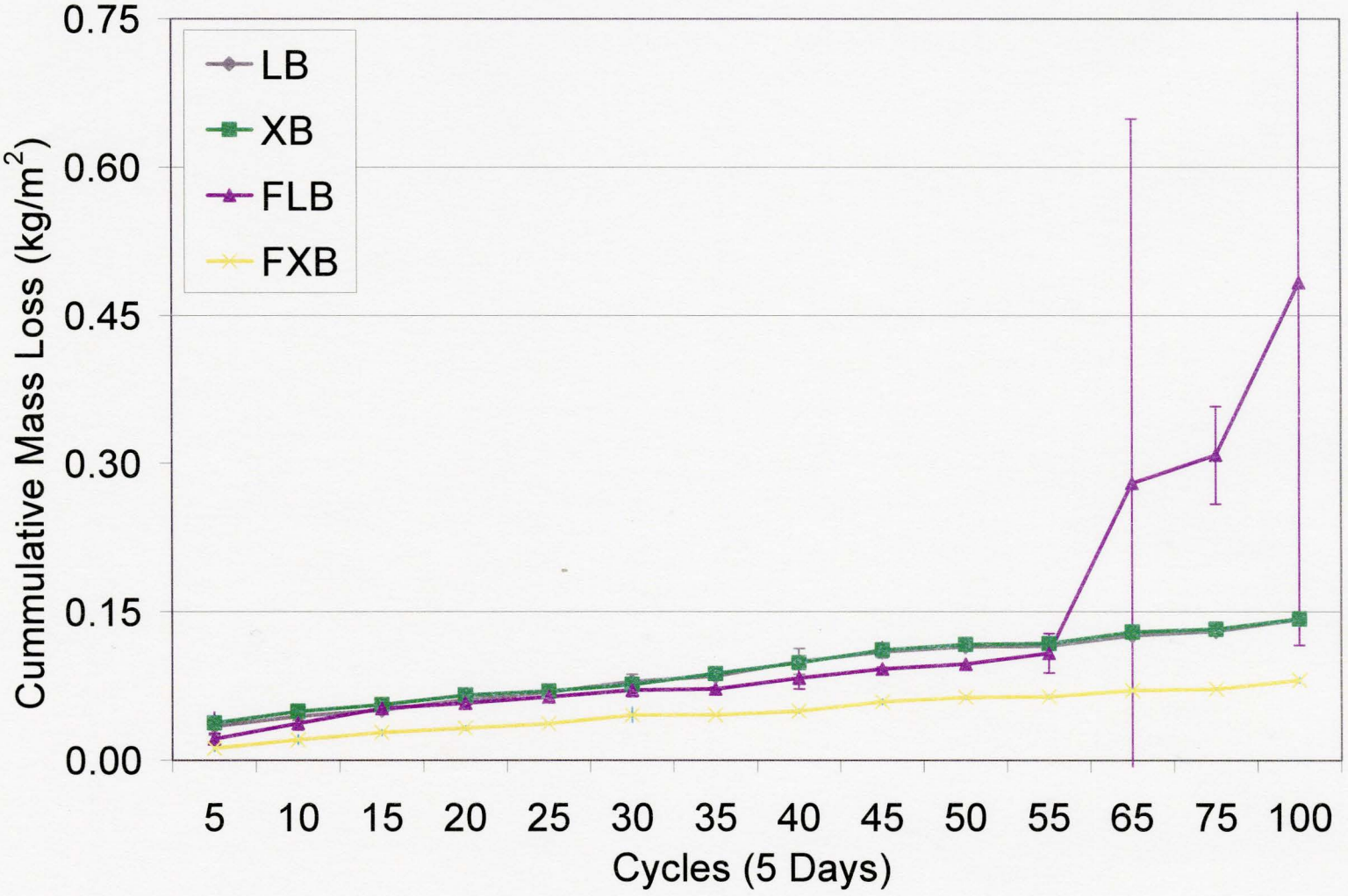

Figure 5.36 Cumulative Mass Loss in 3% NaCl Solution for Various Production Methods After 100 F/T Cycles

At the conclusion of 100 freeze-thaw cycles, specimens L, X, FL, and FX were nearly pristine in their appearance, and the integrity of the finished surface was maintained as judged visually and with handling. No material was observed to come loose from the specimens. The complete cumulative mass loss results for 100 cycles are presented in Figure 5.36.

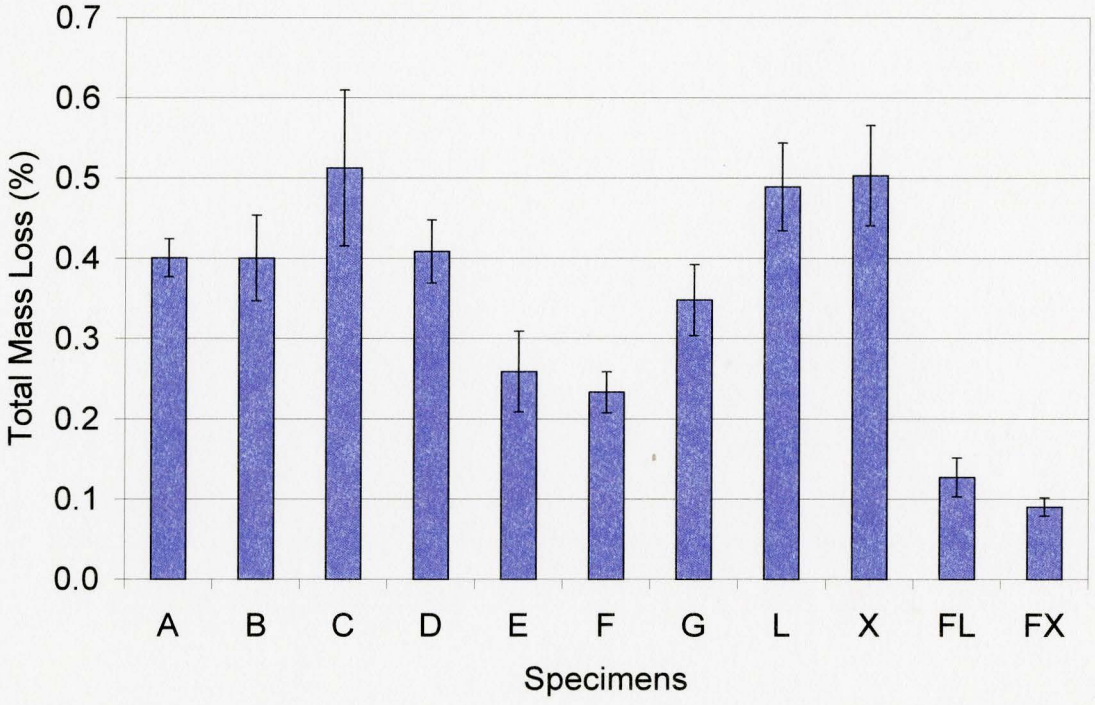

Figure 5.37 Mass Loss for Specimens in 3% NaCl Solution Without FL20B After 100 F/T Cycles

The statistical analysis was performed using the total average percentage mass loss excluding specimen FL20B. Due to the relatively low variance, in all cases the variance of the control specimen, L and the remaining specimens could be considered equal, except for the variance of specimens FX. From Figure 5.37, a comparison of the

variance intervals calculated for L and FX indicates that there is a decrease in mass loss due to freeze-thaw testing for specimen FX; however, this cannot be stated with any statistical certainty. Due to the similarity of specimens A and L discussed previously, a comparison using specimen A may provide more insight. This comparison indicates that there is a statistically significant difference in the mass loss of specimens A and FX, where the total percentage mass loss of FX is up to 77% lower than that of specimen A. The mass loss of specimens X tested in 3% sodium chloride was comparable to the control specimen, while specimen FL achieved a mass loss statistically lower than that of the control specimen by up to 74%.

5.6.5 Summary of Specimen Performance

According to CAN/CSA-A82.1-M87, requirements for freezing and thawing resistance of a brick are that no more than 0.5% dry mass loss of an individual brick, as well as no breakage occur after 50 cycles of freeze-thaw testing (CSA, 1987). CSA Standard CAN3-A82.2-M78 specifies that the testing of freeze-thaw durability be stopped for a specimen that appears to have lost more than 3% of its original mass as judged by visual inspection or has broken in a 50-cycle test (CSA, 1978). The test performed in this study was 100 cycles in length in order to provide additional information on extended performance, as well as to compare the results of specimens tested in NaCl solution with the performance criteria of ASTM C 1262-98.

A summary of the performance of the specimens which were considered to have failed at the conclusion of the freeze-thaw testing are provided in Table 5.1. The total

average percentage mass loss, with respect to the final dry mass of each specimen, is presented for the 100 test cycles. Within the first 50 cycles of testing, the rate of failure was very low; however, in the final 50 cycles of testing, the rate of failure increased dramatically, especially in the final 25 cycles. Of the 10 laboratory fired specimens tested in deionized water, including laboratory scale and plant scale, all 10 failed according to the requirements of CSA A82.2. Several of the specimens containing little or no waste glass also failed within 100 cycles of testing, as well as two of specimens D, which as discussed earlier, suffered unexpected cracking and splitting.

Table 5.1 Summary of Failed Specimens

Specimen	% Waste Glass	Waste Glass Particle Size	Extrusion Location	Firing Location	% Mass Loss After 100 Cycles
A4A	0	-	Lab	Lab	2.83
A6A	0	-	Lab	Lab	2.44
B4A	5	Coarse	Lab	Lab	1.32
B5A	5	Coarse	Lab	Lab	3.84
C6B	5	Fine	Lab	Lab	0.62
D4A	10	Coarse	Lab	Lab	0.57
D5A	10	Coarse	Lab	Lab	23.59
L6A	0	-	Lab	Lab	42.00
L2A	0	-	Lab	Lab	80.57
L29A	0	-	Lab	Lab	39.29
L26A	0	-	Lab	Lab	15.92
L18A	0	-	Lab	Lab	18.47
FX14A	0	-	Plant	Plant	3.92
FL20A	0	-	Plant	Lab	3.47
FL7A	0	-	Plant	Lab	3.55
FL14A	0	-	Plant	Lab	4.20
FL5A	0	-	Plant	Lab	4.08
FL2A	0	-	Plant	Lab	5.87

5.7 Scanning Electron Microscopy of Specimens A to G

Scanning electron microscope (SEM) images of the specimens were created with the assistance of the McMaster University Brockhouse Institute for Materials Research. For all images, the stage tilt was set at 15 degrees, the beam energy was 20 kV, and the spot size of the beam was 50ηm. Specimens were prepared by obtaining a sample, the size of which was approximately 2.5cm square. The surface of interest was the cut surface farthest from the fired edge. The specimens were not polished in order to preserve the integrity of surface pores, and the viewed surface was prepared using a sputtering machine to apply a very thin gold sputter coat. The measured particle sizes of the crushed shale used for specimen preparation ranged from approximately 10μm to 100μm, while waste glass particle sizes ranged from 45μm to 300μm. Exploratory images were obtained for each specimen at a magnification of 25.4 times using the grid shown in Figure 5.38 as a location reference. Figures 5.39 to 5.44 show images obtained for specimens A, B, C, E, F, and G, respectively.

1	4	7
2	5	8
3	6	9

Figure 5.38 Quadrants for Specimen Exploration

Visible in Figure 5.39 are vertical saw marks along the surface of specimen A, created when the specimen was cut to the required size for analysis. A particle within the brick, the longest dimension of which is approximately 1.79 mm, is also clearly visible in the same vertical plane as the saw marks. In general, the surface appears to have some craters along the saw cut portion, but no other distinguishing surface properties.

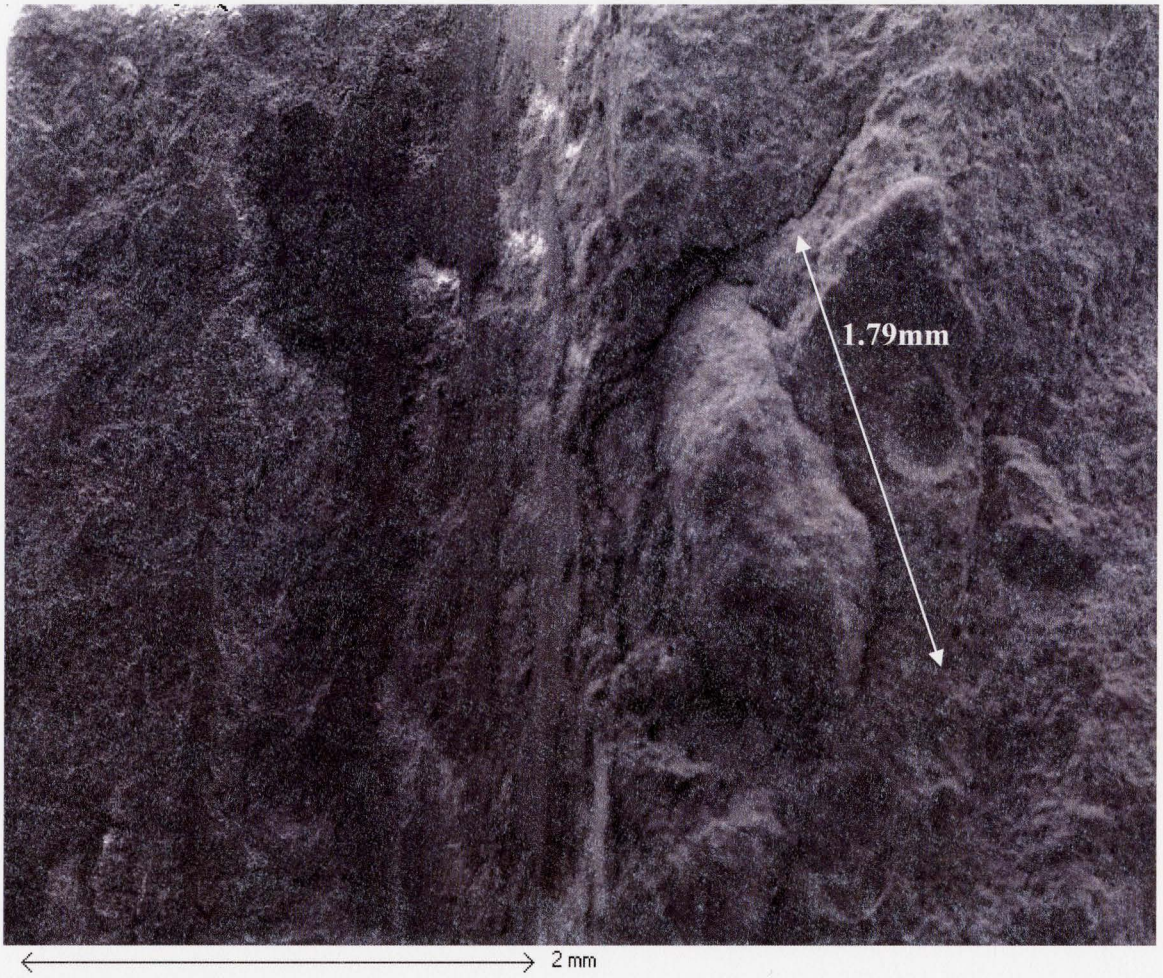

Figure 5.39 Specimen A at 25.4 Times Magnification

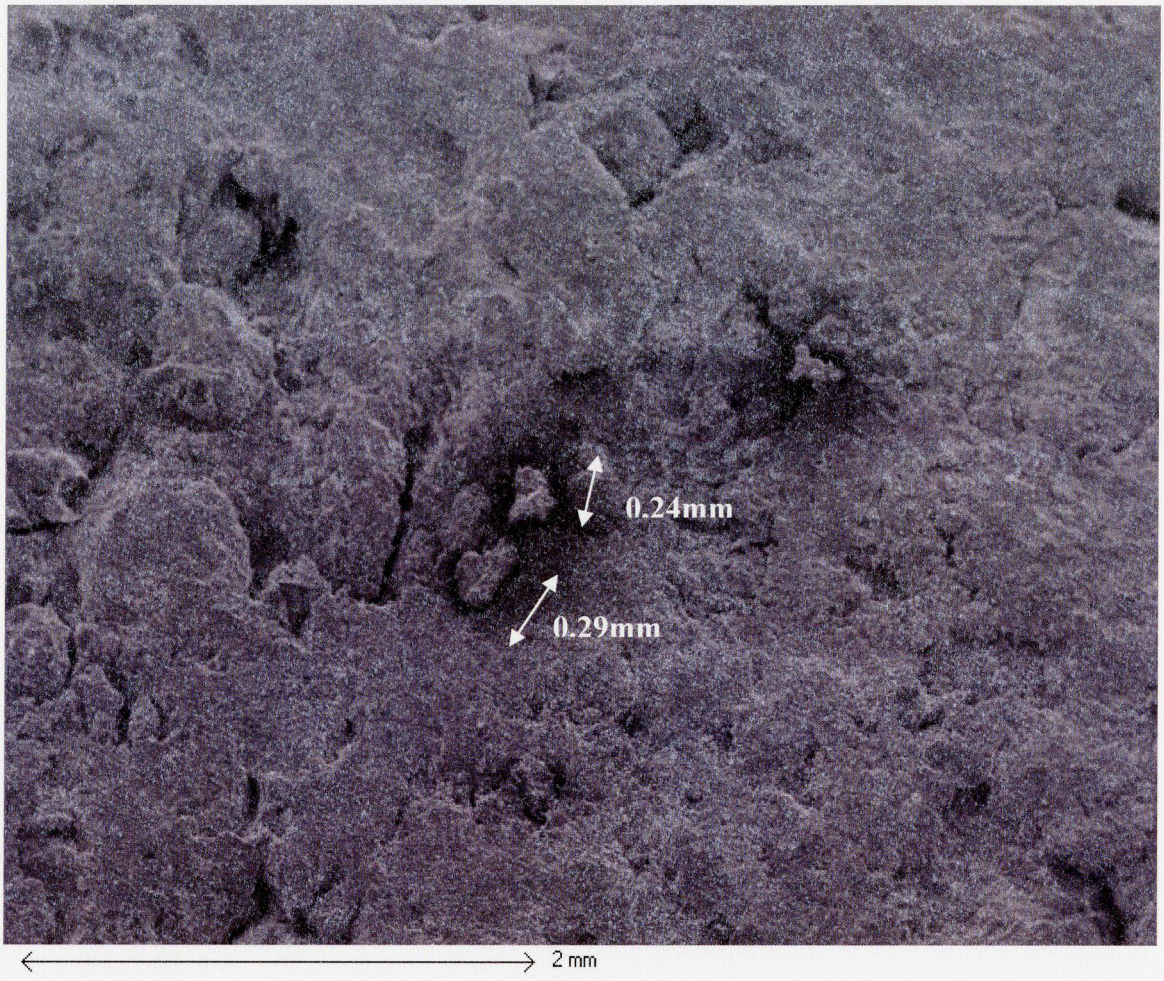

Figure 5.40 Specimen B at 25.4 Times Magnification

The surface of specimen B, Figure 5.40, has some visible particles which are approximately 0.29mm and 0.24mm at their longest dimension. These particles could be waste glass or clay particles that were not completely sintered, or may be the result of the cutting process.

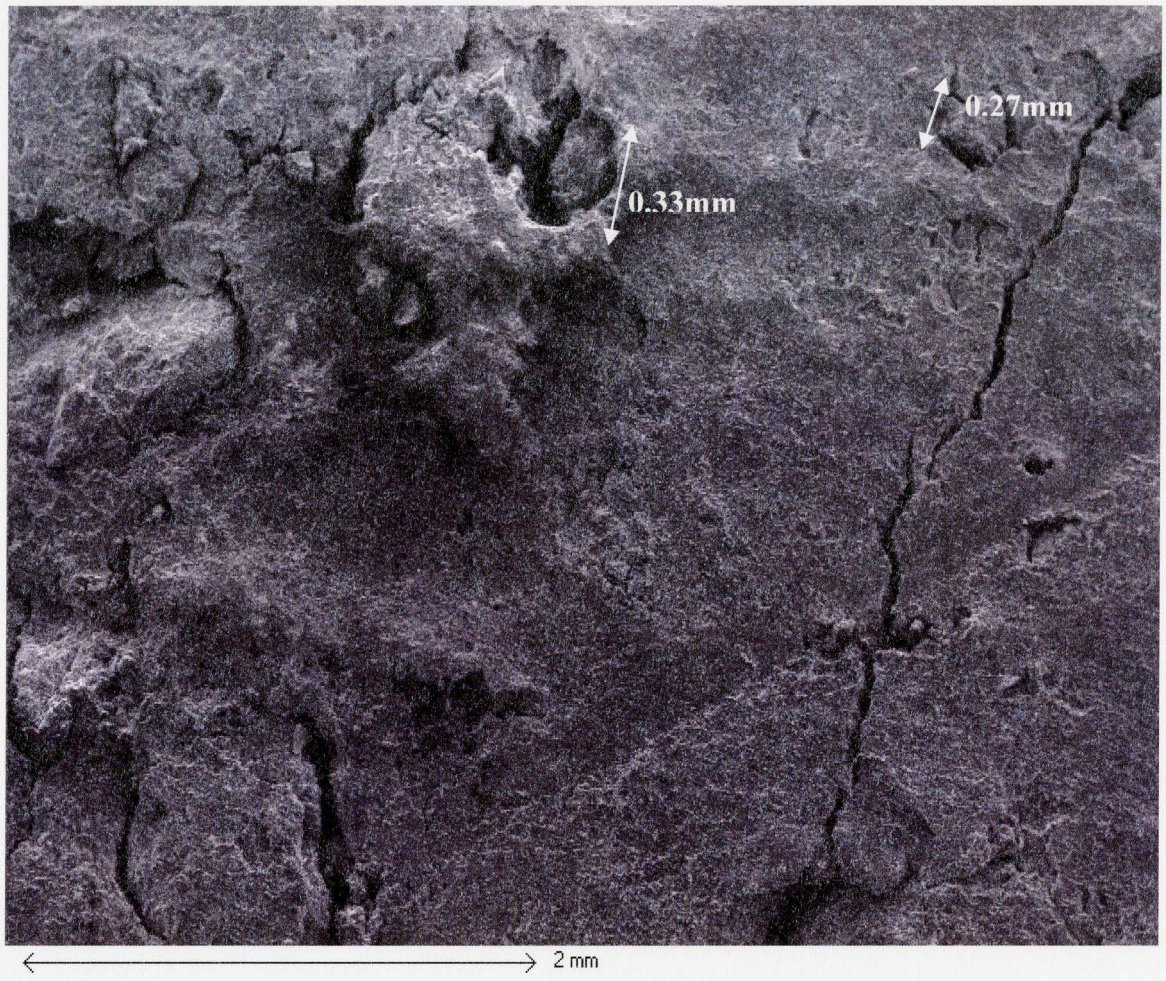

Figure 5.41 Specimen C at 25.4 Times Magnification

On the surface of specimen C, Figure 5.41, a crack is visible, which was caused during sample preparation as the specimens were thinned. Similar to specimen B, some surface particles are visible, the largest of which is approximately 0.33mm, and is therefore most likely an incompletely sintered particle of crushed shale, or a particle of brick dislodged during cutting.

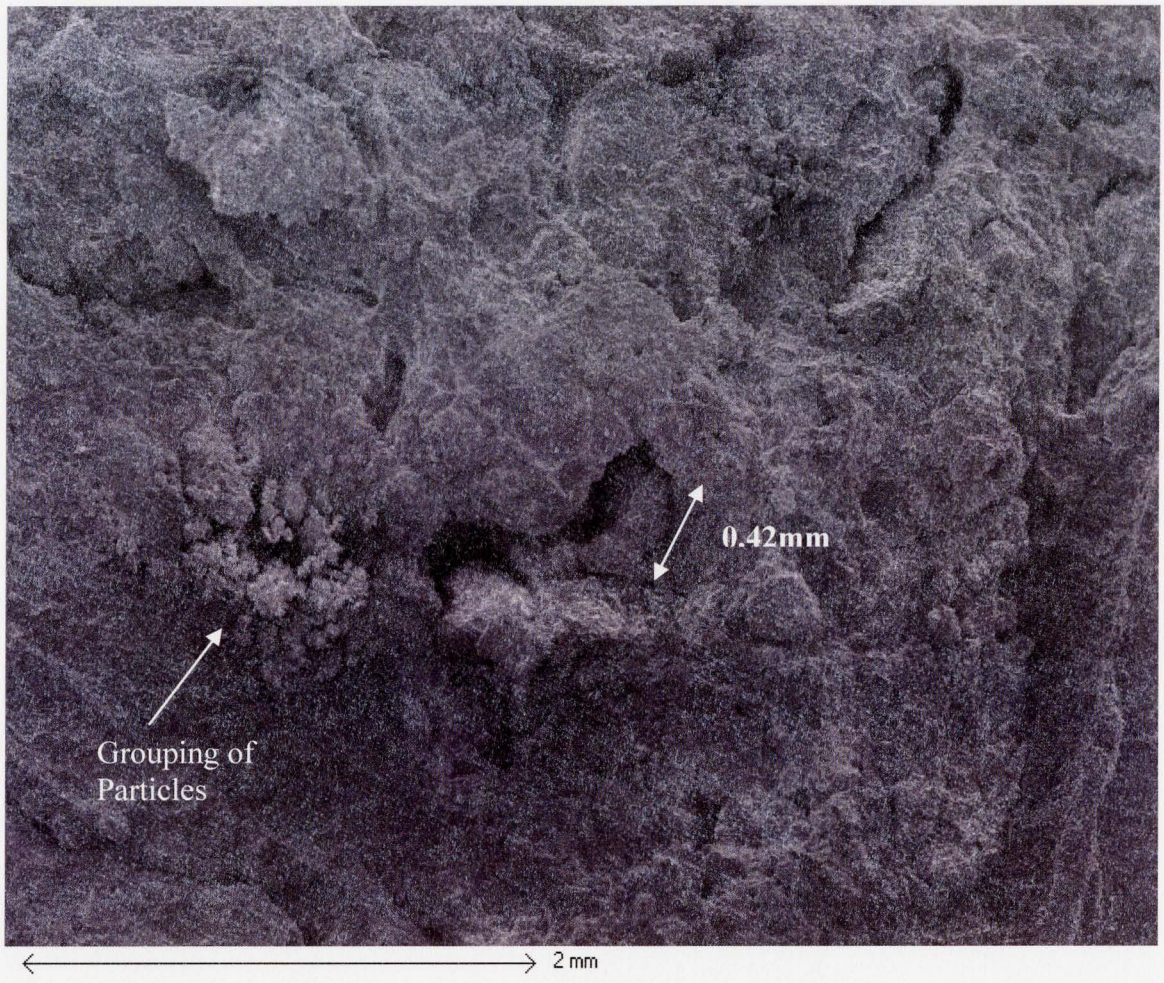

Figure 5.42 Specimen E at 25.4 Times Magnification

In the section of surface of specimen E shown in Figure 5.42, some of the same types of particles seen in specimens B and C are visible near the center of the image, where the marked particle has a length of approximately 0.42mm. A grouping of smaller particles can be seen and are marked in Figure 5.42. The size of this grouping of particles indicates that they may be a group of particles of waste glass, or else a small crystalline formation of vitrified material.

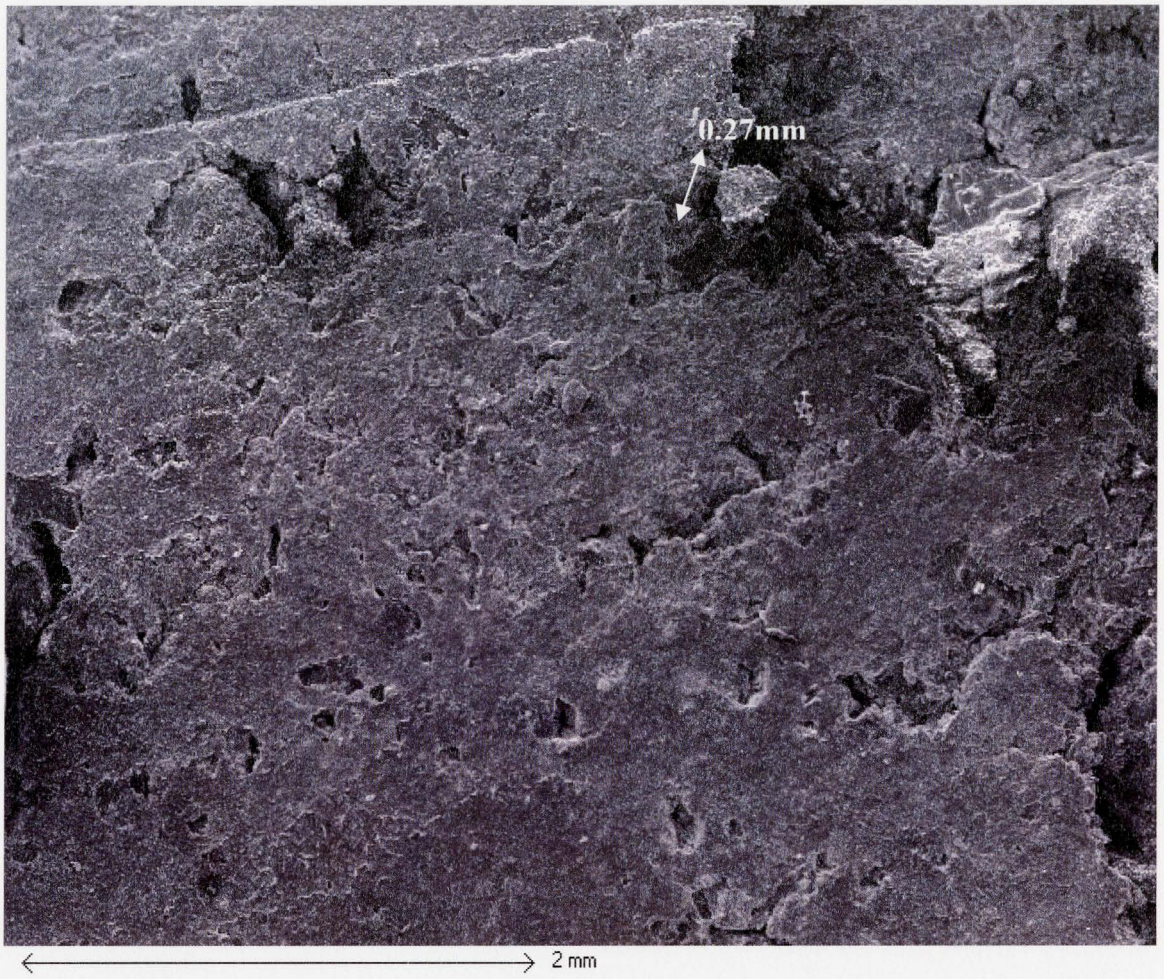

Figure 5.43 Specimen F at 25.4 Times Magnification

Specimen F is shown in Figure 5.43, where an overall less granular surface is observed, with shallow pores throughout. A small particle near the top of the image is similar to those observed for previous specimens, measuring 0.27mm.

Figure 5.44 Specimen G at 25.4 Times Magnification

On the surface of specimen G, Figure 5.44, no particles are observed, only some small craters and marks from cutting which appear horizontally along the bottom of the image. From the images presented in Figures 5.39 to 5.44, it is apparent that the SEM is not able to clearly resolve grain boundaries on an unpolished specimen surface. The next set of images was developed at a magnification of 680 times. At this magnification, small

particles of crushed shale, as well as some of the glass, particles should be within the visible range, up to a maximum length of approximately 150μm.

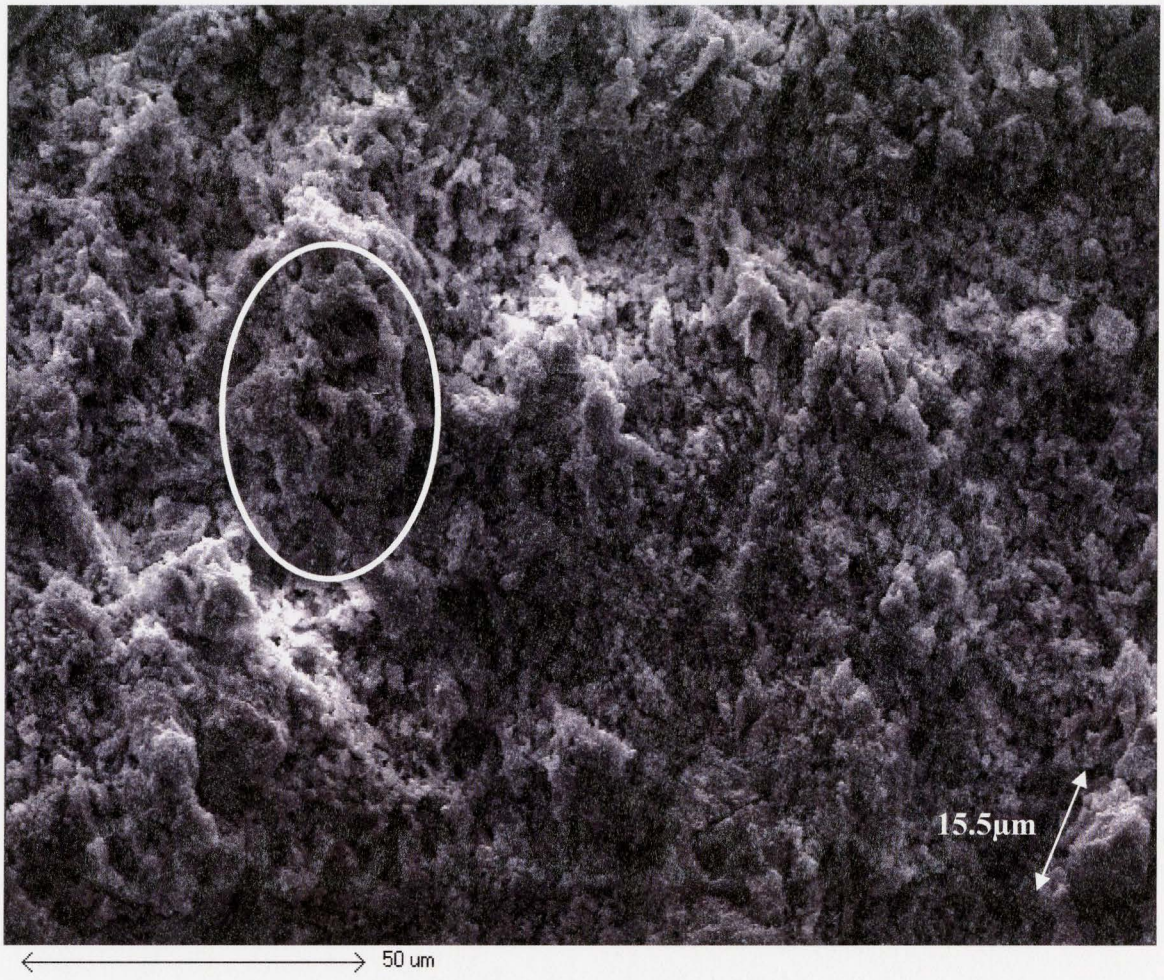

Figure 5.45 Specimen A at 680 Times Magnification

In Figure 5.45, specimen A exhibits signs of vitrification, where pores within the circled section are elongated in shape, and a smooth, glassy looking matrix surrounds the pores. Although some particles are evident, the sizes of which range from 10μm to

15.6μm along their longest dimension, they are too small to be clearly identified as individual particles of crushed shale. The surface appears to have a generally granular appearance.

In Figure 5.46, specimen B can be seen at 680 times magnification in two quadrants (Figure 5.38). The first image appears to be littered with particles that are approximately 2μm to 10μm in length. These particles are too small to be either waste glass or crushed shale, and so they are most likely the result of phase changes within the phyllosilicates present in the crushed shale. Larger particles, approximately 20μm in length are also apparent, and as indicated in the figure, are likely particles of crushed shale. Despite the surface particles, there is evidence of vitrification in the smooth, glassy appearance of the underlying surface, and the elongated shape of pores.

The second image in Figure 5.46 shows in greater detail the achieved vitrification and several clear pores of various sizes. Within the smooth surface, the outlines of particles ranging in size from less than 10μm to approximately 13μm are visible. These apparent particles may also be the result of the flattening and vitrification of the layered phyllosilicates within a much larger particle of crushed shale.

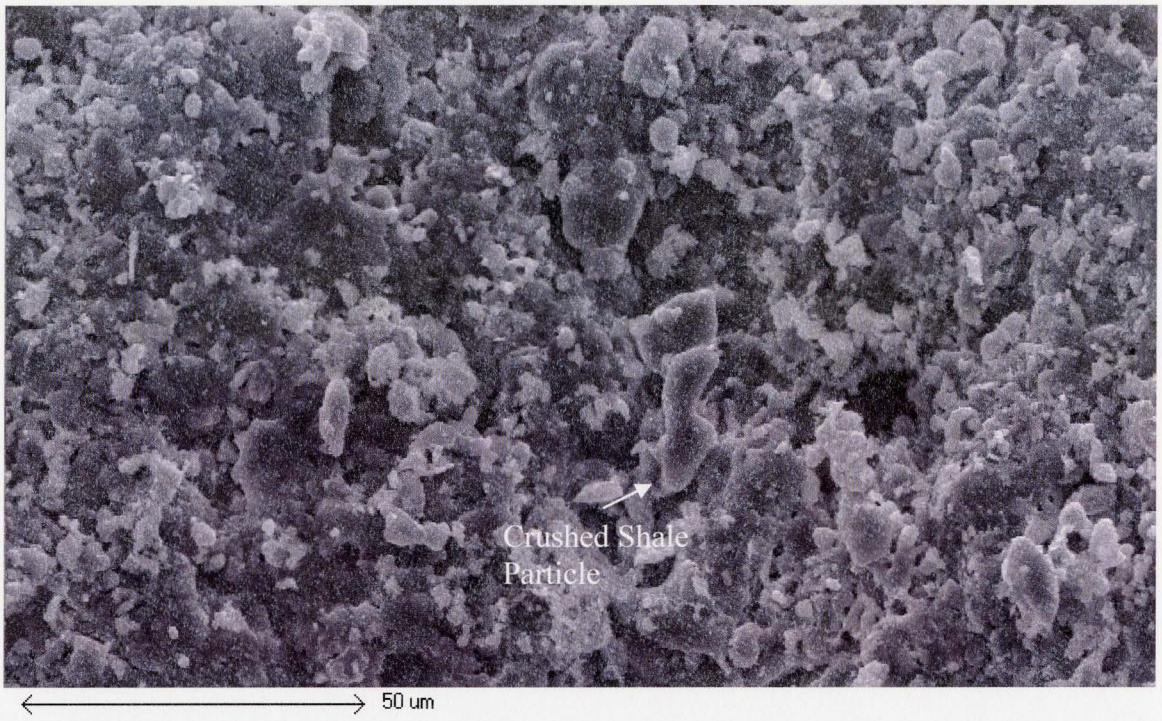

(a)

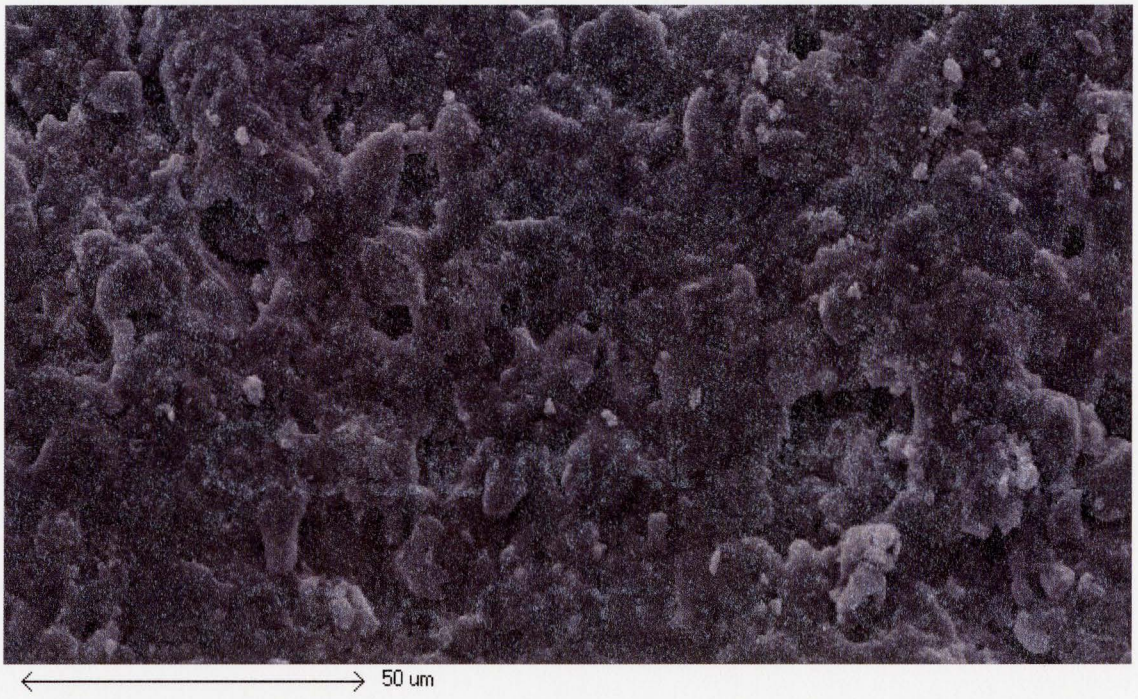

(b)

Figure 5.46 Specimen B at 680 Times Magnification (a) Quadrant 5 (b) Quadrant 7

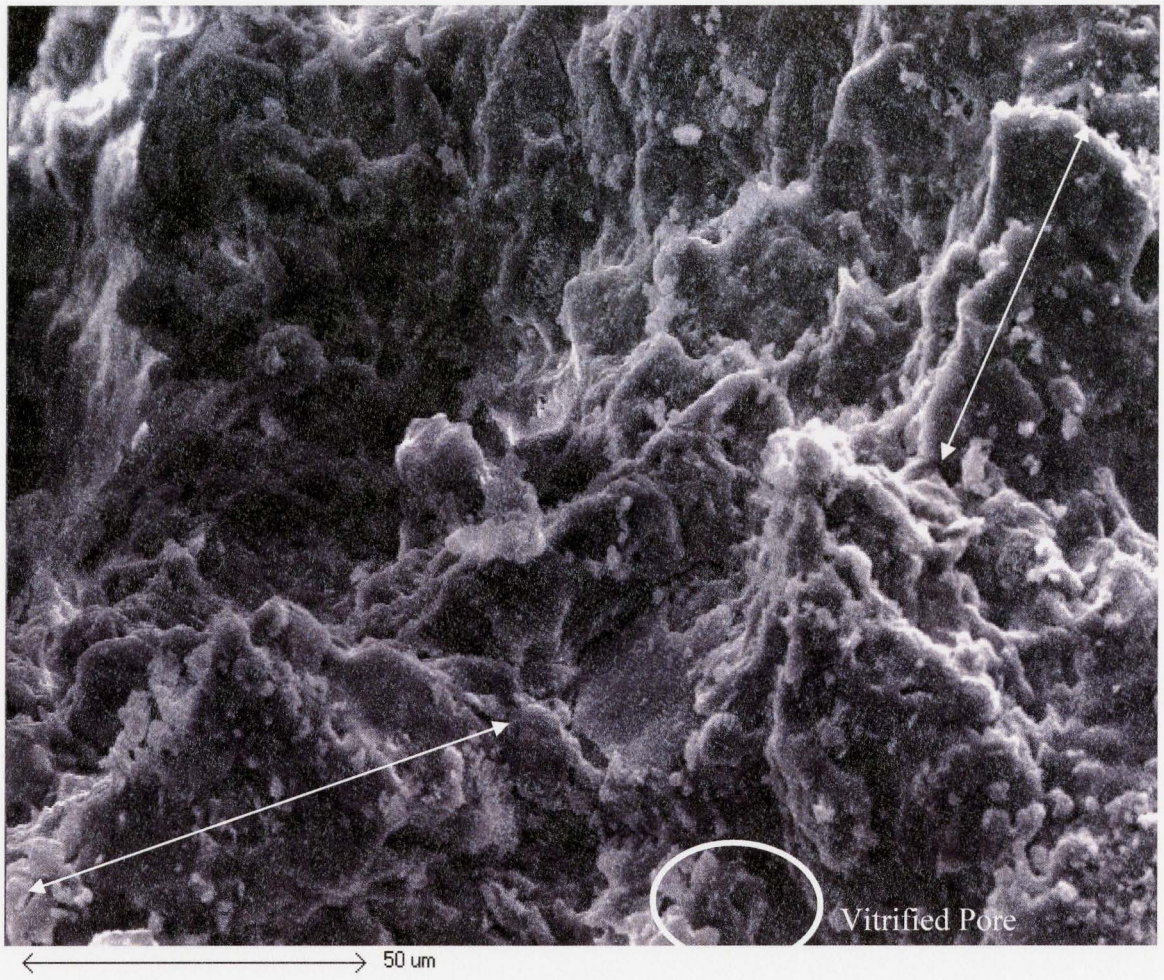

Figure 5.47 Specimen C at 680 Times Magnification, Quadrant 5

In Figure 5.47, specimen C is shown at 680 times magnification. The angle of this particular surface shows several large particles, indicated in the figure, the sizes of which are approximately 50μm. There is an extensive degree of vitrification as the matrix surfaces have a smooth, glassy finish and visible pores are elongated rather than angular.

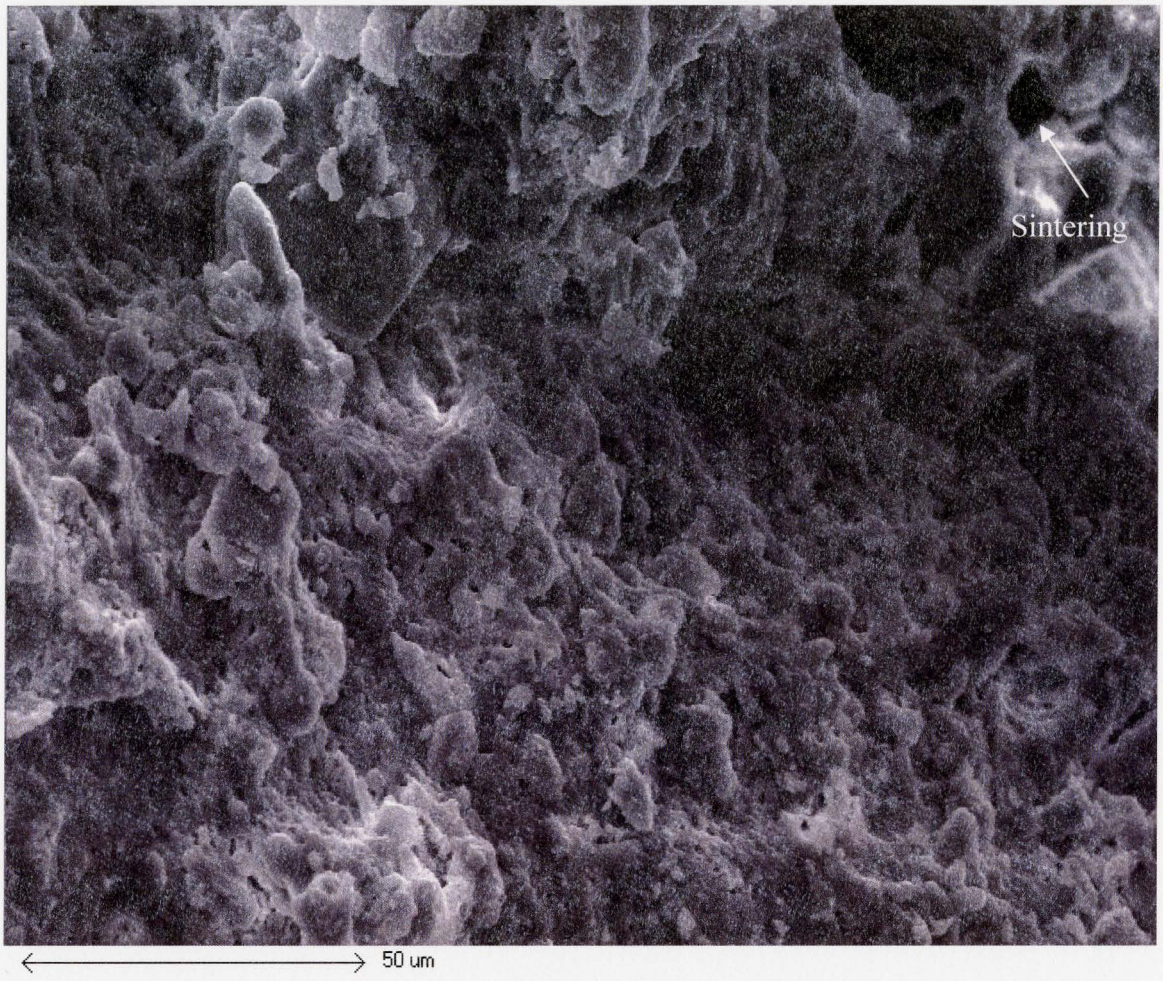

Figure 5.48 Specimen C at 680 Times Magnification, Quadrant 5

In Figure 5.48, again the surface allows larger particles to be observed. In the background where indicated, the first stage of sintering, known as bottlenecking (see Figure 2.1) can be seen between two adjacent and contacting particles, as well as the resulting pore, which is approximately 11μm in length. The remaining matrix appears well vitrified with small pores (1μm) throughout. In the top left corner, a particle, which appears to be slightly smaller than 50μm, is visible within the matrix. The smooth surface

and angled edge of this particle indicate that it is a fine particle of waste glass. Specimen E displays a slightly more layered matrix, Figure 5.49, with a crystalline structure of approximately 50μm visible in the image. This is most likely a particle of crushed shale which has changed phase during firing. Very few small pores are visible in the image and there seems to be a high level of vitrification.

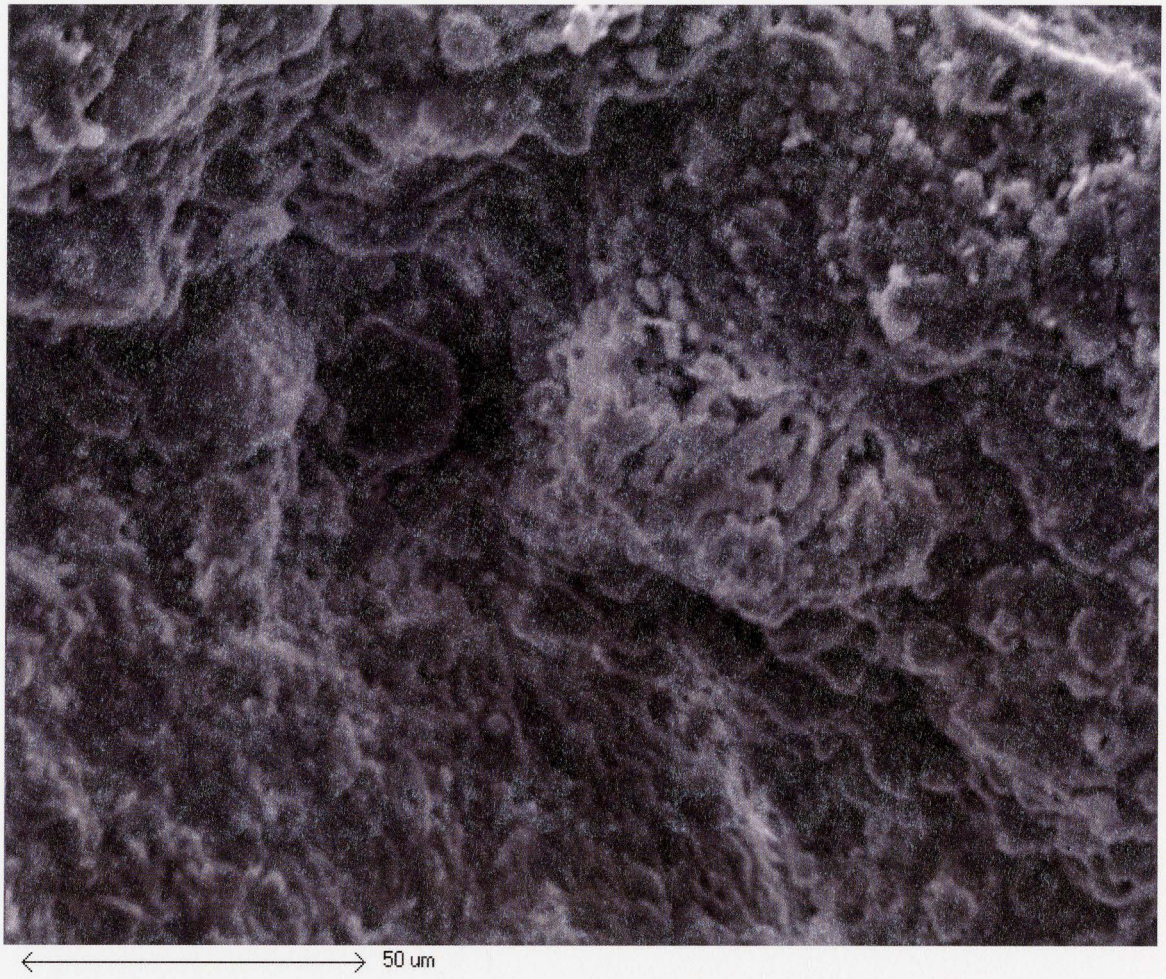

Figure 5.49 Specimen E at 680 Times Magnification

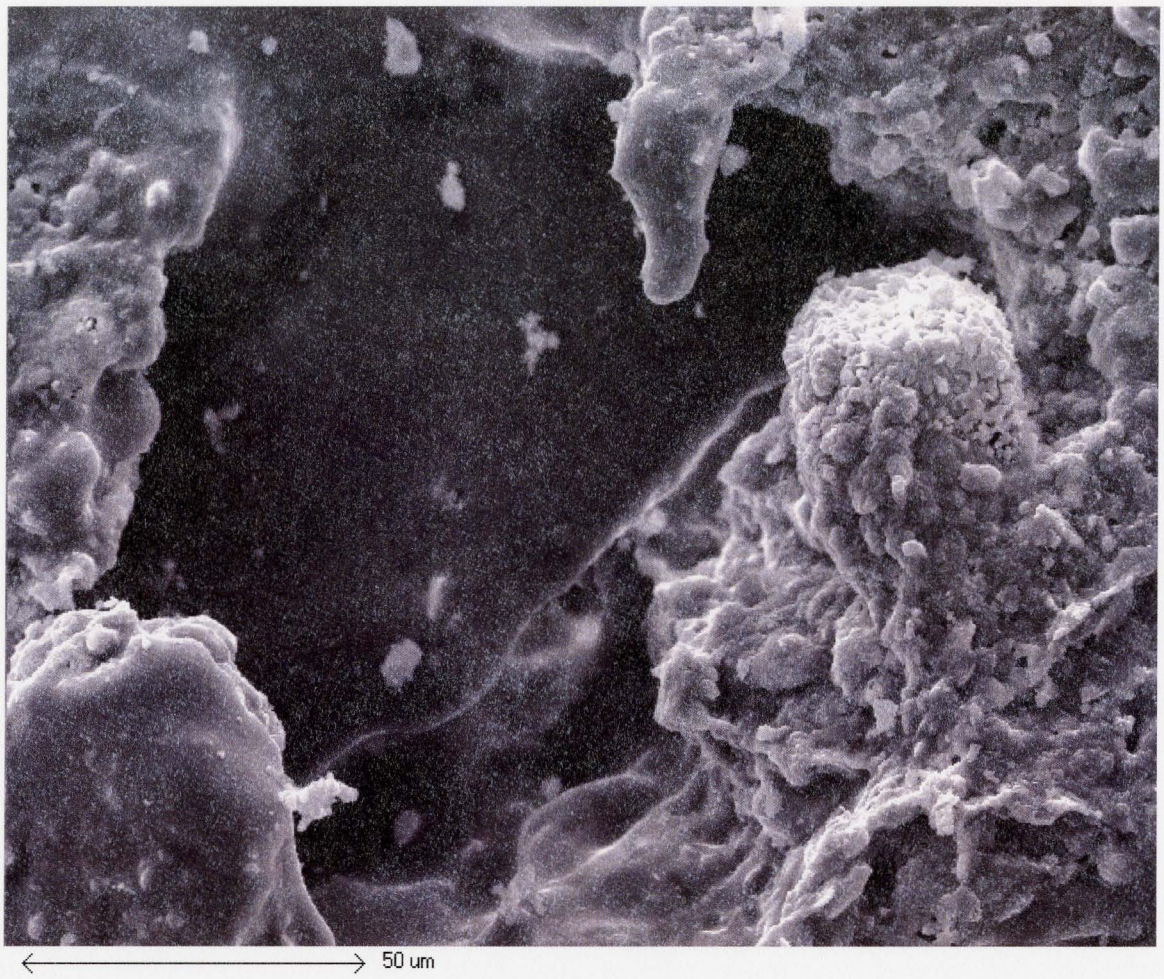

Figure 5.50 Specimen F at 680 Times Magnification, Quadrant 5

With 15% coarse waste glass addition, the first image of specimen F, Figure 5.50, shows a glass particle of size greater than 100μm within a large depression or pore. The very smooth, glassy appearance of the particle, as well as the increased level of vitrification and material flow at its bonded edges, leads to this conclusion that it is in fact a particle of waste glass. The remaining visible matrix consists of well vitrified crushed shale, with a crystalline formation. An image of specimen F in a nearby location, Figure

5.51, shows another waste glass particle surrounded by vitrified crushed shale. A close up view of the crystalline formation is shown in Figure 5.52. Several large pores can be seen within the waste glass particle, which may be the result of the escaping OH^- or CO_2 gasses. Similar to Figure 5.50, the vitrification in the surrounding crushed shale matrix appears to be influenced by increased flow from the glass particle due to the proximity of the particle and the increase in vitrification.

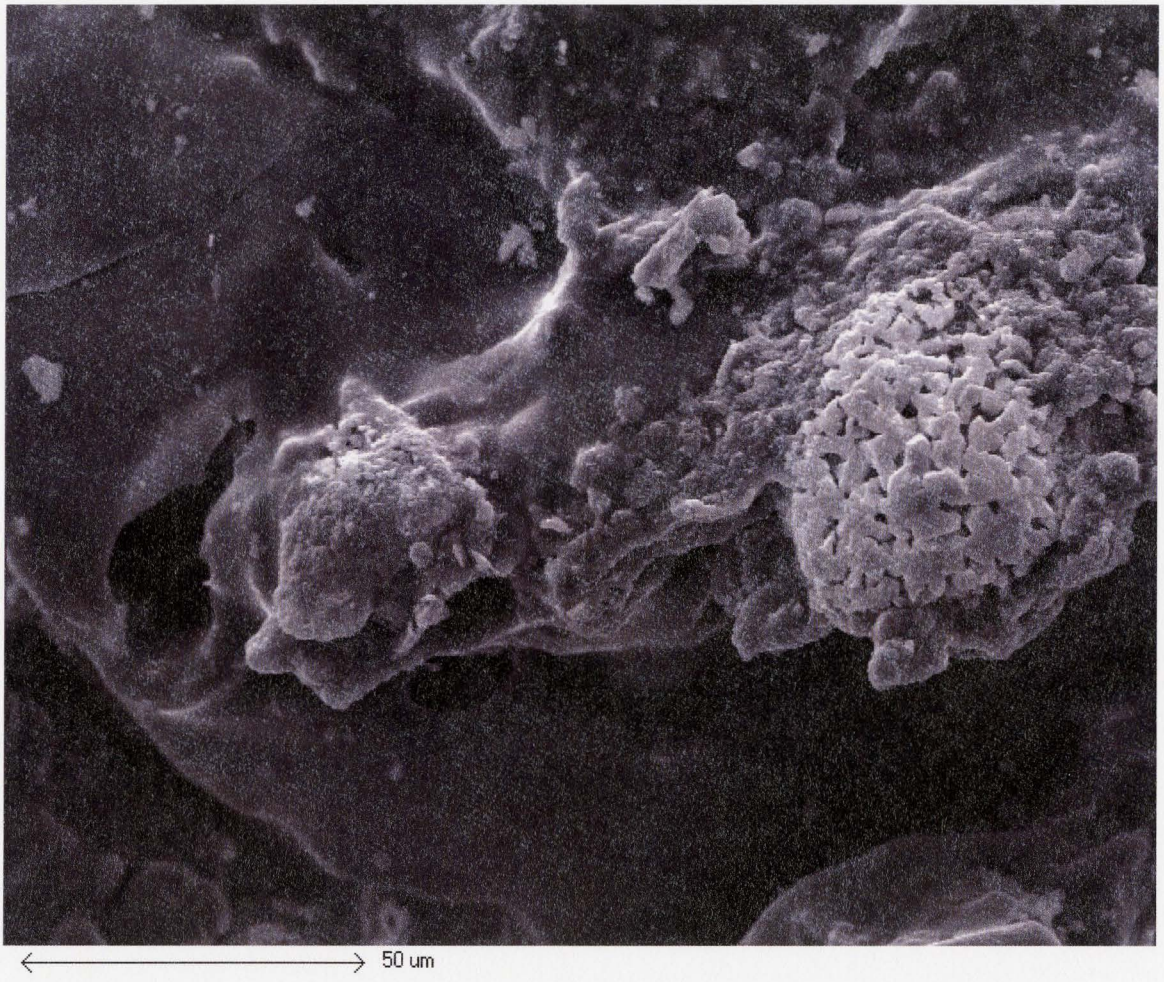

Figure 5.51 Specimen F at 680 Times Magnification, Quadrant 5

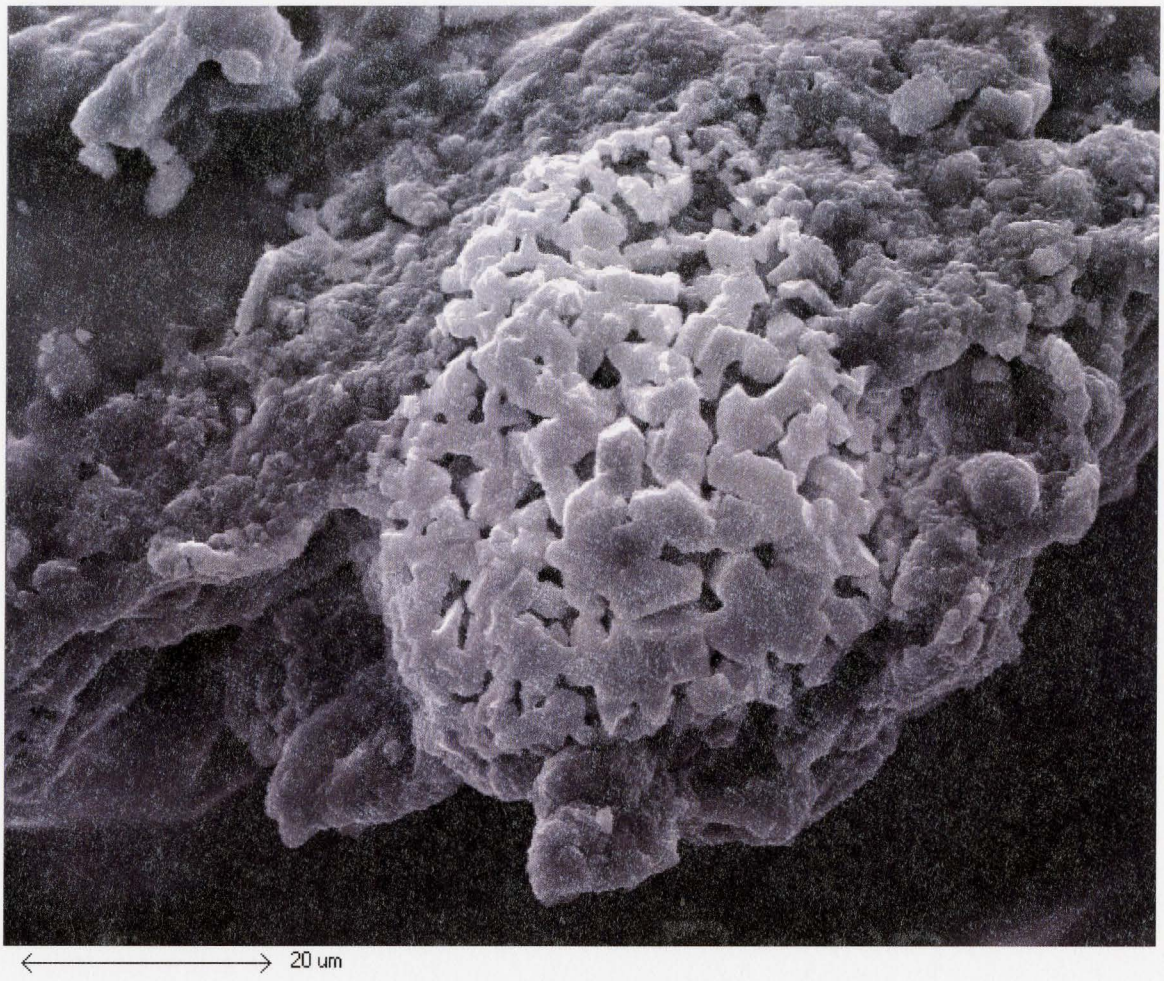

Figure 5.52 Close-Up View of Crystalline Structure, Specimen F

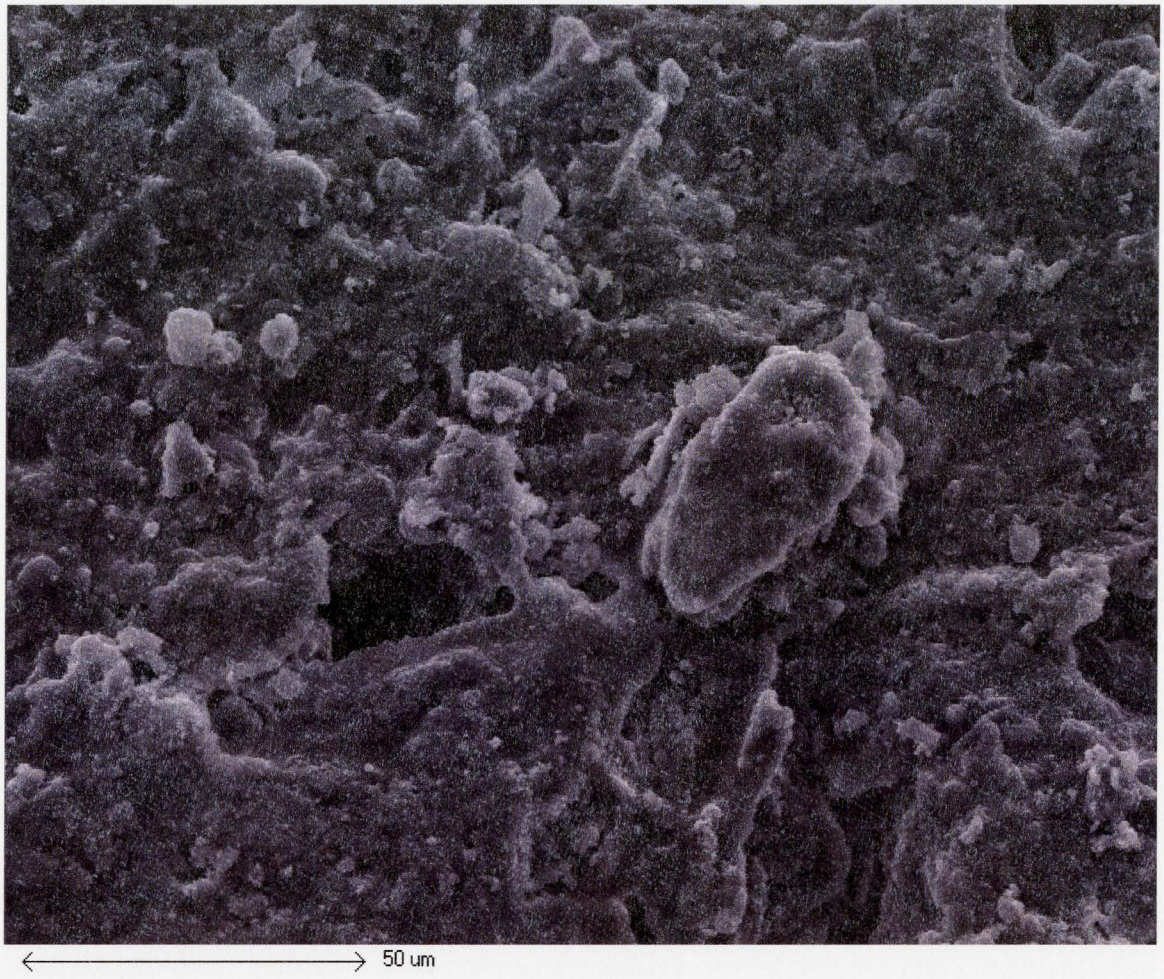

Figure 5.53 Specimen G at 680 Times Magnification, Quadrant 5

Specimen G, containing 15% fine waste glass, shows the same smooth matrix seen in specimens B and C, which contain 5% waste glass. In Figure 5.53, this smooth matrix is apparent as well as a variety of pore sizes, some bottlenecking, and at least one visible particle, the length of which is approximately 43μm. In Figure 5.54, the characteristic vitrification pattern associated with the presence of waste glass can be seen in the upper right of the image, where a particle of length 45μm demonstrates the

particular smooth finish. Again, high levels of vitrification are evident throughout, with extensive elongation of pores and clear bottlenecking.

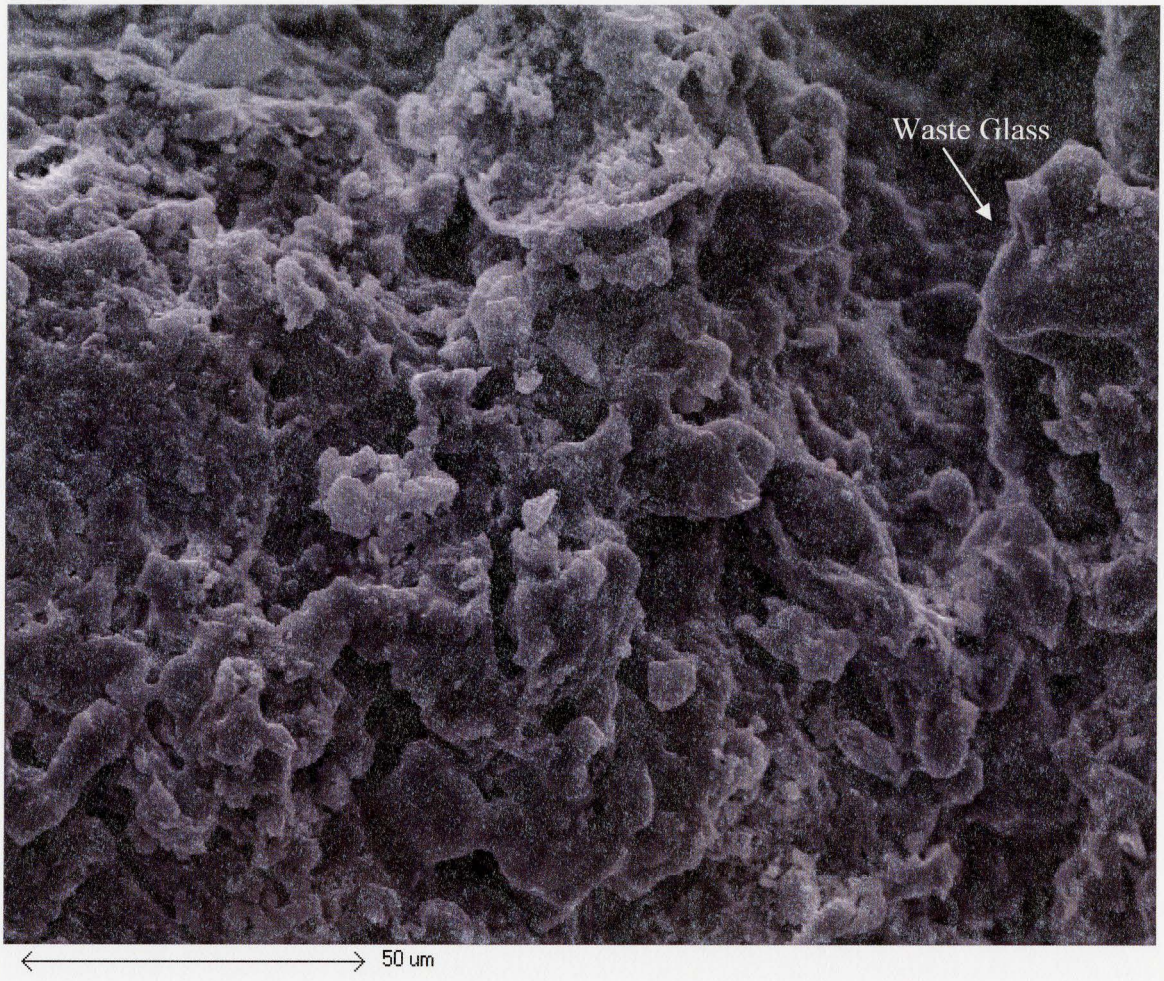

Figure 5.54 Specimen G at 680 Times Magnification, Quadrant 5

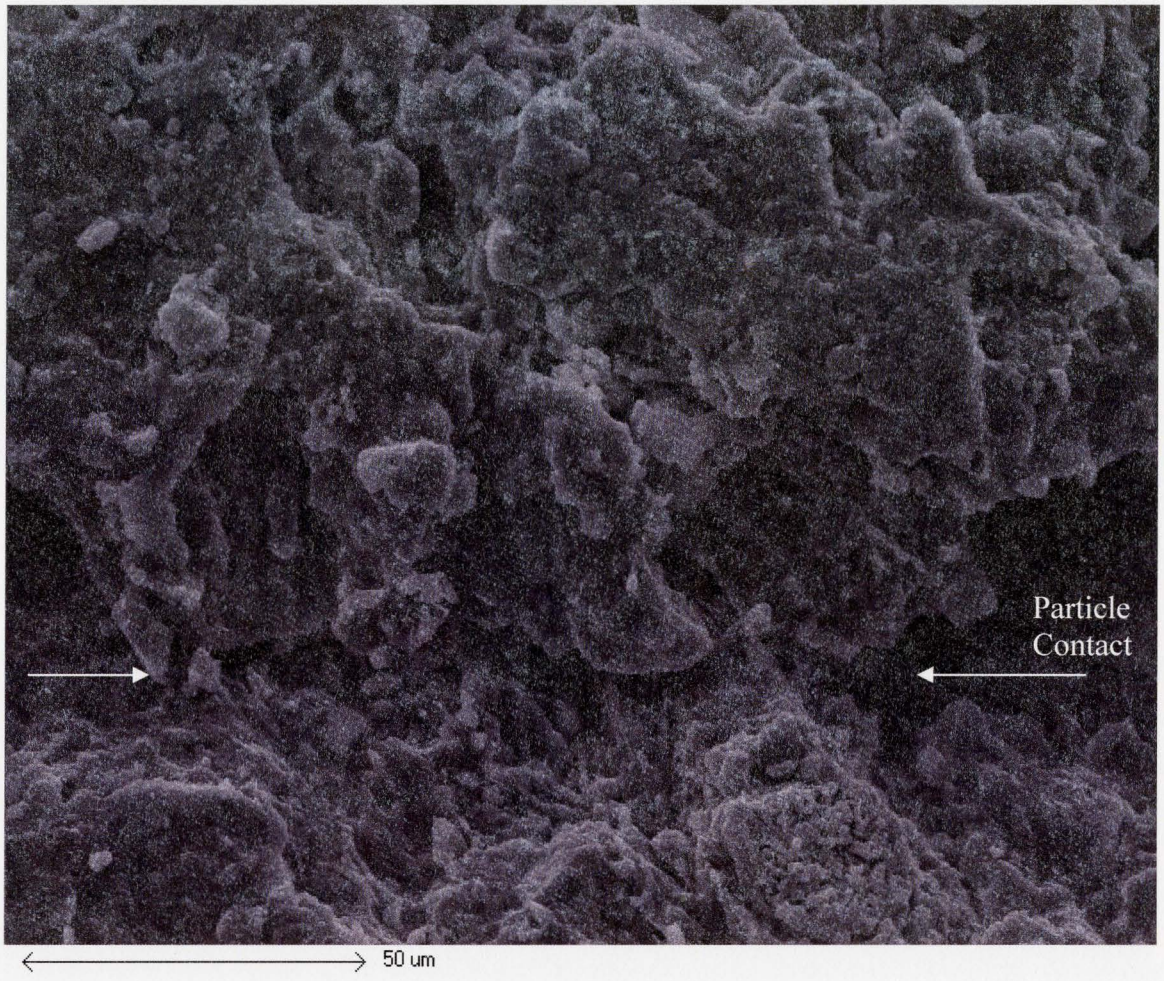

Figure 5.55 Specimen G at 680 Times Magnification, Quadrant 5

In Figure 5.55, the interface between at least two and possibly three larger sized particles is seen. The layered surface finish of the particles indicates that they are crushed shale. Two large pores on the left and right of the image, respectively, are the result of lack of contact between the particles. At the point of contact between the particles, a glassy matrix is apparent with a smoother texture. A crystalline structure is visible at the bottom of the image, on the lower particle.

5.8 Mercury Intrusion Porosimetry

The results of absorption testing, as well as the changes in observed pore size in the SEM images, indicate an important effect of the addition of waste glass. In this regard, mercury intrusion porosimetry is employed with the aim of exploring any relationship between durability and porosity, taking into consideration the percentage addition of waste glass.

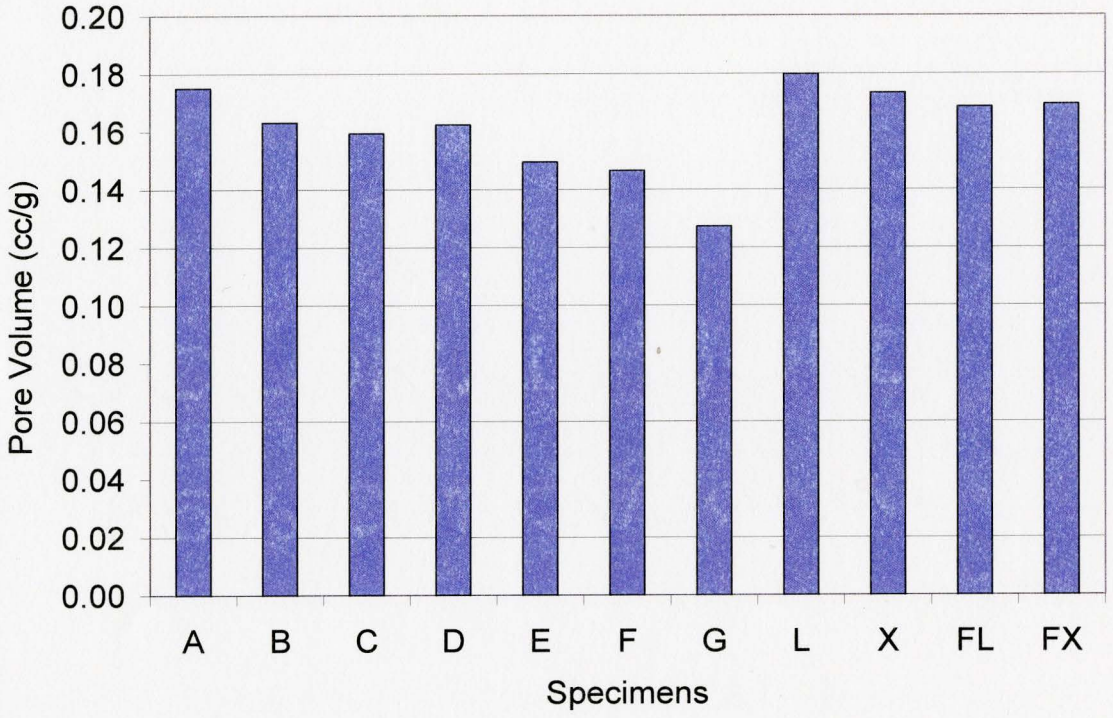

Figure 5.56 Porosity by Mercury Intrusion Porosimetry

Figure 5.56 shows the total porosity of specimens A to G, as well as L, X, FL and FX. As only one of each specimen was tested using mercury intrusion porosimetry, no statistical data can be presented. From Figure 5.56, a decrease in porosity in the

specimens containing waste glass is observed, which is most significant for specimens E, F, and G, containing 10% fine, and 15% coarse and fine waste glass, respectively. The porosity of specimen G is 27.3% lower than that of the control specimen A. Specimens containing fine waste glass exhibit lower porosity than specimens containing the same percentage of coarse waste glass.

The difference in the pore structure of the specimens is also studied by examining the pore distribution for each specimen. The pore size distribution of the control specimen A, shown in Figure 5.57, indicates that the majority of the pores for the specimen are between 0.2μm and 1μm, with the volume falling off rapidly at 0.1μm. The maximum pore volume ranges between 0.5μm and 0.8μm.

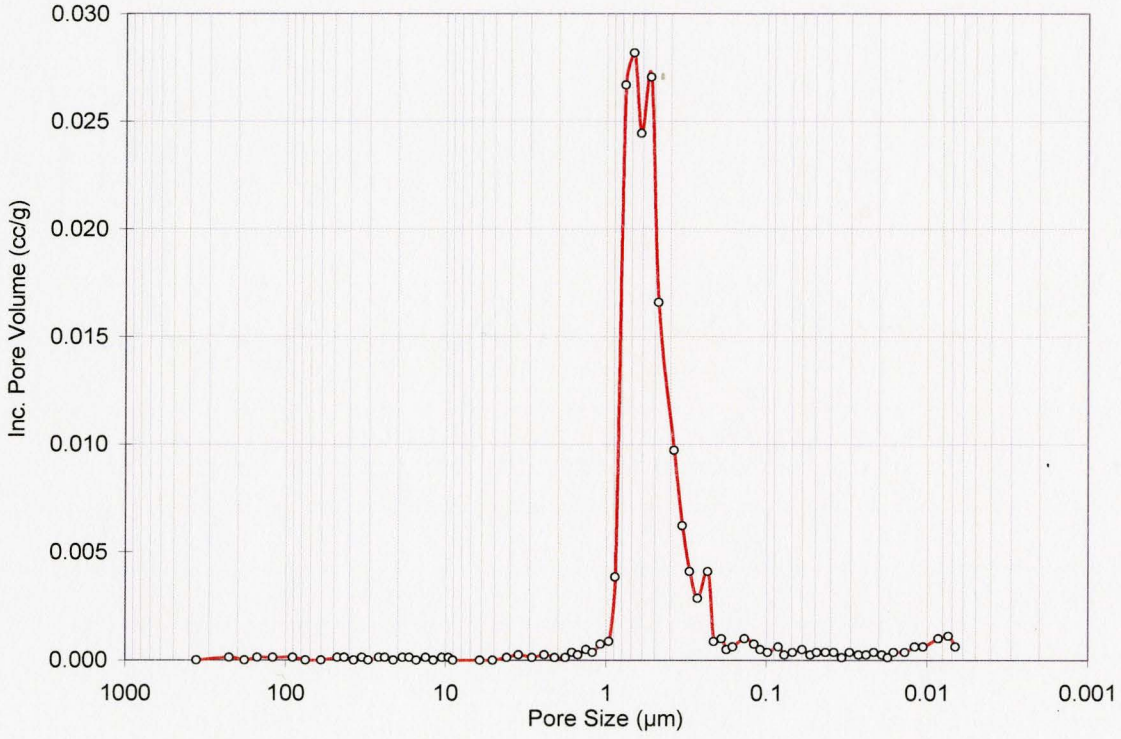

Figure 5.57 Pore Size Distribution of Specimen A

For specimen B, Figure 5.58, the pore distribution occurs over a slightly wider range, with the majority of the pores between 0.1μm and 2μm, and a peak volume between 0.8μm and 0.9μm. In comparison to specimen A, there is a smaller volume of pores in the peak range for specimen B, and a larger volume of pores between the peak and the maximum pore size. Pore size distribution of specimen C, Figure 5.59, is very similar to that of specimen A, with fewer pores between 0.8μm and 2μm, and a larger volume of pores in the peak range than for specimen B. The volume of pores in the peak range is comparable to the results of the control specimen A.

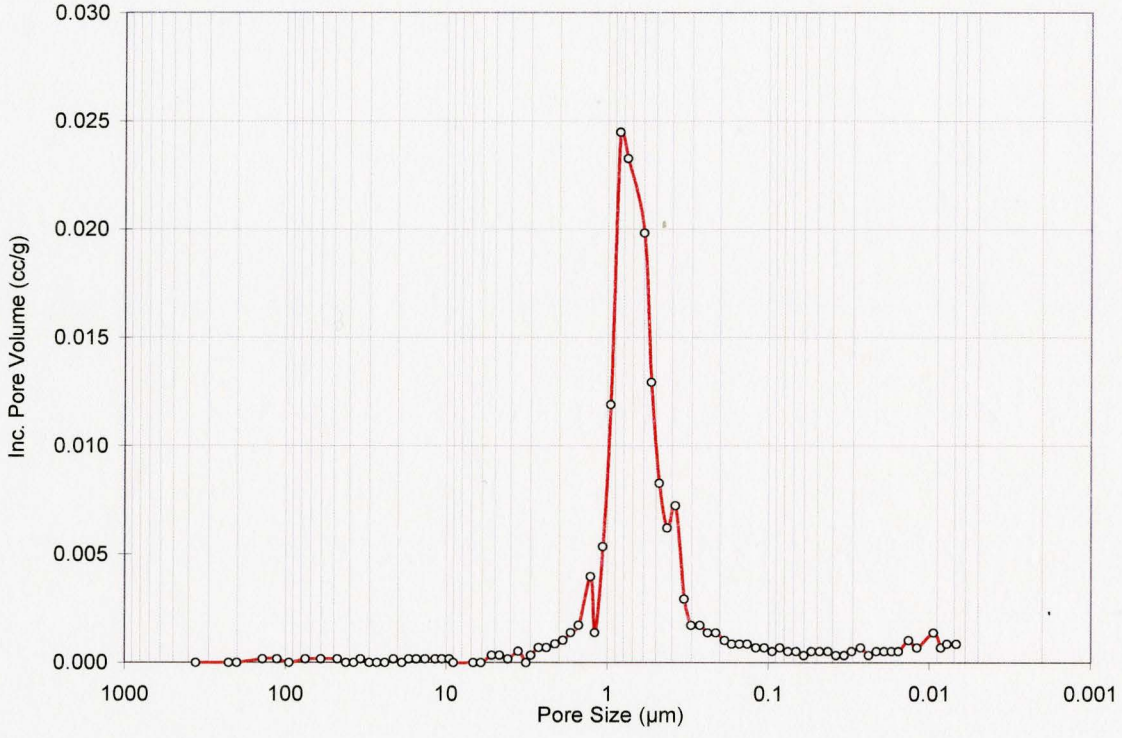

Figure 5.58 Pore Size Distribution of Specimen B

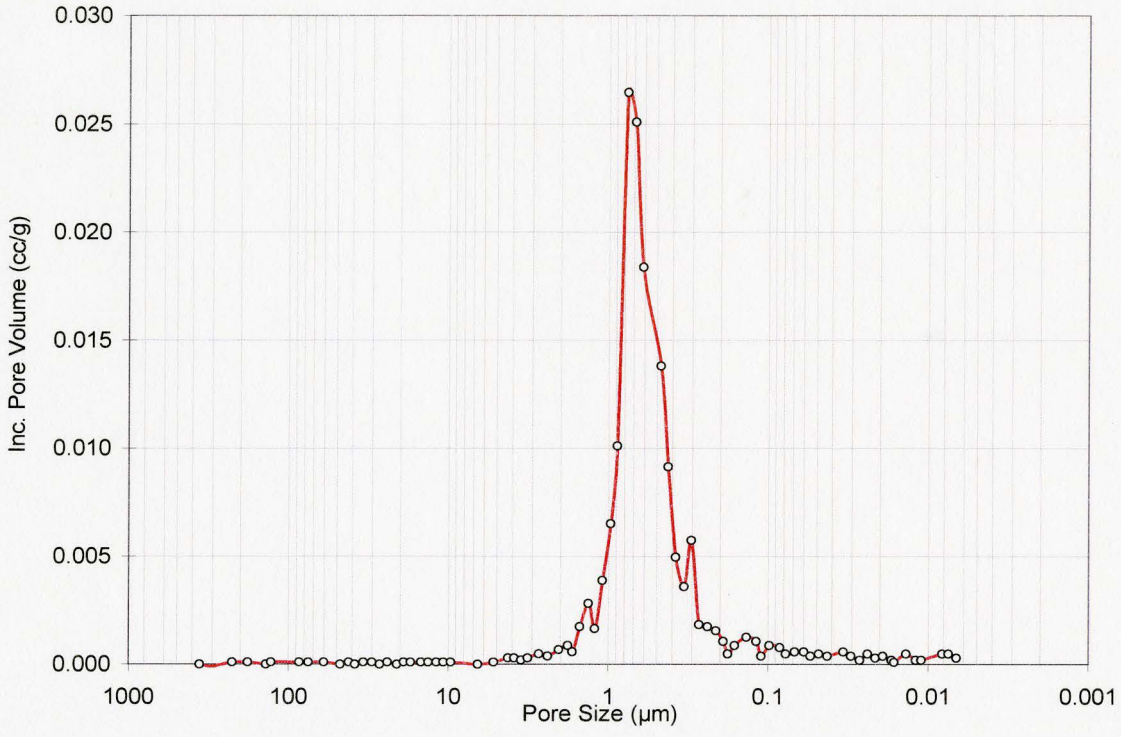

Figure 5.59 Pore Size Distribution of Specimen C

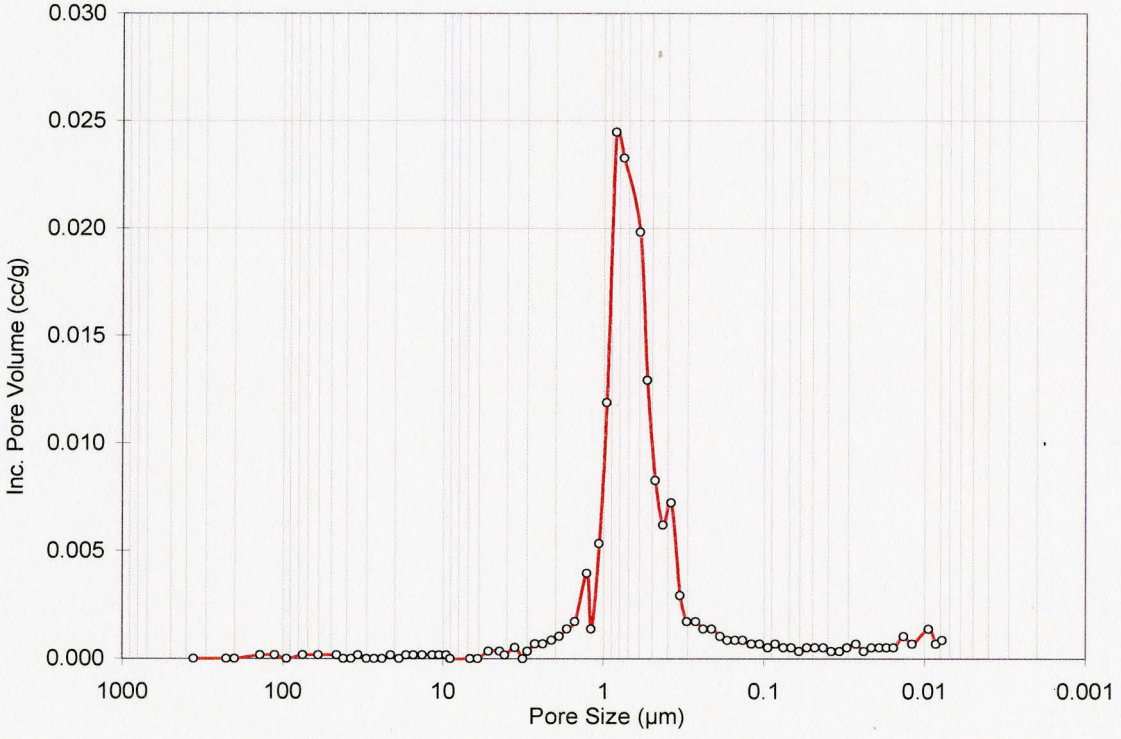

Figure 5.60 Pore Size Distribution of Specimen D

The distribution of the pores in specimen D, Figure 5.60, range between 0.1μm and 2μm, with a peak volume at 0.8μm. The peak volume is comparable to that of specimen A at nearly 0.025cc/g. In specimens B, C and D, there is an increase in pore volume at a pore size of approximately 1.4μm.

Specimen E, Figure 5.61, shows a significant decrease in the peak volume and an increase in the volume of large pores with a diameter greater than 1μm. The peak volume is 0.8μm, and the range in porosity is between 0.1μm and 2μm.

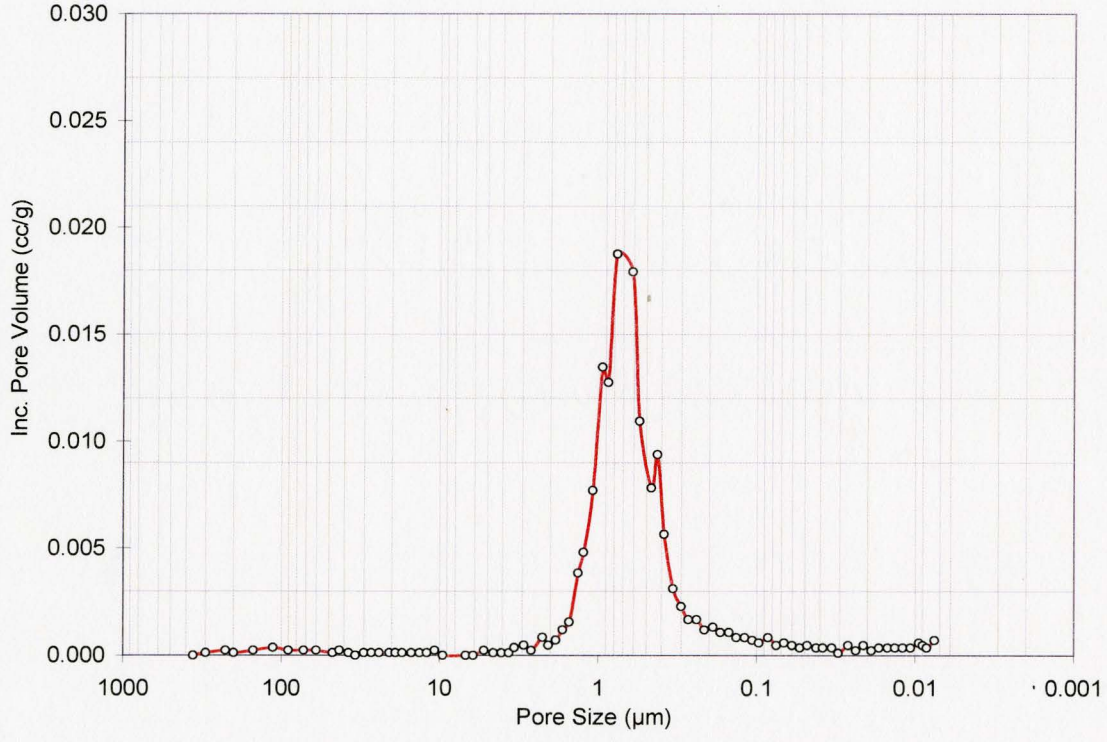

Figure 5.61 Pore Size Distribution of Specimen E

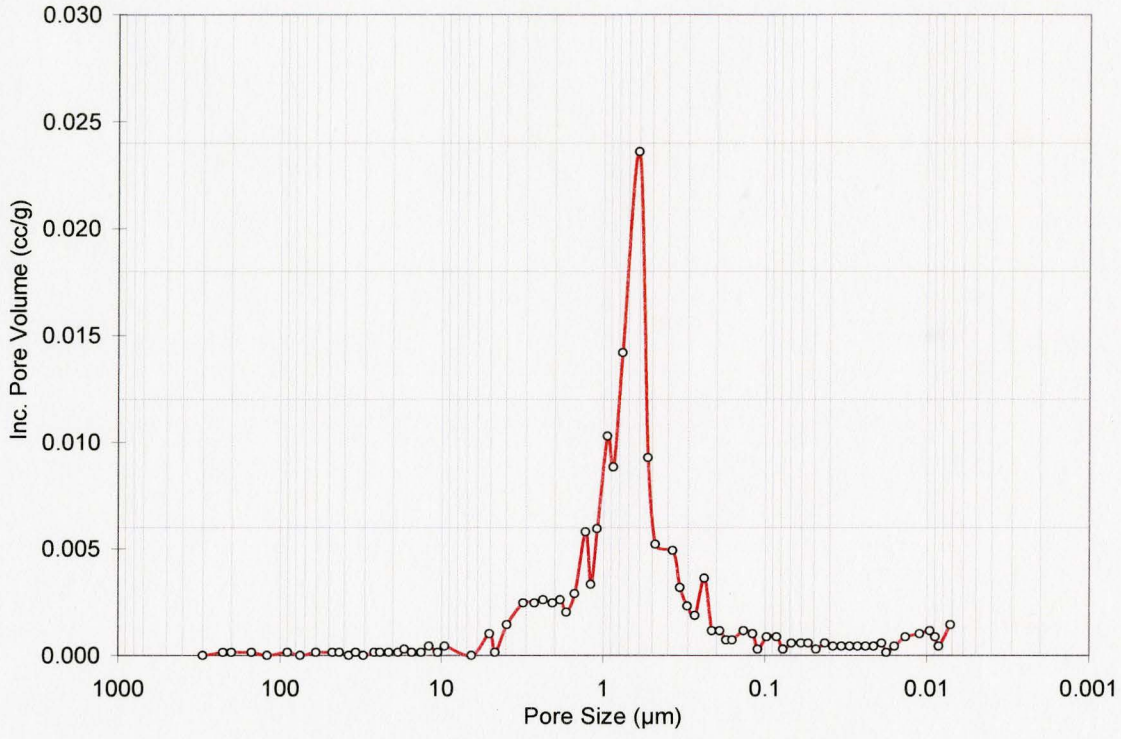

Figure 5.62 Pore Size Distribution of Specimen F

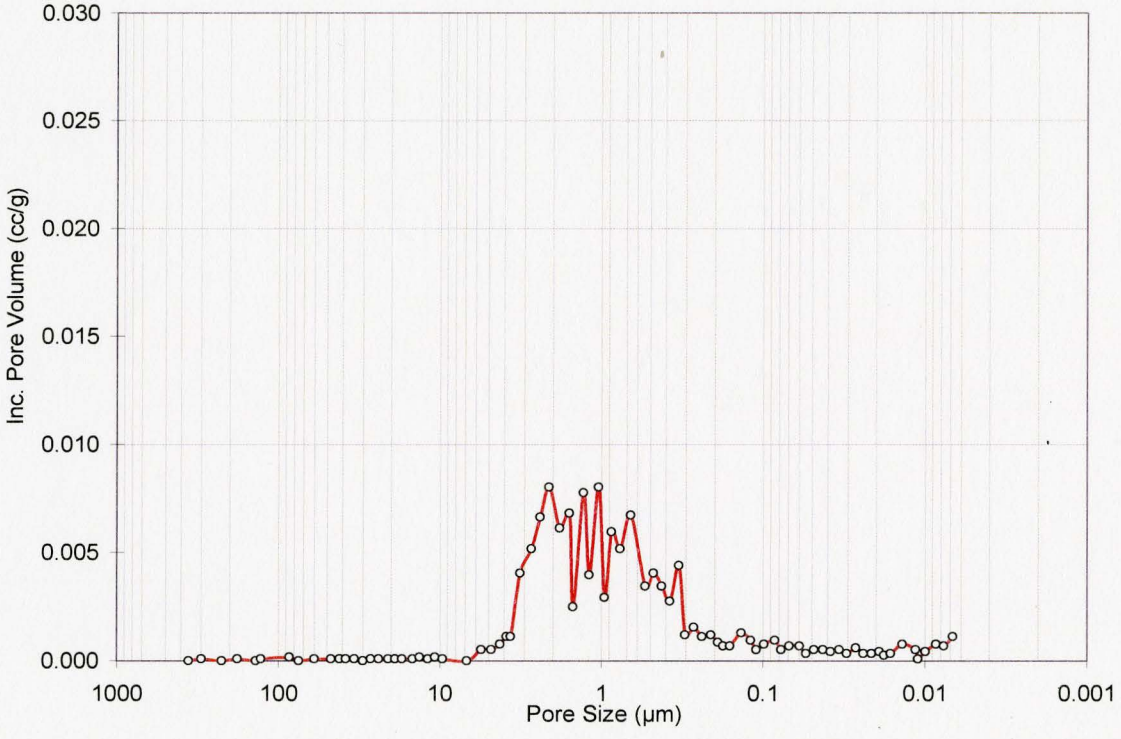

Figure 5.63 Pore Size Distribution of Specimen G

Specimens F and G display the most notable changes in pore size distribution compared to the control specimen A. The range in the pore size is wider, with a significant volume of pores from 0.1μm to 4μm. The peak volume for specimen F, Figure 5.62, occurs at 0.6μm. This peak is at a slightly smaller pore size than the control specimen, despite the increase in volume of large sized pores between 1μm and 4μm. The peak pore distribution is narrow; however, the remaining pore volume is more evenly distributed around the peak.

The results of specimen G, Figure 5.63, are unlike the results for the control specimen or any other specimens containing waste glass. There is a significant increase in the volume of large pores with a diameter greater than 1μm. The range of the majority of the pore sizes is from 0.1μm to 6μm, however there is no peak volume, instead there is a distribution of several peaks between 0.7μm and 2μm. This pore structure is unique from all other tested specimens. The distribution pattern indicates that at 15% fine waste glass addition, the pore size distribution is much broader than in a standard brick, and there is not one specific pore size dominating the distribution, but instead a variety of pore sizes throughout the specimen.

The porosimetry results for specimen L, Figure 5.64, show a very high peak volume of greater than 0.04cc/g at pore size 0.7μm, and a minor peak at pore size 0.4μm. Generally the range of the pore sizes is from 0.2μm to 2μm. The majority of the pores in this specimen are at the two peak volume sizes.

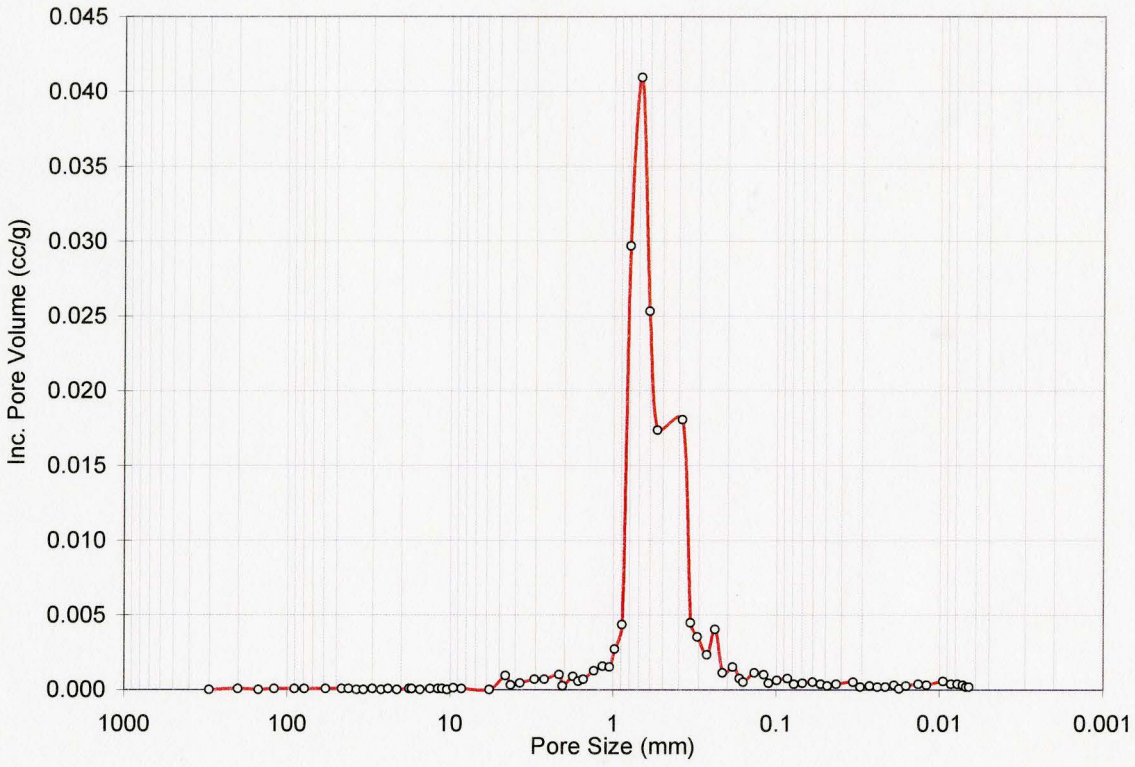

Figure 5.64 Pore Size Distribution of Specimen L

For specimen X, which was extruded in the lab but fired in the plant kiln, the porosity is lower and more comparable to the control specimen A. The two peak volumes of pores occur at 0.75μm and 1μm, Figure 5.65. The distribution of pores is greater, ranging from 0.1μm to 3μm, with a greater volume of large sized pores.

The pore distribution for specimen FL is very similar to that of L, with a slightly lower peak pore volume of 0.035cc/g at 0.7μm, Figure 5.66, and a narrow pore size distribution ranging from 0.1μm to 1.5μm.

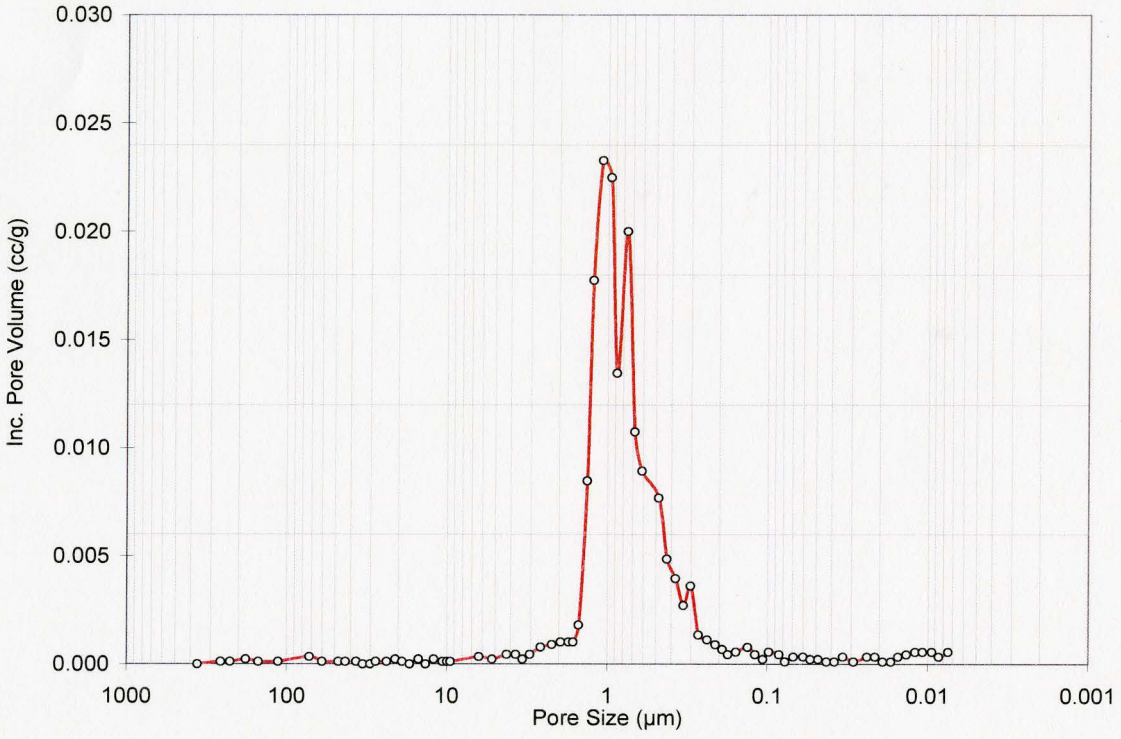

Figure 5.65 Pore Size Distribution of Specimen X

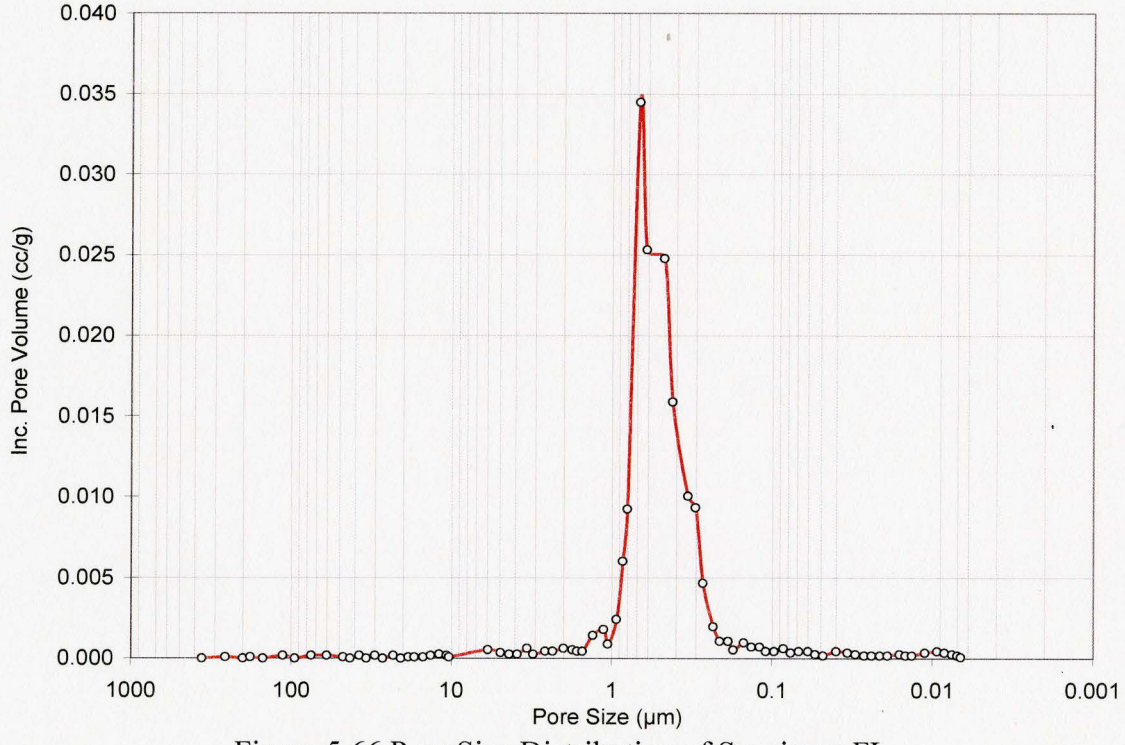

Figure 5.66 Pore Size Distribution of Specimen FL

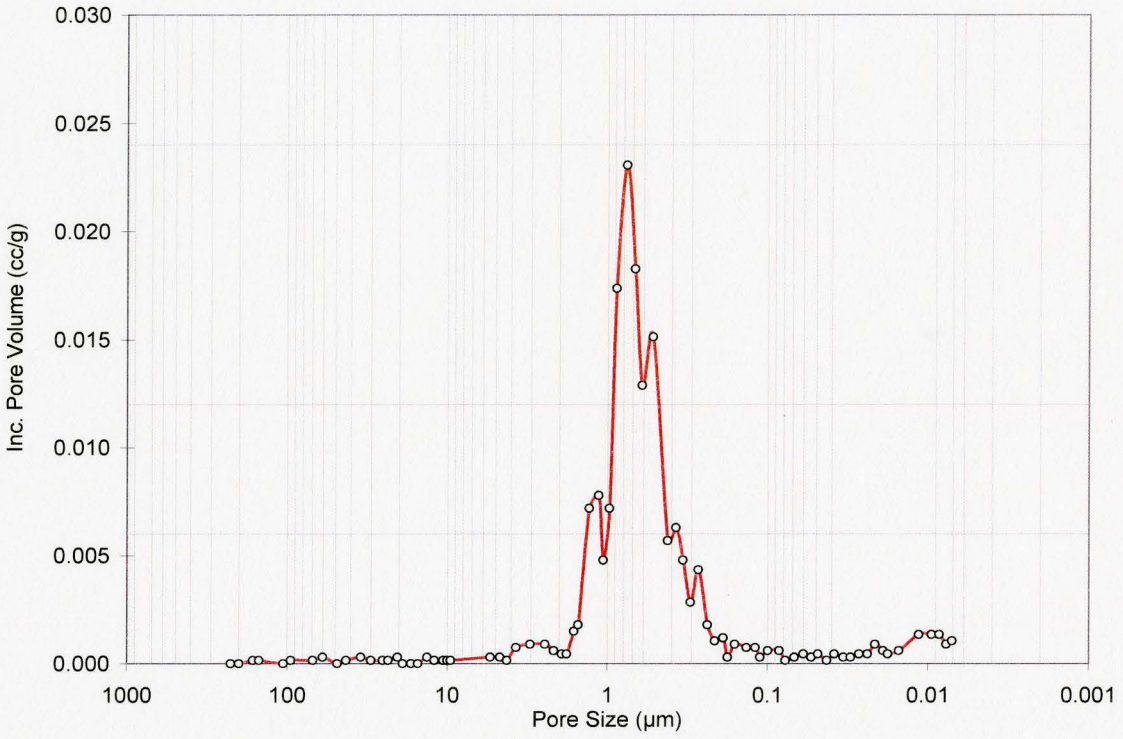

Figure 5.67 Pore Size Distribution of Specimen FX

The porosity of specimen FX is comparable to the control specimen A, and is slightly lower than that of specimens L and X. The distribution ranges from 0.1µm to 4µm, with a main peak volume at 7.5µm, and minor peaks at 0.5µm and 1.3µm, Figure 5.67. Generally the pore structure of the specimens produced exclusively in the factory is more diversified and contains slightly larger pores than the other specimens.

Using the incremental pore size volume measurements, the Maage (1984) durability index was calculated for the tested specimens according to Equation 4.7, and the values are given in Table 5.2. According to this system of durability estimation, all of the specimens tested are expected to be non-durable. For specimens F and G, the index approaches the limit of possible durability, which is 55.

Table 5.2 Porosity and Maage Durability Index

Specimen	Porosity	PV	P3	F_c
A	0.175	0.175	1.212	21
B	0.163	0.163	2.218	25
C	0.159	0.159	1.709	24
D	0.162	0.162	2.229	25
E	0.149	0.149	3.057	29
F	0.147	0.147	5.929	36
G	0.127	0.127	7.875	44
L	0.180	0.180	1.933	22
X	0.173	0.173	2.870	25
FL	0.168	0.168	2.772	26
FX	0.169	0.169	3.186	27

CHAPTER 6 REGRESSION ANALYSES AND DISCUSSION

An analysis comparing the statistical significance of average result values and variances of the mechanical, durability, and absorption properties of tested specimens was performed in Section 5. The analysis was intended to indicate a statistically significant change in properties as a result of the variables of interest in the testing program. In this section, the statistical analysis will be expanded to provide a more complete model to fit the experimental data.

6.1 Multiple Linear Regression

The method of choice for the development of a model of this nature is regression analysis, where the data is used to best fit a model of the form in Equation 6.1.

$$y = \beta_0 + \beta_1 x_1 + \ldots + \beta_i x_i + \varepsilon \qquad \text{Equation 6.1}$$

The form of the model in Equation 6.1 is linear and designed to accommodate multiple results and variables, where the result, y, is influenced by the variables, x, the parameters, β, and the error associated with the fit of the model, ε. The fitting of this model is therefore referred to as multiple linear regression (MLR). In order to determine the best fit of the model, the experimental values are first used to estimate the parameters. These estimated parameters form the equation above, into which the variable values are substituted. The resulting model values, $\tilde{y}$, are subtracted from the experimental values, y,

in order to find the residual values, *e*. A model is considered to have a good fit when the sum of the squared residual values is minimized. This is an iterative process which can be calculation intensive; however the use of matrix notation, Equation 6.2, can greatly simplify the computations required (Montgomery and Runger, 1999).

$$\beta = (X'X)^{-1}X'y \qquad \text{Equation 6.2}$$

In addition to the development of the model equation, analysis of the variance in the model can provide insight into the quality and significance of the model and its ability to account for variation in predicted values. This analysis of significance is based on the theory of hypothesis testing, where the tested hypothesis is that the parameters, β, are not equal to zero, and are therefore significant to the model (Quinn, 2005).

For each tested property, y, namely initial rate of absorption, absorption ratio, compressive strength, modulus of rupture, and freeze-thaw mass loss, a model was fit using multiple linear regression, where the variables, x, included percentage of waste glass addition, particle size of waste glass, extrusion method, firing method, and freeze-thaw solution. The resulting parameters, β, were used to calculate the predicted result, $\tilde{y}$, and the fit and significance of each model was evaluated based on assessment of residual plots, and the test for lack of fit through analysis of variance (ANOVA). The significance of the variance was determined with the critical value of the F-probability distribution for α of 0.05%, where p is the number of parameters, and n the number of observations, or results. In this analysis, hypothesis tests are used to determine significance, where the two

possible hypotheses for a regression model, Equation 6.3, are H_0, in which all the parameters equal zero, and H_1, in which at least one parameter does not equal zero, giving the model a significance in its fit to the data. (Montgomery and Runger, 2003)

$$H_0: \beta_1 = \beta_2 = \ldots = \beta_k = 0 \qquad \text{Equation 6.3}$$

$$H_1: \beta_j \neq 0 \text{ for at least one parameter}$$

If the calculated value, F_o is greater than the critical value, $F_{p,n-p;\alpha}$, H_0 should be rejected, indicating that the form of the model has at least one significant parameter. All specimens were modelled together, so that the effects of both waste glass addition and production method could be considered at one time. Table 6.1 summarizes the variable names that were considered in the model formation.

Table 6.1 Table 6.1 Linear Regression Variables

	Glass Particle Size	% Waste Glass	Extrusion Method	Firing Method	Freeze-Thaw Solution
Variable	x_1	x_2	x_3	x_4	x_5
	1 Coarse	0	1 Lab	1 Lab	1 NaCl
	0 Fine	5	0 Plant	0 Plant	0 Deionized
		10			
		15			

The results of the regression analysis were checked using an existing linear regression program (Paez, 2004) in order to confirm the results, as well as to gain additional statistical information such as the coefficient of determination (R^2), a quantity

which is used to judge the adequacy of the model based on the ratio of the model error and the total error. A coefficient of determination close to unity indicates a well fit model (Montgomery and Runger, 2003).

6.2 Initial Rate of Absorption Regression Model

A model was fit to the resulting experimental IRA data using matrix methods (Quinn, 2005). The resulting parameters and model form, Equation 6.4, estimated the influence of the variables of interest on the initial rate of absorption. The final term is a measure of the interaction between the particle size and percentage addition. The R^2 value for the model was 0.858, which indicates significance of fit.

$$\tilde{y}_{ira} = 24.273 + 5.681x_1 - 1.167x_2 + 4.036x_3 - 2.6999x_4 \qquad \text{Equation 6.4}$$

The residual plots are provided in Figure 6.1. Some observations from the plots may indicate areas for improvement in the fit of the model. For variable x_2, percentage of waste glass addition, there is a pattern in the sign of the coefficient for 10% and 15% addition. Residuals for 10% addition are positive, while for 15% addition they are negative. This effect may be caused by the outliers at 5% and 15% addition. Variables x_3 and x_4 show a wider range of error for the specimens extruded and fired in the laboratory as opposed to those prepared in the plant. This increased variation may mean that the fit of the model is less accurate than it could be and is compromising between the two states

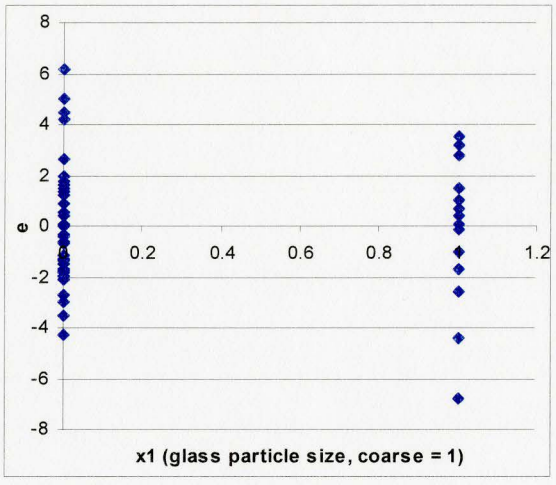

(a)

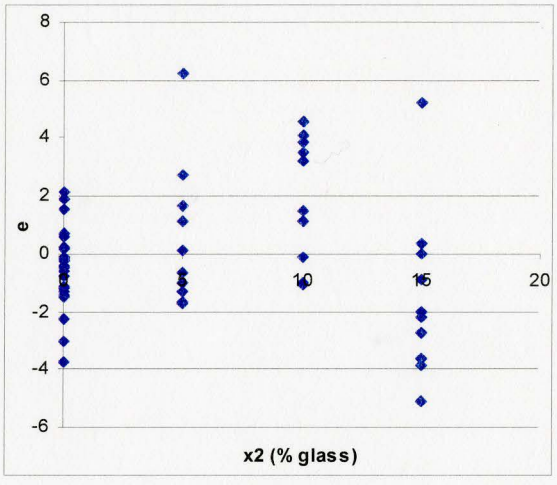

(b)

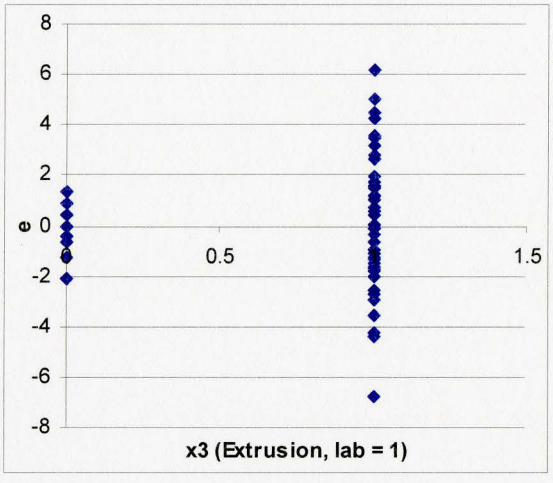

(c)

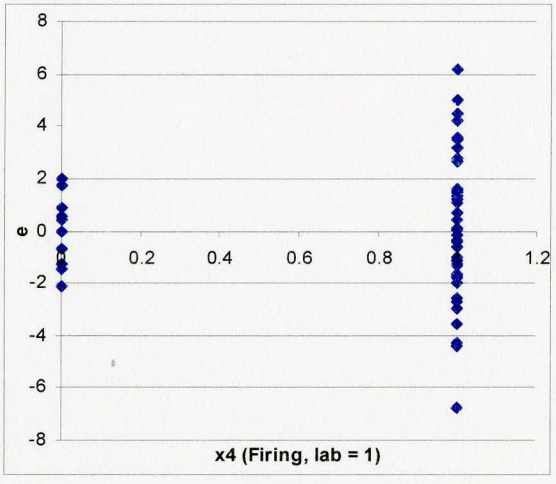

(d)

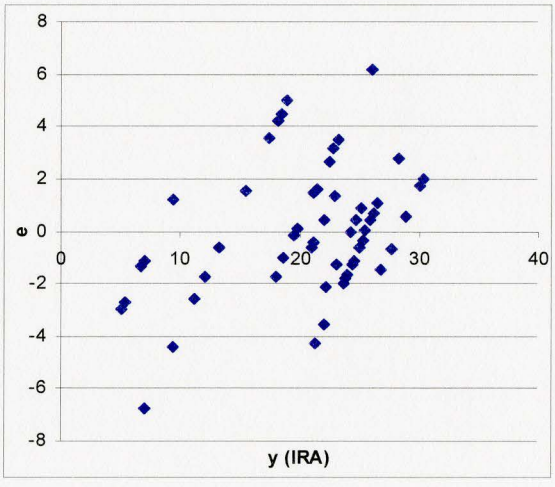

(e)

Figure 6.1 Residual Plots for IRA Residual VS (a) x1 (b) x_2 (c) x_3 (d) x_4 (e) y

of production. Also it may indicate a level of variation in the process that is not explained by extrusion and firing alone. The variation in (e) indicates a possible pattern as IRA increases, where there is a cyclic increase and decrease in the values. There appears to be two outliers at 5% and 15% waste glass addition.

The ANOVA table for the IRA, Table 6.2, was calculated with a critical F value of 2.57, and therefore the model is considered to have significance in terms of the chosen parameters and data obtained experimentally for IRA, where at least one of the coefficients is not equal to zero. The coefficient values from Equation 6.4 are plotted in Figure 6.2 along with the corresponding confidence intervals for a Student t-table probability of 0.05%. As indicated in the ANOVA table, at least one of the coefficients is significant; however, it appears that all of the parameters are significant to the model based on the confidence intervals, with glass particle size as the most influential parameter. As the particle size of the waste glass increases from fine to coarse, the IRA increases. The percentage of waste glass has a small effect on the IRA, where increasing waste glass percentage would be expected to decrease the IRA slightly. As expected from the residual plots, the firing and extrusion method are also influential, where extrusion in the laboratory caused an increase in IRA, while firing in the laboratory decreases the IRA.

Table 6.2 ANOVA Values for IRA

Variation	Sum of Squares	DOF	Mean Square	F_o
SSR	1981.073	4	495.2682	75.30416
SSE	328.8451	50	6.576903	
SST	2309.918	54		

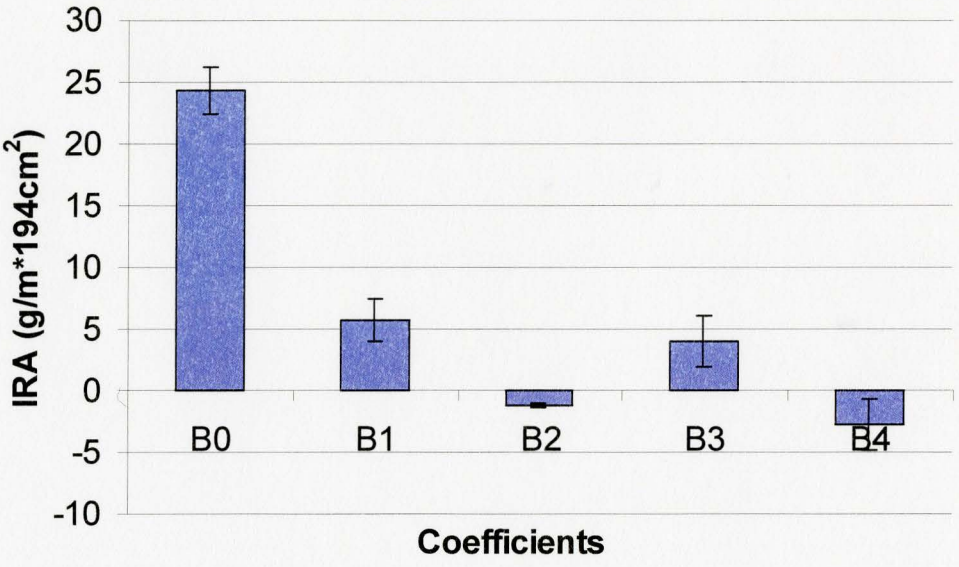

Figure 6.2 IRA Coefficients and Confidence Intervals

6.3 Absorption Ratio Regression Model

The absorption ratio was chosen for modelling because it represents both the cold water and boiling water absorption values. A linear model was fit, Equation 6.5, and the residuals were plotted for assessment of the quality of the model, Figure 6.3. The R^2 value for the model was 0.855, which indicates significance of fit.

$$\tilde{y}_{cb} = 0.799 + 0.029x_1 - 0.012x_2 - 0.0045x_3 + 0.03x_4 \qquad \text{Equation 6.5}$$

Table 6.3 ANOVA Values for Absorption Ratio, C/B

Variation	Sum of Squares	DOF	Mean Square	Fo
SSR	0.220973	4	0.055243	72.24274
SSE	0.038235	50	0.000765	
SST	0.259208	55		

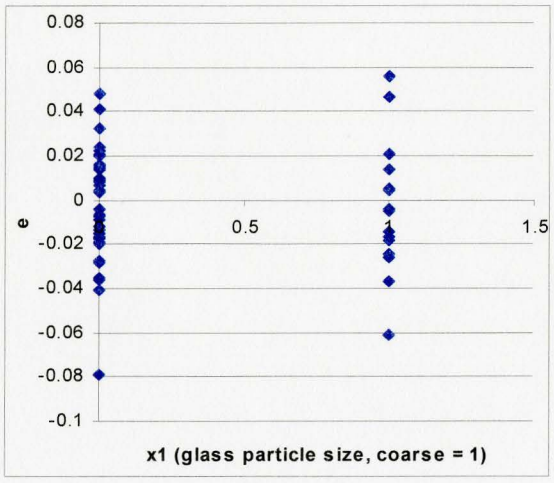

(a)

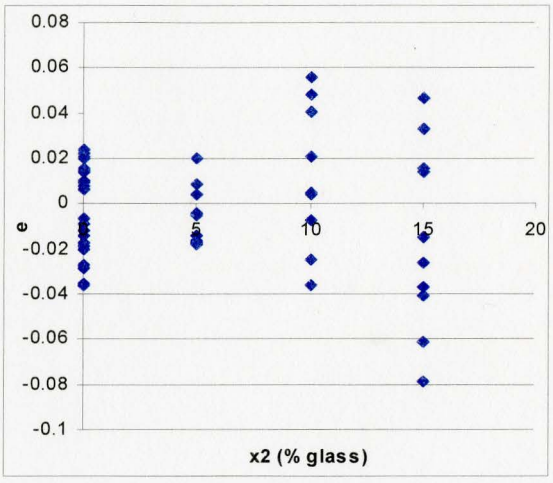

(b)

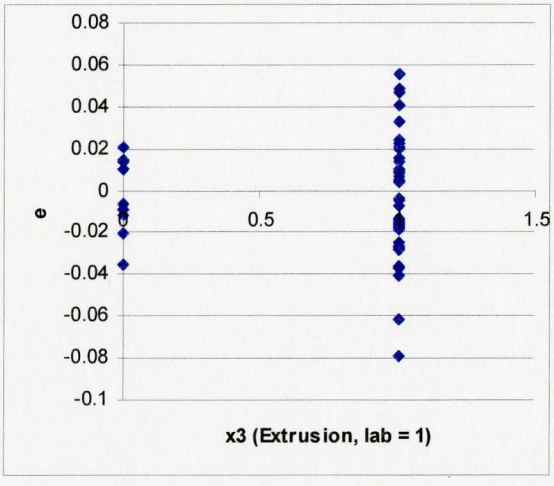

(c)

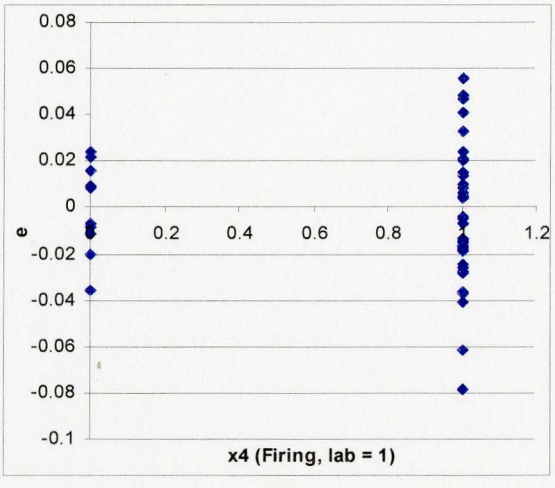

(d)

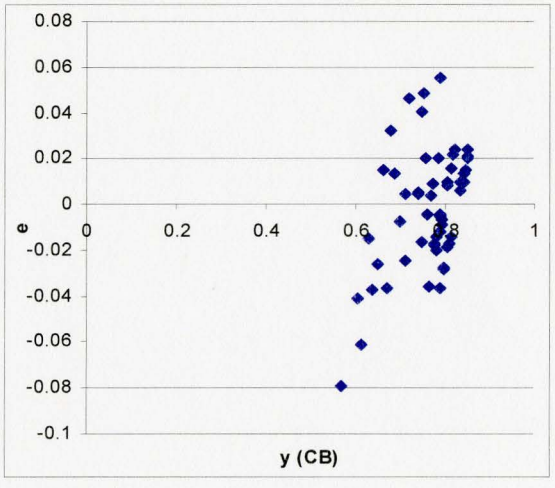

(e)

Figure 6.3 Residual Plots for C/B Ratio Residual VS (a) x1 (b) x_2 (c) x_3 (d) x_4 (e) y

The residual plots for the absorption coefficient show good variation for variables x_1 and x_2, although the variance of the residuals is slightly greater at higher percentages of waste glass in Figure 6.3 (b). As was seen for the IRA results, the variation of the residuals is much higher for the laboratory specimens in both extrusion and firing for the C/B ratio. The residual distribution versus the experimental results shows a very good distribution. Although there is a large range in the results, this range is evenly distributed. There are not any obvious outliers detected in the data.

The ANOVA table for the C/B, Table 6.3, was calculated with a critical F value of 2.57. The ANOVA values indicate that at least one of the coefficients, β, is significant in the model. From Figure 6.4, β_3 is most likely insignificant, as the coefficient is very small, and the confidence interval crosses the horizontal axis. The coefficients β_0, β_1, β_2 and β_4 are significant in the model, where the first coefficient is the average value, β_1 is percentage of waste glass added, β_2 is the influence of waste glass addition, and β_4 is the influence of the firing method. The influence of the average is the greatest due to the very small variation in C/B ratio among the tested specimens. The model indicates that the addition of waste glass in increasing percentages would be expected to decrease the C/B ratio, while firing the specimens in the laboratory causes the C/B ratio to increase. The use of coarse size waste glass increases the C/B ratio as well. The fit of the model could be improved by excluding extrusion method as a variable as it does not influence the results.

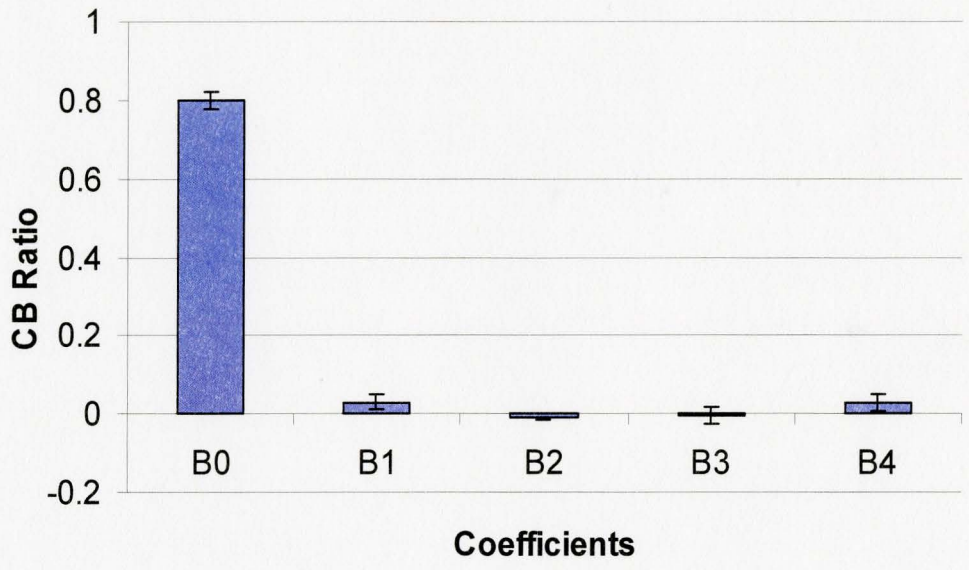

Figure 6.4 C/B Ratio Coefficients and Confidence Intervals

6.4 Modulus of Rupture Regression Model

The model fit to the results of the modulus of rupture (MOR) data accounted for two testing techniques. While specimens A to G were tested in accordance with the CSA method of testing (CSA, 1978), specimens X, L, FX, and FL were tested using the four point load method. As noted, the four point load test method led to both higher values of MOR and smaller variations in the results. This method also accentuated flaws in the full scale laboratory specimens fired in the laboratory kiln, which gave poor results for these specimens. The model is therefore a compromise between the two methods of testing, and is not expected to accurately reflect either method on its own. The linear model, Equation 6.6, is analyzed for quality of fit using residual plots, Figure 6.5. The R^2 value for the model was 0.70, which is a lower than ideal value, indicating a potential lack of fit for the data.

$$\tilde{y}_{mor} = 14.95 - 1.318x_1 - 0.377x_2 + 0.165x_3 - 8.424x_4 \qquad \text{Equation 6.6}$$

The residual plots for the modulus of rupture variables show some indications of lack of fit, as expected, due to the two methods of testing. The distribution of the residuals for specimens containing no glass or fine glass is much larger than the residuals for the specimens containing coarse glass. This result is influenced by the specimens tested using the four point load method, none of which contained waste glass. This result is also apparent in the residual versus the waste glass percentage. At 0% waste glass, the variation is very large, while the remaining values have much lower variation and are not randomized, with the residual moving from negative to positive with increasing waste glass addition.

The testing of specimens A to G, all of which were extruded and fired in the laboratory, using the CSA method may have caused the uneven distribution of residuals in (c), and therefore it is not possible to distinguish the influence of the testing method from that of the extrusion method. The failure mechanism in MOR for full scale specimens fired in the laboratory kiln was due to cracks developed along the plant impressions formed during extrusion. The distribution of the residuals in (c) and (d) may be the result of this failure mode, the testing method, or the effect of the firing method.

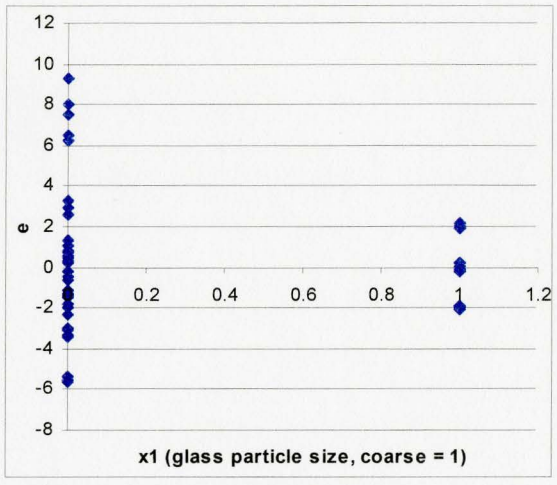

(a)

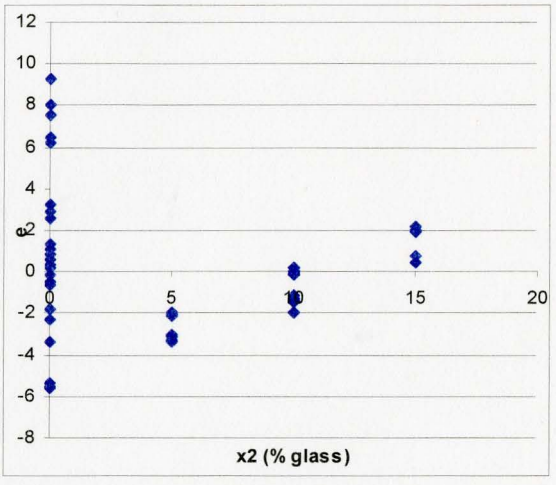

(b)

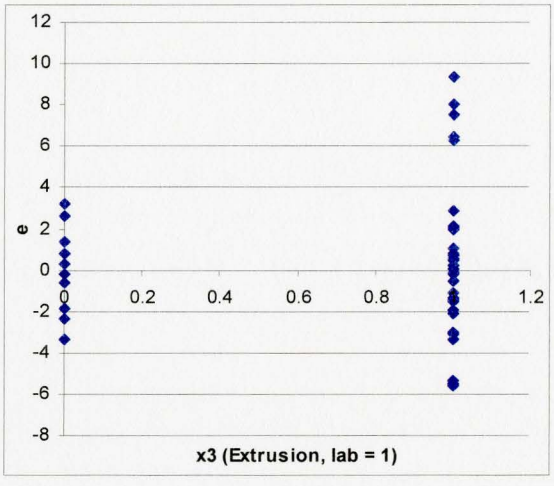

(c)

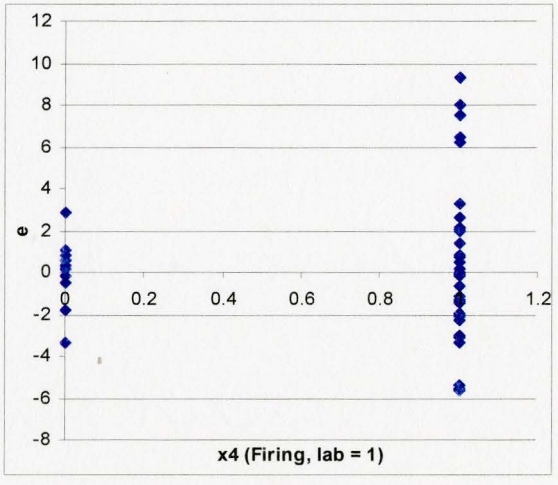

(d)

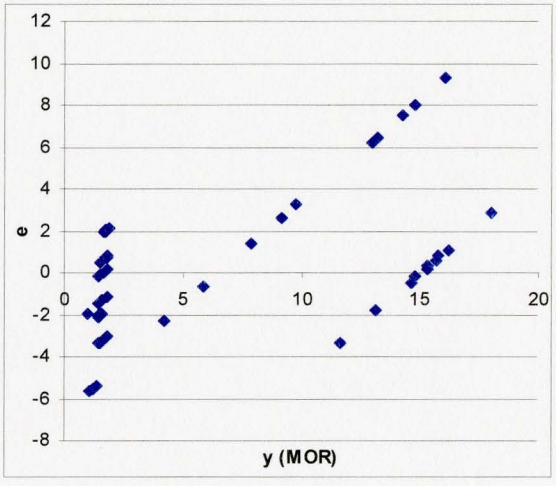

(e)

Figure 6.5 Residual Plots for MOR Residual VS (a) x1 (b) x_2 (c) x_3 (d) x_4 (e) y

There are clear patterns in the residual distribution versus the experimental results in (E). At the low values of MOR, determined with the CSA testing method, there is a reasonably random and approximately equal distribution of residuals about the horizontal axis. When the four point load test method was employed, resulting in higher MOR values, a parallel pattern of increasing variation with increasing MOR is observed, with two levels of variation in the highest MOR values.

Table 6.4 ANOVA Values for Modulus of Rupture

Variation	Sum of Squares	DOF	Mean Square	Fo
SSR	1322.16	4	330.5399	28.6712
SSE	564.9032	49	11.52864	
SST	1887.063	54		

This contradiction is a result of the unexpected failure of the full scale laboratory fired specimens. The ANOVA results for the modulus of rupture, Table 6.4, with a critical F value of 2.574 indicates that at least one of the coefficients of the model is significant, however the lack of fit from the residual plots and R^2 value indicates that the model is less than ideal. The results are greatly influenced by the different methods of testing; however no variable was used to identify the testing methods.

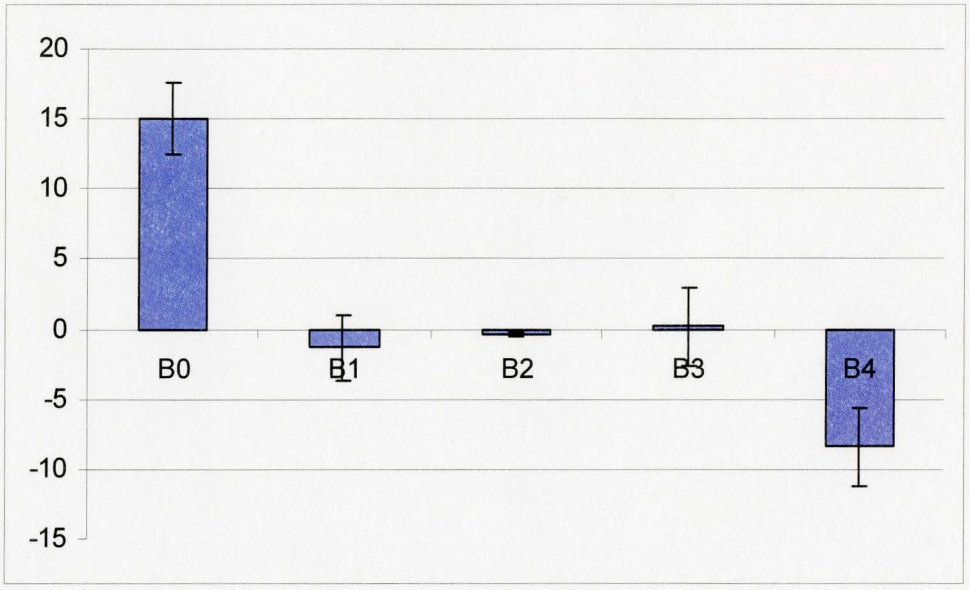

Figure 6.6 MOR Coefficients and Confidence Intervals

The graph of the coefficients and their confidence intervals, Figure 6.6, provides a more detailed view of the performance of the model. There is evidence of lack of fit since the coefficients, excluding β_0 and β_4 all have extremely large confidence intervals compared to the value of the coefficient and are small, and all confidence intervals cross the horizontal axis. In the case of β_1, and β_3 which is the influence of waste particle size and extrusion, the confidence interval not only crosses the horizontal axis, but is much larger than the coefficient itself. The only parameter which has significance is the average coefficient, β_0, and the influence of firing location, β_4, although the confidence interval of this coefficient is large.

Analysis of the residual plots and the ANOVA values for the MOR model indicated that the fit of the model is poor; however the data in its current form would not allow a better model. In order to create a better fitting model, a variable was added to

account for the difference in the testing method. This would make a comparison between waste glass addition and production method difficult, it would; however, allow the determination of the relative importance of the testing method

As a result of the poor performance of the model, an additional variable, x_5, was added to account for the testing method, where an x_5 value of zero indicated that the CSA method was used, and a model was refit for the MOR results. The modified model took the form of Equation 6.7. The variables fit to the model were limited to the percentage of waste glass addition, waste glass particle size and their interaction. The difference in the two models is substantial not only in form, but the average value, β_0, falls from 14.95 MPa to 1.203 MPa.

$$\tilde{y}_{morMOD} = 1.203 + 0.0296x_1 + 0.0272x_2 + 4.343x_3 - 4.246x_4 + 11.659x_5 \qquad \text{Equation 6.7}$$

The residual plots for the modified model are shown in Figure 6.7. When compared to the original model, the distribution of the residuals shows very clearly the difference between the two testing methods. There is a much larger variation of residuals for the specimens tested using the four point loading method as seen in (e). The distribution of the residuals for the modified model compared to the experimental values shows that the results from the four point loading method are well distributed, but indicate that the two testing methods are not comparable.

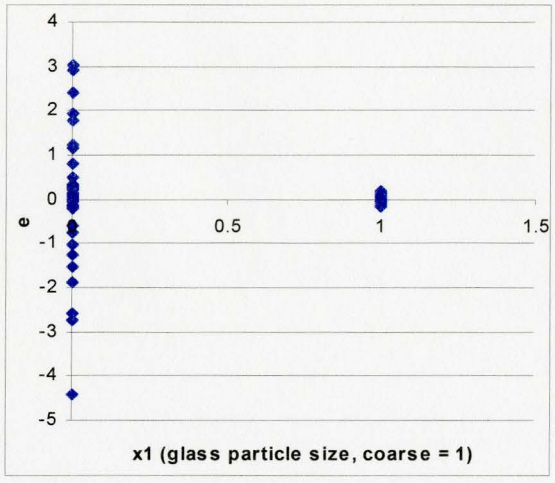

(a)

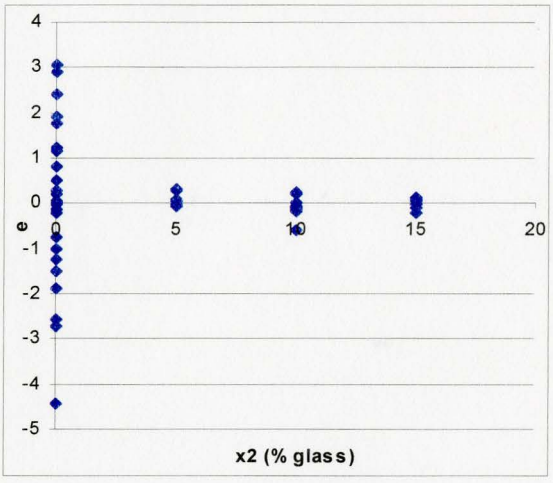

(b)

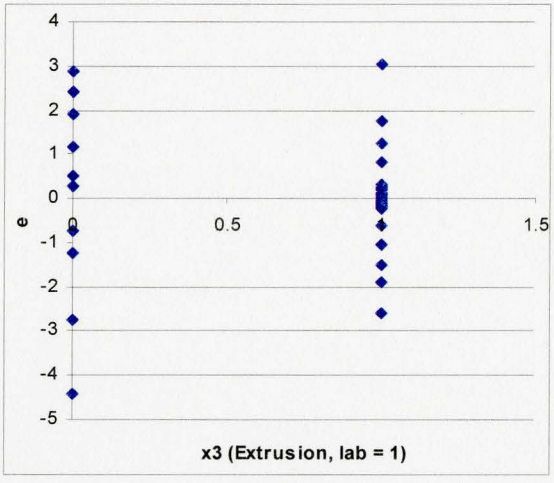

(c)

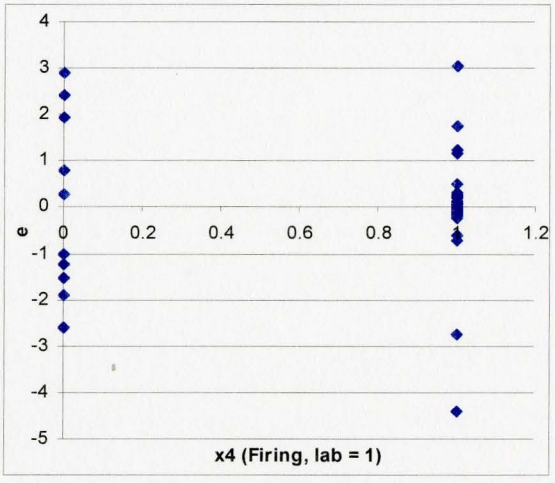

(d)

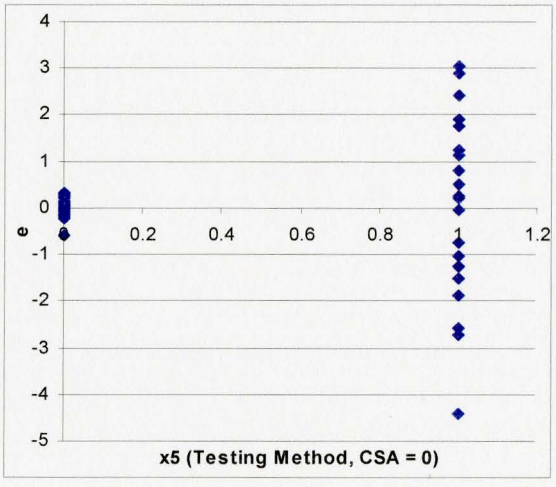

(e)

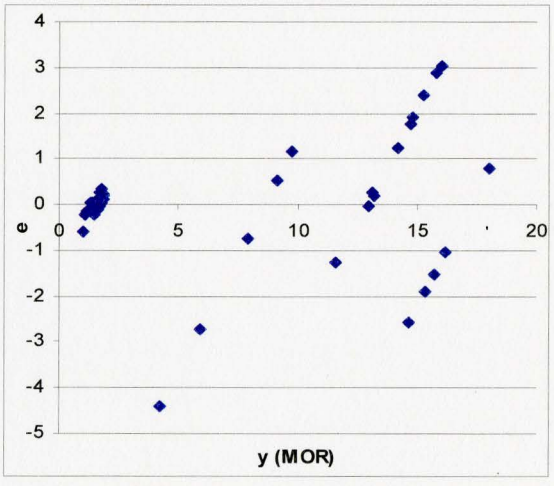

(f)

Figure 6.7 Modified MOR Residual VS (a) x1 (b) x_2 (c) x_3 (d) x_4 (e) x_5 (f) y

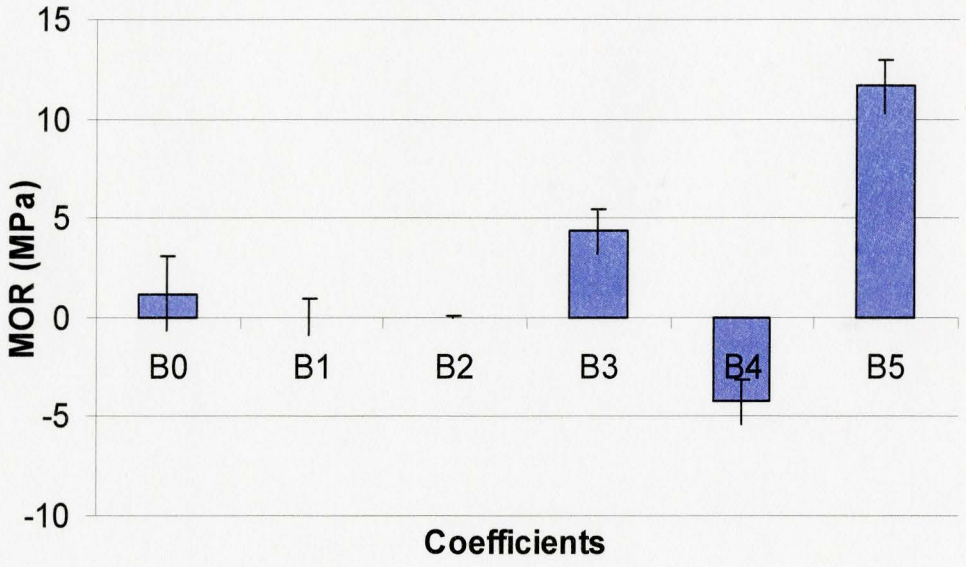

Figure 6.8 Modified MOR Model Coefficients and Confidence Intervals

Table 6.5 ANOVA Values for Modified MOR Model

Variation	Sum of Squares	DOF	Mean Square	Fo
SSR	1809.28	5	361.856	223.3031
SSE	77.78258	48	1.620471	
SST	1887.063	54		

The ANOVA table for the modified MOR model, Table 6.5, provides an F_o value of 223.3, while the critical value is 2.338. With an R^2 value of 0.959, the model in this form provides a much better fit to the data and allows comment on the influence of the testing method. The coefficients for the modified model, Figure 6.8, show that the method of testing used is more influential than the tested variables, which is not an ideal result of the testing program. In order to obtain meaningful results from the data, it is

therefore necessary to divide the data by testing method. In this way, although the results of waste glass addition and production method cannot be directly compared, their influences may be discussed separately.

Table 6.6 ANOVA Values for MOR Data Specimens A to G

Variation	Sum of Squares	DOF	Mean Square	Fo
SSR	0.667289	2	0.333645	10.7674
SSE	0.960584	31	0.030987	
SST	1.627873	34		

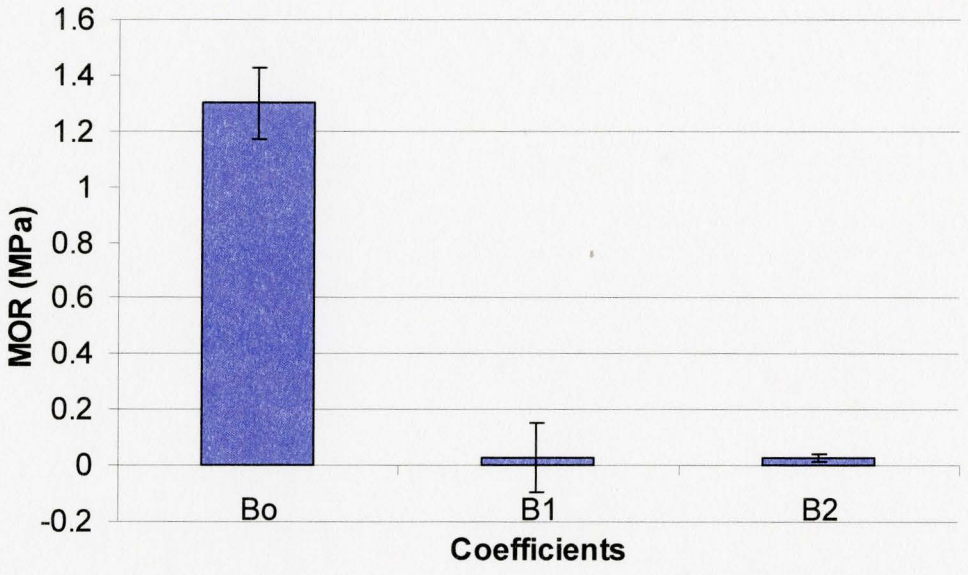

Figure 6.9 MOR Model Coefficients and Confidence Intervals for Specimens A to G

The results of the models in which the results are divided provided additional insight into the performance of the specimens in MOR testing. Specimens A to G were fit with variables x_1 and x_2, resulting in an R^2 value of 0.41 for the model. The ANOVA

results in Table 6.6 indicate that at least one coefficient is not equal to zero with a critical F value of 2.92, and in Figure 6.9, both β_1 and β_2 are insignificant, leaving only the average value as significant.

Table 6.7 ANOVA Values for MOR Data Specimens L, X, FL, FX

Variation	Sum of Squares	DOF	Mean Square	Fo
SSR	2763.986	2	1381.993	305.8218
SSE	76.82212	17	4.518948	
SST	2840.808	20		

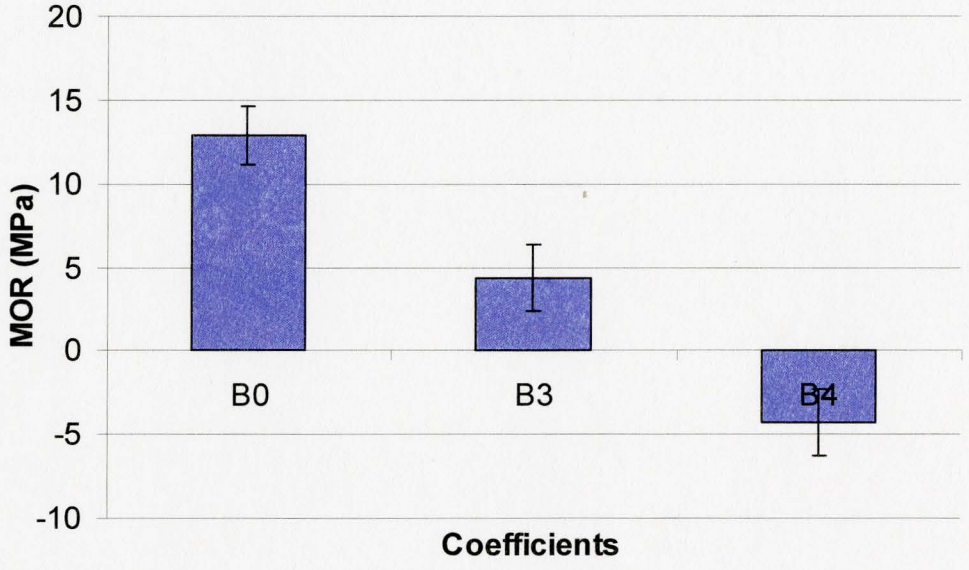

Figure 6.10 MOR Model Coefficients and Confidence Intervals for L, X, FL, FX

Specimens L, X, FL, and FX were fit with variables x_3 and x_4, resulting in an R^2 value of 0.706 for the model. The ANOVA results in Table 6.7 indicate a good fit to the

model and that at least one coefficient is not equal to zero with a critical F value of 3.59. In Figure 6.10, both β_3 and β_4 are significant, indicating that the production method influences the resulting MOR by decreasing the strength with lab firing and increasing it with lab extrusion.

6.5 Compressive Strength Regression Model

The model fit to the compression testing data, Equation 6.8, utilized a larger set of data than the other models due to some uncertainty in the results. The compression testing could not be completed at one location due to equipment failure, and so additional specimens were tested in order to make up for the possible influence of testing facilities, as the initial compressive strengths seemed to be affected by testing facility. The R^2 value for the model was 0.583, which may indicate lack of fit or a less than ideal model form for the data.

$$\tilde{y}_{comp} = 79.043 - 16.336x_1 + 3.407x_2 - 8.083x_3 - 5.565x_4 \qquad \text{Equation 6.8}$$

The fit of the model was assessed using residual plots, Figure 6.11. Although there appears to be a pattern of higher variance for no or fine glass (a), this value is influenced by the variation of the full scale specimens tested at different facilities, for which there was an increased range in the results. The residuals of the percentage waste addition are mostly positive excluding the results at 10% waste addition, where some negative residuals occur. These negative residuals may be outliers, which cause the

remainder of the residuals to be more positive. The results observed previously for laboratory extrusion and firing are repeated in (c) and (d), where the residual range for the laboratory extruded or fired specimens is larger than for the plant specimens. Comparing the residuals to the experimental results, there is a good range of residual distribution; however there are outliers at the extreme negative for low compression values and at the extreme positive for high compression values. Overall, there is no clear evidence of lack of fit of the compression model from the residual plots.

Table 6.8 ANOVA Values for Compressive Strength

Variation	Sum of Squares	DOF	Mean Square	F_0
SSR	14397.65	4	3599.413	19.54112
SSE	10315.03	56	184.1969	
SST	24712.68	61		

The ANOVA table for the compression results, Table 6.8 gives, a calculated F_0 value for the data of 19.54, which is higher than the critical F value, 2.466. From Figure 6.12, the coefficients for production method are of little to no significance to the model as the confidence intervals for β_3 and β_4 cross the horizontal axis, and are therefore statistically likely to be equal to zero. This result may be due to the increased variance for specimens FL and FX, which do not contain waste glass, and would therefore sway the result of the importance of this factor. A better form of the model would separate the production methods from the waste glass addition, however as discussed for the modulus

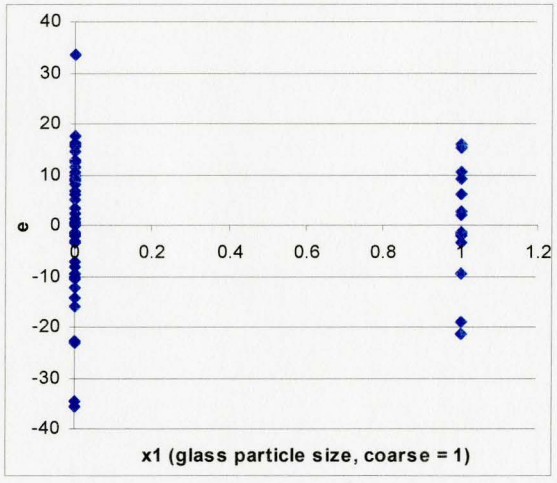

(a)

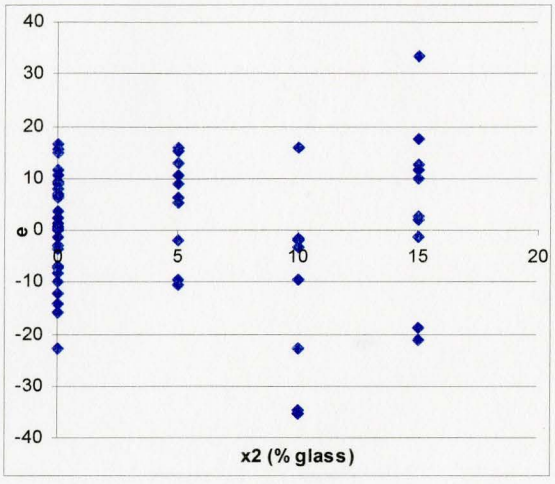

(b)

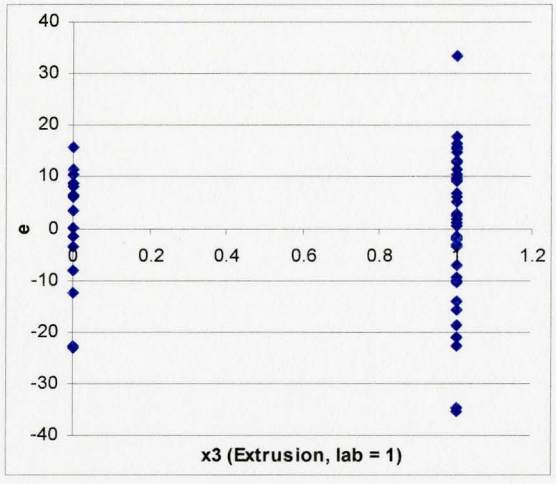

(c)

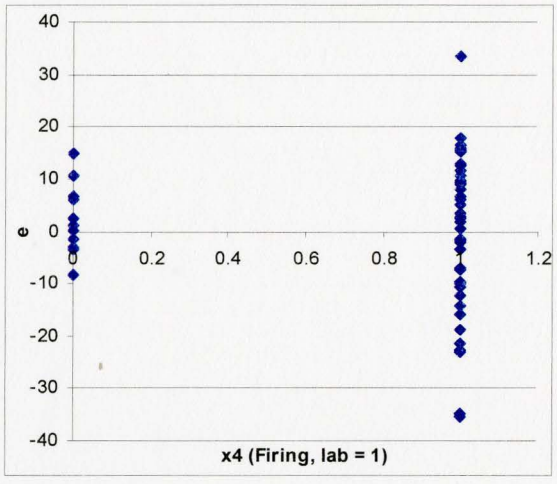

(d)

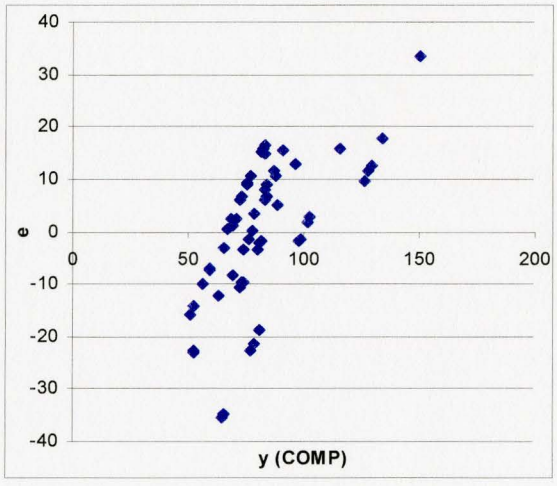

(e)

Figure 6.11 Residual Plots of Compression Residual VS (a) x1 (b) x_2 (c) x_3 (d) x_4 (e) y

of rupture model, this would make the comparison of results very difficult. Other coefficients in the model, including percentage waste glass addition and particle size, are more significant in their influence on the results. A better fitting model may be achieved by introducing a separate variable to account for the variation in testing facilities.

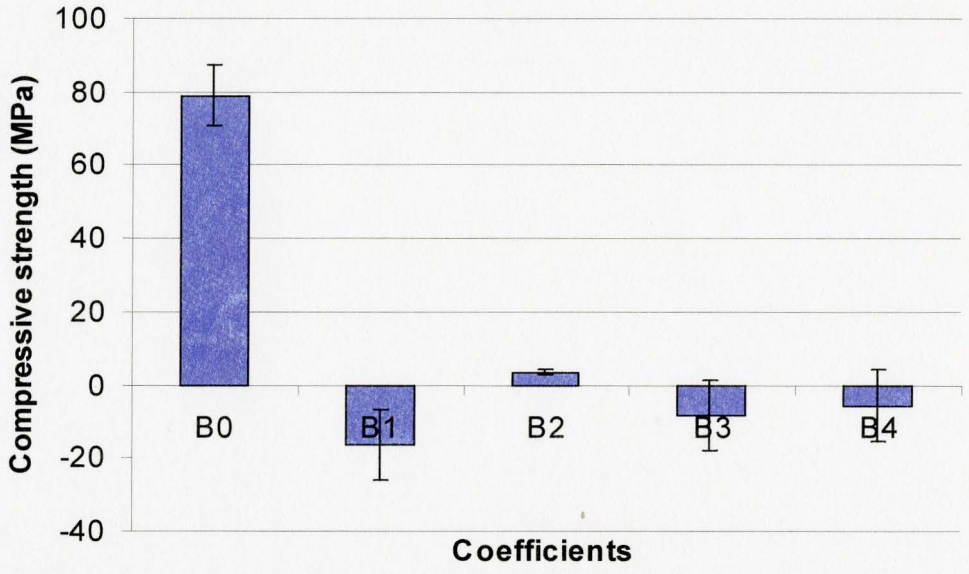

Figure 6.12 Compressive Strength Coefficients and Confidence Intervals

6.6 Freeze-Thaw Durability Regression Model

The data for the freeze-thaw durability testing was modelled for all specimens at both 50 cycles and 100 cycles in order to compare the limits of the CSA failure criteria with the results of extended testing. An initial review of the data revealed several outliers where catastrophic failure of the specimens had occurred. In order to fit a representative model while still accounting for the failure of these specimens, the measured mass loss of

any specimens that failed due to mass loss beyond 0.5% or due to cracking was replaced with a value of 0.5% at 50 cycles. At 100 cycles, the failed specimens were represented with a mass loss value of 1%.

6.6.1 Freeze-Thaw Durability Regression Model After 50 Cycles of Testing

The model for the first 50 cycles of testing, Equation 6.9, resulted in an R^2 value of only 0.402. This may indicate a poor fit for the data; however the residual plots, Figure 6.13, show a good distribution of residuals for the variables. Both extrusion and firing location, (c) and (d), show a clear pattern for the plant specimens, with residuals occurring at a defined high and low.

$$\tilde{y}_{ft50} = 0.054 - 0.0082x_1 - 0.0077x_2 + 0.132x_3 + 0.045x_4 + 0.122x_5 \qquad \text{Equation 6.9}$$

The lack of clear evidence of poor fit in the residual graphs is not clarified by the ANOVA table, Table 6.9. Although the calculated F_0 value is higher than the critical value of 2.349, the regression error is higher than ideal.

Table 6.9 ANOVA Values for Freeze-Thaw Durability at 50 Cycles

Variation	Sum of Squares	DOF	Mean Square	Fo
SSR	0.577102	5	0.11542	10.2133
SSE	0.858875	76	0.011301	
SST	1.435977	81		

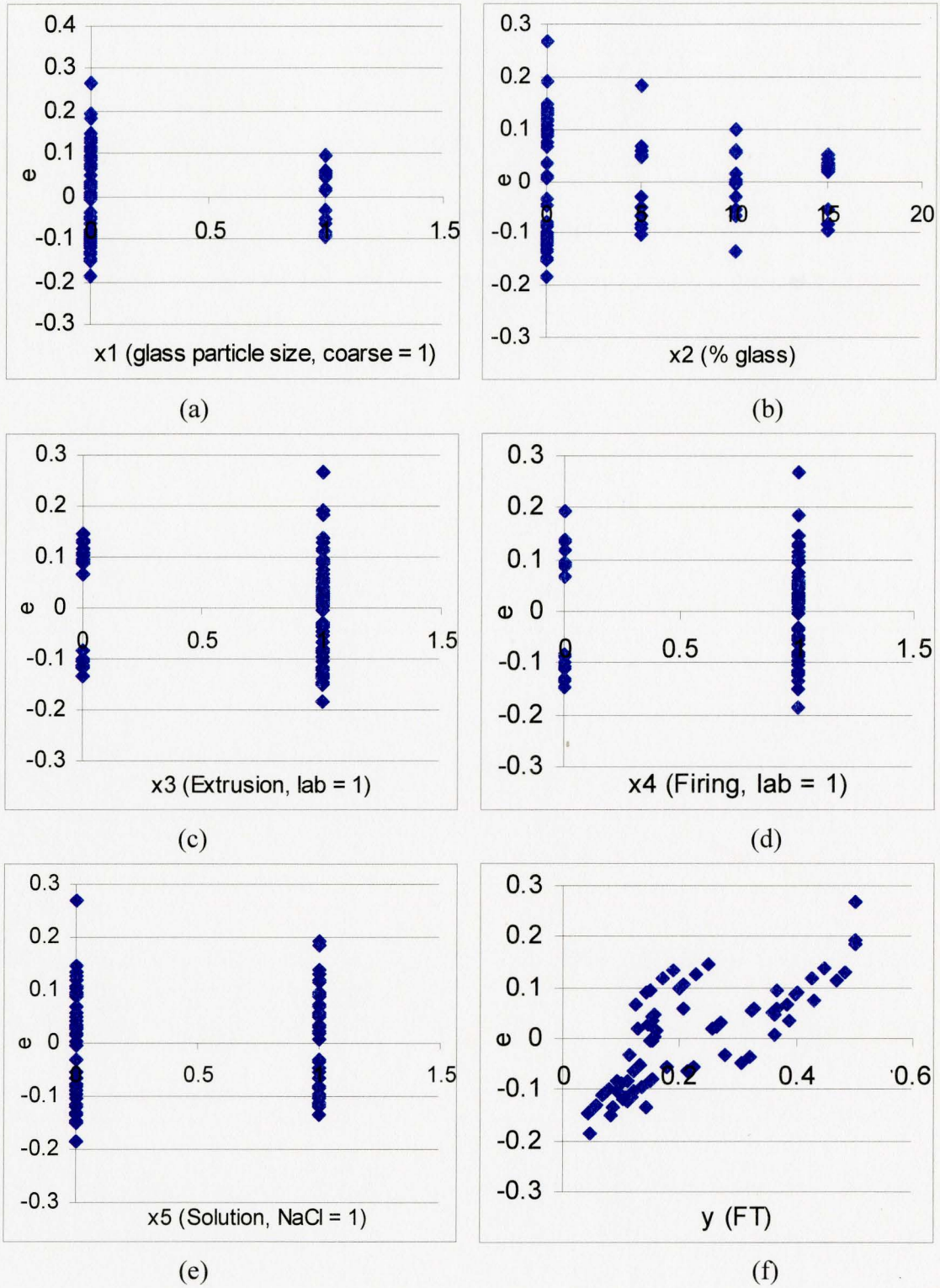

Figure 6.13 Residual Plots for Freeze-Thaw at 50 Cycles VS (a) x1 (b) x_2 (c) x_3 (d) x_4 (e) x_5 (f) y

The coefficients in Figure 6.14 indicate that the most influential variables are the extrusion method, β_3 and the testing solution for the specimens, β_5. The remaining variables are considered insignificant due to large confidence intervals or in the case of percentage waste glass addition, β_2, by a relatively small influence. The fit of the model is therefore affected by the inclusion of insignificant variables.

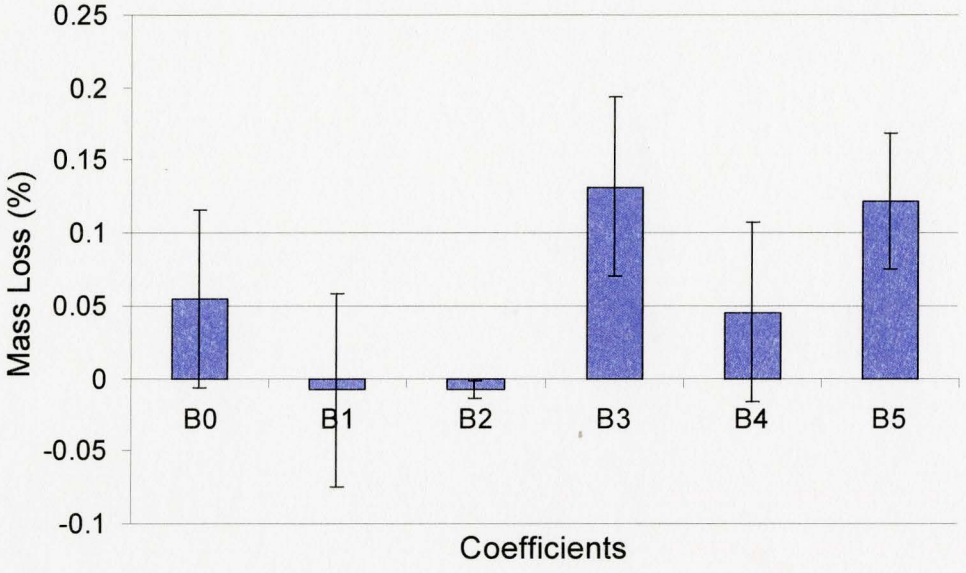

Figure 6.14 Freeze-Thaw Durability Coefficients and Confidence Intervals, 50 Cycles

6.6.2 Freeze-Thaw Durability Regression Model After One Hundred Cycles of Testing

By continuing the testing of freeze-thaw durability beyond the recommended 50 cycles, more complete information was obtained in terms of long term performance. From this data, the model in Equation 6.10 was developed for 100 cycles of durability testing.

$$\tilde{y}_{ft100} = 0.677 + 0.11x_1 - 0.031x_2 - 0.0275x_3 + 0.122x_4 - 0.280x_5 \quad \text{Equation 6.10}$$

The model for 100 cycles had a fit similar to the model for 50 cycles of testing, with an R^2 value of only 0.364, indicating that there is variability in the data not explained by the current model form. The residual plots, Figure 6.14, show a consistent range of variation, however the distinct levels of variation noted at 50 cycles are again observed in (c) and (d) for extrusion and firing in the plant. The outliers in (f) are necessary to account for the failed specimens despite the influence they may have on the model.

Table 6.10 ANOVA Values for Freeze-Thaw Durability at 100 Cycles

Variation	Sum of Squares	DOF	Mean Square	Fo
SSR	3.389421	5	0.677884	8.687673
SSE	5.930149	76	0.078028	
SST	9.31957	81		

By investigating the variance of the model, Table 6.10, the calculated F_0 value of 8.688 is found to be larger than the critical F value of 2.342; however there is a large error associated with the fit of the model. Although at least one of the coefficients is non zero, the model indicates that some of the coefficients are of little or no importance, and that there exists variance in the model that is not accounted for by the current variables. Figure 6.15 shows the coefficients and their confidence intervals at 100 cycles of freeze-

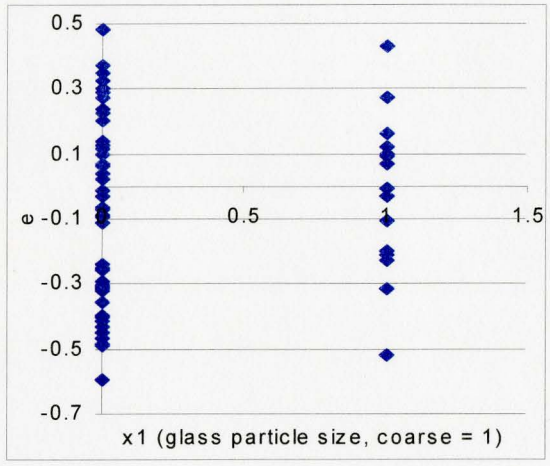

(a)

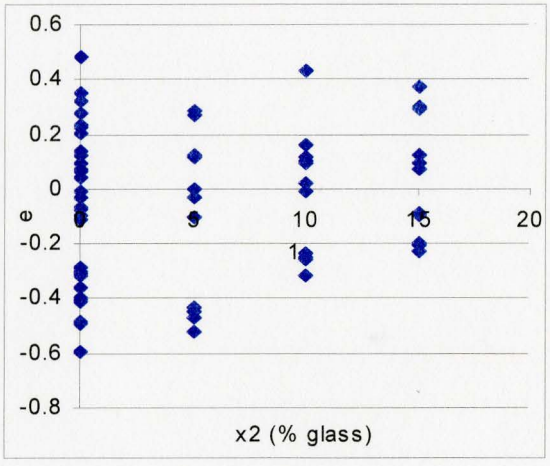

(b)

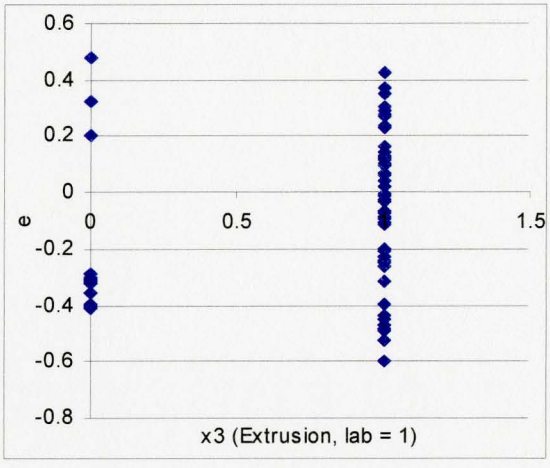

(c)

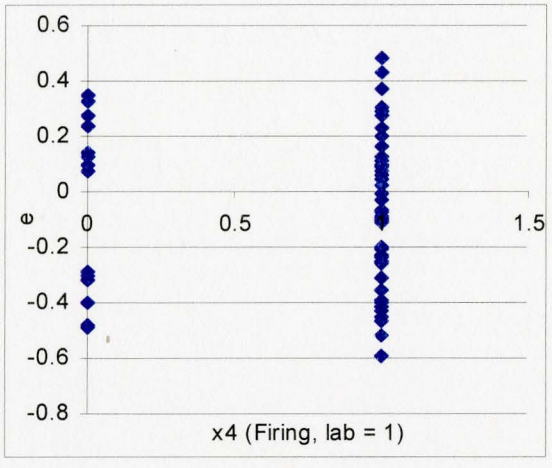

(d)

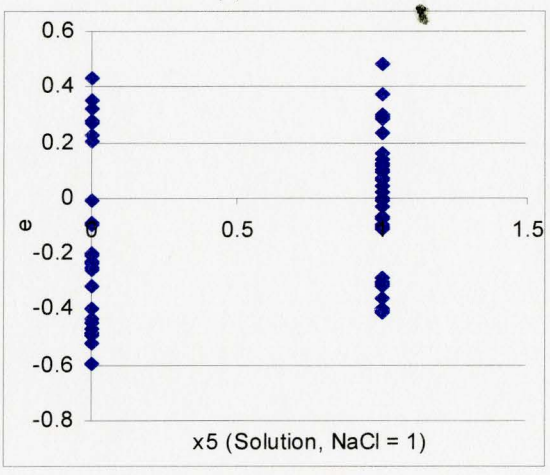

(e)

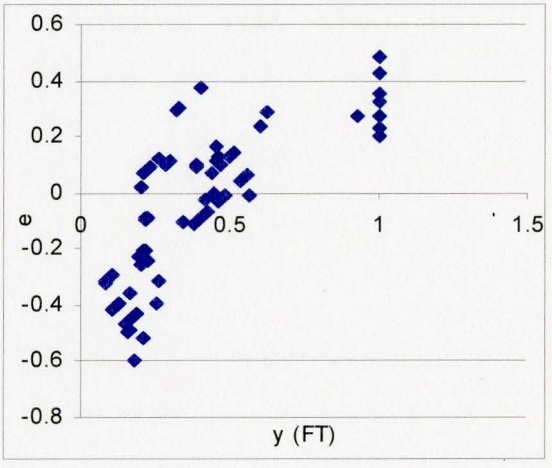

(f)

Figure 6.15 Residual Plots, Freeze-Thaw 100 Cycles VS (a)x_1 (b)x_2 (c)x_3 (d)x_4 (e)x_5 (f)y

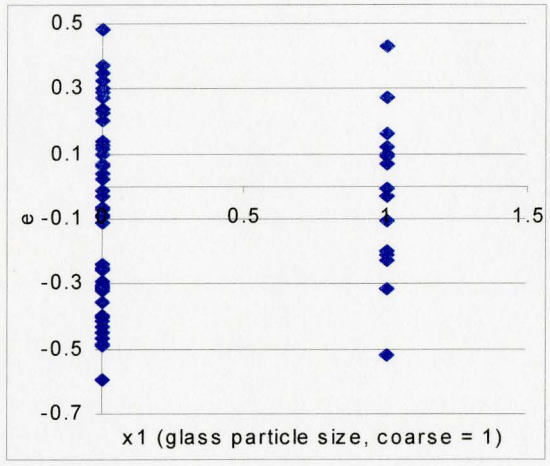

(a)

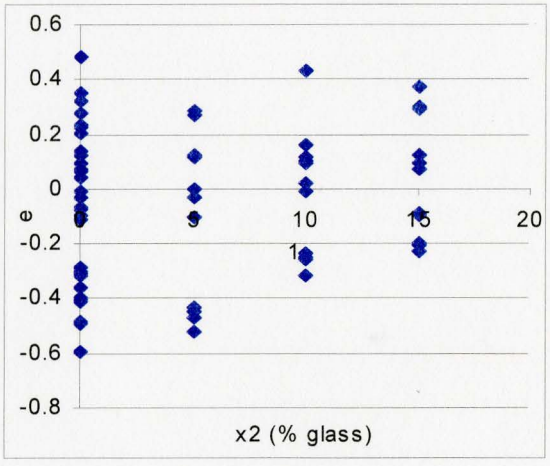

(b)

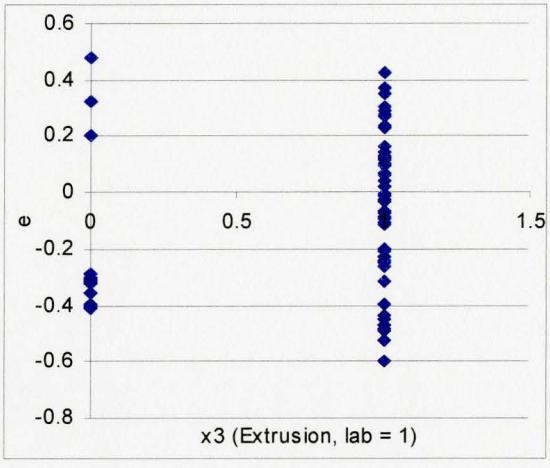

(c)

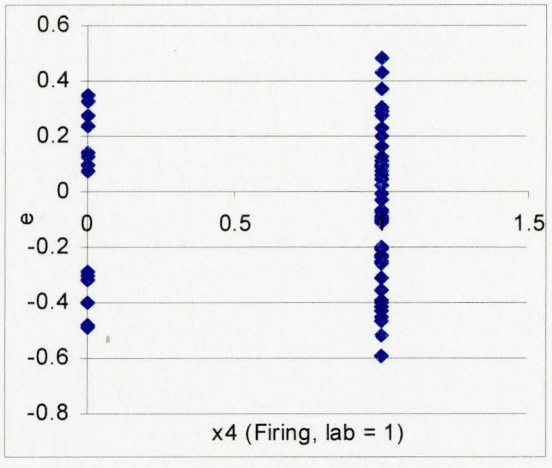

(d)

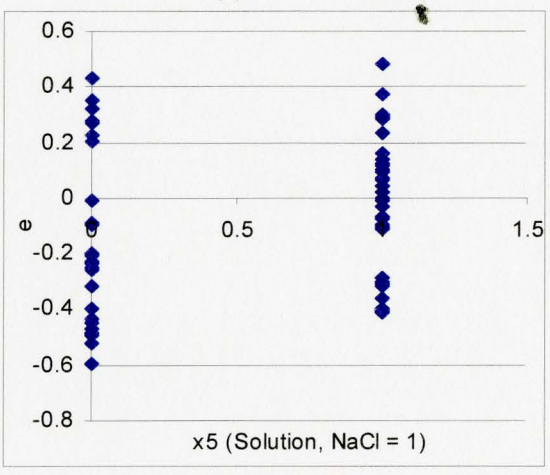

(e)

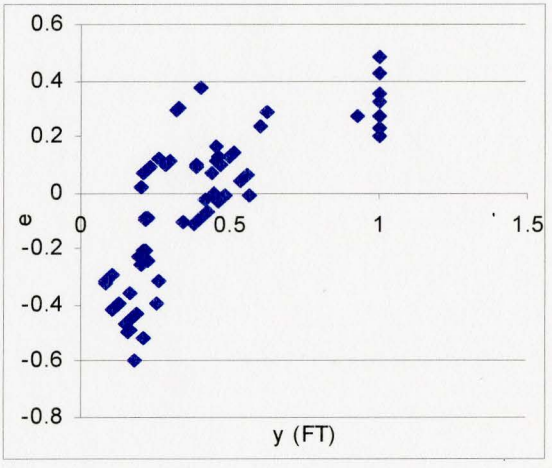

(f)

Figure 6.15 Residual Plots, Freeze-Thaw 100 Cycles VS (a)x_1 (b)x_2 (c)x_3 (d)x_4 (e)x_5 (f)y

majority of the initial mass loss occurred in the small scale, laboratory extruded specimens. At 100 cycles, the extrusion method was no longer influential, as the plant specimens began to lose mass at an increasing rate. As the mass loss increased, especially for the large specimens, the data began to reflect the visually observed results. The specimens tested in deionized water had an increase in mass loss, causing coefficient β_5 to reverse in direction.

6.7 Discussion

The testing program was performed in order to establish the effect of the addition of waste glass to fired clay brick. In this investigation, several variables were considered, including waste glass particle size, percentage of waste glass addition, and production method, in order to determine the optimal combination for production purposes. The ultimate aim of the addition of waste glass was to potentially improve brick properties while maintaining quality and ease of production. The performance of the test specimens was ascertained through absorptive, mechanical, durability and microstructural investigative testing.

6.7.1 Effects of the Addition of Waste Glass

From the results presented for absorption, strength, and durability properties for specimens with waste glass content, there was a significant effect on the properties of the specimens, especially with additions of waste glass exceeding 5% by mass.

The absorption properties, including the initial rate of absorption, the cold water and boiling water absorption, and the absorption ratio, had observable improvement with the addition of waste glass. The initial rate of absorption decreased significantly with the addition of waste glass at 10% fine, 15% coarse and 15% fine. Modelling of the IRA results indicated a correlation between both the increasing percentage of waste glass, which tended to decrease IRA, and the particle size of the waste glass, where coarse particles tended to increase the optimal IRA. Both the 24 hour cold water absorption and the 5 hour boiling water absorption measured values showed a decrease in absorption for specimens containing 10% fine, as well as 15% coarse and fine waste glass, indicating a decrease in pores in general for specimens with increased waste glass addition. This effect is reflected in the absorption ratio values; however, due to the decrease in both numerator and denominator of the ratio, the effects are not as noticeable when presented in absorption ratio form. Modelling of the C/B ratio, therefore, shows only a slight significance of addition of waste glass, despite the results observed at the CWA and BWA levels.

Overall, the absorption properties of specimens containing waste glass tend to improve when compared to the control specimen. The resulting improvement in absorption was similarly reported by Shutt et al, Smith, and Sanders (1972; 2004; 2003), who observed decreasing C/B ratios beyond 5% waste glass addition. From the SEM analysis, a greater level of vitrification in the matrix, as well as glassy flow, was observed for specimens E, F, and G. This increase in vitrification and flow would lead to a

decrease in pores as the initial bottleneck formation at the sintering point of adjacent particles becomes more fluid and elongated.

Based on the mercury intrusion porosimetry analysis, there was a significant decrease in the overall porosity of the specimens as percent waste glass addition was increased, where specimen G had a porosity 27% lower than specimen A. The particle size of the waste glass influenced this decrease in porosity, where the fine waste glass caused a greater rate of decreased porosity than the coarse waste glass. In addition to the general decrease in porosity, the distribution of the pores within the fired clay bodies was altered by the addition of waste glass. The control specimen had a narrow range of pore sizes, all within 0.9 μm, and a clear peak in pore volume between 0.5μm and 0.7μm. Specimens B, C, and D shared this general pore distribution, with the majority of the pores in the specimen being the same size, and with a peak volume of nearly 0.025cc/g. At 10% fine waste glass addition, specimen E, the pore size distribution began to widen and the peak was significantly reduced. At 15% fine waste glass addition, specimen G, the distribution of pores ranged over 2.7μm, and there was no longer a clear peak pore size within the specimen. The change in the distribution of the pores, especially the balance of the pore sizes over a greater range, appears to influence the experimental absorption ratio results, as the greatest change in absorption occurred in specimens with the most altered pore distributions.

The strength and durability properties of the specimens containing waste glass were also influenced by changes at the microscopic level. The compressive strength of the specimens containing 10% coarse, 15% coarse and 15% fine waste glass increased

significantly, by as much as 45%. There was a large variation in the results for the specimen containing 10% fine waste glass; however, the average value for these specimens was higher than that of the control specimen. The compressive strength model indicated that the percentage of waste glass was the most influential variable for the increase of the compressive strength, while the use of coarse glass detracted slightly from this beneficial influence. The compressive strength values achieved were much higher than those discussed in the literature (Shutt et al, 1972; Leshina and Pivnev, 2002; Smith, 2004; Youssef et al, 1998), however the general trends reported by both Shutt et al. and Leshina and Pivnev at 20% to 30% waste glass addition were recreated with only 15% waste glass addition. This is most likely due to the use of smaller waste glass particle sizes for the tested specimens but may also be a result of differing size effects for the specimens tested in the literature.

The modulus of rupture strength for specimens containing waste glass was tested using the CSA method, which resulted in lower than expected values and no statistical evidence of improvement. There is a general trend of increasing average strength as waste glass addition increases, and full testing using the four point loading method would be expected to result in improved MOR values for increasing waste glass addition when compared to the control specimen. The MOR model for the small scale specimens showed a very slight influence of waste glass addition. At the microscopic level, the increase in vitrification and glassy phase in the specimens containing 10% and 15% waste glass created a denser fired specimen, as was seen in the decreasing porosity values

obtained through mercury intrusion porosimetry analysis. This increased density and more complete sintering improved the maximum compressive strength.

The particle size of the waste glass is less influential in mechanical strength then in absorption properties, as both coarse and fine particles improve strength at a comparable rate. The MOR values obtained using the CSA method of testing were not comparable to the results reported in the literature review.

The freeze-thaw durability of specimens containing waste glass was determined according to a modified method in both deionized water and 3% sodium chloride solution. The results of 100 cycles of testing in deionized water were unexpected. At 50 cycles of testing, the majority of the specimens were still below the CSA recommended mass loss limit of 0.5% and were performing moderately well in terms of surface finish. In the final 50 cycles of testing, specimen failure increased dramatically. Of the 21 specimens tested for waste glass addition, 7 failed with high mass loss and breaking. Of those failed specimens, all contained at most 10% coarse waste glass. The specimens with 10% fine waste glass and 15% either coarse or fine waste glass did not experience failure, and visually, appeared nearly pristine at the conclusion of the testing in both deionized water and sodium chloride solution. The difference in mass loss compared statistically does not reflect this decreased rate of failure for specimens containing higher percentages of waste glass due to the large variation in the data; however the model fit to the data separately at both 50 and 100 cycles supports the significance of the addition of waste glass to the improvement in durability.

The specimens tested in sodium chloride solution experienced less mass loss than those tested in deionized water, with only one documented failure. No visible surface damage or cracking for any of the specimens. This result was captured in the model of the freeze-thaw results at 100 cycles. Specimens E and F, containing 10% fine and 15% coarse waste glass, respectively, had a statistically significant decrease in mass loss when compared to the control specimens.

As discussed, the SEM images indicated that increased vitrification with higher percentage addition of waste glass tended to decrease the amount of mass loss for specimens E, F, and G. The low R^2 values for the freeze-thaw models indicate a missing influential variable in the model. The change in pore distribution, density, or pore connectivity may be the influencing factor in the decrease of mass loss experienced by the specimens. Based on the mercury intrusion porosimetry results, the Maage (1984) frost resistance number, when calculated for the tested specimens, indicated that all of the tested specimens could be considered nondurable based on the pore sizes and distribution, despite extensive freeze-thaw durability testing indicating that only specimens A, B, C, and D experienced failure in the specimens tested with waste glass addition. Based on the experimental results, the Maage method is not accurate for predicting the durability of bricks produced with waste glass; however the experimental evidence suggests that there is a clear connection between the pore distribution and the resulting durability of the specimen.

The mass loss for the specimens tested in sodium chloride solution was much lower than expected, with the specimens appearing unaffected by the vigorous freeze-

thaw cycling. This result could not be explained by any difference in the microstructure of the specimens due to waste glass addition since the control specimen also performed better than the same control specimen tested in deionized water. One possible theory to explain this result draws on the behaviour of a freezing salt solution, in this case 3% NaCl, which is comparable to freezing sea water. As discussed by Rice and Chau (1997), the freezing of the upper layer of the NaCl solution results in the formation of ice crystals which exclude the dissolved NaCl into a brine solution. Whether this phenomenon is occurring on the microscopic scale within pores of the brick specimens, or on the macroscopic scale within the testing containers, the hypothesis is that this system allows pressure from the freezing water to be accommodated by the partially frozen brine solution. The pressurization of the brine solution prevents damage to the matrix surrounding the pores of the brick, which in turn, limits damage to the specimen itself.

The variables of testing, including percentage of waste glass addition and particle size, are in most cases significant enough to influence the resulting absorptive, mechanical, and durability properties. As the percentage of waste glass is increased, there is a statistically significant decrease in initial rate of absorption, cold waster absorption and boiling water absorption, while the strength properties, as indicated by compressive strength and modulus of rupture, increase. This improvement in properties was statistically significant at additions of 10% and 15% waste glass, however even at additions of 5% waste glass, the properties of the brick specimens were at least maintained in comparison with the control specimens.

The particle size of the waste glass was also influential in most cases. For initial rate of absorption, modelling indicated that the decrease in absorption was directly affected by the choice of particle size, where fine particles, ranging from 300μm to 45μm, were more beneficial than coarse particles. At 10% waste glass addition, the CWA and BWA were significantly decreased for the specimens containing fine waste glass, but not coarse waste glass. At 15%, the decrease in CWA and BWA for specimen G was greater than for that of F, and therefore the fine particles had a greater influence on the improvement of properties than the large particles. Modelling of the compression and MOR results indicated that the particle size did not influence the improvement in strength as significantly as the percentage of waste glass addition. The porosity and pore distribution was also most affected by fine particles, which led to a higher density and wider pore size distribution.

6.7.2 Effects of Production Method

Analysis of the absorption, strength, and durability properties resulting from the variation of production methods indicated that there was a significant effect on the properties of the specimens depending on the location and method of both extrusion and firing of the specimens.

The initial rate of absorption increased for small scale specimens fired in the plant kiln, while large scale specimens extruded in the plant and small scale laboratory fired specimens were comparable. The IRA results observed for specimens containing waste glass are therefore directly comparable with expected plant trial results. A model fit to the

IRA data included the specimens containing waste glass and those with various production methods, and reinforced the conclusion that the addition of waste glass, especially fine waste glass, will improve the initial rate of absorption for specimens extruded in the plant, however the plant kiln will increase the rate of absorption from the optimum achieved in the laboratory kiln. This increase in absorption for specimens fired in the plant kiln may be due to a less complete vitrification caused by the larger scale of production and the location of the specimen on the kiln car.

Although the ratio of the CWA and BWA did not indicate a significant difference in mean values as a result of production method, the values did indicate a general trend of improvement in absorption as production is moved from the laboratory to the plant, with firing location as the most influential factor. The improvement in properties from laboratory production to plant production indicates that the results observed with waste glass addition are conservative. Although both the CWA and BWA improved dramatically with 10% fine and 15% waste glass addition, the improvement is expected to be even greater in a plant scale trial.

A comparison of the pore structure for specimens produced in the laboratory and factory as determined by mercury intrusion porosimetry indicates that the firing location influences the porosity, where firing in the plant kiln tends to reduce the porosity of the specimen and increase the range of pore sizes. Specimen L had a very high peak volume and a narrow pore size distribution, which was comparable to control specimen A. The results obtained experimentally for the initial rate of absorption contradict the measured

decrease in porosity; however the absorption ratio results are consistent with the measured distribution of pores.

The strength properties for the different production methods also indicated a significant influence of the method of extrusion and firing of the specimen. The specimens both extruded and fired in the laboratory had an increase in strength when compared to the control specimen L. The results of the control specimen A and the plant specimen FX were similar, and therefore it is expected that the properties of specimens containing waste glass produced in a plant setting would follow the same trend as the small scale specimens.

The modulus of rupture of the specimens with differing production methods varied from the control specimen. The modulus of rupture increased significantly with both extrusion and firing in the plant, where specimen FX achieved an average MOR value twice that of the control, L. As discussed previously, the use of the four point loading modulus of rupture test for specimens L, X, FL, and FX resulted in much higher MOR values than those of specimens A to G, however if the trend within the production method specimens holds true, the results in specimens A to G can be considered extremely conservative. Production of specimens containing waste glass in a plant setting would lead to a significant improvement in MOR performance. Support for the use of the four point loading method is provided by data reported in the literature review, the values for which are comparable to those obtained using the four point loading method to within 2 MPa at the control level (0% waste glass).

The results of the freeze-thaw durability for the specimens of varying production methods caused some concern in their performance. At the completion of 100 cycles of testing, all 10 specimens fired in the laboratory kiln and tested in deionized water had failed through excessive mass loss by way of surface spalling and chipping, as well as splitting and delamination. The results for the control specimen L were not comparable to the control specimen A, however the performance of the plant fired specimens were comparable, and no significant difference in their mean existed. Modelling of the freeze-thaw results indicated that no conclusion could be made with respect to the influence of production method due to the large variation at 100 cycles, however at 50 cycles the laboratory extrusion was a significant factor in increased mass loss. Density was slightly lower for specimens extruded in the lab, and according to the Maage method for prediction of freeze-thaw durability, all of the specimens could be considered non-durable. Experimental results indicated that specimens fired in the plant were much more durable than the laboratory fired specimens, despite the predicted durability factor.

When tested in 3% sodium chloride solution, mass loss for the full size specimens, FL and FX, was significantly lower at both 50 cycles and 100 cycles, while the small scale specimens, L and X, were similar to the control specimen A. The mass loss for specimens tested in NaCl solution was significantly lower than that of specimens tested in deionized water. The mass loss experienced by the laboratory specimens was in general much greater than that of the plant specimens, and therefore the slight improvements in durability as a result of waste glass addition can be considered conservative, with lower mass loss values expected in a full scale plant trial.

6.7.3 Firing, Porosity and Durability

The addition of particles of waste glass in percentages ranging from 5% to 15% resulted in changes at the microscopic level which affected both absorptive and mechanical properties of fired clay brick. These changes occurred in both the vitrified matrix of the bricks and the final pore distribution. The effects on the matrix and pore structure were observed using scanning electron microscopy and mercury intrusion porosimetry. Increased vitrification and glassy flow was observed for specimens containing a minimum of 10% waste glass. Increased vitrification was confirmed by elongation of the visible pores, as well as an extensive glassy matrix, while there was also an increase in the crystalline phase visible as waste glass content was increased.

Results of the mercury intrusion porosimetry, as well as the experimental results for absorption and durability indicated that the addition of waste glass as low as 5% by mass decreased porosity, and increased both the range in size and the variation in volume of pores within the fired clay brick specimens. This increase in range and decrease in porosity improved the absorption properties by limiting the volume of water absorbed by the specimens, and providing increased durability in freeze-thaw testing. This improvement in durability especially may be directly related to the porosity, where a greater variety of pore sizes seems to be more capable of resisting damage. Known relationships which explain this phenomenon, including Maage's (1984) durability index do not accurately predict the experimental results, and further efforts by Korath et al (1998) attempt to correct this issue. Although the results of this testing program do not allow the development of a more comprehensive durability index, they do further support

the correlation between pore structure and durability, as well as the possible relationship between the tensile strength and durability. There is also a significant influence of waste glass addition on the overall porosity and pore structure, and as a result, on the durability of the specimens.

CHAPTER 7 CONCLUSIONS AND RECOMMENDATIONS

7.1 Conclusions

A comprehensive experimental program was undertaken to evaluate the effects of adding waste glass to fired clay brick. Various observations and conclusions were drawn from the study and are presented, in a topical manner, according to mechanical properties, absorptive properties, microstructural properties, durability issues, and production methods. The following conclusions are based on the observed characteristics of the tested specimens as a result of the addition of waste glass.

7.2 Mechanical Properties

1) The compressive strength of the specimens containing 10% coarse, 15% coarse and 15% fine waste glass increased significantly, by as much as 104%. Percentage of waste glass was the most influential variable in the increase of the compressive strength.

2) The modulus of rupture strength for specimens containing waste glass was tested using the CSA method, which was found to be inappropriate for the specimens, resulting in high variance and low strength values. As a result, the four point loading method was adopted and gave results comparable to those in the literature.

3) The MOR values obtained for the laboratory scale specimens using the CSA method of testing were not comparable to results reported in the literature review.

4) The particle size of the waste glass is less influential in mechanical strength than in absorption properties, as both coarse and fine particles improved strength at a comparable rate.

7.3 Absorptive Properties

1) Modelling of the IRA results showed a direct correlation between both the increasing percentages of waste glass addition, which tended to decrease IRA, and the particle size of the waste glass, where fine particles tended to decrease the IRA at a greater rate than the coarse particles.

2) Both the 24 hour cold water absorption and the 5 hour boiling water absorption decreased significantly for specimens containing 10% fine, as well as 15% coarse and fine waste glass.

7.4 Microstructural Properties

1) A greater level of vitrification in the matrix was observed for specimens containing 10% fine, as well as 15% coarse and fine waste glass.

2) There was a significant decrease in the overall porosity of the specimens as the percentage of waste glass was increased. The particle size of the waste glass influenced this decrease in porosity, where fine waste glass caused a greater rate of decreased porosity than the coarse waste glass.

3) The distribution of pore sizes within the fired clay bodies was altered by the addition of waste glass. This change in the distribution of the pores, especially the volume balance of the pore sizes over a greater range, significantly influenced the absorption properties.

7.5 Durability Issues

1) The method for freeze-thaw durability testing recommended by CSA CAN3-A82.2-M78 is not accurate for determination of a quantifiable mass loss or a repeatable result. A method was developed which combined the specifications of CSA with those of ASTM C 1262-98, "Standard Test Method for Evaluating the Freeze-Thaw Durability of Manufactured Concrete Masonry Units and Related Concrete Units" and led to more readily measured mass loss results.

2) The specimens tested in 3% sodium chloride solution performed better than those tested in deionized water, with only one documented failure due to a high level of mass loss, and no visible surface damage or cracking for any of the specimens.

3) Specimens with 10% fine waste glass and 15% waste glass did not experience any significant freeze-thaw damage at the conclusion of 100 cycles of testing in both deionized water and 3% sodium chloride solution.

4) The change in pore distribution, density, or pore connectivity may be the influencing factor in the decrease of mass loss experienced by the specimens with increased waste glass content.

5) Based on the experimental results, the Maage method is not accurate for predicting the durability of bricks produced with waste glass; however, the experimental evidence

suggests that there is a direct relationship between the pore distribution and the resulting durability of the specimen.

6) The suggestion by Ravaglioli (1976) that a larger percentage of pores exceeding 1.4μm results in improved durability may be more representative of the observed experimental results.

7) The modified freeze-thaw approach provided a reliable test method to accurately quantify the mass loss due to freeze-thaw action; however, the results of this method are relative in nature and cannot be directly compared to the CSA standard. For this reason, the results are not expected to be directly indicative of field performance.

7.6 Production Method

1) There is a significant effect on the properties of the specimens, including strength, durability, absorption, and microstructure, depending on the location of both extrusion and firing of the specimens.

2) The initial rate of absorption increased for small scale specimens fired in the plant kiln, while specimens produced in the plant as well as specimens fired in the lab were comparable to one another in terms of IRA.

3) The CWA and BWA values indicated a general trend of improvement in absorption as production was moved from the laboratory to the plant, with firing location as the most influential factor.

4) Extrusion location influenced the porosity, where extrusion in the lab tended to increase the porosity of the specimens.

5) The firing location influenced the distribution of the pores in the sample. The results obtained experimentally for the initial rate of absorption contradict the measured decrease in porosity; however the absorption ratio results are consistent with the measured distribution of pores. For this reason, pore distribution may be more influential than general porosity on absorption.

6) The specimens both extruded and fired in the laboratory had an increase in strength when compared to the plant control specimen.

7) The modulus of rupture increased significantly with both extrusion and firing in the plant, despite lower than expected values for those full scale specimens fired in the lab.

8) At 50 cycles of freeze-thaw testing, laboratory extrusion was a significant factor in increased mass loss.

9) The mass loss experienced by the laboratory specimens was in general much greater than that of the plant specimens.

In conclusion, the addition of waste glass to fired clay brick resulted in an improvement of the absorption, mechanical and durability properties at the laboratory scale. These improvements can be considered conservative when compared to the expected results at the plant scale, as preparation and firing in the plant also improved properties compared to the laboratory specimens.

7.7 Recommendations and Future Research

The purpose of this experimental research program was to investigate the influence of the addition of waste glass on fired clay brick in order to determine the

feasibility of replacing non-renewable resources used as raw material, such as clay and crushed shale, with non-recycled waste material diverted from landfills. Ideally, the method of waste glass addition would be optimized in order to improve strength and durability of bricks while easily incorporating the waste glass addition into current production methods, and decreasing the energy consumed in the firing process.

From the test results discussed in this thesis, several recommendations can be made with respect to the addition of waste glass to fired clay brick. At 5% waste glass addition, there is no statistical improvement in the properties of the brick; however, generally there is a slight trend of improvement. This trend is especially clear with the use of fine particles of glass ranging in size from 45μm to 150μm. At 5% waste glass addition, the shrinkage and colour darkening effect of the waste glass are negligible. Based on these results, 5% of the current raw material could be replaced without any impact on the resulting product, and with the possibility of improved properties.

With the addition of 10% coarse waste glass, the results are comparable to those achieved with 5% waste glass; however, there is a slight increase in darkening and shrinkage. When fine waste glass is used at 10% addition, there is a statistically significant improvement in properties, especially durability and absorption.

At 15% waste glass addition, there is a statistically significant improvement in properties for both coarse and fine waste glass addition. The strength properties are improved significantly, and absorption properties are improved as a result of the alteration of the pore structure and distribution in the specimens. As a result of the high percentage of waste glass, there is a marked increase in shrinkage and warping, as well as

a noticeable darkening of the fired product. This result may be further refined by lowering the firing temperature of the plant kiln; however it will be necessary to find a balance between the improved strength and durability properties achieved through the increased sintering, and the aesthetic concerns at the current firing temperature. Due to the increased cost of preparing fine particles of waste glass, as well as the large jump in the improvement of properties at 15% fine waste glass addition, the optimum waste glass addition for the purpose of factory scale implementation based on the percentages tested should be 10% fine waste glass or 15% coarse waste glass depending on which properties are to be optimized. If strength properties are of the greatest interest, fine waste glass particles are ideal to minimize cost, however to achieve a balanced improvement in properties overall, especially absorption and durability, fine waste glass at 10% should be used.

Based on the testing methods employed in this thesis, further development of the modified freeze-thaw test should be carried out. The purpose of the modification from the recommended CSA methods is to provide repeatable and numerically quantifiable results. The development of a freeze-thaw test method on the basis of microanalysis methods such as SEM and mercury intrusion porosimetry should be further explored, as it may provide a more reliable method for the prediction of durability without the need for tedious and lengthy testing.

The use of waste glass as a fluxing agent and replacement for raw material in the production of fired clay bricks serves to optimize an ancient technology in order to meet the needs of a changing modern world. In the quest to produce a stronger, more durable,

and more economical product, it is possible through this method to also balance the need for environmental stewardship and waste management by utilizing a waste additive as a viable material alternative.

REFERENCES

Anderson, Michael, Elliot, Mark, and Hickson, Celia. 2002. Factory-scale proving trials using combined mixtures of three by-product wastes (including incinerated sewage sludge ash) in clay building bricks. *Journal of Chemical Technology and Biotechnology* 77: 345-351.

Arkhipov, I.I., Nemchenok, Z.O., and Rempel, A.M. 1979. Using waste for the production of ceramic tiles. *Glass and Ceramics* 36, no. 10: 588-589.

ASTM International. 2006. *C1262-98 Standard Test Method for Evaluating the Freeze-Thaw Durability of Manufactured Concrete masonry Units and related Concrete Units.* ASTM: West Conshohocken.

Baulez, B., Mayayo, M.J., Yuste, A., Fernandez-Niento, C., and Gonzalez Lopez, J.M. 2004. TEM study of mineral transformations in fired carbonated clays: Relevance to brick making. *Clay Minerals* 39: 333-344.

Botton, Gianluigi. 2005. Introduction to Electron Microscopy MATLS 731. Hamilton: McMaster University. Photocopied.

Bowles, Joseph E. 1992. *Engineering Properties of Soils and Their Measurement.* 4th ed. Toronto: McGraw-Hill, Inc.

Brick Industry Association. 2004. Technical Notes on Brick Construction. Virginia.

Canadian Standards Association. 1978. *CAN3-A82.2-M78 Methods of Sampling and Testing Brick.* Rexdale: Canadian Standards Association.

Canadian Standards Association. 1987. *CAN3-A82.1-Burned Clay Brick.* Rexdale: Canadian Standards Association.

Carlson, Thomas A. 1975. *Photoelectron and Auger Spectroscopy.* New York: Plenum Press.

Carretoro, M. I., Dondi, M., Fabbri, B., and Raimondo, M. 2001. The influence of shaping and firing technology on ceramic properties of calcareous and non-calcareous illitic-chloritic clays. *Applied Clay Science* 20: 301-306.

Chang, Raymond. 1998.*Chemistry, 6th Ed.* Boston: McGraw-Hill.

Coussy, Olivier. 2005. Poromechanics of freezing materials. *Journal of the Mechanics and Physics of Solids.* 53: 1689-1718.

Cultrone, Guiseppe, Rodriguez-Navarro, Carlos, Sebastián, Eduardo, Cazalla, Olga, and José de la Torre, Maria. 2001. Carbonate and silicate phase reactions during ceramic firing. *European Journal of Mineralogy* 13: 621-634.

Cultrone, Guiseppe, Sebastián, Eduardo, Elert, Kerstin, José de la Torre, Maria, Cazalla, Olga, and Rodriguez-Navarro, Carlos. 2004. Influence of mineralogy and firing temperature on the porosity of bricks. *Journal of the European Ceramic Society* 24: 547-564.

Drysdale, Robert G., Hamid, Ahmad A., and Baker, Lawrie R. 1994. *Masonry Structures Behavior and Design.* New Jersey: Prentice-Hall Inc.

Elert, Kerstin, Cultrone, Guiseppe, Rodriguez Navarro, Carlos, and Sebastián Pardo, Eduardo. 2003. Durability of bricks used in the conservation of historic buildings – influence of composition and microstructure. *Journal of Cultural Heritage* 4: 91-99.

Everett, D. H. 1961. The thermodynamics of frost damage to porous solids. *Transactions of the Faraday Society* 57: 1541-1551.

Goldstein, Joseph I. 2003. *Scanning Electron Microscopy and X-Ray Microanalysis.* New York: Kluwer Academic/Plenum Publishers.

Grimshaw, Rex W. 1971. *The Chemistry and Physics of Clays and Allied Ceramic Materials.* London: Ernest Benn Limited.

Heinrich, Kurt F. J. 1981. *Electron Beam X-Ray Microanalysis.* Toronto: Van Nostrand Reinhold.

Hlavac, J. 1983. *The Technology of Glass and Ceramics.* New York: Elsevier.

Jena, Akshaya, and Gupta, Krishna. 2005. Pore structure characterization techniques. *American Ceramic Society Bulletin* 84: 3 28-30.

Koroth, Surej R., Feldman, Dorel, and Fazio, Paul. 1998. Development of new durability index for clay bricks. *Journal of Architectural Engineering* 4, no. 3: 87-93.

León y León, Carlos A. 1998. New Perspectives in Mercury Porosimetry. *Advances in Colloid and Interface Science* 76-77: 341-372.

Leshina, V.A. and Pivnev, A.L. 2002. Ceramic wall material using glass waste. *Glass and Ceramics* 59: 9-10.

Liew, Abdul G., Idris, Azni, Samad, Abdul A., Wong, Calvin H.K., Jaafar, Mohd S., and Baki, Aminuddin M. 2004. Reusability of sewage sludge in clay bricks. *Journal of Material Cycles and Waste Management* 6: 41-47.

Liu, Wansheng, Li, Shuzhen, and Zhang, Zhanying. 1991. Sintered mosaic glass from ground waste glass. *Glass Technology* 32, no.1: 24-30.

Maage, M. 1984. Frost resistance and pore size distribution in bricks. *Materials and Structures* 17, no.101: 345-350.

Malhotra, S.K., and Tehri, S.P. 1996. Development of bricks from granulated blast furnace slag. *Construction and Building Materials* 10, no. 3: 191-193.

Mallidi, Srinivasa Reddy. 1996. Application of mercury intrusion porosimetry on clay bricks to assess freeze-thaw durability. *Construction and Building Materials* 10, no. 6:461-465.

Matteucci, F., Dondi, M., and Guarini, G. 2002. Effect of soda-lime glass on sintering and technological properties of porcelain stoneware tiles. *Ceramics International* 28: 873-880.

Montgomery, D.C., and Runger, G.C. 1999. *Applied Statistics and Probability for Engineers*. 2nd ed. Toronto: John Wiley & Sons.

Montgomery, D.C., and Runger, G.C. 2003. *Applied Statistics and Probability for Engineers*. 3rd ed. Toronto: John Wiley & Sons.

Montriro, S.N. and Vieira, C. M. F. 2004. Solid state sintering of red ceramics at lower temperatures. *Ceramics International* 30: 381-387.

Motz, H., Geiseler, J. 2001. Products of steel slags an opportunity to save natural resources. *Waste Management* 21: 285-293.

National Brick Research Centre. 2003. *Reducing Fuel Consumption in Brick Manufacturing*. Section 10. From material presented at Clemson University, South Carolina, June 26.

National Brick Research Centre. 2005. *Mercury Porosimetry Results, Brampton Brick.* Anderson: Clemson University.

Nishigaki, Masahide. 2000. Producing permeable blocks and pavement bricks from molten slag. *Waste Management,* 20: 185-192.

Ontario Ministry of Northern Development and Mines. 2003. Ontario Industrial Minerals. Queens Printer for Ontario.

Paez, Antonio. 2004. CIV ENG 4H03Analysis of Transportation Systems CIV ENG 4H03. *OLSREP Matlab Linear Regression Analysis*. Hamilton: McMaster University.

Park, Young Jun, Heo, Jong. 2002. Conversion to glass-ceramics from glasses made by MSW incinerator fly ash for recycling. *Ceramics International* 28: 689-694.

Quinn, Shannon L. 2004. Chemical Engineering 4C3/6C3 Engineering Statistics. Copies Plus, Hamilton.

Ravagioli, A. 1976. Evaluation of the frost resistance of pressed ceramic products based on the dimensional distribution of pores. *Transactions and Journal of the British Ceramic Society* 75, no.5:92-95.

Riccardi, M.P., Messiga, B., Duminuco, P. 1999. An approach to the dynamics of clay firing. *Applied Clay Science* 15: 393-409.

Rice, Warren and Chau, David S.C. 1997. Freeze desalination using hydraulic refrigerant compressors. *Desalination* 109: 157-164.

Sanders, John. 1998. Glass addition to brick. *Brickyard Road* 2, no. 4: 14-18.

Shackelford, James F. 2005. Introduction to Materials Science for Engineers, 6th Ed. Pearson Prentice Hall, New Jersey.

Shih, Pai-Haung, Wu, Zong-Zheng, & Chiang, Hung-Lung. 2004. Characteristics of bricks made from waste steel slag. *Waste Management* 24: 1043-1047.

Shutt, T.C., Campbell, H, & Abrahams, J.H. Jr. 1972. New building materials containing waste glass. *Ceramic Bulletin* 51, no. 1.

Smith, Andrew S. 2004. *To demonstrate commercial viability of incorporating ground glass in bricks with reduced emissions and energy savings*. The Waste & Resource Action Programme, Banbury.

Toledo, R., dos Santos, D.R., Faria, R.T. Jr., Carrió, J.G., Auler, L.T., Vargas, H. 2004. Gas release during clay firing and evolution of ceramic properties. *Applied Clay Science* 27 151-157.

Wardeh, G. and Perrin, B. 2006. Analysis of strains in baked clay based materials during freezing and thawing cycles. *Journal of Building Physics* 29, no. 3: 201-216.

Wardeh, G. and Perrin, B. 2006. Identification of liquid pressure in pores of baked clay tiles during freezing and thawing cycles. *Journal of Building Physics* 29, no. 4: 269-278.

Weng, Chih-Huang, Lin, Deng-Fong, & Chiang, Pen-Chi. 2003. Utilization of sludge as brick materials. *Advances in Environmental Research* 7: 679-68.

Youssef, N.F., Abadir, M.F., & Shater, M.A.O. 1998. Utilization of soda glass (cullet) in the manufacture of wall and floor tiles. *Journal of the European Ceramic Society* 18: 1721-1727.